



HAL
open science

Applications of stochastic geometry in the modeling and analysis of wireless networks

Yassine Hmamouche

► **To cite this version:**

Yassine Hmamouche. Applications of stochastic geometry in the modeling and analysis of wireless networks. Networking and Internet Architecture [cs.NI]. Ecole nationale supérieure Mines-Télécom Atlantique, 2020. English. NNT : 2020IMTA0212 . tel-03199210

HAL Id: tel-03199210

<https://theses.hal.science/tel-03199210>

Submitted on 15 Apr 2021

HAL is a multi-disciplinary open access archive for the deposit and dissemination of scientific research documents, whether they are published or not. The documents may come from teaching and research institutions in France or abroad, or from public or private research centers.

L'archive ouverte pluridisciplinaire **HAL**, est destinée au dépôt et à la diffusion de documents scientifiques de niveau recherche, publiés ou non, émanant des établissements d'enseignement et de recherche français ou étrangers, des laboratoires publics ou privés.

THÈSE DE DOCTORAT DE

L'ÉCOLE NATIONALE SUPÉRIEURE MINES-TÉLÉCOM
ATLANTIQUE BRETAGNE PAYS DE LA LOIRE - IMT ATLANTIQUE

ÉCOLE DOCTORALE N° 601
*Mathématiques et Sciences et Technologies
de l'Information et de la Communication*
Spécialité : *Télécommunications*

Par

Yassine HMAMOUCHE

Applications of Stochastic Geometry in the Modeling and Analysis of Wireless Networks

Thèse présentée et soutenue à Brest, le 21 Octobre 2020

Laboratoire : Lab-STICC Pôle : CACS/COM Département : Signal et Communications

Thèse N° : 2020IMTA0212

Rapporteurs avant soutenance :

Lina Mroueh Professeur ISEP-Paris, France
Harpreet Dhillon Professeur Virginia Tech, USA

Composition du Jury :

Président :	Sébastien Houcke	Professeur IMT Atlantique, France
Rapporteurs :	Lina Mroueh	Professeur ISEP-Paris, France
	Harpreet Dhillon	Professeur Virginia Tech, USA
Examineurs :	Martin Haenggi	Professeur University of Notre Dame, USA
	Marco Di Renzo	Directeur de Recherche Centrale Supelec, Univ. Paris-Saclay, France
	Halim Yanikomeroglu	Professeur Carleton University, Canada
Dir. de thèse :	Samir Saoudi	Professeur IMT Atlantique, France
Co-encadrant :	Mustapha Benjillali	Professeur INPT Rabat, Maroc

ACKNOWLEDGEMENT

The research presented in this thesis was carried out at the Signal and Communications Department, IMT Atlantique, Brest, France. I acknowledge the financial support of pôle de Recherche Avancée en Communications (PRACOM) and the Regional Council of Brittany, France.

My sincere and deep thanks go to my thesis supervisors Professor Samir Saoudi and Professor Mustapha Benjillali for their high expertise and great experience, which provided me with the inspiration and high energy to carry out scientific research during the three years of my thesis. I would also like to thank them for their flexibility, support, and guidance. Many thanks to them for having helped me to find my way in this fascinating topic of research and for having facilitated the connection with other international research laboratories.

I would like to extend my profound recognition to Professor Halim Yanikomeroglu for hosting me for a 3-month scientific research visit in his research group in the Department of Systems and Computer Engineering at Carleton University. I thank him for giving me the opportunity to work with such a talented group of researchers and for providing me with guidance and insights based on a wealth of experience. I also thank him for accepting to examine this work and for being a member of my thesis committee.

I would like to thank Professor Marco Di Renzo for being available to attend the individual follow-up committee of my thesis. I thank him so much for his humility and his high expertise. His original ideas and suggestions allowed me to find valuable analytical leads. I also thank him for accepting to examine this work and for being a member of my thesis committee.

I am grateful to Professor Sébastien Houcke who honoured me by chairing the jury of my thesis.

I would also like to thank Professor Lina Mroueh and Professor Harpeet Dhillon for accepting to be the rapporteurs of my dissertation work. I thank them for their positive remarks and recommendations that allowed me to improve the quality of my thesis report.

I have the great honour to have Professor Martin Haenggi as examiner of my thesis. I am deeply grateful to him for accepting to evaluate my work with an unprecedented thoroughness and refinement. I also thank him for the wealth of his publications, which were of immense importance to me during the three years of my thesis.

I have special thanks to all my family for their encouragement and support. I especially acknowledge the support and love of two great women in my life; my mother and my wife. I thank them for their patience and sacrifices.

To my children for being the light that illuminates my life.

TABLE OF CONTENTS

List of Figures	10
List of Tables	11
List of Abbreviations	13
List of Symbols	16
Publications	17
Introduction	19
A Brief History of Stochastic Geometry	19
The Paradigm of Spatial Point Process	21
Poisson Point Process Essentials	25
Stochastic Geometry in New Generation Wireless Networks	30
Key Performance Metrics	31
Scope and Contribution of the Thesis	36
1 Diverse Point Processes for Diverse Network Configurations	39
1.1 Taxonomy of State-of-the-art Point Processes	39
1.1.1 Stationary Deterministic Lattices	40
1.1.2 Hardcore Point Processes	40
1.1.3 Softcore Repulsive Point Processes	43
1.1.4 Aggregative Point Processes	47
1.1.5 Wide Versatile Point Processes	50
1.2 Stochastic Geometry Statistical Analysis	53
1.2.1 Comparison Between Point Processes	53
1.2.2 Modeling Real Nodes Deployment	55
1.3 Chapter Summary	57

2	Stochastic Geometry Based Modeling and Analysis of Wireless Networks	60
2.1	Modeling and Conceptual Choices	60
2.1.1	Network Elements	60
2.1.2	Propagation Effects	61
2.1.3	Cell Association Strategies	64
2.1.4	Transmitter-Receiver Direction of Analysis	65
2.1.5	Nodes Mobility	66
2.1.6	Spatio-temporal Traffic Modeling	67
2.2	Stochastic Geometry Based Analytical Techniques	69
2.2.1	The Baseline Two-Step Approach	69
2.2.2	Coverage Probability New Abstraction	71
2.2.3	The Relative Distance Process Based Approach	71
2.2.4	Finite Networks Assumption	73
2.2.5	Nakagami Fading on the Desired Signal	74
2.2.6	The Factorial Moment Based Approach	75
2.2.7	The Plancherel-Parseval Approach	76
2.2.8	The Gil-Pelaez Inversion Approach	77
2.2.9	The Laplace Transform Inversion Approach	77
2.2.10	The Interference Approximation Approach	78
2.2.11	MGF-based Average Rate	79
2.3	Chapter Summary	79
3	Stochastic Geometry for 5G/B5G Wireless Networks	81
3.1	Stochastic Geometry and Promising RAN Architectures For 5G/B5G	81
3.1.1	Terrestrial Heterogeneous Networks	81
3.1.2	Non-Terrestrial Networks	82
3.1.3	UDNs via Infrastructure Densification	83
3.1.4	Cloud Radio Access Networks	87
3.1.5	Virtualized Radio Access Networks	88
3.1.6	Fog Radio Access Networks	89
3.2	Stochastic Geometry in Higher-Frequency Bands	90
3.2.1	mmWave Communications	90
3.2.2	TeraHertz Communications	91
3.2.3	Visible Light Communications	91

TABLE OF CONTENTS

3.2.4	Free-Space Optical Communications	92
3.3	Stochastic Geometry and 5G/B5G Enabling Technologies	93
3.3.1	Cognitive Wireless Networks	93
3.3.2	Non-Orthogonal Multiple Access Techniques	94
3.3.3	In-Band Full-Duplex Technology	95
3.3.4	Physical Layer Security	96
3.4	Chapter Summary	96
4	A Stochastic Geometry Based Approach to Tractable 5G RNPO	98
4.1	Introduction	98
4.1.1	Related Works	98
4.1.2	Motivation and Contribution	99
4.2	System Model and Assumptions	99
4.2.1	Path Loss process with shadowing and RNPO parameters	101
4.3	Coverage Probability Analysis	103
4.3.1	Association Policy Under the H-LOS Probability Model	103
4.3.2	Coverage probability	106
4.3.3	The Regime of UDNs	108
4.3.4	The Regime of Optimal Network Density	108
4.4	Numerical Results	112
4.4.1	Validation of the Model	112
4.4.2	Operational Regimes	112
4.4.3	Optimal Network Density	115
4.5	Chapter Summary	115
5	Stochastic Analysis of UDNs With Resource Capacity and User Scheduling	117
5.1	Introduction	117
5.1.1	Related Works	118
5.1.2	Motivation and Contribution	119
5.2	System Model and Assumptions	119
5.2.1	Cellular Network and Channel Model	119
5.2.2	Cell Association Model	120
5.2.3	Scheduling Modeling	120
5.3	Coverage Probability and Ergodic Rate Analysis	121
5.3.1	Approximation of the Process of BSs with Available Resource Capacity	122

5.3.2	Coverage probability	124
5.3.3	Average Achievable Rate	130
5.4	Numerical Results	130
5.5	Chapter Summary	132
6	Uplink Coverage and Handoff Rate with Realistic Power Control Models	134
6.1	Introduction	134
6.1.1	Related Works	135
6.1.2	Motivation and Contribution	135
6.2	System Model and Assumptions	136
6.2.1	Cellular Network Model and Association Scheme	136
6.2.2	Channel Model and Power Control Scheme	136
6.2.3	Distribution of Link Distances and the Process of the Interference Field	138
6.2.4	Mobility Model	139
6.3	Uplink Coverage Probability Analysis	139
6.3.1	Case of Stationary Active UEs	139
6.3.2	Case of Moving Active UEs	140
6.4	Numerical Results	143
6.4.1	Validation of the Analytical results	144
6.4.2	The DSBPC and the Uplink Performance of UDNs	144
6.4.3	The Impact of Mobility on the Uplink Performance	146
6.5	Chapter Summary	148
7	Uplink Energy Efficiency Distribution with Aerial Users	150
7.1	Introduction	150
7.1.1	Related Works	151
7.1.2	Motivation and Contribution	152
7.2	System Model	152
7.3	Uplink Energy Efficiency Distribution	156
7.3.1	Distribution of the serving UE	157
7.3.2	Interference from active terrestrial users	159
7.3.3	Interference from active aerial users	159
7.4	Numerical Results	160
7.5	Chapter Summary	162

TABLE OF CONTENTS

Résumé long en français	163
Conclusion	174
7.5.1 Stochastic Geometry and Molecular Communications	174
7.5.2 Stochastic Geometry in the Era of Machine Learning	175
7.5.3 Stochastic Geometry as a Multi-objective Analytical Tool	176
7.5.4 Grothendieck Toposes as Mathematical Bridges for Stochastic Geometry	177
Bibliography	178

LIST OF FIGURES

1	The paradigm of spatial point process	22
2	The tendency from regularity to clustering	25
3	Simulation of non-homogeneous PPP	28
4	Main performance metrics used in the stochastic geometry abstraction	31
5	Perturbation of a regular lattice	45
6	Point process as a superposition of PPP and stationary lattice	48
7	Poisson line process in VANET	50
8	Comprehensive taxonomy of point process used in the literature	51
9	Typical shape of pair correlation function	54
10	Estimation of summary statistics	59
11	Typical realizations of the BPP abstraction	74
12	Illustration of the H -LOS setup.	104
13	Validation of analytical results	112
14	Association probability scaling with BS density	113
15	Coverage probability scaling with BS density	113
16	BS density in the optimal regime	114
17	Coverage probability scaling with network parameters	114
18	Voronoi tessellation with minimal and maximal disc.	123
19	The scaling of coverage probability with SIR threshold	131
20	The scaling of coverage probability with network and users densities.	132
21	Coverage probability as a function of system parameters	133
22	Average rate as a function of resource capacity, transmit power , and BS height .	133
23	Uplink system model of chapter 6.	138
24	Validation of the analytical model	144
25	The scaling of the uplink coverage probability with system parameters	145
26	The handoff rate as a function of the serving UE velocity and the BS density . .	147

LIST OF FIGURES

27	The induced uplink coverage probability as a function of system parameters . . .	148
28	Uplink system model of chapter 7	153
29	Aerial priority bias as a function of system parameters	161
30	Mean load approximation of the uplink EE	161
31	The uplink EE as a function of the aerial priority bias	161

LIST OF TABLES

1	A proposed reading path to get started with SG in wireless networks	21
1	Analytical tractability of PPs	52
1	Typical configuration of BSs and users in a stochastic geometry based modeling	61
2	Key path loss models used in stochastic geometry abstraction	63
3	Analytical techniques vs Association policy	80
4	Defining the intervals of integration	143

LIST OF ABBREVIATIONS

μ Wave	Microwave
3GPP	3rd generation partnership project
5G	Fifth generation
6G	Sixth generation
AF	Amplify-and-forward
ASE	Area spectral efficiency
AtG	Air-to-ground
AWGN	Additive white Gaussian noise
B5G	Beyond 5G
BBU	Baseband unit
BPM	Bounded path loss model
BPP	Binomial point process
CCDF	Complementary cumulative distribution function
CAPEX	Capital expenditure
CoMP	Coordinated multipoint
C-plane	Control plane
CR	Cognitive radio
C-RAN	Cloud radio access network
CRE	Cell range expansion
DSBPC	Dual-slope bounded power control
DSPM	Dual-slope path loss model
D2D	Device-to-device
DAS	Distributed antenna system
dex	Directionally convex
DF	Decode-and-forward
DPP	Determinantal point process
DUDA	Decoupled uplink-downlink access
EE	Energy efficiency
EM	Electromagnetic
eMBB	enhanced mobile broadband
F-RAN	Fog radio access network

FSO	Free space optical
GPP	Ginibre point process
GSPP	Geyer saturation point process
HD	Half duplex
HetNet	Heterogeneous network
HPPP	Homogeneous Poisson point process
IBFD	In-band full-duplex
ICIC	Inter-cell interference coordination
IDT	Inhomogeneous double thinning
IPPP	Inhomogeneous Poisson point process
LED	Light-emitting diode
LGCP	Log Gaussian Cox process
LOS	Line-of-sight
MAC	Medium access control
MC	Molecular communication
MCMC	Markov chain Monte Carlo
MCP	Matérn cluster process
MGF	Moment generating function
MHPP	Matérn hardcore point process
MIMO	Multiple-input and multiple-output
ML	Machine learning
mmWave	Millimeter wave
NLOS	Non-line-of-sight
NOMA	Non-orthogonal multiple access
OPEX	Operational expenditure
PCP	Poisson cluster process
PDF	Probability density function
PGFL	Probability generating functional
PHCP	Poisson hardcore process
PHP	Poisson hole process
PL	Perturbed lattice
PLP	Poisson line process
PMF	Probability mass function
PP	Point process
PPP	Poisson point process

PF	Proportional Fair
QoE	Quality of experience
QoS	Quality of service
RAN	Radio access network
RN	Relay node
RNPO	Radio network planning and optimization
ROI	Return on investment
RRH	Remote radio head
RR	Round-Robin
RWP	Random waypoint
SDN	Software-defined networking
SG	Stochastic geometry
SI	Self interference
SIC	Successive interference cancellation
SINR	Signal-to-interference-plus-noise ratio
SPP	Strauss point process
SSI	Simple sequential inhibition
SWIPT	Simultaneous wireless information and power transfer
TCP	Thomas cluster process
TTC	Time-to-content
UAV	Unmanned aerial vehicles
UDN	Ultra-dense network
UE	User equipment
U-plane	User plane
UPM	Unbounded path loss model
URLLC	Ultra-reliable and low latency communications
VAD	Voronoi area distribution
VANET	Vehicular ad hoc network
VLC	Visible light communications

LIST OF SYMBOLS

Symbol/Function	Description
$\mathbb{E}\{\cdot\}, \mathbb{P}\{\cdot\}$	Expectation and probability measures
$\mathcal{L}_X(s) = \mathbb{E}\{e^{-sX}\}$	Laplace functional of a random variable X
$\Psi_X(w) = \mathcal{L}_X(-jw)$	Characteristic function of a random variable X such that $\sqrt{j} = -1$
$\mathbb{1}(\cdot)$	Indicator function
$F_m(x) = {}_2F_1(1, -m; 1 - m; -x)$	Shorthand such that ${}_2F_1(\cdot, \cdot; \cdot; z)$ is the Gauss hypergeometric function for $z \in \mathbb{C}$
$\Gamma(a, x) = \int_x^\infty t^{a-1} e^{-t} dt$	The upper incomplete gamma function for $a, x \in \mathbb{R}$
$\gamma(a, x) = \int_0^x t^{a-1} e^{-t} dt$	The lower incomplete gamma function for $a, x \in \mathbb{R}$
$\psi^{-1}(\cdot)$	The inverse function of a function $\psi(\cdot)$
W_0	The principal branch of the Lambert W function

PUBLICATIONS

Journal Papers:

- **Y. Hmamouche**, M. Benjillali, S. Saoudi, and D. B. da Costa, “Uplink Energy Efficiency Distribution with Aerial Users in Cellular Networks”, IEEE Wireless Communications Letters, to appear.
- S. Alfattani, W. Jaafar, **Y. Hmamouche**, H. Yanikomeroglu, A. Yongacoglu, N. D. Dao, and P. Zhu, “Aerial platforms with reconfigurable smart surfaces for 5G and beyond”, IEEE Communications Magazine, to appear.
- **Y. Hmamouche**, M. Benjillali, S. Saoudi, H. Yanikomeroglu, and M. Di Renzo, “New Trends in Stochastic Geometry for Wireless Networks: A Tutorial and Survey”, Proceedings of the IEEE, to appear.

Conference Papers:

- **Y. Hmamouche**, M. Benjillali, and S. Saoudi, “Closed-form Coverage Probability under the Idle Mode Capability: A Stochastic Geometry Approach”, in Proc. 9th International Symposium on Signal, Image, Video, and Communications (ISIVC’18), pp. 135-140, 27-30 November 2018, Rabat, Morocco.
- **Y. Hmamouche**, M. Benjillali, and S. Saoudi, “A Stochastic Analysis of UDNs With Resource Capacity and User Scheduling”, in Proc. IEEE Wireless Communications and Networking Conference (WCNC’19), 15-18 April 2019, Marrakech, Morocco.
- **Y. Hmamouche**, M. Benjillali, and S. Saoudi, “A Stochastic Geometry Based Approach to Tractable 5G RNPO with a New H-LOS Model”, in Proc. IEEE Wireless Communications and Networking Conference (WCNC’19), 15-18 April 2019, Marrakech, Morocco.
- **Y. Hmamouche**, M. Benjillali, S. Saoudi, and H. Yanikomeroglu, “Uplink Coverage and Handoff Rate with Realistic Power Control Models and Blind Cell Search”, in Proc. IEEE International Symposium on Personal, Indoor and Mobile Radio Communications (PIMRC ’20), 31 August - 3 September 2020, London, UK.
- **Y. Hmamouche**, M. Benjillali, and S. Saoudi, “On the Role of Stochastic Geometry in Sixth Generation Wireless Networks”, in Proc. 10th International Symposium on Signal,

Image, Video and Communications (ISIVC '20), 7-9 April 2021, Saint-Etienne, France.

INTRODUCTION

Stochastic geometry (SG) is a field of applied probability that aims to provide tractable¹ mathematical models and appropriate statistical methods to study and analyze random phenomena on the plane \mathbb{R}^2 or in larger dimensions [1]. Its development was driven by applications in several scientific areas such as forestry, image analysis, geophysics, neurophysiology, cardiology, finance, and economics. In the context of communication networks, user equipment (UE) and base stations (BSs) are treated a realization over an enormous number of possibilities, where designing the system for every network realization would be time-consuming and resource-intensive [2,3]. Instead, using tools from SG [1–8], the location of nodes is assessed statistically in order to evaluate spatial averages, which inherently considers all possible network realizations and generally capture the main dependencies of the network performance connectivity (capacity/throughput and reliability). This is broadly understood if we see the concept of using a statistical distribution to abstract the variety of potential network topologies as actually similar to the approach of considering a statistical distribution to model the infinite possibilities of multipath fading and shadowing.

A Brief History of Stochastic Geometry

SG as a concept of geometric probability is a field that can be stretched back at least 300 years. Indeed, the bond between probability theory and geometry reverts back to the 18th century when several challenging problems and imagined experiments raised by prominent mathematicians, pondering about the impact of varying randomly geometric forms on the probability of specific events. We quote particularly the Buffon’s needle problem² (1733), and afterwards

1. The term “tractable” is a key feature in stochastic geometry-based analytical models where it serves to characterize the mathematical flexibility of the model and even its ability to produce closed-form analytical expressions. In several cases of analysis, various assumptions are adopted to increase the tractability of the modeling choices.

2. Buffon’s needle problem asks to find the probability that a needle of a given length will land on a line, given a window with equally spaced parallel lines far apart by a given distance. It provides a theoretical scheme to statistically determine the number π .

questions related to Sylvester's four-point problem³ (1864) and Bertrand's paradox⁴ (1889). A short historical outline of these early days of geometric probability may be found in [9].

Since the 1950s, the framework of geometric probability broadened substantially and framed as an academic area. In particular, the focus mainly switched to models involving a typical number of randomly selected geometric objects. As a consequence, the four distinguishable mathematical strands of *integral geometry theory* [10], *random set theory* [11], *random measures theory* [12], and *point process (PP) theory* [4–8] started to play a prominent role in the geometric probability, which since then was called stochastic geometry. Integral geometry gives a unified approach for defining integrands over curves, surfaces, volumes, and higher-dimensional manifolds by using tools from probability theory, group theory, and projective geometry. Random sets generalizes the concept of random vectors, by addressing random entities whose number of components is unknown. Random measures theory is focused on studying the properties of measures established on random elements. In the special case where these measures are integer-valued, random measures reduce to PPs considered as an important subclass of random measures. Discussions on how early problems on geometrical probability have led to the construction of primary results on these pillar theories of SG, can be found in [13]. Moreover, for the sake of exploratory data analysis, parameter estimation, and model fitting, SG has been endowed with a statistical theory in similarity with the traditional probability theory. More statistical analysis and parameters estimation can be found in [14].

In the context of communication networks, the paper [15] is the first to consider tools from SG to evaluate connectivity in a network of stations represented by a Poisson point process (PPP). In particular, it was only by the late 1990s that important ideas from SG found their way to modeling and analysis of communication networks [2, 3], where tools based on Poisson Voronoi tessellations and Delaunay triangulations were proposed to derive geometric characteristics of hierarchical links between stations. Interestingly, the seminal results were reported a decade later, where the baseline mathematical framework was characterized in the case of a generative downlink single-tier wireless network [16, 17]. Since then, generalizations to more advanced SG models have been gradually adopted in subsequent works. For example, extensions to multi-tier networks are reported in [18, 19] and to the uplink direction are analyzed in [20]. More discussions about such early extensions can be found in [21–24].

3. Sylvester's four-point problem asks for the probability that four points scattered randomly in a given window region have a convex hull, i.e., it will be possible to connect any two points within the shape constructed by the four points with a straight line that does not leave the shape.

4. The Bertrand paradox asks for the probability that the chord of a circle will be longer than the side of an equilateral triangle inscribed in this circle.

Table 1 – A proposed reading path to get started with SG in wireless networks

References	Main topics	Suitability to researchers			
		A concept primer	A technical primer	Intermediate reader	Advanced reader
[39, 40]	On the importance of using SG to grasp the implications of modern networks tendency towards heterogeneity.	•			
[24]	Generative analytical techniques to derive coverage probability under the assumptions of Rayleigh fading and PPP distributed nodes.		•		
[41]	Generative techniques used to derive the transmit-receive distance distribution.		•		
[21]	SG models, up to 2008, in the study of communication networks.	•	•		
[22]	Applications of SG, percolation theory, and random geometry in interference characterization of ad hoc networks.	•	•	•	
[23]	SG models, up to 2013, in the study of heterogeneous and cognitive networks.	•		•	
[42, 43]	Stochastic interference characterization in ad hoc networks.			•	
[44]	Stochastic interference characterization in cellular networks.			•	
[1, 4–8, 10–12]	SG theory in conjunction with related mathematical strands, e.g., integral geometry theory, random set theory, and PP theory.			•	•

Table 1 suggests some key references to help a non-specialist reader familiarize with the field of using SG in wireless networks and keep the subsequently discussed concepts less arcane.

The Paradigm of Spatial Point Process

The PP theory plays an important role in SG, since i) the building blocks of many important SG models are based on PPs inasmuch as points are the most elementary types of geometrical objects; ii) it is common to parameterize geometric objects and map them with PPs in suitable state spaces, e.g., a line process in \mathbb{R}^2 can be seen as a PP on a cylinder [10]. Next, we will address the key properties of the PPP considered as the baseline and widely used PP, due to its practical mathematical attributes, where some key results can produce surprising consequences [2–4, 4–8].

In the context of communication networks, spatial PPs have become a burgeoning strand of SG models to evaluate the following aspects [4–8]

- The statistical properties of a given set of points.
- The possibility of having a point at a specific location.
- How to build a model of points with minimal error assumptions based on an empirical set of points.
- Describing more general random geometric objects made up of unit random elements.

In contrast to earlier applications in queuing theory, where time has a natural order in one-dimensional PPs, the concept is quite different in higher dimensions ($d \geq 2$), where there is no natural order of points. Instead, the most common way is to consider the *cumulative counting process* of a spatial PP Ψ , defined for each bounded set $B \subset \mathbb{R}^d$ as the number of points x_i

falling into B ,

$$\Psi(B) = \sum_{x_i \in \Psi(B)} \mathbb{1}_B(x_i). \tag{1}$$

As illustrated in Fig. 1, a probability space $(\Omega, \mathcal{F}, \mathbb{P})$ is established to capture the uncertain outcomes of a real-world experiment. In fact, the states ω_i occur randomly depending on various socioeconomic factors to give birth to the points x_i . \mathbb{P} is the probability function that associates each event ω_i with its probability, Ω is the sample space such that $\mathbb{P}(\Omega) = 1$ and \mathcal{F} is its σ -algebra. A random variable X_i maps each event ω_i of Ω to an element x_i from a separable complete metric space $\Upsilon \subseteq \mathbb{R}^d$ where $\mathcal{B}(\Upsilon)$ its Borel σ - algebra⁵. The locations (x_i) of nodes in a communication network are then generated by random variables (X_i) such that the probability that a point is located in a given location x_i is $\mathbb{P}_{X_i}(x_i) = \mathbb{P}(X_i^{-1}(x_i)) = \mathbb{P}(\omega_i)$. The PP Ψ is now introduced as a random counting measure that describes the set of (x_i) by counting their number inside given bounded sets of Υ (sets A, B , and C in Fig. 1). Interestingly, Ψ can be observed as a random set consisting of random variables (x_i) as its elements. $N(\cdot)$ can be written for any bounded $B \in \mathbb{R}^d$ as In a more general way, we consider the n th factorial moment measure given

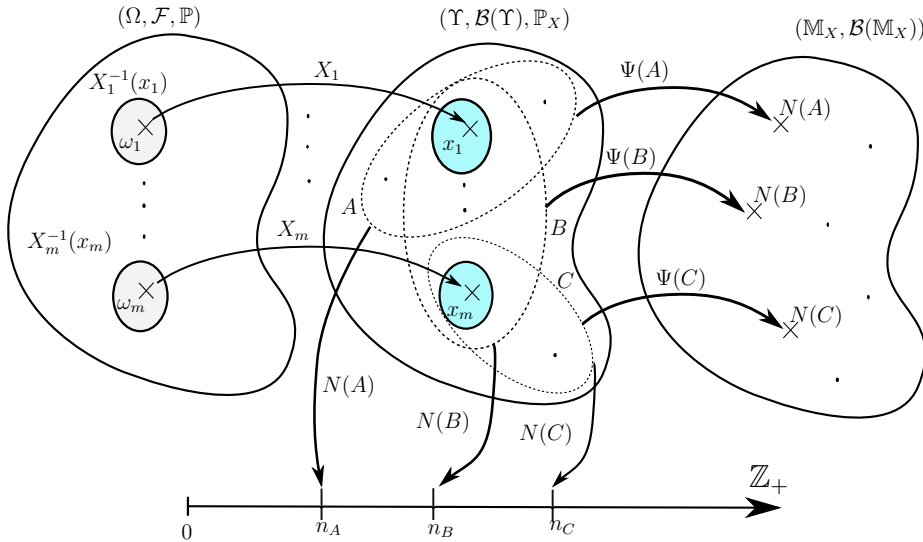


Figure 1 – Point process representation. The random variables $(X_i)_i$ map each event ω_i in the sample space Ω into an element x_i from $\Upsilon \subseteq \mathbb{R}^d$. The PP Ψ maps each bounded region $B \in \Upsilon$ with a measure n from \mathbb{M}_X that counts the number of points $(x_i)_i$ falling into B .

5. The smallest collection of sets $A^{(k)}$ of Borel subsets A of Ω [7].

by

$$\begin{aligned}
\mathbb{M}^{(n)}(A_1, \dots, A_n) &= \mathbb{E} \left(\Psi^{(n)}(A_1 \times \dots \times A_n) \right) \\
&= \mathbb{E} \left(\sum_{x_1, \dots, x_n \in \Psi}^{\neq} \mathbb{1}_{A_1 \times \dots \times A_n}(x_1, \dots, x_n) \right) \\
&= \int_{A_1} \dots \int_{A_n} \varrho^{(n)}(x_1, \dots, x_n) dx_1 \dots dx_n, \tag{2}
\end{aligned}$$

where \neq indicates the sum over pairwise distinct n -tuples and $\varrho^{(n)}(\cdot) : A_1 \times \dots \times A_n \rightarrow \mathbb{R}^+$ is the product density function w.r.t. the Lebesgue measure. Without loss of generality and for notation simplicity, we consider that when $x_i \in \Psi$, x_i will refer to a random variable that captures the potential location of the point x_i in \mathbb{R}^d . However, when x_i is used as a parameter of a PDF (or more generally of a product density function) inside a given integral for example, x_i will refer to the integration variable over a bounded set covered by the PP Ψ .

The nearest neighbor distance and the contact distribution function

One important metric related to the cumulative counting process in (1), is the probability mass function (PMF) of $N(\cdot)$ defined as the probability that there will be exactly n points inside B , i.e., $\mathbb{P}(N(B) = n)$. A particular type is *the void probability* defined as $\text{void}(B) = \mathbb{P}(N(B) = 0)$. When $B = b(y, r)$ is the ball⁶ of radius r and centered at the typical⁷ point y , $\text{void}(b(y, r))$ can be interestingly interpreted as the probability that the distance between y and the closest point of Ψ is larger than r . That is, when $y \in \Psi$, we talk about the nearest neighbor distance distribution $G_y(\cdot)$ defined as the distribution of the distance between y and the nearest point of $\Psi \setminus \{y\}$. In simple probability terms,

$$G_y(r) = \mathbb{P}(d(y, \Psi \setminus \{y\}) \leq r | y \in \Psi) \tag{3}$$

$$= \mathbb{P}(N(b(y, r) \setminus \{y\}) > 0 | y \in \Psi) = 1 - \mathbb{P}(N(b(y, r)) = 1 | y \in \Psi), \tag{4}$$

where $d(y, \Psi \setminus \{y\})$ is the distance between the fixed location y and the nearest point of Ψ except y .

6. A different shape may be taken instead of a ball depending on the dimension d of the Euclidean plane and the isotropy of Ψ .

7. In PP theory, the typical point of a PP Ψ is often considered. In wireless network analysis, it is termed as the typical UE for the downlink analysis and the typical BS for the uplink analysis. Formally, it is a point that has been chosen by a selection procedure in which each point in the process has the same chance of being selected [4, 6].

When $y \notin \Psi$, we consider *the contact distribution function* $F_y(\cdot)$ that represents the smallest radius necessary for the ball centered at y to contact a point in Ψ . Formally,

$$F_y(r) = \mathbb{P}(d(y, \Psi) \leq r) = 1 - \mathbb{P}(N(b(y, r)) = 0). \quad (5)$$

$G_y(\cdot)$ and $F_y(\cdot)$ are important first-order summary characteristics of a given PP [14] enabling to capture *clustering* or *regularity* in PPs. Typically, they are equal for the case of the totally random PP, which is the PPP, while $G > F$ for clustered PPs (Cox, Nymann-Scott, etc.), and $G < F$ for regular PPs (shifted regular lattices, hard-core, and soft-core repulsive PPs, etc.), as illustrated in Fig. 2. More discussions about PPs comparison and classification will be brought in the sequel.

The reduced Palm probability

We consider the typical point y from a stationary PP Ψ and we shift Ψ such as y lies at the typical fixed location o (the origin). For a given set $B \subset \mathbb{R}^d$, $G_y(\cdot)$ can be seen as the ratio between the mean number of points except y in the ball of radius r and centered at o , and the mean number of points inside B . Formally, it is the ratio between *the reduced Campbell measure* expressed as $\mathbb{E}_o^!(\Psi(B)) = \mathbb{E}(\sum_{y \in \Psi \cap B} \mathbb{1}_{\mathcal{A}}(\Psi_{-y} \setminus \{y\}))$, and the average number of points inside B expressed as $\lambda \nu(B)$, where \mathcal{A} is the event $N(b(y, r) \setminus \{y\}) > 0$, Ψ_{-y} is the shifted PP Ψ such as y lies at o , and $\nu(B)$ is the Lebesgue measure or the d -dimensional volume of the subset B .

The previous interpretation of the nearest neighbor distance $G_y(\cdot)$ is called *the reduced Palm probability* measure denoted by $\mathbb{P}_o^!$ as [1, 4, 6–8]

$$\mathbb{P}_o^!(\Psi \in \mathcal{A}) = \frac{1}{\lambda \nu(B)} \mathbb{E} \left(\sum_{y \in \Psi \cap B} \mathbb{1}_{\mathcal{A}}(\Psi_{-y} \setminus \{y\}) \right), \quad (6)$$

where the index o is to mention the shifting of Ψ towards o , the superscript $!$ is to refer that the typical point in the origin o is not counted, i.e., $\mathbb{P}_o(\Psi \setminus \{y\} \in \mathcal{A}) = \mathbb{P}_o^!(\Psi \in \mathcal{A})$, and $\Psi \in \mathcal{A}$ mentioning that Ψ has the property \mathcal{A} .

The marked point process

A generalization of the PP Ψ is the concept of marked PP where each point $x_i \in \Psi$ is assigned a further quantity m_{x_i} , called marks, that provides extra information on the object represented by x_i . For example, when considering a PP incorporating BSs, marks can be the

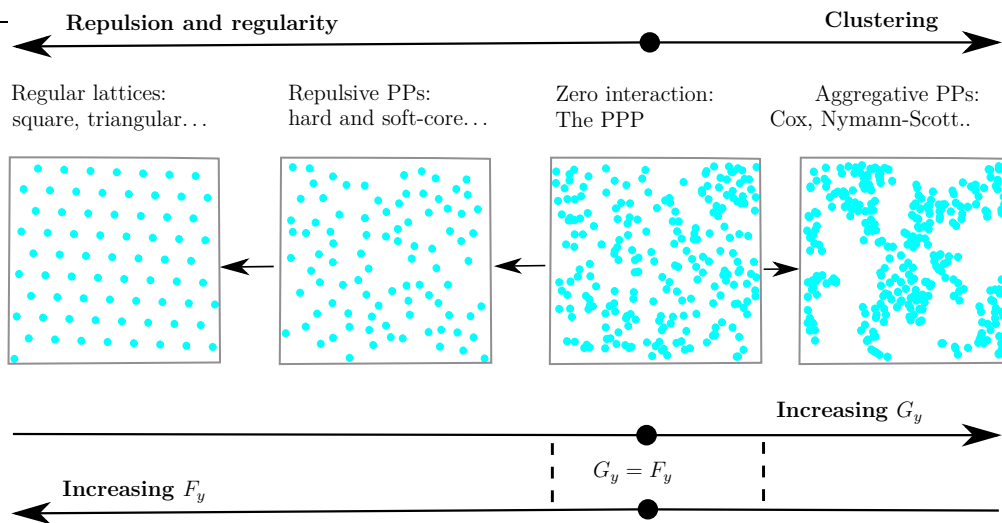


Figure 2 – The tendency towards regularity or clustering of PPs. Typically, increasing regularity reduces G_y and increases F_y simultaneously, while increasing clustering have a dual impact on G_y and F_y .

coverage area of each BS x_i [4], the fading gain between a BS x_i and the typical UE [51, 52], or the BS tier in a multi-tier network [53].

Poisson Point Process Essentials

The PPP is considered as the most popular PP given its tractability and analytical flexibility [4–8]. In the following, we will discuss key properties underlying such tractability.

In general, a PPP Ψ of density $\lambda(\cdot)$ and intensity measure $\Lambda(\cdot)$ such as for a given $B \subset \mathbb{R}^d$, $\Lambda(B) = \int_B \lambda(x)dx$, is characterized by a PMF as

$$\mathbb{P}\{\Psi(B) = n\} = \frac{\Lambda(B)^n}{n!} e^{-\Lambda(B)}. \quad (7)$$

Slivnyak-Mecke theorem

For a homogeneous PPP (HPPP) $\Psi \subset \mathbb{R}^2$ with density λ and shifted such as its typical point y will be located at the origin of the ball $b(o, \epsilon)$ of radius $\epsilon \ll 1$, The number of points falling in disjoint Borel sets are independent. The nearest neighbor distance $G_y(\cdot)$ can be expressed via

the reduced Palm probability as

$$G_y(r) = \mathbb{P}(d(y, \Psi \setminus \{y\}) \leq r | y \in \Psi) \quad (8)$$

$$= \lim_{\epsilon \rightarrow 0} \mathbb{P}_y^{\downarrow}(\Psi \in (N(b(o, r) \setminus b(o, \epsilon)) \neq 0) | N(b(o, \epsilon)) = 1) \quad (9)$$

$$= 1 - \exp(-\pi\lambda r^2) = 1 - \mathbb{P}(N(b(y, r)) = 0) = F_y(r). \quad (10)$$

Hence, the points modeled by PPP are totally independent, that is why the PPP is sometimes referred to as a zero-interaction PP [6]. In a more general way, the previous similarity in (10), between the nearest neighbor distance distribution and the contact distance distribution, may be seen as the equivalence between the reduced Palm probability of Ψ in the typical point y located at the origin o and its original distribution counting y . In other words, the spatial averages observed at $o \notin \Psi$, are equivalent in distribution to those observed at o of $\Psi \cup \{o\}$, which means that conditioning on the typical point does not affect the distribution of the PPP. This is the well-known *Slivnyak-Mecke theorem* [4–8], formally expressed as

$$\mathbb{P}_y^{\downarrow}(\Psi \in \cdot) = \mathbb{P}(\Psi \in \cdot). \quad (11)$$

This theorem is extensively used in the literature. For instance, in a wireless network where the typical UE is located at the origin o , the Slivnyak-Mecke theorem can be used to derive the mean interference at o , conceiving that the serving BS x_0 belongs to the PP of interferers, but however, it does not contribute towards the interference [16–19, 54]. Another valuable application is the transmit-receive distance distribution derived as in [4, Example 1.4.7] [41, 55–58].

Finite Poisson point process

For a fixed number n of nodes inside a given network area W , if $k \leq n$ nodes are located in a certain subset $B \subset W$, the remaining area $W \setminus B$ contains necessarily $n - k$ nodes, which introduces dependence between points of W , and hence the PPP is not so accurate to model such finite networks. Alternatively, the BPP is considered as the most relevant PP for such scenarios [41, 59–62]. It is worth mentioning that according to (6), the probability that a point $x \in W$ belongs to B is proportional to the number of points falling inside B . Equivalently,

$$\mathbb{P}(x \in B) = \frac{\Lambda(B)}{\Lambda(W)}, \quad (12)$$

and then the probability density function (PDF) of $x \in B$ is

$$f(x|\Psi(W) = n) = \frac{\lambda(x)}{\Lambda(W)}. \quad (13)$$

In a more formal way, the conditional multivariate PDF $f(x_1, \dots, x_n|\Psi(W) = n)$ defined w.r.t. the Lebesgue measure on $(\mathbb{R}^d)^n$ is expressed as

$$f(x_1, \dots, x_n|\Psi(W) = n) = \frac{\prod_{i=1}^n \lambda(x_i)}{\Lambda(W)^k}. \quad (14)$$

Interestingly, the concept of (14) is explored to capture the structure of point patterns exhibiting inter-point interactions. That is, it is used in a more refined structure called the *Papangelou conditional intensity* to construct the family of Gibbs PPs [14, 63–65] and fitting statistical models to specific spatial point patterns via *pseudolikelihood maximization* [66]. More generally, (14) is the building block in the definition of *the reduced Palm distribution* [8].

Simulation of Poisson point process

The equivalence property between a conditional PPP and a binomial distribution in a bounded window W , is typically used in simulation studies to generate a stationary PPP of density λ [14, 63]. Practically, we first generate a Poisson variate \mathcal{N} with parameter $\lambda\nu(W)$ and next we generate \mathcal{N} independent and uniformly distributed (iud) points inside W . The resulted PP inside W is equivalent to a PPP with density λ . Besides, (14) is considered as the key to generate an inhomogeneous PPP (IPPP). For example, we consider the realization of a 2-dimensional IPPP with density $\lambda(x, y) = 240(6x^5 + 4y^3)$ on the window $W = [0, 1] \times [0, 1]$. The PDF of a given point located in (x, y) is $f(x, y) = \lambda(x, y)/480$ bounded by 5. Using the accept-reject method \mathcal{N} times, where \mathcal{N} is generated by a Poisson variate with parameter $\tilde{\lambda} = 480$, we draw uniformly g on $[0, 1]$ and accept (x, y) such as $f(x, y)/5 \leq g$. Fig. 3 describes the realization of the previous process in W . A valuable application of such technique in cellular networks modeling and analysis can be found in [67, Section VI].

Campbell and probability generating functional theorems

In the previous analysis, the PPP were constructed based on the PMF in (7). In the following, a PPP Ψ can be constructed through probability densities on bounded subsets and generalizing the construction to the whole plane.

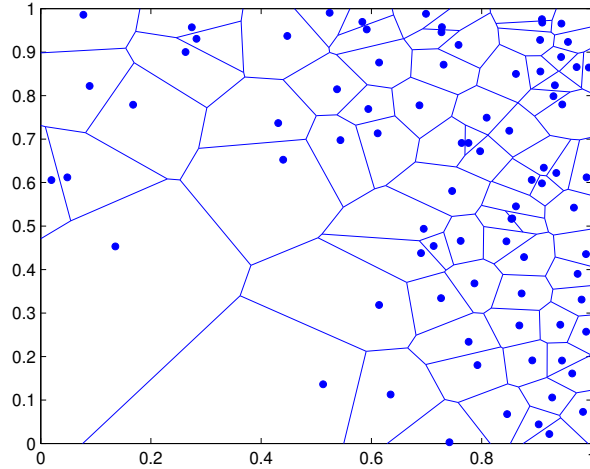


Figure 3 – Realization of a non homogeneous PPP on the window $W = [0, 1] \times [0, 1]$ with density $\lambda(x, y) = 240(6x^5 + 4y^3)$. Voronoi tessellation shows cells boundaries based on the spatially nearest points.

In fact, for any real positive function f defined over \mathbb{R}^d , the probability generating functional (PGFL) of a PPP Ψ , named equivalently the Laplace functional, is expressed as [4–7]

$$\mathcal{L}_\Psi(f) = \mathbb{E} \left\{ \exp \left(- \sum_{x_i \in \Psi} f(x_i) \right) \right\} = \mathbb{E} \left\{ \exp \left(- \int_{\mathbb{R}^d} f(x) \Psi(dx) \right) \right\} \quad (15)$$

$$\stackrel{(a)}{=} \exp \left(- \int_{\mathbb{R}^d} (1 - e^{-f(x)}) \Lambda(dx) \right), \quad (16)$$

where (a) follows by using the conditional PDF expression in (14) as in [4].

The expression (16) is considered to derive two fundamental results widely explored in SG-based modeling and analysis of wireless networks, namely the Campbell and PGFL theorems. In fact, by considering $tf(x) \rightarrow f(x)$ in (16) with $t \geq 0$ and differentiating w.r.t. t at $t = 0$, we obtain the Campbell theorem, as

$$\mathbb{E} \left(\sum_{x_i \in \Psi} f(x_i) \right) = \int_{\mathbb{R}^d} f(x) \Lambda(dx). \quad (17)$$

While by replacing $e^{-f(x)} \rightarrow f(x)$ in (16), we obtain the PGFL theorem for the PPP Ψ , as

$$\mathbb{E} \left(\prod_{x_i \in \Psi} f(x_i) \right) = \exp \left(- \int_{\mathbb{R}^d} (1 - f(x)) \Lambda(x) \right). \quad (18)$$

Preserving the Poisson law

Sometimes, it is necessary to consider some transformations on the PPP used to model node locations in order to obtain more insightful and tractable results. In the following, we consider popular operations preserving the Poisson law and extensively explored in the literature [4–8].

- *Superposition*: The union of independent PPPs (Ψ_k) with intensities (Λ_k) is a PPP $\Psi = \bigcup_k \Psi_k$ with intensity measure $\Lambda = \sum_k \Lambda_k$. As an illustration, the superposition of independent K-tier networks is investigated in [18, 19, 39, 54, 58, 68]. The superposition of two independent layers of line-of-sight (LOS) and non-line-of-sight (NLOS) BSs are considered in [69–71]. The superposition of independent PPPs to abstract the network of several competitive operators is considered in the context of infrastructure sharing [72], spectrum sharing [73–75], or both [76–78].
- *Independent thinning*: is a selection process Ψ^p of specific points from the primary PPP Ψ such that each point x is randomly and independently selected with a probability $p(x)$. Accordingly, Ψ^p yields a PPP of intensity measure equals to $\int_{\mathbb{R}^d} p(x)\Lambda(dx)$ [4, Proposition 1.3.5.]. Typically, independent thinning is used to generate the family of Cox PP (e.g., Neymann-Scott, log-Gaussian) considered as a generalization of the PPP and used to capture clustered point patterns [1, 6, 79]. Also, the nodes of a given network can be thinned independently given their ability to be in LOS or NLOS transmissions with the typical UE [69–71], to operate in half-duplex (HD) or IBFD mode [80], or to use device-to-device (D2D) channels as in [81]. ALOHA, the popular algorithm used in the medium access control (MAC) layer to track simultaneous packet transmissions in the network, is considered in [4, 82] as an independent thinning of nodes willing to transmit data.
- *Displacement*: is a random transformation of points of Ψ from \mathbb{R}^d to some new location in Ψ^p from $\mathbb{R}^{d'}$ according to a probability p . The new PP inherits the Poisson law and its intensity measure is $\Lambda'(A) = \int_{\mathbb{R}^d} p(x \in A)\Lambda(dx)$, $A \subset \mathbb{R}^{d'}$, as given by the displacement theorem [4, Theorem 1.3.9]. Valuable applications can be found in [4, 51, 83, 84]. In some settings, a given point $x \in \Psi$ may be moved deterministically with probability 1 into a function $f(x) \in \Psi^f$ [56, 58], and hence the new PP remains a PPP with intensity measure $\Lambda'(A) = \Lambda(f^{-1}(\cdot))$. This property is also known as the mapping theorem [6]. A typical application is studied in [85, 86], where the authors considered an arbitrary path loss model and a generalized fading model, and next derived a sequence of equivalence relations between the so-called shotgun cellular system and a stochastically equivalent system, namely *the canonical model*.

Stochastic Geometry in New Generation Wireless Networks

With exponential digitalization of modern society, 5G/B5G networks are envisioned to play a major role in the process of achieving higher data rates, hyper-connectivity, and ultra-low latency [25,26]. To achieve such requirements, future 5G/B5G wireless networks are expected to be more heterogeneous due to various targeted verticals with specific demand, in addition to the use of higher-frequency bands (e.g., millimeter-wave (mmWave) [27], teraHertz communications [28], and visible light communications (VLC) [29]) enabling to build high-speed short-range networks. Also, environmental objects will be coated with intelligent meta-surfaces that can reflect incident signals in a customized way to optimise/recycle signal propagations in future networks [30]. The use of unmanned aerial vehicles (UAVs) will be a common and mature technology, where they can be used as flying-BSs to support terrestrial coverage in isolated regions, enhance capacity in traffic overloaded user hotspots, and even used as flying-UEs for delivery or supervision purposes [31]. Interestingly, end terminals will be gradually equipped with computing and/or storage capabilities, in a fog radio access architecture (F-RAN) fashion [32], enabling to emerge from the paradigm of ubiquitous connectivity to that of *ubiquitous wireless intelligence*.

Consequently, as the complexity and heterogeneity of modern wireless networks is continuously increasing, tools from artificial intelligence and machine learning (ML) will be crucial to learn static and dynamic components of the wireless environment and then help to make optimal control decisions for system-level performance. Also, SG adopted as a powerful model-driven tool for the evaluation of wireless networks during the last decade, is expected to remain an effervescent area of research in the foreseeable future, due typically to the following reasons: First, spatial arrangement of transmitters and receivers will continue to play a major role in the prediction of performance metrics in 5G/B5G wireless networks, e.g., performance scaling laws in ultra-dense networks (UDNs) [33,34], impact of coupling UE and BS locations on system-level performance (see Table 1). Second, a cross-fertilization between SG and ML can be made to achieve better results in terms of accuracy and flexibility. Typically, SG can be integrated as a hypothesis class in the learning process of ML to evaluate the family of subset selection problems [35,36]. Third, despite the ability to build a programmable and controlled wireless environment in 5G/B5G networks, thanks to F-RAN and massive adoption of meta-surfaces, it is actually impossible to control all facets of the environment, e.g., building sway generated by winds and thermal expansion of materials [37] or beams misalignment in higher-frequency communications [38]. Hence, the need to model such uncontrolled network aspects with random

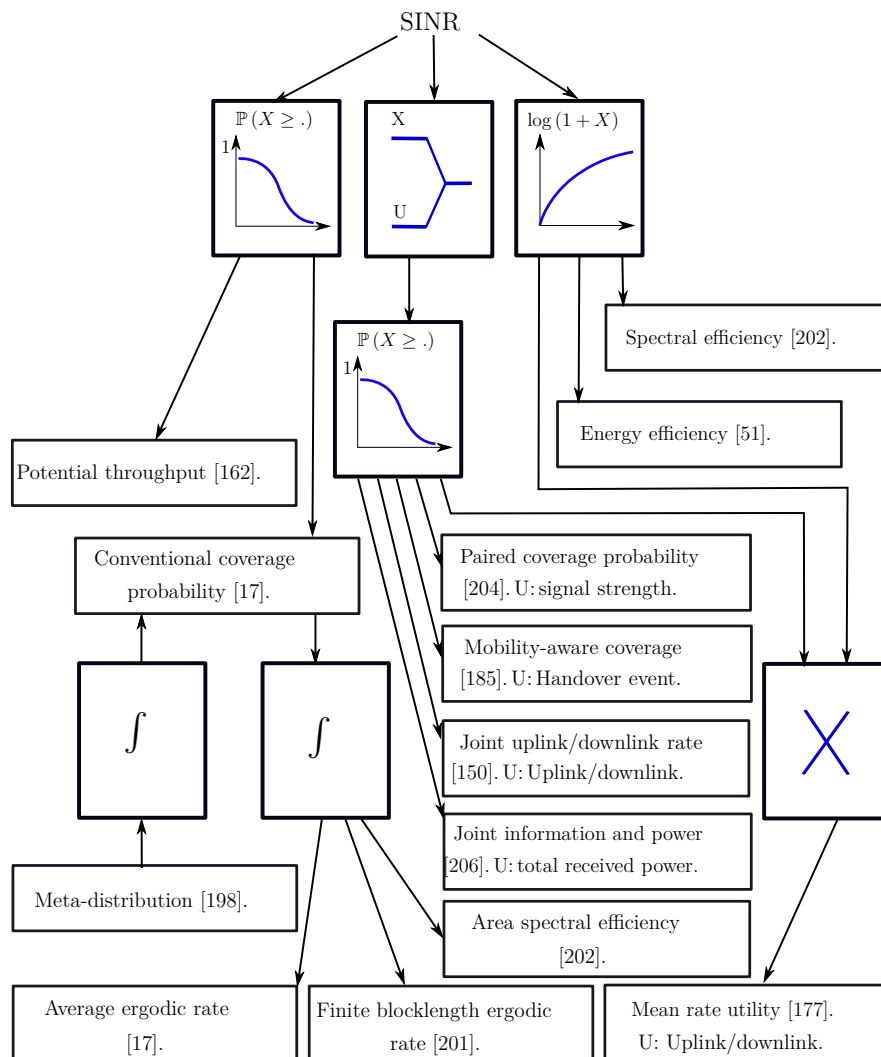


Figure 4 – Main performance metrics used in the SG abstraction.

processes, and then the ubiquitous need for SG.

Key Performance Metrics

Since Shannon's work [188], the received SINR has been considered as the first-order predictor of link reliability and users QoE, where almost all performance metrics conceived to date are closely related to it. For instance, the bit error rate depends on $Q(a\sqrt{\text{SINR}})$ and the data rate follows $\log(1 + \text{SINR})$, where $Q(\cdot)$ is the Q -function and a is a constant depending on modulation and detection. A review of the largely fragmented literature of SG-based arts for modeling and analysis of wireless networks reveals that almost all the adopted performance metrics are

typically based on six key operations of SINR, as illustrated in Fig. 4. In the following, we will consider the definition of key representative performance metrics.

Spectral efficiency

The spectral efficiency S_e is conceived as the maximum information rate that can be transmitted over a given bandwidth B . In the simplest case of AWGN and optimal theoretical link performance, the Shannon-Hartley theorem defines S_e in units of [nats/s] as

$$S_e \triangleq B \log(1 + \text{SINR}). \quad (19)$$

Energy efficiency (EE)

The EE \mathcal{E} evaluates the number of bits that can be successfully transmitted with unit energy. It is generally expressed under the form [51, 138, 197]

$$\mathcal{E} = \frac{S_e}{\varpi P_{\text{tx}} + \alpha}, \quad (20)$$

where P_{tx} is the BS transmit power and ϖ and α are some positive constants depending on the power consumption model.

Mean rate utility

It is particularly defined in the context of a generic IBFD link [177], as

$$\mathcal{R}_u(T_{\text{DL}}, T_{\text{UL}}) = \mathbb{P}(S_e^{\text{DL}} \geq T_{\text{DL}}) S_e^{\text{DL}} + \mathbb{P}(S_e^{\text{UL}} \geq T_{\text{UL}}) S_e^{\text{UL}}, \quad (21)$$

where T_{DL} and T_{UL} are, respectively, the required spectral efficiency thresholds in the downlink and the uplink.

Conventional coverage probability

The coverage probability P_c , as opposed to outage probability P_o , is defined as the probability that the typical user can reach a target SINR T [17]. It is expressed as

$$P_c(T) = 1 - P_o(T) = \mathbb{P}(\text{SINR} \geq T), \quad (22)$$

which also can be interpreted as the success probability of the typical transmission/link averaged over all spatial links [7, 42, 105]. Formally, we first condition on the BS process and the typical UE is located at the origin \mathbf{o} of the PP Ψ , and next average over all the spatial links, as

$$P_c(\mathsf{T}) = \mathbb{E} \{ \mathbb{P}^{\mathbf{o}}(\text{SINR} \geq \mathsf{T} | \Psi) \}. \quad (23)$$

Meta-distribution

Expression (23) can be rephrased as the reduced Palm expectation over the PP realization, which does not provide insights about how concentrated are the well covered areas or what are the link success probabilities. The Meta-distribution concept is interestingly introduced in [198] to obtain fine-grained information about the performance, as

$$\overline{F}(\mathsf{T}, u) = \mathbb{P} \{ \mathbb{P}^{\mathbf{o}}(\text{SINR} \geq \mathsf{T} | \Psi) > u \}, \quad u \in [0, 1]. \quad (24)$$

The coverage probability in (23) becomes then $P_c(\mathsf{T}) = \int_0^1 \overline{F}(\mathsf{T}, u) du$.

Average ergodic rate

Another quantity of interest is the average ergodic rate τ , also known as the Shannon throughput, accounting for the mean data rate achievable over a cell. It is obtained in units of [nats/s/Hz] as [17–19]

$$\tau \triangleq \mathbb{E} \{ \log(1 + \text{SINR}) \}. \quad (25)$$

The average ergodic rate in (25) may actually require the preliminary calculation of P_c [16, 17, 68], since

$$\tau = \int_{t>0} \mathbb{P} \{ \log(1 + \text{SINR}) > t \} dt = \int_{t>0} \mathbb{P} (\text{SINR} > e^t - 1) dt = \int_{x>0} \frac{P_c(x)}{x+1} dx. \quad (26)$$

Finite blocklength ergodic rate

From an information-theoretic angle, (25) is a reasonable performance metric for modern wireless networks supporting enhanced mobile broadband (eMBB) services where codewords length is sufficiently large to maximize throughput and induce very small packet error probability. However, in the context of ultra-reliable and low latency communications (URLLC), the throughput is not a key requirement of the system, and the trade-off between low latency and

ultra-high reliability requires generally the use of short packets [199] [200]. In such a context, the ergodic rate of communication is approximated as [201, Equation 296]

$$\tau^*(n, \epsilon) \approx \mathbb{E} \left\{ C - \sqrt{\frac{V}{n}} \mathcal{Q}^{-1}(\epsilon) + \frac{1}{2n} \log(n) \right\}, \quad (27)$$

where n is the blocklength, ϵ is the error probability, $C = \log(1 + \text{SINR})$ is the capacity of an AWGN channel, and V is the channel dispersion approximated as a function of SINR in [201, Equation 293].

Area spectral efficiency

The concept of area spectral efficiency (ASE) has been introduced for the first time in [202, Equation (65)] to measure, for a partially loaded system, the maximum average data rate per unit area per unit bandwidth supported by a cell. Formally,

$$\text{ASE} = \frac{1}{|\mathcal{A}|} \sum_{k=1}^{N_s} \mathbb{E} \{ \log(1 + \text{SINR}_k) \}, \quad (28)$$

where $|\mathcal{A}|$ is the area of interest, N_s is the total number of active users inside $|\mathcal{A}|$, and $\mathbb{E} [\ln(1 + \text{SINR}_k)]$ is the ergodic rate of the k th user.

Under the SG abstraction, ASE in (28) can be simplified as

$$\text{ASE} = \lambda \mathbb{E} \{ \log(1 + \text{SINR}) \}, \quad (29)$$

where the expectation averages over different network and fading realizations, and λ is the density of active BSs [203].

In realistic scenarios, a minimum SINR constraint γ_0 is required for the system operational regime [70], which induces a constrained variant of the area spectral efficiency as

$$\text{ASE}_c = \lambda \mathbb{E} \{ \ln(1 + \text{SINR}) \} \mathbb{1}(\text{SINR} \geq \gamma_0). \quad (30)$$

Potential throughput

The potential throughput considered in [83, 162, 165], is another variant of the area spectral efficiency. It is defined in units of [bps/Hz/m²] as

$$P_{\text{th}}(\mathsf{T}) = \lambda \log(1 + \mathsf{T}) \mathbb{P}\{\text{SINR} \geq \mathsf{T}\}. \quad (31)$$

Interestingly, it has been demonstrated in [34] that (29), (30), and (31), are ordered as follows

$$P_{\text{th}} \leq \text{ASE}_c \leq \text{ASE}.$$

Paired coverage probability

A new definition of coverage probability is considered in [204, 205], such that the typical UE is in coverage as well as, i) it receives a sufficiently good signal strength, i.e., the short-term average signal-to-noise ratio $\overline{\text{SNR}}$ is greater than a certain threshold T_s , ii) it receives a good signal quality, i.e., the SIR is greater than another threshold T_q . Formally,

$$P_c(\mathsf{T}_s, \mathsf{T}_q) = \mathbb{P}(\overline{\text{SNR}} \geq \mathsf{T}_s, \text{SIR} \geq \mathsf{T}_q). \quad (32)$$

(32) is shown to capture more system-level parameters than (22), and enables deriving tractable closed-form expressions.

Mobility-aware coverage probability

In [185, 186], the authors introduced a mobility-aware coverage probability, where handoffs may cost service delays or drops. (22) is updated as

$$P_c(\mathsf{T}) = \mathbb{P}(\text{SINR} \geq \mathsf{T}, \overline{\mathsf{H}}) + (1 - \beta) \mathbb{P}(\text{SINR} \geq \mathsf{T}, \mathsf{H}), \quad (33)$$

where H is the handoff event, and $\beta \in [0, 1]$ reflects system sensitivity to QoS impairment when handoff occurs.

Joint uplink and downlink rate coverage

It is defined as the fraction of users with sufficient spectral efficiency (or SINR) in the uplink and downlink simultaneously [150]. It is expressed as

$$\mathcal{R}(\mathsf{T}_{\text{DL}}, \mathsf{T}_{\text{UL}}) = \mathbb{P}\left(\mathsf{S}_e^{\text{DL}} \geq \mathsf{T}_{\text{DL}}, \mathsf{S}_e^{\text{UL}} \geq \mathsf{T}_{\text{UL}}\right). \quad (34)$$

Joint information and power coverage

The joint information and power coverage \mathcal{P} , is introduced in [206] to evaluate the performance of simultaneous wireless information and power transfer (SWIPT). It is expressed as

$$\mathcal{P}(\mathsf{T}_i, \mathsf{T}_e) = \mathbb{P}(\mathsf{S}_e \geq \mathsf{T}_i, \mathsf{E} \geq \mathsf{T}_e), \quad (35)$$

where E is the total received power at the energy harvester.

Scope and Contribution of the Thesis

In this thesis, I will use powerful analytical tools from stochastic geometry to model and analyze the downlink and uplink of wireless networks. The results introduced in the present thesis can be extended to a broad range of setups. In a nutshell, the contributions can be summarized as follows

- We review the largely fragmented literature, up to 2020, in wireless applications leveraging PP models, and provide for the first time a comprehensive taxonomy of them. We additionally review the key statistical methods used to compare between PPs and fit some empirical data.
- We present in a refined tutorial fashion for non-specialists, the analytical techniques developed to date in the literature of SG-based modeling and analysis of wireless networks, where we delve into their key mathematical sequence steps.
- We outline key modeling properties of new 5G/B5G technologies including emerging RAN architectures and enabling technologies.
- We investigate the importance of introducing generalized shadowing and conventional RNPO parameters into the cell-selection model. Using tools from SG, we derive the coverage probability by considering an SINR distribution equivalence between a 3D network with shadowing and RNPO parameters and a 2D network in which they are ignored. An

intermediary result is a closed- form expression generator encompassing the Q -function based- expression in [17].

- We investigate the impact of antenna elevation, resource capacity, and user scheduling on the performance of ultra-dense networks (UDNs). Using tools from stochastic geometry (SG), we extend a recently introduced definition of coverage probability by inducing a generic thinning that can capture BSs with available resource capacity to transmit users data. Analytical results are then derived for the coverage probability and the average achievable rate, where we obtain closed-form expressions allowing to assess UDNs performance in a more tractable and meaningful fashion compared to the conventional definition of coverage probability. Besides, our results showed that BS height and user density are so detrimental to coverage probability and average rate in UDNs, while inherent resource capacity and the transmit power have reduced impact as network density increases, which suggests new insights into the role of these parameters in UDNs.
- We characterize, based on stochastic geometry, the uplink coverage probability with a unified power control scheme built upon realistic path loss models and user equipment (UE) constrained transmit power. To improve their uplink connectivity, active UEs are next assumed to move in a random direction without prior knowledge of their nearest base station location, namely the blind cell search (BCS) movement. A tractable expression of the uplink handoff rate is then derived and the induced uplink coverage probability following the BCS movement is evaluated. The results show different echoes of the uplink coverage probability depending on the serving UE profile (stationary or mobile) and the considered path loss model.
- Considering two classes of terrestrial and aerial users with distinctive characteristics in terms of shadowing and system-level parameters (density, height, consumed power, and power control factor), we evaluate the uplink energy efficiency (EE) distribution at the typical ground base station. We first characterize the priority bias of each user layer to assess its degree of penetration among the total population of active users. Next, tractable approximations of the desired signal and the interference distribution are performed, enabling to derive the uplink EE. Our results demonstrate that an aggregation of the system-level parameters through the aerial priority bias needs to meet a given constraint to mitigate interference from aerial users and enhance EE distribution.

DIVERSE POINT PROCESSES FOR DIVERSE NETWORK CONFIGURATIONS

Although the PPP model provides tractable results and many useful closed-form expressions, its accuracy has been recently questioned [65,67,87,88]. In fact, given the zero interaction assumption of the PPP, it cannot capture the geometry of real networks, where nodes are negatively correlated, i.e., spatial inhibition and repulsion, or positively correlated, i.e., spatial aggregation and clustering. In realistic networks, radio planning engineers are generally interested to deploy BSs on theoretical points where there will be a sufficient traffic demand and then an adequate return on investment (ROI). Hence, realistic deployments have commonly an increasing tendency towards clustering in user hotspots (e.g., events, urban area) and a tendency towards repulsion and regularity when users are equally likely scattered [89–91]. That is, since the received SINR is sensitive to the interaction degree between nodes location, capturing the geometry of such nodes through an appropriate PP, will directly impact the accuracy of network performance evaluation [40,67,89–93].

In the following, we will review the alternative PPs used in the literature to model nodes location that exhibit interaction, in addition to outline the key methods used to infer them. Also, we will discuss the relevant literature works applying them in a variety of communication scenarios. Finally, we will develop a comprehensive classification of these PPs according to several attributes (e.g., the degree of interaction between points, the PP family, the ability to characterize interference at an arbitrary point when transmitters are scattered according to this PP, and the analytical tractability of such interference characterization).

1.1 Taxonomy of State-of-the-art Point Processes

A more universal way to classify PPs is by considering the interaction degree between points. In fact, point locations can interact negatively with each other to build a well-crafted and regular structure or even an intermediate repulsive structure that can be either hard-core or soft-core.

Conversely, a decrease in repulsion may be equivalent to an increase in randomness and then a tendency towards the paradigm of zero interaction PP, i.e., the PPP. Afterwards, a positive interaction between points will induce clustered points (see Fig. 2).

1.1.1 Stationary Deterministic Lattices

Traditionally, deterministic lattices, e.g., regular hexagonal lattice, or perfect square lattice, are often considered as an ubiquitous assumption in academia and research to model the location of nodes in a wireless network [42]. Formally, a 2-dimensional stationary regular lattice can be expressed under the form

$$\Lambda_{\text{grid}} = \{c\mathbf{G} + U : c \in \mathbb{Z}^2\}, \quad (38)$$

where \mathbf{G} is the generator matrix of the grid and U is a uniformly distributed random vector over the Voronoi cell of the origin to ensure the stationarity of lattices.

However, despite the main advantage of regular lattices, where it is generally more efficient to design good channel access schemes as compared to networks where node locations are perceived as random or in motion, tractable network performance evaluation is only possible for specific user locations in the cell (cell edges, etc.), and a generalization over the entire cell requires complex and time-consuming Monte Carlo simulations [16, 17]. Also, with the proliferation of heterogeneous networks (HetNets¹) where cells radii vary considerably with differences in transmission power, grid models are seen as very idealized, yielding very optimistic results of performance evaluation [16, 17]. Typically, when comparing the results obtained from the PPP and lattice models with real deployments, we observe that the PPP model provides a lower bound of reality, while perfect lattices give an upper bound. An accurate PP lies then somewhere between the two extremes. It is neither perfectly periodic, nor completely independent.

1.1.2 Hardcore Point Processes

In such a family of PPs, there are no points at a distance smaller than a specific minimum threshold δ , also known as the hardcore distance. In the following, we will discuss the key variants of hardcore PPs.

- *Matérn hardcore point process (MHPP)*: There are generally two popular variants of MHPP used in the literature of wireless networks modeling and analysis, namely MHPP

1. There is a slight abuse of meaning with the term of non homogeneous networks modeled by a PP with location-dependent density.

type I and MHPP type II [94]. MHPP I deletes all pairs of points with pairwise distance less than δ such that the density of the resulting PP is $\lambda = \lambda_p \exp(-\pi\lambda_p\delta^2)$, where λ_p is the density of the parent PPP. In MHPP II, the process MHPP I is changed into a dynamic scheme by considering the parent PPP as marked by the uniform speed arrival times $t \in [0, 1]$, which results on a density $\lambda = [1 - \exp(-\lambda_p\pi\delta^2)] / \pi\delta^2$. For $\lambda_p \rightarrow \infty$, we note that MHPP I suggests that no point could survive after the dependent thinning process, while MHPP II predicts that the remaining points are correlated with $1/\pi\delta^2$. Performance analytical evaluation of networks modeled by the MHPP is generally challenging given the reduced tractability of the contact and nearest neighbor functions, which enables to only derive approximations for the mean and the MGF of the interference. For instance, tight bounds of the mean interference in MHPP I and MHPP II are investigated in [95,96] and the contact distribution is evaluated in [97]. More theoretical analysis of the MHPP can be found in [1,94].

- *Simple sequential inhibition (SSI)*: Another fashion to capture point patterns that exhibit inhibition, is by exploring sequential PPs, in which points are added one by one based on a given sequence. The most popular sequential process is the simple sequential inhibition (SSI) process, where each point is generated uniformly in a given window and independently from the previous points. The added point is rejected if it lies closer than the hardcore distance from the previous accepted points, and retained otherwise. Next, another point is generated and the process is ended if and only if we achieve the desired number of points inside the window or no other point can be added. A representative example is the art in [98], where the amount of regularity in MHPP I, MHPP II, and SSI is evaluated through some regularity metrics.
- *The family of Gibbs point process–Poisson hardcore process (PHCP)*: An alternative way to capture point patterns that exhibit repulsion, is to proceed through the multivariate PDF in (2), which renders the construction and interpretation of the PP simpler, in addition to flexible simulations. Typically, the simulation of the multivariate PDF can be approximated for example by considering the equilibrium distribution of a Markov chain, also known as *Markov Chain Monte Carlo* (MCMC) algorithms, e.g., *Métropolis-Hastings* algorithms [14, Page 149]. A representative family of PPs based on this approach is the class of Gibbs PPs, also known as Markov PPs [99]. Formally, for a given finite spatial point pattern $u = \{x_1, \dots, x_{n(u)}\}$, the multivariate PDF of a finite Gibbs PP Ψ is expressed as

$$\varrho^{(n)}(u) = \exp \left(V_0 + \sum_{i=1}^{n(u)} V_1(x_i) + \sum_{i < j \leq n(u)} V_2(x_i, x_j) + \dots \right), \quad (39)$$

where $\exp(V_0)$ is a normalizing factor ensuring that $\varrho^{(n)}(\cdot)$ is a PDF, and for $k \geq 1$, V_k is a function reflecting the interaction order between points.

It is worth mentioning that the exponential form in (39) is not arbitrary but driven by the formulation of a maximization problem of the entropy in physics, expressed generally on the basis of logarithmic functions. Typically, statistical analysis has shown that the pairwise interaction is generally sufficient to model inter-points interaction [14]. That is, the Gibbs PP is commonly known as pairwise interaction PP. The multivariate PDF of a stationary Gibbs PP Ψ , i.e., $V_1(x) = \log(\beta), \forall x \in u$, is simplified as

$$\varrho^{(n)}(u) = \kappa \beta^{n(u)} \prod_{i < j \leq n(u)} h(\|x_i - x_j\|), \quad (40)$$

where $\|x_i - x_j\| = d(x_i, x_j)$, $\kappa = \exp(V_0)$, and $h(\cdot)$ is a function dependent on the mutual distance between points.

The Poisson hardcore process (PHCP) is established as a special case of the Gibbs PP, such that $\forall x_i, x_j \in u$,

$$h(\|x_i, x_j\|) = \begin{cases} 1 & \text{if } \|x_i - x_j\| > \delta \\ 0 & \text{if } \|x_i - x_j\| \leq \delta. \end{cases} \quad (41)$$

In wireless networks modeling and analysis, the PHCP was initially investigated via simulations in pattern recognition of deployed nodes that exhibit repulsion [65]. Some analytical investigations of the PHCP are next considered, to approximate for example performance metrics of a two-tier HetNet as in [100].

- *Poisson hole process (PHP)*: Another way to conceptualize hardcore repulsion between points is to consider independent realizations of two HPPPs Ψ_1 and Ψ_2 , with respective densities λ_1 and λ_2 . Next, A PHP Ψ is conceived by considering Ψ_2 as a parent PP depriving it of points located in holes (exclusion regions) of radius δ around the points of Ψ_1 . The density of Ψ is then expressed as [6], $\lambda = \lambda_2 \exp(-\pi\lambda_1\delta)$. PHP belongs to the family of Cox PPs, i.e., doubly stochastic PPPs, where it is roughly considered as capturing clustering rather than inhibition, this is well understood since creating holes

in one region forces nodes to cluster in other regions.

Several valuable applications of the PHP are reported in the literature. For instance, in cognitive networks [101], the holes are interpreted as the guard regions around primary users, where the PHP models secondary users allowed to transmit as long as they are located outside the holes, which reduces the detrimental effect of interference. In HetNets [100, 102], the PHP is explored to capture dependence between tiers, where small cells are not allowed to be deployed very close to macro cells. In [103], the authors proposed the use of the PHP to model a multi-cell D2D underlaid cellular network. Generally, despite the flexible construction of the PHP as compared to previous hardcore PPs, a complete characterization of interference and then SINR distribution is unfeasible. To overcome such limitation, two approaches are considered in the literature: i) Derive relatively tight bounds and approximations of the MGF of the interference [101, 103, 104], or ii) approximate the PHP realization with either a PPP or a tractable clustering PP [6, 102].

1.1.3 Softcore Repulsive Point Processes

A smooth way to generate inhibition between points is to increase the tendency towards repulsion and regularity without setting a deterministic restriction via hardcore distances. In the following, we will outline the key softcore PPs used in the literature of wireless networks modeling and analysis.

- *The family of Gibbs point process–Strauss point process (SPP)*: It is a special case of Gibbs PPs by defining for a constant $0 < \gamma < 1$, the function h in (40), as

$$h(\|x_i, x_j\|) = \begin{cases} 1 & \text{if } \|x_i - x_j\| > \delta \\ \gamma & \text{if } \|x_i - x_j\| \leq \delta. \end{cases} \quad (42)$$

The multivariate PDF in (40) is then simplified as

$$\varrho^{(n)}(u) = \kappa \beta^{n(u)} \gamma^{s_\delta(u)}, \quad (43)$$

where $s_\delta(u)$ counts the number of unordered pairs of distinct points in u spaced apart by less than δ .

When $s(u)$ increases, the PDF in (43) is integrable and goes towards 0, which decreases the tendency towards clustering. γ helps then to softly adjust the repulsiveness intensity, where the SPP is typically reduced to a PPP when $\gamma = 1$ and to a PHCP when $\gamma = 0$.

Practically, it is revealed in [64,65] that the SPP is an optimal candidate for point patterns that exhibit a tendency towards repulsion. However, despite its easy interpretation and construction, the finite SPP is geared towards time consuming simulations and does not have closed-form expressions for the moments, while generalizations to infinite Gibbs PP renders the analysis even more complicated.

- *Determinantal point processes (DPPs)*: To overcome the previous limitations of SPP, a DPP Ψ acting over a given Borel $B \subseteq \mathbb{C}^d$ is constructed in such a way that it preserves the smart structure of Gibbs PPs in (40), but with a closed-form multivariate PDF w.r.t. the Lebesgue measure on $(\mathbb{C}, \mathcal{B}(\mathbb{C}))$ [105–111]. That is, for two functions $h : B^n \rightarrow \mathbb{R}^+$ and $C : B^2 \rightarrow \mathbb{C}$, we have

$$\mathbb{E} \left\{ \sum_{x_1, \dots, x_n \in \Psi}^{\neq} h(x_1, \dots, x_n) \right\} = \int_B \cdots \int_B \varrho^{(n)}(x_1, \dots, x_n) h(x_1, \dots, x_n) dx_1 \cdots dx_n, \quad (44)$$

$$\text{and } \varrho^{(n)}(x_1, \dots, x_n) = \det (C(x_i, x_j))_{1 \leq i, j \leq n}, \quad (45)$$

where \neq denotes that the finite points are pair-wise distinct, $\det(\cdot)$ denotes the determinant function, and the matrix C is called the kernel of the DPP.

The repulsiveness of the DPP Ψ stems from the observation that the determinant of a complex covariance matrix can not be greater than the product of its eigenvalues [111], and then $\varrho^{(n)}(x_1, \dots, x_n) \leq \prod_{i=1}^n \varrho^{(1)}(x_i)$, where equality holds in a PPP. Furthermore, motion-invariance of Ψ implies that the kernel C_0 is real depending only on the distance between pairs of points. That is, its Fourier transform, i.e., spectral density, exists and is defined as

$$\varphi(x) = \mathcal{F}(C_0)(x) = \int_B C_0(y) e^{-2\pi jxy} dy, \quad (46)$$

where the existence of the associated DPP Ψ to C_0 is constrained by checking $|\varphi| \leq 1$ [109, Proposition 5.1].

Depending then on the formulation of the covariance function C_0 or the spectral density φ , several versions of motion-invariant DPPs are constructed with different levels of repulsiveness and tractability [105, 106, 111]. For instance, Ψ is a Gauss DPP if for every $u \in \mathbb{R}^2$, $C_0(u) = \lambda \exp(-\|u/\gamma\|^2)$, where λ is the spatial intensity of the Gauss DPP and γ is a parameter to adjust the repulsiveness of the DPP, such as $\pi\lambda\gamma^2 \leq 1$ for the

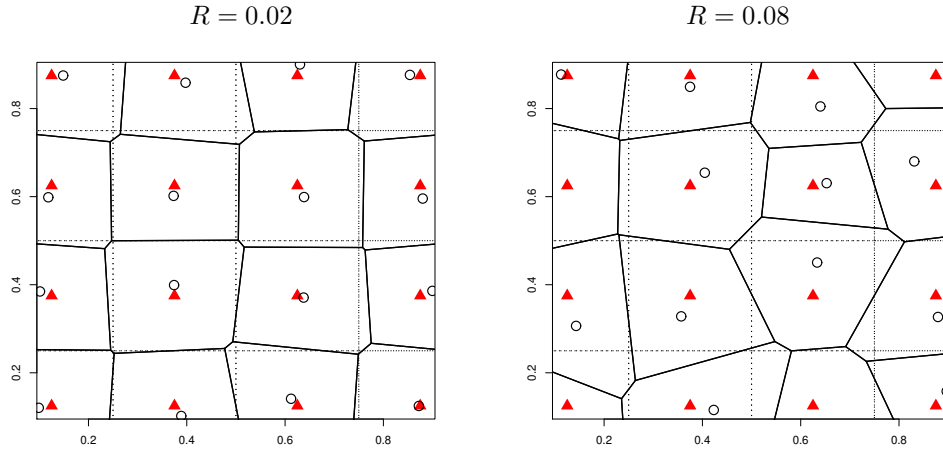


Figure 5 – Two realizations of the square lattice with uniform perturbation on the disk $b(0, R)$. The dotted lines reflect borders of the Voronoi tessellation of the square lattice without perturbation (red triangles) and the solid lines that of the Voronoi tessellation of the perturbed lattice (circles).

existence condition. The Cauchy DPP is obtained when $C_0(u) = \lambda / (1 + \|u/\gamma\|^2)^{m+1}$ and an existence condition such that $\pi\lambda\gamma^2 \leq m$, where λ is the intensity of the process and α and m , are shape parameters to tune repulsiveness. The generalized gamma DPP is defined with a spectral density $\varphi(u) = \lambda(m\gamma^2 / (2\pi\Gamma(2/m))) \exp(-\|u\gamma\|^m)$, where the existence condition is $\lambda m\gamma^2 \leq 2\pi\Gamma(2/m)$.

For more tractability and mathematical convenience, another form of motion-invariant DPPs is introduced, namely the scaled Ginibre PP (β -GPP), by considering a kernel as $C(x, y) = c\pi^{-1} e^{-\frac{c}{2\beta}(|x|^2 + |y|^2)} e^{\frac{c}{\beta}x\bar{y}}$, where the resulting density λ is scaling with c as $\lambda = c/\pi$ [107–110] and β to seamlessly adjust the repulsion intensity. It is worth mentioning that in addition to the availability of closed-form moments of DPPs, a scaled β -GPP $\Psi = (X_i)_{i \in \mathbb{N}}$ enhances mathematical tractability due to the fundamental property in which $(X_i^2)_{i \in \mathbb{N}}$ are mutually independent and follow a $\Gamma(i, \beta/c)$, $\forall i \in \mathbb{N}$ [109, Proposition 1].

Relevant applications of the DPP have been reported in the literature. For instance, the authors of [105] investigated the goodness-of-fit of a real deployment scenario of nodes with three motion-invariant DPPs: the Gauss model, the Cauchy model, and the Generalized gamma model, where it is revealed that the latter provides the best fit accuracy at the expense of reduced tractability due to the spectral density based construction of the model. Analytical investigation of the scaled β -GPP is explored in [107–110], where tractable expressions of the contact distribution function and the Ripley's K -function (see next paragraphs) are derived; however, the distribution of SINR is yet of intractable formulation.

- *Perturbed lattice (PL)*: At this stage, the above-discussed repulsive PPs differ in terms of their construction approaches, tractability, and capability to fit real deployment scenarios. However, one common shortcoming is their inability to softly capture point patterns that exhibit *perfect regularity*. Accordingly, the perturbed lattice (PL) is adopted in the literature of wireless network modeling and analysis, such that the degree of perturbation allows to tune softly the process from a deterministic lattice (no perturbation) to highly random deployments (i.e., PPP) [51, 64, 65, 112–116]. Formally, the construction of a perturbed lattice Λ_{pert} is based on (38), as

$$\Lambda_{\text{pert}} = \Lambda_{\text{grid}} + X_c = \left\{ c\mathbf{G} + U + X_c : c \in \mathbb{Z}^2 \right\}, \quad (47)$$

where X_c , $c \in \mathbb{Z}^2$, is a family of i.i.d. random variables, uniformly distributed on a disk of radius R . In other words, R is a control knob to tune the degree of perturbation (see Fig. 5). R needs generally to be upper-bounded to avoid collision between nodes after perturbation, e.g., in the case of triangular lattice, R needs to verify $0 \leq R < r_s\sqrt{3}/2$ where r_s is the radius of the circumscribed circle of the perfect lattice.

Given its ability to capture wide range of point patterns between the PPP and deterministic lattices, the PL is extensively investigated in the literature of wireless networks modeling and analysis. For instance, analytical bounds of the average interference and signal-to-interference ratio (SIR) distribution are studied in [112, 113]. In [64, 65, 113, 114], the PL is used to model realistic node deployments that exhibit repulsion. Interestingly and given the observation that the best SINR distribution is achievable under perfect lattices [17], the authors of [115, 116], proposed to proceed on the basis of a novel algorithm, namely *the triangular lattice fit*, to deactivate some empty BSs, i.e., BSs serving no UE, in such a way to render the structure of activated BSs as regular as possible, which will enable to maximize the overall performance.

Evaluating the amount of regularity in the location of transmitters and/or receivers is typically an important metric to predict the performance of a given wireless network. A review of the sparse literature shows that there are generally two judicious tools to evaluate the amount of regularity in a point pattern. i) *The coefficient of variation (CoV)* metrics, introduced for the first time in [117]. They are constructed based on specific geometrical characteristics of point patterns, such as the area of Voronoi cells, the length of Delaunay triangulation edges, and the nearest neighbor function. CoV metrics are typically normalized by a given constant [118] such that their value in the context of

the PPP equals 1. Valuable applications can be found in [98, 114–116]. ii) *The average deployment gain* introduced in [65, Equation (11)] to measure the minimum horizontal gap in terms of the mean square deviation between the two curves of the SIR distribution under the PPP and the point pattern under investigation.

- *Combination of PPP and stationary grid:* Due to the observation that all the nodes of a PL are subject to random perturbation, the authors of [64] confirmed via experiments on realistic deployments that PLs cannot accurately capture spatial dependence between nodes. Alternatively, the authors of [119] proposed a new approach to capture soft repulsion between nodes as a combination of two extreme sub-structures, namely a totally random PP (i.e., PPP) and a stationary deterministic lattice. That is, the repulsiveness of the outcome PP is softly tuned based on the ratio between the densities of the PPP and the stationary grid (see Fig. 6).

1.1.4 Aggregative Point Processes

There are several aspects exhibiting clustering in realistic wireless networks. For instance, there will be a tendency towards clustering for indoor transmitters covering building's interior, or transmitters serving clustered users around hotspots, or even vehicles clustered due to traffic and intersections. Also, UEs of a D2D communication network need to lie in close proximity of each other, and sometimes, the clustering of nodes may be logically induced by some MAC protocols [120–125]. In such circumstances of geometrically and logically induced clustering, aggregative PPs are required for an accurate evaluation of networks performance. A common way to capture the clustering of nodes is by considering a further generalization of the PPP via the IPPP, where the distance-dependent density of the IPPP increases in regions of interest. However, one main shortcoming of the IPPP is its non-stationarity, which limits the use of tractable simplifications considered in the case of stationary PPs and also ceases the concept of the typical user where the performance evaluation becomes dependent on the location of the user under investigation. In the following, we review the key aggregative PPs used in the literature to overcome such limitation.

- *Cox cluster point process:* A further generalization of the finite² IPPP is the stationary finite Cox process constructed by randomizing the parameters of the IPPP model. Typically, the intensity of the IPPP becomes a random variable mapped with realizations of

2. Stationarity or homogeneity of a PP implies implicitly infinite point patterns. In other words, it is realistic to consider large inhomogeneous point patterns as part of a stationary PP while IPPP is generally a finite PP [14].

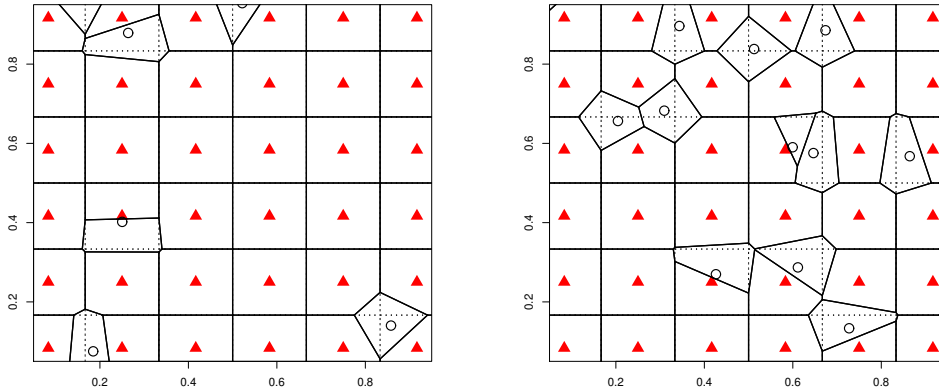


Figure 6 – Two realizations of the proposed PP constructed as a superposition of a stationary perfect lattice (red triangles) and a PPP (black circles).

a stationary random field with positive values (i.e., the intensity field). The Cox PP is also known as a doubly stochastic PP since its construction is tracked on two steps: i) Generate realizations of the random field $\{\Lambda(y)\}$, i.e., parent points. Next, ii) conditioned on a realization $\Lambda(y)$ of the random field, point pattern is generated with an IPPP of density $\lambda(y) = \Lambda(y)$, i.e., daughter points, where parent points are not observable and do not form part of the resulted point pattern. Depending on the construction way of the random field $\{\Lambda(y)\}$, several flexible families of the Cox PP may be established. For instance, the log Gaussian Cox process (LGCP) is considered when the logarithm of the random field is a real-valued Gaussian process. In other words, the clustering of point patterns in LGCP may be smoothly adjusted by acting on the mean and variance of the distribution, where a zero variance is equivalent to the PPP case, and an increasing variance (with constant mean) is equivalent to an increasing tendency towards clustering. Another interesting doubly stochastic PP is the α -stable Cox PP [126,127], in which the random field follows the α -stable distribution. The shot-noise Cox PP [128] is obtained by generating the random field by a general PP Ψ_p , where at each parent point $x \in \Psi_p$, the daughter points Ψ_d are generated by an IPPP with density $m_x \psi(y - x)$, where m_x is the average number of points clustered around x , and $\psi(\cdot)$ is the PDF of the distance between a daughter point y of the cluster and x . The density of the outcome Cox PP is

then expressed as

$$\lambda(y) = \sum_{x \in \Psi_p} m_x \psi(y - x), \quad \forall y \in \Psi_d. \quad (48)$$

The Cox PP is typically investigated in vehicular ad hoc networks (VANETs) [?, 79, 130], where a doubly stochastic process is useful to capture the randomness of roads (modeled by a Poisson line process (PLP)) as well as that of nodes location (modeled by a 1D PPP) (see Fig. 7). Alternatively, and based on empirical data of realistic networks, the authors of [127] observed that user-centric capacity-driven behavior of modern BS deployments is accurately captured by heavy-tailed distributions of the BS density, particularly the α -stable distribution. In [126], analytical investigation in addition to empirical data fitting is obtained by considering a generalized PPP setup with α -stable distributed BS density. In [131], the spatial clustering degree of users (i.e., level of heterogeneity) is captured via the LGCP, where it is observed that the network performance decreases when users are clustered without being correlated to BSs location.

- *Poisson cluster process (PCP)*: In Cox cluster PP, the number of parent points follows a general PP while that of daughter points follows a PPP. The PCP, however, is based on a reciprocal approach where the number of parent points follows a PPP while that of daughter points follows a general PP. A representative family is the Gauss-Poisson PP, in which daughter points are either no points, one, or two points, with respective probabilities p_0 , p_1 , and $p_2 = 1 - p_0 - p_1$ [6]. Another special case of the PCP is when daughter points are scattered i.i.d. around the origin and their number is Poisson distributed, which yields the family of the Neyman-Scott PP, also considered as a special case of the shot-noise Cox PP. That is, considering the parent PP as HPPP and based on the expression of $\psi(\cdot)$ in (48), two important models of the Neyman-Scott PP are commonly constructed, namely the Matérn cluster processes (MCP), where daughter points are i.u.d in a ball $b(x, \delta)$ centered at each parent point $x \in \mathbb{R}^d$, and Thomas cluster processes (TCP), where daughter points are symmetric normal distributed.

Based on simulations and model fitting, relevant works in the literature compared empirical data of existing shared networks [132] and vehicular networks [133] with the accurate PP from MCP, TCP, and LGCP. Results showed that the LGCP is the most suitable PP to characterize point patterns that exhibit strong tendency towards clustering, while analytical flexibility is in favour of the others, as performed in [120–125] for MCP and TCP, and in [134, 135] for the Gauss-Poisson PP.

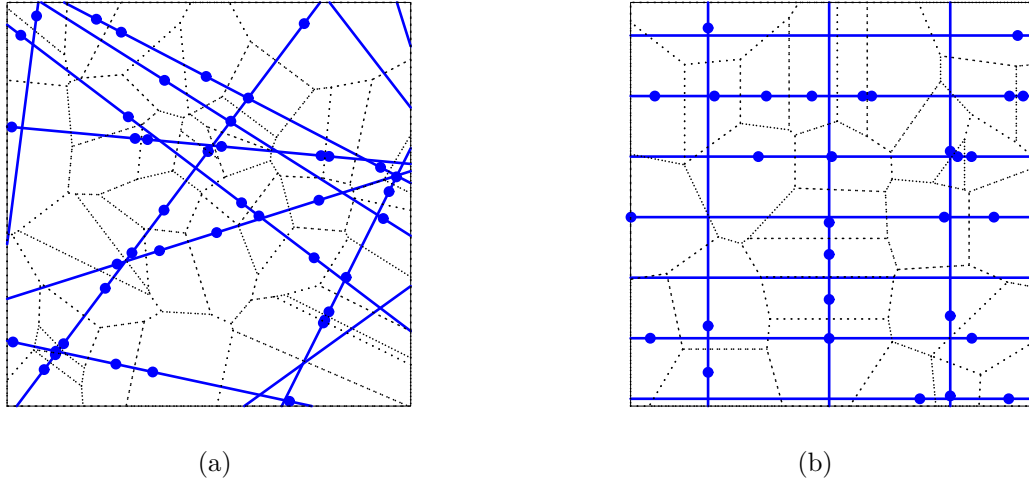


Figure 7 – Two realizations of roads (solid lines) modeled by a Poisson line process (a) and by a deterministic set of lines (b). Vehicles (dots) are modeled by a 1D PPP with similar densities in (a) and (b). Voronoi tessellation (dotted lines) reflects the association region of each vehicle.

- *The conditional thinning approach:* A tractable generative approach to capture the tendency of nodes towards clustering (i.e., reduced homogeneity) is by considering a specific independent thinning. Typically, the authors of [136, 137] introduced a specific thinning of retention probability p conditioned on the serving BS and complementarily dependent on the empty probability of other BSs [138] (i.e., the probability that a BS does not serve any user). A value of $p = 1$ is equivalent to a uniform distribution of users, while a decreasing value of p is equivalent to clustering of users around the serving BS.

1.1.5 Wide Versatile Point Processes

Despite diversity of the previous discussed PPs, they are restricted to capture point patterns that exhibit either repulsion or clustering. However, in realistic deployments, we usually find a combination of repulsion and aggregation at different levels, and hence a compelling need for more general PPs. In the following, we consider a third type of PPs, namely *the wide versatile PPs*, that with regard to their typical construction may capture both repulsion and clustering.

- *Geyer saturation point process (GSPP):* The first PP is the GSPP seen as a natural generalization of the SPP. Actually, when γ in (43) is below 1, the GSPP is equivalent to an SPP and then captures repulsiveness. However, in the case of clustering (i.e., $\gamma > 1$), the multivariate PDF in (43) is not integrable for $s(u) \rightarrow \infty$. To overcome this, the

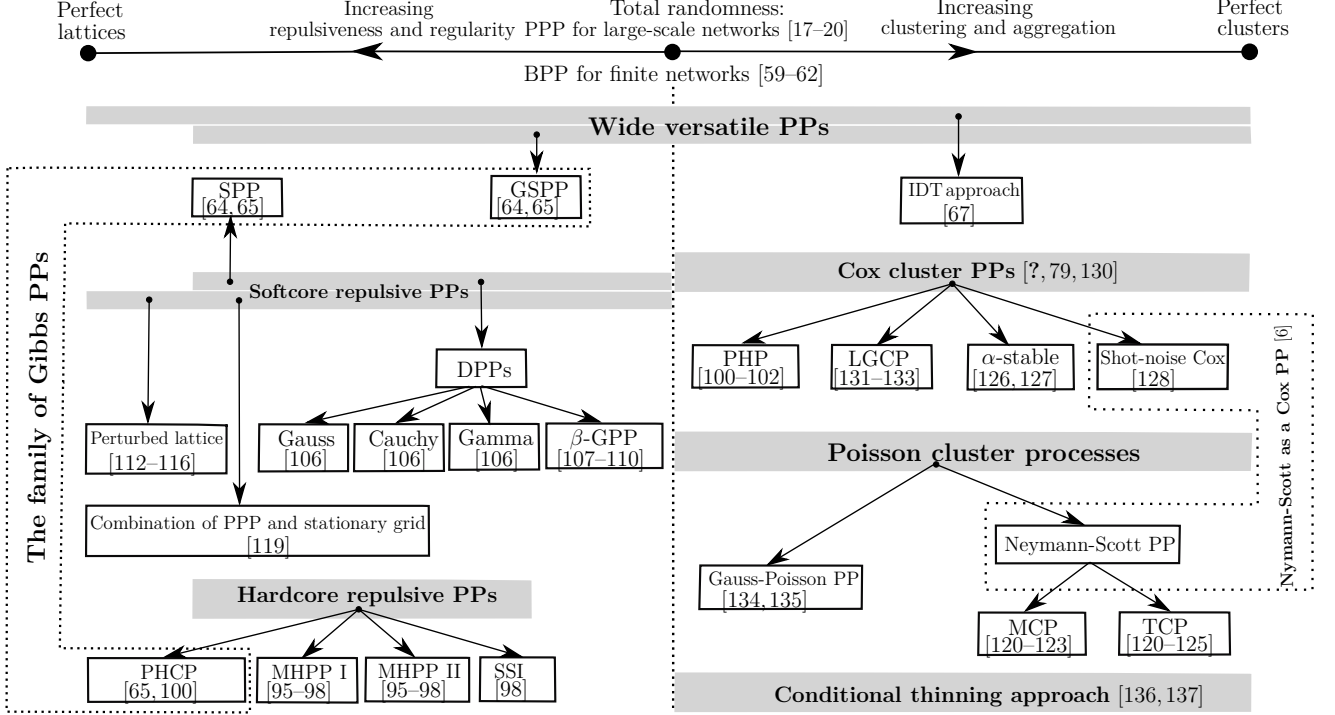


Figure 8 – Taxonomy of PPs and frameworks used to model nodes in wireless communication networks.

GSPP is then saturated as

$$\varrho^{(n)}(u) = \kappa \beta^{n(u)} \gamma^{\min(s(u), t)}, \quad (49)$$

where t is a constant to bound the trend of $s(u)$. If t is large enough, the GSPP can capture both repulsion and clustering depending on the fluctuation of γ . Moreover, if $t = 0$ or $\gamma = 1$, the GSPP is equivalent to a PPP.

- *The inhomogeneous double thinning (IDT) approach:* The second PP is an analytical framework, namely the inhomogeneous double thinning (IDT) approach, introduced in [67] in such a way to capture the interaction degree between points based on the superposition of two conditionally independent IPPPs. In fact, by conditioning on the serving BS, the first IPPP captures the fluctuation degree of the distance between the typical user and the serving BS (via the F -function), while the second IPPP captures the fluctuation degree of the distance between the typical user and interfering BSs (via Ripley's K -function). Interestingly, based on two triplets of parameters (i.e., one triplet for the F -function and the other triplet for the K -function), it is observed that the IDT model can accurately fit the structure of a wide range of wireless networks, where nodes

Table 1 – Taxonomy of PPs in terms of the ability to characterize the interference and analytical tractability.

Point process	Modeling use cases				Interference characterisation	References	Analytical tractability	Comments
	Regularity	Repulsion	Clustering	Independence				
Stationary regular lattice	•				Exact mean	[42, 88]	High	- More efficient to design good channel access schemes as compared to networks where node locations are perceived as random or in motion. - System-level performance evaluation requires complex and time-consuming Monte Carlo simulations. - Do not capture the geometry of Hetnets.
PPP				•	Exact PGFL	[17]	High	- Enhanced tractability and mathematical convenience, more simplifications compared to other PPs, captures randomness of network geometry. - Cannot capture the geometry of realistic scenarios, where nodes are highly correlated (repulsion or clustering).
BPP				•	Exact PGFL	[61]	Medium	- The PPP version to model finite networks. - Reduced tractability as compared to the PPP.
MHCPP		•			Approximate mean	[95, 96]	Low	- Capture the mutual repulsion between nodes. - Underestimates the density of transmitters in high density of the parent PPP points, which affects the interference estimation.
SSI					Unknown	[98]	Unknown	Overcomes the limitations of MHCPP in terms of underestimating the density of transmitters in high density of the parent PPP points.
PHCP		•			Exact PGFL	[100]	Low	- Easy interpretation of the model and flexible simulations.
SPP		•			Unknown	[64, 65]	Unknown	- GSPP: Suitable for a wide range of PPs ranging from the aggregative family to the repulsion one.
GSPP		•	•	•	Unknown	[64]	Unknown	- No closed form expressions for the moments. - Can resort to time consuming simulations.
PHP			•		Approximate PGFL	[101, 102, 104]	Medium	Enables to conceptualize hard-core repulsion between points based on the tractability of two independent HPPPs.
DPP		•			Exact PGFL, Exact mean	[105–110]	Low	- The moments are known as they are described by certain determinants of matrices - Involving analysis of the contact distribution function and the SINR's distribution
Perturbed lattice	•	•		•	Approximate mean	[112, 113]	Medium	- Enables to softly capture point patterns that exhibit perfect regularity. - All nodes of a PL are subject to random perturbation, which reduces the accuracy to capture spatial dependence between nodes in realistic deployments.
Superposition of PPP and Shifted lattice	•	•		•	Approximate PGFL	[119]	Medium	- Overcomes the limitations of the perturbed PL. - Involving analysis of the SINR's distribution.
Alpha-stable Cox			•		Exact PGFL	[126]	Low	- Superior accuracy to statistically model the varying BS density in different areas. - Involving analysis of the SINR's distribution inducing reduced computational efficiency.
LGCP			•	•	Unknown	[131–133]	Unknown	- Its construction is based on elegant simplicity as the random field is a real-valued Gaussian process. - Can serve as a universal model to fit realistic multi-network empirical data.
PCP			•		Exact PGFL	[121–124, 134, 135]	Medium	Enables to capture spatial coupling between user and BS locations, which is in line with the 3GPP simulation models.
Conditional thinning approach			•	•	Exact PGFL	[136, 137]	High	Captures the tendency of users towards clustering (i.e., reduced homogeneity) around the serving BS.
IDT approach	•	•	•	•	Exact PGFL	[67]	Medium	Captures the interaction degree between points based on the superposition of two conditionally independent IPPPs

location can exhibit spatial repulsion and/or clustering.

Fig. 8 illustrates a comprehensive taxonomy of the PPs used in the literature of wireless networks modeling and analysis. Typically, the gray bar reflects the range of variation in the degree of interaction of each PP family. For instance, hard-core PPs can only reflect structures with hard-core repulsion distance, without being able to capture totally random structures (PPP or BPP) or perfect lattices. DPPs which are part of soft-core PPs, can capture structures ranging from the PPP to some repulsive structures below perfect lattices. However, other soft-core PPs such as perturbed lattice and the combination of a PPP and a stationary grid can model more point patterns ranging from PPP to perfect lattices. Interestingly, the IDT approach can model structures ranging from the two extremes.

Table 1 classifies the PPs, used in the SG literature for modeling and analysis of wireless networks, by various degrees of tractability and mathematical complexity. An important key measure of interest is the ability of the PP to permit the derivation of the PGFL of the interference at a given arbitrary point, which in turn allows to derive various performance metrics

(e.g. coverage probability, ergodic rate). Three classes of PPs are identified; those enabling to derive the interference's PGFL, those failing to derive it so that an approximation of the PGFL or of the interference mean value is made, and those with unknown PGFL and mean value of the interference.

Since SG is also endowed with an important statistical theory [14], the PPP is typically leveraged as a reference PP to build statistical tools that enable to characterize the class of a given PP (totally random, clustered, or repulsive) or even to compare between PPs. Subsequently, we will review the key statistical methods used in the literature of wireless networks modeling and analysis to characterize PPs or fit them to realistic empirical data.

1.2 Stochastic Geometry Statistical Analysis

Several tools are used in the theory of PPs and spatial statistics to detect deviations from the PPP and characterize the interaction between points, particularly in terms of type, strength, and range [1, 6, 14]. These tools are also used as fitting methodologies to identify an appropriate PP model for some empirical data, [64, 65, 87, 109].

1.2.1 Comparison Between Point Processes

Using the observation that the contact function and the nearest neighbor function are identical in the PPP, the J -function is introduced in spatial statistics for $r > 0$ as

$$J_y(r) = \frac{1 - G_y(r)}{1 - F_y(r)}. \quad (50)$$

That is, $J(r) = 1$ in the case of a PPP. In clustered PPs, an arbitrary point of the plane is likely to be farther away from a given point of the PP rather than in the context of the PPP, whereas in the other direction, clustered points tend to lie closer to their nearest neighbors, hence $F_y(r) < G_y(r)$ and then $J_y(r) < 1$. Similarly, $J_y(r)$ is greater than 1 in the case of repulsive PPs. However, it is possible to construct sometimes a non-Poisson PP that checks $J(r) = 1$, which reduces the accuracy of the J -function in characterizing PPs [14].

An alternative approach is by considering second-order summary characteristics such as the pair correlation function [119], defined for a PP $\Psi \subset \mathbb{R}^d$, $\forall x, y \in \Psi$ as

$$g(x, y) = \frac{\varrho^{(2)}(x, y)}{\varrho^{(1)}(x)\varrho^{(1)}(y)}, \quad (51)$$

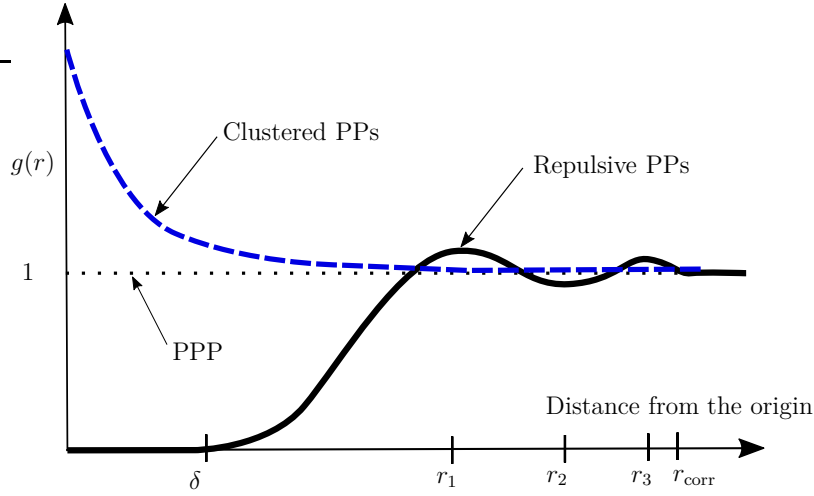


Figure 9 – Typical shape of pair correlation function for the three classes of PPs.

where $\varrho^{(1)}(\cdot)$ and $\varrho^{(2)}(\cdot)$ are, respectively, the first and second moment densities of Ψ .

When Ψ is isotropic, $g(x, y)$ is only dependent on the distance r between points x and y but not on their locations. That is, for a completely random PP (i.e., the PPP), x and y are totally independent and then $g(r) = 1$. In clustered PPs, $\varrho^{(2)}(x, y)$ is likely to overcome $\varrho^{(1)}(x)\varrho^{(1)}(y)$, then $g(r) > 1$ for small r and converges to 1 as r increases. For hardcore repulsive PPs, where inter-points distance is almost greater than a certain barrier distance δ , the pair correlation function equals to 0 when $r < \delta$. As r becomes greater than δ , $g(r)$ can exceed 1 and fluctuates around it with increasing r .

Fig. 9 describes the overall trend of $g(r)$ as a function of the PP class. Typically, r_{corr} is the distance describing the approximate size of clusters. r_1 is the distance to the closest neighbors with most frequent short inter-point distance. r_2 is the distance at which $g(r)$ contacts its first minimum after r_1 , and can be interpreted as the distance to regions with a small number of points beyond the nearest neighbors. r_3 is the second maximum of $g(r)$, interpreted as the distance to the regions with further neighbors [14].

Other popular second-order summary statistics used to capture inter-points correlation are Ripley's K and L -functions defined for a stationary PP of density λ and $r \geq 0$ as

$$K(r) = \frac{\mathbb{E}_o^{\dagger}(\Psi(b(o, r)))}{\lambda} \quad \text{and} \quad L(r) = \sqrt{\frac{K(r)}{\pi}}. \quad (52)$$

We note that $K(r) = \pi r^2$ and $L(r) = r$ in the case of a PPP. Repulsive and clustered PPs are however, respectively, characterized by smaller and larger K and L -functions as compared to

the PPP. More discussions about PPs statistics and nodes real deployment characterization can be found in [14, 40, 64, 65, 67, 87, 88, 92, 93, 109].

Characterizing PPs based on their summary statistics is generally not sufficient to study the impact of inter-point interaction on macroscopic properties [14, 64, 65]. Interestingly, the authors of [142, 143] developed PP ordering based on the directionally convex (dcx) order, where for two given real-valued PPs Ψ and Φ of the same dimension, Ψ is said to be less than Φ in dcx, if and only if for all directionally convex³ function f on \mathbb{R}^d , $\mathbb{E}\{f(\Psi)\} \leq \mathbb{E}\{f(\Phi)\} < \infty$ and we denote $\Psi(\cdot) \leq_{\text{dcx}} \Phi(\cdot)$. Typically, it has been shown in [142, Proposition 3.4 and Corollary 3.1] that the dcx order cover PPs comparison based on the pair-correlation and K -functions, where the largest PP in terms of dcx order is generally the one with the greatest pair-correlation and K -function, assuming the same mean number of points in the observation window. That is, the PPP is also taken as the reference PP on dcx-based comparison, where repulsive and clustered PPs are, respectively, smaller and larger in dcx order as compared to the PPP. They are then referred to as *sub and super-Poisson*, respectively.

In general, sub- and super-poissonianity can occur simultaneously but at different spatial scales, e.g., clustering at large scales and regularity at small scales. As an illustration, using the *spatstat* package in the **R** language, Fig. 10 shows the estimation of summary statistics $J(r)$, $g(r)$, and $K(r)$ of an homogeneous PPP generated in the window $W = [0, 10] \times [0, 10]$. We can see in particular the fluctuation of summary statistics with the range of observation.

1.2.2 Modeling Real Nodes Deployment

In the following, we will review the statistical methods used to fit several PP candidates to empirical data of realistic networks. Next, we will investigate the various metrics explored in the literature to select the best fitted PP model, i.e., the goodness-of-fit.

Fitting the structure of nodes

In classical statistics, *the likelihood function* describes the probability of observing data samples given some model parameter θ [14, 66]. Similarly, in the context of SG, the parameters of the PP model are approximated from existing point pattern $\mathbf{x} = \{x_1, \dots, x_n\}$, where the likelihood function is maximized, yielding to parameter estimation that best fits the data samples, e.g., the ratio between the number of point patterns and the window area is a natural estimator for the parameter density of an HPPP, the hardcore distance in inhibitive PPs is simply estimated

3. For any x, y, z and $u \in \mathbb{R}^d$, such as $x \leq y$, $z \leq u$ and $y + z = x + u$, we have $f(y) + f(z) \leq f(x) + f(u)$.

by the minimum inter-point distance in the empirical data, etc.. The general formulation for the likelihood function of three classes of representative PPs, namely the HPPP, the IPPP, and finite Gibbs PP, can be found in [66]. However, due to the lack of closed-form expressions for the normalizing function rendering the likelihood function a PDF, the maximization problem for the likelihood function when considering several PPs beyond the PPP, is generally intractable [14, 66]. To overcome such limitation, *the pseudolikelihood function* of a given PP is defined in terms of the conditional intensity at a given point of the sample pattern [66, Equations (6), (7)]. Also, when the conditional intensity is not available or parameter estimators are of reduced accuracy, which is typically the case for aggregative PPs, *the minimum contrast method* is proposed. That is, the key idea is to define PP parameters that minimize the gap between the summary statistic of this PP and the estimated one from empirical data. This gap, as a function of the PP model parameters θ , is typically expressed as

$$\Delta(\theta) = \int_{s_1}^{s_2} |\widehat{S}^m(r) - S_\theta^m(r)|^n dr, \quad (53)$$

where $\widehat{S}(r)$ is the estimated summary statistic from empirical data over a range radius $s_1 \leq r \leq s_2$ and $m, n > 0$ are parameters in the method.

Metrics for the goodness-of-fit

After the fitting procedure of several PP candidate models to the empirical data, comes the goodness-of-fit phase where the best fitted PP to empirical data is selected. In the following, we outline the key techniques used in the literature for the goodness-of-fit procedure:

- *Summary statistics simulated envelope test (3SET)*: The most common approach for hypothesis testing is by evaluating the gap between summary statistics curves of the empirical data and the fitted PP model. In fact, by simulating the summary statistics of the fitted PP model, we end up getting the lower and upper envelopes that reflect the confidence interval. Next, the fitted PP model is considered as a good model if the curve of the estimated summary statistic of the empirical data, falls into the envelope with increased probability. Otherwise, the PP model may be rejected based on the 3SET method. Typically, the K and L -functions are the most popular summary statistics considered for the 3SET method [64, 65, 106, 109]. However, other summary statistics such as G , F , and J -functions are investigated in [106, 109, 144]. Besides, if the curve of the estimated summary statistic of the empirical data lies within the envelope of several fitted PP models, a specific quantity may be considered to select the most suitable PP model,

namely the root mean square deviation (RMSD), defined from (53) as

$$\text{RMSD} = \sqrt{\frac{1}{N} \sum_{k=1}^N (\widehat{S}(r_i) - S_{\theta}(r_i))^2}, \quad (54)$$

where N is the number of samples.

- *SINR distribution*: Since the SINR distribution is tightly related to the network geometry (i.e., inter-points interaction), it is used as an evaluation metric to select the most suitable PP model for empirical data. Given the typical user y located at the origin of the point pattern Ψ and connected to the nearest point $x_0 \in \Psi$, the downlink SINR is generally evaluated as

$$\text{SINR}(x_0; y) = \frac{P_{\text{tx}} h_{x_0} \ell(\|x_0\|)}{\sigma^2 + \sum_{x_i \in \Phi \setminus \{x_0\}} P_{\text{tx}} h_{x_i} \ell(\|x_i\|)}, \quad (55)$$

where P_{tx} is the BS transmit power, $\ell(\cdot)$ is the path loss function, h_x is a random variable that captures multipath fading and/or shadowing between user y and BS x , and σ^2 is the variance of noise power.

Based mainly on simulations, the SINR distribution of the empirical data and the fitted PP models are evaluated w.r.t. a threshold in dB, then the suitable model is selected using envelope matching and eventually the RMSD method [64, 65, 113, 145].

- *Geometry-based evaluation metrics (GBEM)*: Two main geometry characteristics are considered in the literature as higher-order properties in PP model selection, namely the Voronoi area distribution (VAD) [2, 64, 118, 146] and the Delaunay triangulation edges length distribution (DTELD) [98, 114–116]. The use of VAD and its dual DTELD is actually justified given the observation that coverage regions of BSs in a cellular network generally converge to Voronoi cells [4, Proposition 5.5.11], where the VAD is commonly approximated in the case of a PPP by a generalized gamma function [118].

1.3 Chapter Summary

With a comprehensive exploration of all the above-mentioned references related to proposals for modeling wireless networks with PPs beyond the PPP, it is almost straightforward to infer that such PPs are more accurate than the PPP for modeling emerging wireless architectures. However, they are mathematically less tractable to derive the contact distance function, the nearest neighbor function, and hence we can only approximate the interference and performance behavior. Also, modeling node locations with the previous PPs does not provide a significant

change to system design insights as compared to the PPP case [6, 24, 42, 67]. Accordingly, in some analytical contexts, it is generally more appropriate to favor mathematical tractability with physically meaningful insights on system design, rather than increasing modeling accuracy but with a huge loss on tractability and mathematical flexibility. In other words, the tractability of the PPP sometimes justifies its possible inaccuracy. Subsequently, we consider four recent results that endorse even the accuracy of the PPP relatively to other beyond-PPPs:

- In [51, Theorem 3], the authors support analytically the assumption that modeling node locations through PPP is a realistic hypothesis since a given general model for a large structure of node locations can be seen under the effect of sufficiently strong lognormal shadowing, i.e., greater than approximately 10 dB, as equivalent to the PPP model. In other words, instead of modeling node locations with a given general PP under lognormal shadowing, we can equivalently consider a perturbation of node locations, which may lead to a totally random structure depending on the intensity of shadowing.
- In [139–141], the authors showed that the slope of the SIR distribution is the same for almost all motion-invariant PPs, i.e., the SIR distribution of a given network model is a shifted version of the other network models. For example, the horizontal gap between the PPP and the triangular lattice is approximately a constant of 3.4 dB for a wide range of SIR regimes. Interestingly, instead of modeling point patterns of a given network by a less-tractable but more accurate PP, one can use the PPP, i.e., the reference network model, endowed with its enhanced tractability and add some weight to the outcome network performance being evaluated under the PPP assumption.
- In [136, 137], the authors explored the PPP under a tractable generative model, namely the conditional thinning approach, which allows capturing smoothly a wide range of clustered point patterns ordered from a totally random structure to a very clustered one. Consequently, the PPP can be harnessed in a meaningful way to create new PPs that are endowed with similar tractability as the PPP but can also capture inter-points interactions.
- In [67], and since the IPPP is the most tractable alternative to the PPP, the authors introduced the IDT approach that can be used as the most tractable version of the PPP, and fully able to capture a wide range of network models from clustered PPs to stationary deterministic lattices.

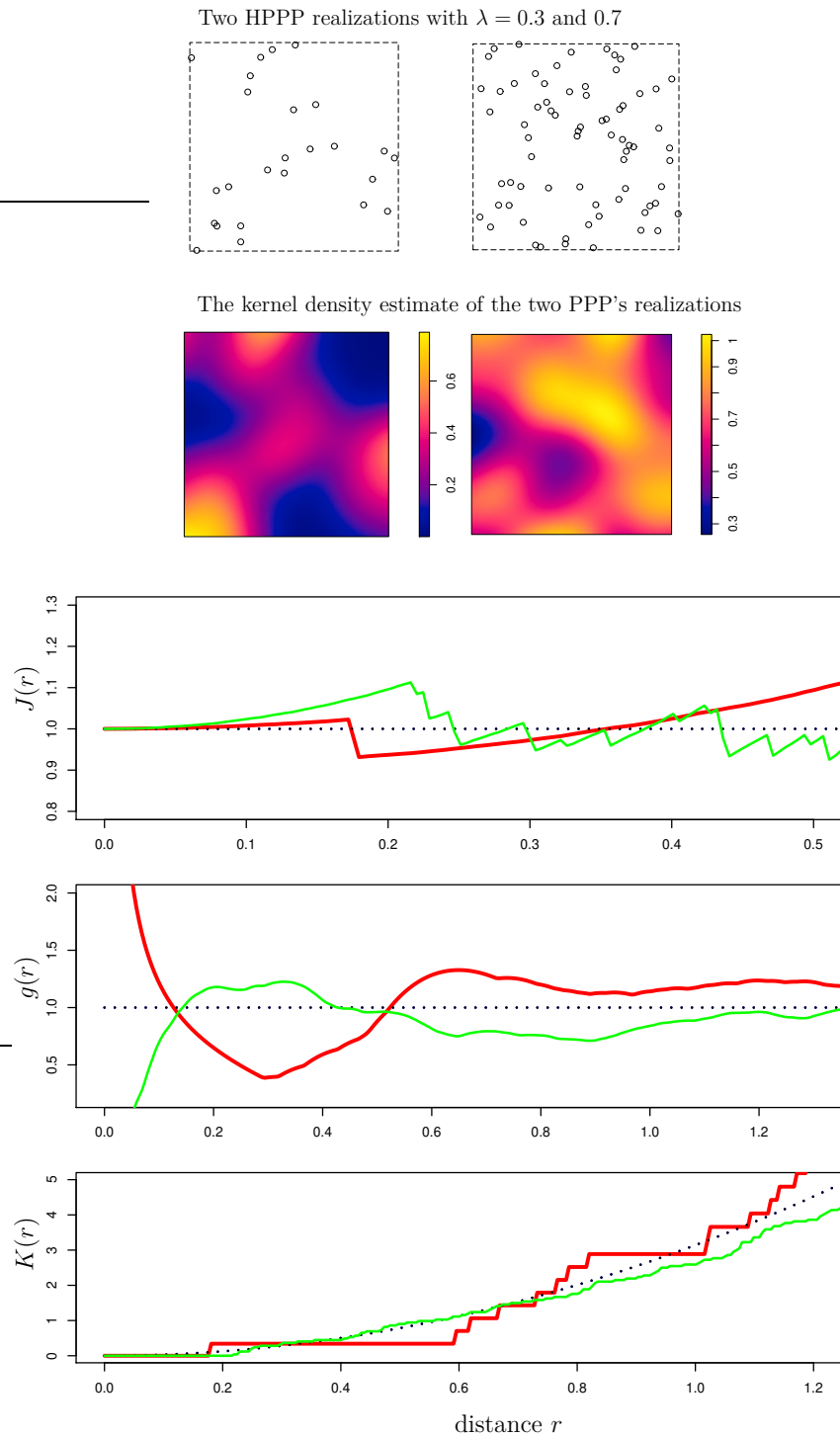


Figure 10 – Estimation of summary statistics $J(r)$, $g(r)$, and $K(r)$ of two HPPP realizations with increasing density. The red bold line is for $\lambda = 0.3$, the green thin line is for $\lambda = 0.7$, and the dotted lines are the theoretical values of the summary statistics assuming an infinite expansion of the window W .

STOCHASTIC GEOMETRY BASED MODELING AND ANALYSIS OF WIRELESS NETWORKS

Modeling wireless networks is commonly considered as a set of conceptual choices to study a real or an imaginary communication scenario. Such model preferences are typically related to i) network elements, e.g., location model (deterministic, random, or mobile), node type (transmitter, receiver, or both), ii) their attributes, e.g, transmit power and antenna types, iii) the environment characteristics in which they operate, e.g, propagation effects, and iv) the interplay properties between nodes, e.g., association policy, coordination, and spatial interaction. In some cases, we can also include analytical and experimental tools used in the study, in addition to the considered key performance metrics. In the following, we will review the plethora of modeling choices made in the literature of SG-based modeling and analysis.

2.1 Modeling and Conceptual Choices

2.1.1 Network Elements

Based on the SG approach, elements of a wireless network are deemed to be hierarchically modeled in such a way that subscribers are 0-level stations, BSs are 1-level stations directly connected to 0-level stations, switching centers are 2-level stations directly connected to BSs, and so on [2, 138]. Besides, depending on the system model being considered, network elements can be partially or entirely distributed according to particular PPs and receiver/transmitter locations can be correlated¹ or not, e.g., coupling of users and BSs location in a user-centric

1. This term should not be confused with temporal and spatial correlation in BS activity factors where the former is induced by the mobility of receivers across neighboring transmitters, while the latter is induced by correlation through interference and load traffic between neighboring transmitters [147].

Table 1 – Typical configuration of BSs and users in a stochastic geometry based modeling

Configuration of BSs	Configuration of UEs	UE-BS coupling?	Adopted PP		Comments
			For BSs	For UEs	
Uniformly random	Uniformly random	No	PPP	PPP	Total independence between UEs and BSs [17–19].
Uniformly random	Uniformly random	Yes	PPP	PPP	UE-BS coupling can be captured through i) a specific dependent thinning as in [136] [137], or via ii) a power control scheme in uplink networks as in [20, 148–153].
Uniformly random	Uniformly random	Yes	BPP	BPP	Correlation between UEs and BSs is introduced via the finite number of BSs and UEs in a given area [59–62].
Uniformly random	Clustered	Yes	PPP	MCP, TCP	UEs are clustered around transmitters, seen as the parent points [122–124].
Uniformly random	Clustered	No	PPP	MCP, TCP	The analysis is focused on the clustering aspect of UEs [154–156].
Clustered	Uniformly random	No	MCP, TCP, Gauss-Poisson PP.	PPP	The analysis is focused on the clustering aspect of BSs [120, 121, 134, 135].
Clustered	Clustered	Yes	TCP	TCP	UEs and BSs are clustered around the same hotspots [125].
Uniformly random	Repulsive	Yes	PPP	PHP	A typical application is when some UEs are allowed to transmit only if they are outside exclusion regions around specific UEs or BSs [101, 103].
Repulsive	Uniformly random	No	Regular lattice, Soft and hardcore PPs.	PPP	Typical configuration in rural areas where repulsion is required between BSs without necessarily coupling with UE locations [88, 95, 109, 119, 157].

capacity-driven cell deployment. Table 1 summarizes the state-of-the-art main configurations used for modeling the location of users and BSs.

2.1.2 Propagation Effects

In a wireless network composed of many spatially dispersed nodes, communication is typically impaired by various deficiencies like wireless propagation effects introduced by i) the attenuation of radiated signals with blockages (shadowing), ii) receiving multiple copies of the same transmitted signal (multipath fading), and iii) signal losses with distance (path loss). In general, the received power at the typical receiver located at a distance r from the transmitter, is expressed as

$$P_{\text{rx}} = P_{\text{tx}} \ell(r) \prod_k Z_k, \quad (56)$$

where P_{tx} is the reference transmitted power, $\ell(\cdot)$ is the path loss function, and $\{Z_k\}$ are independent random variables accounting for propagation effects.

It is worth mentioning that the effect of shadowing is generally captured via log-normal distributed random variables where key parameters are fitted from field measurements. However, in view of the analytical intractability of such distribution PDF, a common approach in SG-

based frameworks is to absorb shadowing model into the intensity function of a new PPP by means of the displacement theorem. Representative examples can be found in [24, 51, 54, 56, 83, 85, 86, 158, 159]. Also, modeling shadowing via random variables fails to reflect the distance-dependence of blockage effects given that shadowing intensity needs to naturally grow with increased transmit-receive distance, particularly in higher-frequency bands where signals are more vulnerable to blockages. That is, the authors of [160] proposed to capture blockages effect via the product $\prod_{i=1}^M \gamma_i$, where $0 \leq \gamma_i \leq 1$ is the ratio of power loss due to the i th blockage, and M is the random number of blockages intersecting the transmit-receive link. Using tools from random shape theory [160], M is shown to follow a Poisson distribution with parameter dependent on the blockages density, the link distance, and the average dimensions of blockages.

Regarding path loss functions, Table 2 summarizes the key models used in the literature of SG-based modeling and analysis. Typically, the great majority of works consider the simplistic single slope unbounded path loss model (UPM) (model #1 in Table 2) given its ability to derive reliable and tractable results especially for sparse networks wherein the average separation distance between nodes is greater enough to ignore the effect of singularity at the model (when $r = 0$). However, this effect cannot be ignored in environments with higher path loss exponent [161] or networks with very high infrastructure density [33, 162, 163], where the single slope UPM is deemed as inaccurate. In fact, the SINR-invariance property obtained under the single slope UPM [17], such that the overall SINR is independent from infrastructure density in the interference-limited regime, has reopened the discussion on the reliability of UPM since it is not conceivable that splitting cells indefinitely through the addition of new BSs, will maintain the same SINR distribution. A key aspect to overcome this limitation is to revisit the single slope UPM. The authors of [33, 162] introduced the multi-slope UPM (model #2.1 in Table 2) enabling to ascertain that the SINR-invariance property is no longer valid when the near-field path loss exponent is surprisingly under the dimension of the network, which turns out to *near-universal outage* as network density increases. A similar effect is assessed when considering the bounded path loss model (BPM) in [164], the single slope UPM accounting for BSs antenna elevation in [71], and the stretched exponential path loss model in [165].

Furthermore, based on extensive field measurements, it has been reported in [166] and the references therein that mmWave signals are very sensitive to blockages as compared to sub-6 GHz. Hence, considering LOS and NLOS paths in such environment is of great importance. That is, the authors of [69, 158] considered a revisited path loss model that incorporates LOS and NLOS transmissions, as

Table 2 – Key path loss models used in stochastic geometry abstraction

#	Path loss function	Parameters	Comments	References
1	$\ell(r) = Kr^{-\alpha}$	$K = \ell(1) = \left(\frac{\lambda}{4\pi}\right)^2$, where λ is the wavelength, α needs to be greater than 2 to bound the interference.	Popular model in the literature given its tractability. However, it is inaccurate in some situations due to its singularity.	[17–19]
2	For $n \in \mathbb{N}$, $\ell(r) = \begin{cases} \ell_0(r), & R_0 \leq r < R_1 \\ \ell_1(r), & R_1 \leq r < R_2 \\ \dots \\ \ell_{n-1}(r), & R_{n-1} \leq r < R_n \end{cases}$	$\forall 0 \leq i \leq n-1$, $\ell_i(r) = K_i r^{-\alpha_i}$, $\alpha_i \leq \alpha_{i+1}$, $\alpha_{n-1} > 2$, $K_0 = 1$, and $K_i = \prod_{k=1}^i R_k^{\alpha_k - \alpha_{k-1}}$	Generalization of model #1 when $\alpha_i = \alpha_{i+1}$ $\forall 0 \leq i \leq n-1$ and of model #3.3 when $\alpha_0 = 0$.	[33, 162]
		$\ell_i(r) = K_i (1 + r^{\alpha_i})^{-1}$, $\alpha_i \leq \alpha_{i+1}$, $\alpha_{n-1} > 2$, $K_0 = 1$, and $K_i = \prod_{k=1}^i \left(\frac{1 + R_k^{\alpha_k}}{1 + R_k^{\alpha_{k-1}}} \right)$	Generalization of model #3.2 when $\alpha_i = \alpha_{i+1}$ $\forall 0 \leq i \leq n-1$.	[170]
3	$\ell(r) = K(1+r)^{-\alpha}$; $\ell(r) = K(1+r^\alpha)^{-1}$; $\ell(r) = K \min(1, r^{-\alpha})$	$K = \ell(0) > 0$, $\alpha > 2$	Non-singular path loss models adopted especially for dense urban scenarios.	[42, 164]
4	$\ell(r) = K(r^2 + h^2)^{-\alpha/2}$	$K = \ell(1) > 0$, $\alpha > 2$, $h > 0$	Near-universal outage in high network density.	[71]
5	$\ell(r) = Ke^{-\alpha r^\beta}$	$K = \ell(0) > 0$, $\alpha, \beta > 0$	Accurate model for short to moderate distances, i.e., 5m-300m, in UDNs.	[165]
6	$\ell(r) = p_{\text{los}} \ell_{\text{los}}(r) + p_{\text{nlos}} \ell_{\text{nlos}}(r)$	$\ell_{\text{los}}(r) = K_{\text{los}} r^{-\alpha_{\text{los}}}$, and $\ell_{\text{nlos}}(r) = K_{\text{nlos}} r^{-\alpha_{\text{nlos}}}$ where K_{los} and K_{nlos} are, resp., intercepts of the LOS and NLOS paths, while α_{los} and α_{nlos} are, resp., LOS and NLOS path loss exponents.	mmWave communications: $p_{\text{los}}(r) = \mathbb{1}_{r \leq R_c}(r)$, where R_c is a fixed radius and $p_{\text{nlos}}(r) = 1 - p_{\text{los}}(r)$.	[69, 158]
			mmWave communications: $p_{\text{nlos}}(r) = 1 - p_{\text{los}}(r) - p_{\text{out}}(r)$, $p_{\text{out}}(r) = \max(0, 1 - A_{\text{out}} e^{-a_{\text{out}} r})$ $p_{\text{los}}(r) = (1 - p_{\text{out}}(r)) e^{-a_{\text{los}} r}$ where A_{out} , a_{out} , and a_{los} are fitting parameters.	[83, 159]
			Lower frequency bands (sub-6 GHz): $p_{\text{los}}(r) = e^{-ar^2}$, where a is a parameter to fit 3GPP models and $p_{\text{nlos}}(r) = 1 - p_{\text{los}}(r)$.	[171]
			Lower frequency bands (sub-6 GHz): 3GPP case1: $p_{\text{los}}(r) = \begin{cases} 1 - \frac{r}{R_1} & , r \leq R_1 \\ 0 & , r > R_1 \end{cases}$ 3GPP case2: $p_{\text{los}}(r) = 0.5 - \min \left\{ 0.5, 5 \exp \left(-\frac{R_1}{r} \right) \right\} + \min \left\{ 0.5, 5 \exp \left(-\frac{r}{R_2} \right) \right\}$.	[70]
			UAV-aided communication networks: $p_{\text{los}}(\theta) = 1 / [1 + a \exp(-b[\theta - a])]$, where a and b are fitting parameters and θ is the elevation angle.	[167, 168]
			$\ell_{\text{los}}(r) = K_{\text{los}}(r^2 + h^2)^{-\frac{\alpha_{\text{los}}}{2}}$, and $\ell_{\text{nlos}}(r) = K_{\text{nlos}}(r^2 + h^2)^{-\frac{\alpha_{\text{nlos}}}{2}}$	Lower frequency bands (sub-6 GHz): the same probability models as [70].
$\ell_{\text{los}}(r) = K_{\text{los}}(1 + r^{\alpha_{\text{los}}})^{-1}$, and $\ell_{\text{nlos}}(r) = K_{\text{nlos}}(1 + r^{\alpha_{\text{nlos}}})^{-1}$	Lower frequency bands (sub-6 GHz): $p_{\text{los}}(r) = \min \left(\frac{18}{r}, 1 \right) \left(1 - e^{-\frac{r}{36}} \right) + e^{-\frac{r}{36}}$.	[173]		

$$\ell(r) \approx \begin{cases} \ell_{\text{los}}(r) & \text{with probability } p_{\text{los}} \\ \ell_{\text{nlos}}(r) & \text{with probability } p_{\text{nlos}} = 1 - p_{\text{los}}. \end{cases} \quad (57)$$

In [83,159], the authors included an outage state in addition to LOS and NLOS states to accurately capture the sensitivity of mmWave communications to blockages. Generally, the model in (57) is a building block for other sophisticated models depending on the approximation of the LOS probability p_{los} and the preferences for ℓ_{los} and ℓ_{nlos} . For instance, the authors of [70] introduced a composite model of (57) and the multi-slope UPM wherein the LOS probability is mapped with representative models adopted by the 3rd generation partnership project (3GPP). The LOS probability in [167,168] is approximated with a modified sigmoid function to characterize the air-to-ground (AtG) channel in UAV aided communication networks. A comprehensive survey of channel modeling for UAV communications can be found in [169].

2.1.3 Cell Association Strategies

In microwave (μ Wave) multi-tier wireless networks, various layers of BSs are deployed, where BSs of the i th tier Ψ_i ($i = 1, \dots, K$) transmit data with a given transmit power p_i . In such a context, shadowing is a slowly varying effect and the typical UE located at y commonly selects the serving BS x_0 based on *the strongest average received power strategy (without fading)* [24,58], as

$$x_0 = \arg \max_{x \in \Psi_i, \forall i=1, \dots, K} p_i \ell(\|x - y\|), \quad (58)$$

where $\ell(\cdot)$ is the path loss function (see Table 2).

Expression (58) induces then an exclusion region of radius δ_0 around y wherein no interfering BS to x_0 exists. That is, δ_0 is expressed as

$$\delta_0 = \min_{x_0 \in \Psi_i, \forall j=1, \dots, K} \left\{ \ell^{-1} \left(\frac{p_i}{p_j} \ell(\|x_0 - y\|) \right) \right\}. \quad (59)$$

However, the association criterion in (58) may sometimes lead to heavily loaded BSs especially those transmitting with the highest power, i.e., macro BSs, which reduces the average achievable rate and the efficiency of deploying small cells. An alternative way is then to associate users with BSs providing the highest data rate [39,174], which can be captured via a measure of BSs load. Accordingly, the authors of [19] endowed BSs of each tier i by some adjustable bias B_i , where the typical UE y selects the serving BS as that providing the maximum average

power weighted by its bias, namely *the biased cell association*. (58) becomes

$$x_0 = \arg \max_{x \in \Psi_i, \forall i=1, \dots, K} p_i B_i \ell(\|x - y\|). \quad (60)$$

Bias B_i can then improve the capacity of HetNets by offloading users from overloaded cells to lighter ones, namely, load balancing, which is similar to cell breathing through cell range expansion (CRE) [175, 176].

In the single-tier case where BSs send data with the same transmit power, using the association strategy in (58) turns into associating users with their spatially closest BS, which is equivalently named *the nearest-neighbor cell association* [17, 58, 71, 136], or extended to *the n th nearest serving BS policy* as [41, 55–59, 61]. Furthermore, considering system models incorporating various propagation groups, with various path loss exponents (model #6 in Table 2), the association policy in (58) is equivalently referred to as *the smallest path loss cell association* [69, 70, 159].

Last but not least, in environments where shadowing is expected to be less slowly-varying, e.g., sensitive transmissions to blockages, interferers may be closer to the typical UE than the serving BS and then no exclusion region in (59) is considered. That is, we need to consider the shadowing effect Z_x , which renders that the typical UE connects to the strongest BS instantaneously, namely *the maximum instantaneous power-based cell selection*, or equivalently *the max-SINR association policy* [18, 24, 54, 137], such that

$$x_0 = \arg \max_{x \in \Psi_i, \forall i=1, \dots, K} p_i Z_x \ell(\|x - y\|). \quad (61)$$

It is worth mentioning that SG-based modeling and analysis of wireless networks under the previous association policy has taken two directions: i) the first by resorting to the Campbell theorem (17) as in [18, 24, 54, 85, 86, 137], ii) the second by absorbing the shadowing effect into the intensity of a new PPP as in [51, 54, 83, 85, 158, 159], and hence (61) will be consistent with (58).

2.1.4 Transmitter-Receiver Direction of Analysis

In downlink wireless networks, the analysis is generally focused on the received SINR at the level of the typical UE served by one or more BSs [17–19, 54]. However, with the growing interest in symmetric traffic applications, e.g., cloud-storage, the uplink performance analysis is becoming increasingly crucial [20, 148–153]. Typically, analytical evaluation of uplink wireless

networks is generally involved as compared to the downlink, due to the following fundamental changes in the system model: i) The use of location-dependent power control, where each user smoothly adjusts its transmit power to partially/totally invert the effect of path loss [20, 148] and/or lognormal shadowing [149], which mitigates the uplink interference and reduces the user battery consumption, ii) the dependency in the location of concurrent uplink users, which renders the approximation of the users PP more challenging [20, 153].

Interestingly, the authors of [150–152], considered the paradigm of decoupled uplink-downlink access (DUDA), where different association policies are considered for uplink and downlink inducing that the typical UE will not necessarily be prompted to access the same BS for both directions. The DUDA capability is particularly relevant in the scenario of emerging Het-Nets [18, 19, 24, 39, 54], wherein users quality of experience (QoE) is affected by non-uniformity in transmit powers and traffic loads in both downlink and uplink. In such a context, DUDA enables to reduce the transmit power of edge users, which obviously helps to reduce the average uplink interference by about 2 – 3 dB (see [152] and references therein).

Last but not least, the arts in [48, 177] considered the IBFD capability enabling to transmit and receive data simultaneously over the same frequency band, which offers the opportunity to double the spectral efficiency at the expense of extra self interference. More discussions about the use of SG for modeling and analysis of IBFD approach as a potential enabler for 5G/B5G networks will be presented in Chapter 3.

2.1.5 Nodes Mobility

The mobility of transmitters and receivers is a crucial component in the design and performance evaluation of modern wireless networks since it can impinge on traffic load per cell, signaling protocols, handoff algorithms, and location update mechanisms. However, modeling human mobility is generally challenging given its very complex temporal and spatial correlation [178]. A comprehensive survey of user mobility models can be found in [179].

SG as a powerful mathematical tool has been explored in mobility-aware performance analysis of wireless networks. Based on the formalization of the handoff rate, there are typically two directions of analysis adopted in the literature: i) *the trajectory-based handoff*, in which the handoff event occurs as well as the mobile UE crosses a cell border, and then the handoff rate is defined as the average number of crossing cell boundaries of different cells by a moving UE. Hence, the accuracy of such a concept is biased by the efficiency of quantifying the statistical distribution of cells boundary, which is generally consistent with the Buffon’s needle problem. The work in [3] is the first to consider this approach in an SG-based framework, where BSs are

modeled as a 2D PPP, the road system as a PLP, and the location of users as a 1D PPP on the road layout (see Fig. 7). In [180], the authors considered a tractable model for user's mobility, namely *the random waypoint (RWP)*, where a detailed description can be found in [179]. Next, the authors derived the distribution of UE location during one movement period, the handover rate, and the average time of being served by a given BS, also known as the sojourn time. Other representative works using the same approach in the context of HetNets can be found in [181–184]. ii) The second direction is based on *the association-based handoff* where the handoff event occurs as long as another BS verifies the association criterion better than the current serving BS. That is, the handoff rate is defined as the probability of inducing a handoff for a user served by a given BS and moving a random distance in a unit time [185, 186]. A comprehensive tutorial of mobility-aware performance analysis is given considering spatially random and deterministic grid-based topologies in [187].

2.1.6 Spatio-temporal Traffic Modeling

Emerging new data-intensive applications, such as multi-party video conferencing or multiplayer online games, along with latency-critical applications such as smart manufacturing, remote control, or autonomous driving, suggest that the integration of spatio-temporal traffic dynamics in the analysis of 5G/B5G wireless networks will play an increasingly crucial role in their design and deployment. Previous efforts have typically considered one aspect of traffic: i) abstraction based on queuing theory, which primarily evaluates scheduling algorithms and ignores the interaction of traffic with SINR statistics and hence with network geometry; ii) SG-based analysis, which usually does not consider the temporal arrival process of packets and focuses on reliability or throughput in fully buffered networks, i.e. each link always has a packet to send. Interestingly, traffic has recently been abstracted by spatio-temporal modeling that combines tools from SG and queuing theories. In particular, the spatial domain of traffic is captured by modeling nodes via an appropriate PP, while the temporal variation of traffic is captured by the temporal arrival of packets grasped tractably by independent Bernoulli processes [189, 212].

A review of the literature shows that spatio-temporal traffic modeling has been particularly exploited to evaluate two important metrics of interest. First, *delay* that refers to the end-to-end duration from packet initiation at the transmitter to successful decoding at the receiver [191]. This includes the delay in generating a packet, the delay in queuing it, and then the time it takes for the packet to be successfully transmitted within the wireless access network and backhaul links (including the delay incurred in the retransmission mechanism). Delay analysis through

spatio-temporal modeling is generally challenging due to the following major issues: i) The delay is dependent on the system throughput determined by the SINR, which in turn relies on the network geometry and the complex channel fluctuations in large-scale networks. ii) The delay is a long-term measure in which the topology of nodes remains static but random for a fairly long time, which induces a coupling of interference across various time slots. iii) As part of the MAC, a scheduling policy is performed on many queuing nodes in a distributed manner. So, if a queue is idle, the related transmitter does not interfere with the other links; as a result, the service throughput of those links increases allowing their queues to drain faster. Such coupling between each queue and the state of all the other queues renders delay analysis less tractable. To make the analysis feasible, most of the literature focuses on the queuing delay based on the scheduling scheme, and the transmission delay related to the number of transmission trials required until a packet is successfully decoded, while the delay in backhaul links is generally omitted (A comprehensive example of backhaul link delay analysis can be found in [192]). Next, the mean delay is evaluated conditioning on a given realization of the PP, which resorts to a formulation based on the meta-distribution metric that can be derived by applying the Gil-Pelaez theorem or the k -moment inversion. More discussions about the meta-distribution and the Gil-Pelaez technique are brought in the sequel.

Second, the emerging metric of *age of information (AoI)* that measures freshness (timely updating) of the sensed data measurements of the IoT devices at the destination nodes. It is typically defined as the time expired since the previous successfully received update packet at the destination was generated at the source [193]. The requirement for timely updating actually reflects a small average age of status update, i.e., minimizing time-average AoI, which can help in the efficient design of freshness-aware IoT systems. It is worth mentioning that minimizing AoI does not really correspond to maximizing the system throughput, nor guaranteeing a minimum delay in receiving IoT measurements. Intuitively, throughput can be maximized by making sensors send updates as quickly as possible, which can result in higher AoI because the status messages will be pending in the communication system (overloading). In this way, reducing AoI may improve the transmission delay. It is worth mentioning that optimal loading usually requires a perfect balance between overloading the queue and keeping it idle.

Since characterizing the distribution of AoI based on spatio-temporal traffic modeling is known to be notoriously difficult, efforts are mainly devoted to studying some of its easy-constructed variants. For instance, i) work with a lower bound on the average AoI obtained by ignoring the processing time at the source, which mean that a new update packet is instantaneously generated by the source node [194], ii) consider the peak AoI that quantifies the

maximum value of the AoI immediately before an update packet is delivered to the destination node, thus yielding insights into the pessimistic values of the AoI [195, 196].

2.2 Stochastic Geometry Based Analytical Techniques

As discussed before, using non-PPPs helps to accurately capture the system behavior but reduces tractability and mathematical flexibility, which requires resorting to efficient numerical integration (e.g., Quasi Monte-Carlo integration method [106]), or even intractable approximations with limited impact on design insights [106, Equation (25)], [109, Equation (42)], [119, Equation (22)]. Subsequently, we will focus on key approaches considered under the PPP seen as the reference PP. We will also consider its finite version, the BPP. To the best of authors knowledge, eleven techniques are reported in the literature, offering varying degrees of tractability, accuracy, and mathematical flexibility.

To illustrate the key generative sequence steps of each technique, we consider the general common definition of the received SINR at the level of the typical user located in $y \in \mathbb{R}^d$ from a serving BS x_0 , as

$$\text{SINR}(x_0; y) = \frac{h/L(R_0)}{I + W}, \quad (62)$$

where $\ell(\cdot) = 1/L(\cdot)$ is the path loss function (see Table 2). I is the power of the other-cell interference normalized by the BS transmit power P_{tx} , and can be expressed as

$$I = \sum_{k \in \Psi \setminus \{x_0\}} g_k/L(R_k), \quad (63)$$

where (x_k) are BSs location modeled by a HPPP Ψ of density λ , x_0 is the serving BS under a given association strategy, $R_k = \|x_k - y\|$ is the Euclidean distance between the BS x_k and the typical user y , h and $\{g_k\}_k$ are, respectively, fading coefficients of the serving BS and interferers, and W is the noise power normalized by P_{tx} .

2.2.1 The Baseline Two-Step Approach

This is the most popular technique used in the literature to derive coverage probability in (22). In fact, assuming Rayleigh² fading for the desired link, the approach consists on first com-

2. The Rayleigh assumption is generally supported by i) its better tractability and mathematical flexibility incorporated into analysis [17–19, 54], and ii) its ability to give a pessimistic version of the SINR distribution as compared to more realistic fading models, e.g., Nakagami fading [143].

putting the coverage probability by conditioning on R_0 and next averaging w.r.t it. Accordingly, for $h \sim \exp(1)$, the coverage probability in (22) is simplified as

$$P_c(\mathbb{T}) = \mathbb{P} \{h \geq \mathbb{T} \mathbb{L}(R_0)(I + W)\} \quad (64)$$

$$= \mathbb{E}_{R_0} \left\{ \mathbb{P} \left(h \geq \mathbb{T} \mathbb{L}(R_0)(I + W) \middle| R_0 \right) \right\} \quad (65)$$

$$\stackrel{(a)}{=} \mathbb{E}_{R_0} \left\{ \mathcal{L}_W(\mathbb{T} \mathbb{L}(R_0)) \mathcal{L}_I(\mathbb{T} \mathbb{L}(R_0)) \right\}, \quad (66)$$

where (a) follows from the Laplace transform definition and the independence between W and I .

The expectation in (66) is generally expressed under the form $\mathbb{E}_{R_0}(\varphi(R_0)) = \int_0^\infty \varphi(x) f_{R_0}(x) dx$, where the function $f_{R_0}(\cdot)$ reflects a unified framework of the BS association scheme [71]. Typically, when considering the nearest-neighbor cell association [17, 19, 58, 71, 136], $f_{R_0}(\cdot)$ is the PDF of the random variable R_0 , as $f_{R_0}(\xi) = 2\pi\xi e^{-\pi\lambda\xi^2}$. However, if the max-SINR association is considered [18, 24, 54, 137], $f_{R_0}(\xi) = 2\pi\lambda\xi$. Besides, the Laplace transform of the interference can be expressed via the PGFL theorem in (18) as [17, 71]

$$\mathcal{L}_I(\mathbb{T} \mathbb{L}(R_0)) = \exp \left(-\pi\lambda \mathbb{E}_g \left\{ \int_{\vartheta(R_0)}^\infty \left(1 - \exp \left(-g \frac{\mathbb{T} \mathbb{L}(R_0)}{\mathbb{L}(u)} \right) \right) u du \right\} \right), \quad (67)$$

where $\vartheta(\cdot)$ captures the exclusion region of interferers. Typically, $\vartheta(x) = x$ in the nearest-neighbor cell association, where interferers cannot be closer to the typical UE than the serving BS. In the max-SINR association, no exclusion region is considered for interferers and $\vartheta(x) = 0$.

Interestingly, (67) can be further simplified using variable changes as in [68, Equation (34)]. If interference signals are also experiencing Rayleigh fading, (67) will be simplified as

$$\mathcal{L}_I(\mathbb{T} \mathbb{L}(R_0)) = \exp \left(-\pi\lambda \int_{\vartheta(R_0^2)}^\infty \frac{dx}{1 + \frac{\mathbb{L}(\sqrt{x})}{\mathbb{T} \mathbb{L}(R_0)}} \right). \quad (68)$$

Despite the Rayleigh assumption on the intended signal and interferers, coverage probability in (66) is generally expressed under an improper integral requiring a two-fold numerical integration [17, Theorem 1]. Some efforts are made in the literature to derive closed-form expressions or approximations of the coverage probability. For instance, tractable expressions are obtained in [17] by assuming the interference-limited regime or a path loss exponent equals to 4. In [84], a more generalized closed-form expression is proposed assuming an integer value of the path loss exponent. In [207], four approximation techniques are proposed based on the network

operational regime. It has particularly shown that the optimal approximation is achieved by combining the four techniques in accordance with their convergence properties.

2.2.2 Coverage Probability New Abstraction

To develop a closed-form expression of the coverage probability in (66), it has been proposed in [204, 205] to bound the upper endpoint of the integral in (66) by introducing the concept of the paired coverage probability as in (32). That is, (32) is simplified as

$$P_c(\mathsf{T}_s, \mathsf{T}_q) = \mathbb{P} \left(\frac{h \mathbb{1} \{L(R_0) \leq 1/(W\mathsf{T}_s)\}}{IL(R_0)} \geq \mathsf{T}_q \right) = \int_0^{L^{-1}(1/(W\mathsf{T}_s))} \mathcal{L}_I(\mathsf{T}_q L(\xi)) f_{R_0}(\xi) d\xi, \quad (69)$$

which can be further simplified by considering common combinations of i) the standard path loss function of path loss exponent α , ii) additive and constant thermal noise, and iii) the nearest-neighbor cell association, as

$$P_c(\mathsf{T}_s, \mathsf{T}_q) = \frac{1 - \exp \left\{ -\pi \lambda \left(\frac{W}{\mathsf{T}_s} \right)^{\frac{2}{\alpha}} F_{-\frac{2}{\alpha}}(\mathsf{T}_q) \right\}}{F_{-\frac{2}{\alpha}}(\mathsf{T}_q)}. \quad (70)$$

In [208], this technique has been considered to benchmark the performance of UDNs under three representative scheduling schemes in terms of fairness and implementation complexity. Assuming elevated BSs, closed-form expressions are obtained allowing to assess the network performance in a more tractable and meaningful fashion as compared to the conventional definition of coverage probability in (22).

2.2.3 The Relative Distance Process Based Approach

Based on the assumptions of: i) the standard path loss model with path loss exponent α , ii) Rayleigh fading, iii) the nearest BS association policy, and iv) the interference-limited regime, a new way is considered to derive the coverage probability in (64) via the RDP $\Psi^{\mathcal{R}}$ of the PPP Ψ , defined as [198]

$$\Psi^{\mathcal{R}} = \left\{ \frac{R_0}{R_k} \mid x_k \in \Psi \setminus \{x_0\} \right\} \subset [0, 1], \quad (71)$$

where its intensity measure is derived based on (14), as in [141] : $\Lambda(dr) = 2r^{-3}dr$.

When $\Psi^{\mathcal{R}}$ is an IPPP, the PGFL can be expressed as

$$\mathcal{G}_{\Psi^{\mathcal{R}}}^{\text{IPPP}} \{f\} = \exp \left(-2 \int_0^1 \frac{1-f(r)}{r^3} dr \right). \quad (72)$$

In the general case, $\Psi^{\mathcal{R}}$ is not an IPPP, and then (64) is derived based on $\mathcal{G}_{\Psi^{\mathcal{R}}}^{\text{IPPP}}$, as [141, Lemma 1]

$$P_c(\mathsf{T}) = \mathbb{E} \left\{ \mathbb{P} \left(\text{SIR} > \mathsf{T} \mid \Psi \right) \right\} \quad (73)$$

$$= \mathbb{E} \left\{ \prod_{y \in \Psi^{\mathcal{R}}} f(y) \right\} = \frac{1}{1 - \log \left(\mathcal{G}_{\Psi^{\mathcal{R}}}^{\text{IPPP}} \{f\} \right)}, \quad (74)$$

where $f(y) = 1/(1 + \mathsf{T}y^\alpha)$ due to the assumptions i)-iv) considered in this technique.

(73) is actually a special case of the k -th moment, since

$$M_k(\mathsf{T}) = \mathbb{E} \left\{ \left[\mathbb{P}(\text{SIR} > \mathsf{T} \mid \Psi) \right]^k \right\} \stackrel{\text{(a)}}{=} \int_0^1 k u^{k-1} \overline{F}(\mathsf{T}, u) du, \quad (75)$$

where (a) comes from the meta-distribution expression in (24).

It is worth mentioning that $M_1(\mathsf{T})$ is the coverage probability defined in (22). Moreover, using similar steps from (73) to (74), the expression of the k -th moment $M_k(\mathsf{T})$ in (75) can generally be expressed under closed-form expression. However, reshaping the meta-distribution from $M_k(\mathsf{T})$, is an instance of the *Hausdorff moment problem*, which is to derive the inverse k -moment M_k^{-1} . For instance, in [198] two techniques have been considered. The first one is by inverting the $j\omega$ -moment via the Gil-Pelaez theorem [234], which resulted in less tractable expressions of the meta-distribution requiring efficient numerical integration. The second technique is based on approximating the meta-distribution with a beta distribution, where the design parameters are fitted from the first and second moments. This approach has showed an impressive accuracy, but remains relevant only for the measurements considered in study and may diverge for more general setups. In [209], the authors proposed to reconstruct the PDF of the entire meta-distribution defined over the interval $[0, 1]$, by means of shifted Jacobi polynomials via Fourier-Jacobi expansion. The obtained series expansion is infinite, where the coefficients are mapped with the moments of $\mathbb{P}(\text{SIR} > \mathsf{T} \mid \Psi)$ via the binomial expansion. The approach is promising, but needs more investigation on the convergence conditions. In [210], the authors explored binomial mixtures properties to obtain an approximation of the meta-distribution as a function of a finite double sum of the moment sequence. That is, the accuracy of the approach increases with the

length of the moment sequence, which requires however efficient numerical computation.

In [211], the meta-distribution analysis is generalized to PPs beyond the PPP, where the k -th moment of the conditional success probability for a stationary PP can be inferred from that of the PPP by using the same horizontal shift technique introduced in [139–141]. Further extensions of the meta-distribution to other system setups may be found in [212–219].

2.2.4 Finite Networks Assumption

Following a review of the existing state-of-the-art works on modeling and analysis of finite wireless networks, we can generally identify three streams of thoughts ordered in decreasing tractability and mathematical flexibility. The first, considers a typical setup where the reference receiver is located randomly in a compact $C \subset \mathbb{R}^2$, while BSs are uniformly randomly distributed in a disc [59] or a L -sided polygon [60] centered at the reference receiver. The second, extends the first model by considering an arbitrarily-located reference receiver in the disc [220, 221] or L -sided polygon of BSs [61]. The third setup considers an arbitrarily-located reference receiver in an arbitrarily-shaped area that contains finite BSs [62].

As an illustration of the generative analytical background, we consider a typical scenario, in which the reference receiver is arbitrarily located in a disk-shaped finite wireless network, wherein N transmitting BSs are uniformly randomly distributed in a disc C_ξ of radius ξ , i.e., Ψ is a BPP. The reference receiver is located at a distance $0 \leq d \leq \xi$ from the origin of C_ξ and interfering BSs are assumed to be exclusively located in an annular region \mathcal{A} of inner radius r_{in} and outer radius r_{out} from the reference receiver, such as $0 \leq r_{\text{in}} < r_{\text{out}} < \xi$. Fig. 11 illustrates the typical realizations of C_ξ and \mathcal{A} . The density of the BPP is $\lambda = N/\pi\xi^2$, while the probability of having $k \leq N$ interferers inside \mathcal{A} is $\mathbb{P}\{\Psi(\mathcal{A}) = k\} = \binom{N}{k} p^k (1-p)^{N-k}$, where $p = \frac{|\mathcal{A} \cap C_\xi|}{\pi\xi^2}$.

Given Rayleigh fading on the desired link, the coverage probability under such setup is expressed as in (66), where R_0 can be selected uniformly at random from the transmitting BSs [59, 222] (blue points in Fig. 11), or based on the n th nearest serving BS policy [59, 61]. The MGF of the interference can be expressed using similar sequence steps in [4, Page 9], as

$$\mathcal{L}_I(s) = \left(1 - p + p \int_{r_{\text{in}}}^{r_{\text{out}}} f_R(u) \mathbb{E}_g(e^{-sg/L(u)}) du \right)^N, \quad (76)$$

where $s = \text{TL}(R_0)$ and $f_R(\cdot)$ is the PDF of the distance from the reference receiver to interferers,

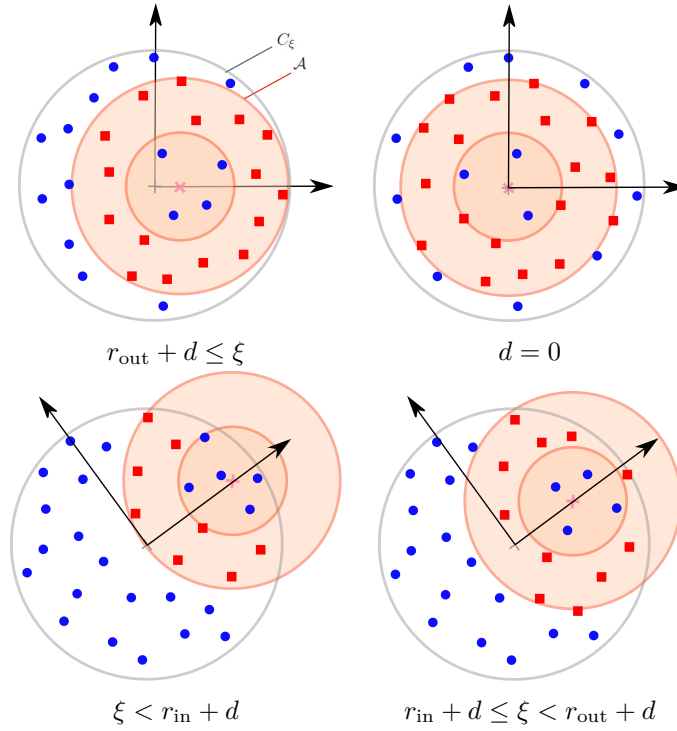


Figure 11 – The typical realizations of C_ξ and \mathcal{A} where the square red points are interferers.

expressed as [222]

$$f_R(u) = \begin{cases} \frac{2\pi u}{|\mathcal{A} \cap C_\xi|}, & r_{\text{in}} \leq u \leq r_{\text{max}} \\ \frac{2u}{|\mathcal{A} \cap C_\xi|} \cos^{-1}\left(\frac{u^2 + d^2 - \xi^2}{2du}\right), & r_{\text{max}} \leq u \leq r_{\text{out}}, \end{cases} \quad (77)$$

where $r_{\text{max}} = \max(r_{\text{in}}, \xi - d)$.

2.2.5 Nakagami Fading on the Desired Signal

Capturing small-scale fading with Rayleigh distribution is particularly justified in NLOS propagation environments. However, in the context of UDNs, where the transmitter-receiver distance is reduced, the likelihood of specular LOS paths increases, and the Rayleigh assumption is no longer realistic. Similar observation is considered in the context of higher-frequency bands where signal propagations are generally sensitive to LOS and NLOS paths [159, 166]. In such scenarios, Rician fading is commonly accepted to capture fading in LOS propagations [223, 224], where it can be well approximated by means of a more tractable Nakagami- m distribution. Also, the Nakagami assumption can actually be seen as a gamma distribution since X^2 is gamma distributed when X is Nakagami distributed, which improves analytical convenience.

We now assume that the desired link h follows a gamma distribution with shape parameter m and scale parameter θ , (64) simplifies then as

$$P_c(\mathbb{T}) = \mathbb{E}_{R_0, I, W} \left\{ \frac{\Gamma\left(m, \frac{\mathbb{T}}{\theta} \mathbb{L}(R_0)(I + W)\right)}{\Gamma(m)} \right\} \quad (78)$$

$$\stackrel{(a)}{=} \mathbb{E}_{R_0} \left\{ \sum_{k=0}^{m-1} \frac{(-1)^k}{k!} \left[s^k \frac{d^k \mathcal{L}_{I+W}(s)}{ds^k} \right]_{s=\frac{\mathbb{T}}{\theta} \mathbb{L}(R_0)} \right\}, \quad (79)$$

where (a) follows from the expansion of the upper incomplete gamma function as $\Gamma(m, x) = \Gamma(m)e^{-x} \sum_{k=0}^{m-1} \frac{x^k}{k!}$.

The computation of coverage probability in (79) requires then a prior evaluation of the k th derivative of $\mathcal{L}_{I+W}(s)$. Assuming the interference-limited regime, i.e., $\mathcal{L}_{I+W}(s) \simeq \mathcal{L}_I(s)$, several frameworks have been proposed in the literature to derive or approximate the k th derivative of the Laplace transform of the interference. For instance, an approximation via Taylor expansions is considered in [225]. In [226–228], The authors proposed the use of the Faà di Bruno’s formula [229], where an alternative formulation under the Bell polynomials is used in [71]. Also, a recursive-technique is proposed in [228, 230], where the expression of the k th derivative is transformed to a lower triangular Toeplitz matrix with positive entries. However, reducing analysis to the interference-limited regime can be seen as less efficient in scenarios where thermal noise is a key player in the network performance, e.g., higher-frequency bands. Interestingly, an alternative framework based on the Alzer’s lemma is suggested in [69, 156], which enables to derive a relatively tight approximation of coverage probability, as

$$P_c(\mathbb{T}) \approx \mathbb{E}_{R_0} \left\{ \sum_{k=1}^m (-1)^{k+1} \binom{m}{k} \mathcal{L}_I(ks) \mathcal{L}_W(ks) \right\}, \quad (80)$$

where $s = \frac{\beta \mathbb{T}}{\theta} \mathbb{L}(R_0)$ and $\beta = \Gamma(1 + m)^{\frac{-1}{m}}$.

It should be noted that this framework is generally suitable whenever the desired link is experiencing a fading model of the form [225, Theorem 1], $\mathbb{P}\{h > u\} = \sum_{n \in \mathbb{N}} e^{-nu} \sum_{k \in \mathbb{N}} a_{nk} u^k$.

2.2.6 The Factorial Moment Based Approach

Considering the max-SINR association policy, the authors of [52, 231–233], conceived the coverage probability experienced by the typical UE y w.r.t. all BSs $x \in \Psi$, as the probability that the k th smallest BS in terms of SINR meets the required target \mathbb{T} . In other words, the typical user is in coverage if at least k BSs meet the required SINR target. Formally,

$$P_c^{(k)}(\mathbb{T}) = \mathbb{P} \left\{ \left[\sum_{x \in \Psi} \mathbf{1} \left(\text{SINR}(x; y) > \mathbb{T} \right) \right] \geq k \right\}. \quad (81)$$

Let's denote by $n \geq 1$, the number of BSs with SINR greather than the required threshold. Next, the authors introduced a key quantity of interest, namely the factorial moment measure $S_n(\mathbb{T})$ of the SINR process [50], defined as the average number of ways that the typical UE can be associated to n different BSs. Formally, it can be expressed as

$$S_n(\mathbb{T}) = \mathbb{E} \left\{ \sum_{x_1, \dots, x_n \in \Psi}^{\neq} \mathbf{1} \left[\bigcap_{i=1}^n \text{SINR}(x_i; y) > \mathbb{T} \mid x_i \in \Psi \right] \right\}. \quad (82)$$

Interestingly, (81) can be simplified via the famous inclusion-exclusion principle [52, 231–233], as

$$P_c^{(k)}(\mathbb{T}) = \sum_{n=k}^{\infty} (-1)^{n-k} \binom{n-1}{k-1} S_n(\mathbb{T}). \quad (83)$$

The sum in (83) is actually finite since $n\mathbb{T}/(1+\mathbb{T})$ needs to be lowered by 1 as demonstrated in [4, Proposition 6.2]. That is, (83) is simplified as

$$P_c^{(k)}(\mathbb{T}) = \sum_{n=k}^{\lceil 1/\mathbb{T} \rceil} (-1)^{n-k} \binom{n-1}{k-1} S_n(\mathbb{T}). \quad (84)$$

The computation of the k -coverage probability in (84) requires then a prior evaluation of $S_n(\mathbb{T})$ for $n \geq k$, which can be derived via higher order Campbell's theorem as in [52, Theorem 6] [233, Theorem 7]. It is worth mentioning that despite the analytical relevance of technique #6 and its ability to reflect several connectivity scenarios of the typical UE, it provides however less-tractable expressions of coverage probability and requires generally a thorough in-depth knowledge of the factorial moment measure and its higher order Campbell's theorem.

2.2.7 The Plancherel-Parseval Approach

For the sake of further generalization, so that the performance evaluation would not be limited to a particular fading distribution that is only valid in some operational regimes, the authors of [4, 5, 16, 17] considered the Plancherel-Parseval theorem [4, Lemma 12.2.1] to derive an exact expression of coverage probability regardless of the fading model. That is, assuming a

generalized fading distribution on both the desired link and interferers, the coverage probability in (65) becomes,

$$P_c(\mathbb{T}) = \mathbb{E}_{R_0} \left\{ \int_{-\infty}^{\infty} \mathcal{L}_I(2j\pi\mathbb{L}(R_0)\mathbb{T}s) \mathcal{L}_W(2j\pi\mathbb{L}(R_0)\mathbb{T}s) \frac{\mathcal{L}_h(-2j\pi s) - 1}{2j\pi s} ds \right\}. \quad (85)$$

2.2.8 The Gil-Pelaez Inversion Approach

An alternative way to incorporate generalized fading, is by using the Gil-Pelaez inversion theorem [234], in which the cumulative distribution function (CDF) F_X of a random variable X can be expressed based on the characteristic function $\Phi_X(\omega)$, as

$$F_X(x) = \frac{1}{2} - \frac{1}{\pi} \int_0^{\infty} \frac{\text{Im}(e^{-j\omega x} \Phi_X(\omega))}{\omega} d\omega. \quad (86)$$

Relevant applications can be found in [83, 159, 198, 235], where the coverage probability in (64) is reformulated as

$$P_c(\mathbb{T}) = \mathbb{E}_{R_0, h, W} \left\{ \mathbb{P}_I \left(I \leq \frac{h}{\mathbb{T}\mathbb{L}(R_0)} - W \mid R_0, h, W \right) \right\} \quad (87)$$

$$= \frac{1}{2} - \frac{1}{\pi} \mathbb{E}_{R_0} \left\{ \int_0^{\infty} \text{Im} \left(\Phi_h \left(\frac{-\omega}{\mathbb{T}\mathbb{L}(R_0)} \right) \Phi_W(\omega) \Phi_I(\omega) \right) \frac{d\omega}{\omega} \right\}, \quad (88)$$

where the characteristic function is obtained as

$$\Phi_I(\omega) = \exp \left(-2\pi\lambda \int_{\vartheta(R_0)}^{\infty} \left[1 - \mathbb{E}_g \left\{ \exp \left(\frac{j\omega g}{\mathbb{L}(u)} \right) \right\} \right] u du \right), \quad (89)$$

such that $\vartheta(\cdot)$ is the function considered in technique #1.

2.2.9 The Laplace Transform Inversion Approach

Another inversion technique to derive the PDF of a random variable X , is by considering the Fourier inversion theorem, also known as the Laplace transform inversion [51, 59, 237, 290], the characteristic function inversion [86, 238], or even the MGF inversion [224]. Generally, the PDF $f_X(\cdot)$ of X is obtained via the Bromwich contour inversion integral, as

$$f_X(y) = \mathcal{L}^{-1} \{ \mathcal{L}_X(s) \} = \frac{1}{2\pi j} \int_{\gamma-j\infty}^{\gamma+j\infty} \mathcal{L}_X(s) e^{ys} ds, \quad (90)$$

where γ is a real constant such as the contour of integration runs from $\gamma - j\infty$ to $\gamma + j\infty$ along a straight line and lies to the right of all the singularities of $\mathcal{L}_X(\cdot)$.

As for the CDF of X , it can be derived equivalently as

$$F_X(x) = \int_0^x f_X(y)dy = \mathcal{L}^{-1} \left\{ \frac{\mathcal{L}_X(s)}{s} \right\} (x). \quad (91)$$

That is , the coverage probability in (87), simplifies then as

$$P_c(T) = \mathbb{E}_{R_0, h, W} \left\{ \mathcal{L}^{-1} \left\{ \frac{\mathcal{L}_I(s)}{s} \right\} \left(\frac{h}{\text{TL}(R_0)} - W \right) \right\}. \quad (92)$$

Similarly to previous inversion techniques, this approach derives exact expressions of coverage probability under generalized fading distribution, but requires involved analysis with limited design insights [233]. A more flexible version is to resort to the characteristic function inversion enabling to avoid contour integration as illustrated in [86, 238].

2.2.10 The Interference Approximation Approach

An alternative way to derive the PDF of the interference without resorting to previous less tractable inversion techniques, is to approximate the interference behavior [23]. Two main approaches are considered in the literature. The first one, is by considering the interference contribution from only some specific transmitters based on the adopted association policy. For example, the k dominant interferers in terms of the received power are considered when assuming max-SINR association criterion [43], while the k -nearest interferers are considered in the case of the nearest [173] or the n th nearest neighbor association policy [220]. This approach enables actually to derive an upper bound of coverage probability, where bound accuracy increases with increasing path loss exponent to justify ignoring the contribution of distant interferers [23]. The second approach is by approximating the distribution of the other-cell interference via well-known distributions with parameters fitting the essential physical parameters that affect interference. Typically, the authors of [239] showed that the interference behavior can be captured by the family of α -stable distributions, while in [240], interference distribution is approximated via gamma distribution.

2.2.11 MGF-based Average Rate

As has been discussed in (26), average ergodic rate is commonly mapped to coverage probability via integration over the positive real axis (Fig. 4). Such approach reduces the use of time-consuming simulations, but requires however the computation of multi-fold numerical integral. An alternative approach is proposed in [241] to derive the average ergodic rate by considering general fading distributions and without necessarily going through the coverage probability expression. A qualitative and quantitative comparisons of the MGF-based framework with the coverage-based conventional approach can be found in [68]. Typically, using [241, Lemma 1], the average ergodic rate in (25) can be simplified as

$$\tau = \mathbb{E}_{R_0, W} \left\{ \mathbb{E} \left\{ \log \left(1 + \frac{h}{1 + \frac{I}{W}} \right) \middle| R_0, W \right\} \right\} \quad (93)$$

$$= \mathbb{E}_{R_0} \left\{ \int_0^\infty \mathcal{L}_W(s) \frac{\mathcal{L}_I(s) \left(1 - \mathcal{L}_h\left(\frac{s}{\mathbb{L}(R_0)}\right) \right)}{s} ds \right\}. \quad (94)$$

Next, the framework was widely adopted in the literature. For instance, the art in [242] evaluated the uplink average ergodic rate when considering representative scheduling schemes in terms of performance and implementation complexity. In [243], the downlink average ergodic rate is investigated under the scenario of multiple cell association in UDNs environment.

2.3 Chapter Summary

Table 3 summarizes the eleven techniques commonly used in the literature to evaluate main performance metrics of wireless networks under the PPP/BPP abstraction. We examined in particular a mapping of these techniques with various association schemes considered in the literature, as well as illustrated the required fading model for each technique.

Table 3 – Key analytical techniques used in wireless networks performance evaluation under the PPP/BPP abstraction.

Analytical techniques	Analytical accuracy	Analytical complexity	Distribution of fading power on		Cell association policies					
			Desired link	Interferers	Strongest average received power	Nearest-neighbor association	Biased cell association	Max-SINR cell association	The n th nearest-neighbor association	Smallest path loss cell association
Technique #1	Approximation	Low	Rayleigh	Generalized	[24, 58]	[17, 58] [71, 136]	[19, 175] [176]	[18, 24, 54] [137]	[57, 58]	[69, 70] [159]
Technique #2	Approximation	Low	Rayleigh	Generalized	-	[204, 205] [208]	-	-	-	-
Technique #3	Approximation	Medium	Rayleigh	Generalized	-	[141, 198]	-	-	-	-
Technique #4	Approximation	Medium	Rayleigh Nakagami	Generalized Nakagami	- -	- [220]	- -	- -	[59, 61]	- [221]
Technique #5	Taylor: Approx. Faà di Bruno: Exact Bell polynomial: Exact Toeplitz matrix: Exact Alzer's lemma: Approx.	Medium	Nakagami	Generalized	[228]	[71, 156] [230]	[226, 227] [228]	-	-	[156]
Technique #6	Exact	High	Rayleigh Generalized	Generalized Generalized	- -	- -	- -	[231, 232] [52, 233]	- -	- -
Technique #7	Exact	High	Generalized	Generalized	-	[17]	-	-	-	-
Technique #8	Exact	Medium	Generalized	Generalized	-	[198, 235]	-	[83, 159]	-	[159]
Technique #9	Exact	High	Generalized	Generalized	-	[224]	-	[86, 237]	-	[238]
Technique #10	Approximation	Low	Nakagami Generalized	Nakagami Generalized	- -	[173, 240] -	- -	- [239]	[220]	- -
Technique #11	Exact	Medium	Generalized	Generalized	-	[242]	[68]	-	[243]	-

STOCHASTIC GEOMETRY FOR 5G/B5G WIRELESS NETWORKS

In this chapter, we will review key aspects and challenges of emerging RAN architectures for 5G/B5G, and subsequently outline major state-of-the-art contributions which, based on SG, can evaluate the key properties of these promising RAN architectures. Also, we will review modeling challenges to capture the properties of 5G/B5G key emerging technologies, and highlight the penetration degree of SG in modeling and analysis of their fundamental attributes.

3.1 Stochastic Geometry and Promising RAN Architectures For 5G/B5G

3.1.1 Terrestrial Heterogeneous Networks

Adding new macro BSs in a homogeneous and regular fashion is typically constrained by increased deployment costs, in addition to heterogeneity in site location availability and users demand. An alternative strategy is to consider the deployment of HetNets, where several classes of low-power and low-cost nodes are deployed in poorly covered small areas or traffic hotspots, overlaid within macro BSs.

The key aspects of a generative SG model consists of K overlaid tiers of BSs, where the BSs of each tier are characterized by some distinctive marks (e.g., transmit power, connectivity threshold, BS density, backhaul type) and the locations of each tier nodes are modeled with a specific PP. Typically, a regular or repulsive PP for macro BSs and clustering PPs for low-power cells [64, 65]. For instance, the downlink SINR of HetNets is evaluated under various BS association policies and fading models in [18, 19, 24, 54, 232, 243]. The uplink analysis of HetNets is studied in [244–246]. Also, given the heterogeneous attributes of BS transmit power in HetNets, the typical UE may be associated to different BSs in uplink and downlink, i.e., DUDA. Further analysis of DUDA in the context of HD HetNets can be found in [150–152],

while DUDA in the context of IBFD HetNets is given in [177] and the references therein. One important use case of small cells in HetNets is to support overloaded macro cells. That is, the impact of CRE on the performance of HetNets is assessed in [137, 175, 176]. Last but not least, the question of mobility is also crucial in HetNets where it is generally governed by several tradeoffs. For example, a mobile UE in HetNets will suffer from frequent handovers, which may increase call drop rate and service delays. However, adding more low-power cells increases the average number of lightly loaded BSs and then reduces interference [247], which can reduce handover failure rate. In all cases, incorporating mobility is very challenging given the complex behavior of UEs movement [178, 179, 187]. Further analysis of mobility-aware HetNets can be found in [181, 182, 184–186].

3.1.2 Non-Terrestrial Networks

A promising frontier for terrestrial HetNets is by extending their deployment to the sky via UAVs [248, 249]. In fact, given their distinctive features, UAVs can be quickly deployed to support coverage in isolated regions and capacity of terrestrial HetNets during flash crowded events. Also, UAVs can even support lightly loaded networks, where the few active users can be served instead by UAVs and then enable some terrestrial macro BSs to switch into idle mode [136, 137, 247], which improves EE and interference mitigation. Sometimes and due to their limited storage and processing capabilities, UAVs may be required to operate as mobile aerial relay nodes (RNs) for ground UEs and BSs [250]. A comprehensive survey about UAV-aided cellular networks can be found in [31]. However, despite the benefits of UAVs as flying nodes, several new challenges are introduced. Among them, the AtG propagation model, which is no longer similar to popular terrestrial models due to UAVs operational altitude and their 3D mobility. The widely used AtG model is typically proposed in [167, 168], and a comprehensive survey about channel modeling for UAV-assisted communications is brought in [169]. Also, given their technical constraints combined with ground UEs QoS requirements, optimal placement of UAVs is another challenging task, which may include UAVs trajectory optimization [251], altitude optimization [168, 252], flight time optimization [253], and UAVs density optimization [254].

Based on SG and its inherent PP theory, spatial locations in UAV-aided wireless networks are totally or partially modeled as randomly distributed according to a PP. This approach is followed in [255], where a unique UAV is assumed to serve randomly scattered terrestrial UEs, among them some random underlay D2D UEs. In [220], a finite network of UAVs whose locations are modeled as a uniform BPP is considered. Assuming Nakagami- m fading for all wireless links, a general expression of the downlink coverage probability is derived by using the

analytical technique #4 and approximations were next made using the dominant interferer-based approach in technique #10. In [256], UAVs and terrestrial BSs are distributed according to two independent PPPs, while terrestrial UEs are modeled by a PCP around the vertical projections of UAVs. In [257], UAVs are aimed to assist public safety networks, where the location of ground BSs surviving after natural disasters are modeled as an independent thinned PPP, while UAVs form a PCP around the locations of damaged BSs. Interestingly, the uplink of UAV-assisted networks is studied in [258], the performance of a UAV backhaul link via ground BSs is evaluated in [259], and the performance analysis of multiple-input and multiple-output (MIMO) combined with NOMA in UAV-aided networks is brought in [260].

3.1.3 UDNs via Infrastructure Densification

Infrastructure densification is envisioned as the workhorse for ubiquitous coverage and capacity improvement in 5G/B5G networks [261–263]. It can be typically realized by adding new transmitters in the area of interest, or by simply increasing the average number of antennas per transmitter/receiver, i.e., MIMO transmissions. Many experts also consider some spatial diversity technologies such as relays, meta-surfaces, and D2D communications, as a form of densification since they allow decentralized opportunistic short-range communication [261]. In the following, we will discuss the main technologies competing in terms of infrastructure densification in HetNets, as well as the key state-of-the-art contributions based on SG.

Small cells

Adding small cells is a common way to emerge from HetNets to UDNs. Several challenges are, however, brought into analysis. For instance, the question of association policy is a key concern, where UEs can access small cells without any logical restriction, namely open access, and hence the need to judiciously adjust cells load via CRE [175, 176] and interference via intercell interference coordination (ICIC) [264]. Also, access to small cells can exclusively be given to some specific UEs belonging to a closed subscriber group (CSG), namely closed access, or consider an hybrid access scheme, in which some additional UEs not registered in the CSG can also access the cell along with registered UEs [267]. Typical challenges may also include, the scaling law of network performance with infrastructure density [33, 70, 71, 162, 164, 165, 172, 262] and qualitative and quantitative comparison between adding new cells, using multi-antenna transmissions, or increasing macro cells storage capacity [265, 266]. More discussions about other representative challenges are given in [261–263].

Infrastructure sharing

A new viable business model for infrastructure densification is by allowing concurrent operators share their mutual infrastructure [268]. This paradigm is expected to lower the time to market of each operator and reduce costs by an average of up to 40% and 15% in terms of capital expenditure (CAPEX) and operational expenditure (OPEX) costs, respectively [269]. Questions related to the optimal sharing strategy between operators, are actually the main concern of research studies. Typically, two extreme variants of infrastructure sharing are considered: Passive sharing, wherein operators can only share site location and common operation costs, while each operator installs and maintains its own equipment, and active sharing wherein operators share their network physical infrastructure and have access to it on the basis of an agreed resource allocation strategy.

Based on the tractability of SG, several mathematical frameworks and PP models have been investigated to quantify the benefits of infrastructure sharing. For instance, the authors of [132] evaluated the goodness-of-fit of some realistic shared-infrastructure networks with various aggregative PP models, where they revealed that LGCP can serve as a universal model to fit realistic multi-network empirical data. In [72], infrastructure sharing is evaluated under a setup of one buyer operator and multiple seller operators, where the aim of the study is to define an optimal buying strategy to meet a target QoS requirement with reduced costs. In [73–75], spectrum sharing between several operators is studied, particularly at mmWave frequencies where antenna beamforming, transmissions sensitivity to blockages, and operators cooperation, can help to mitigate inter-operator interference [270]. In [76–78] both spectrum and infrastructure sharing are investigated.

Multiple-input multiple-output systems

In conjunction with adding new cells and using higher frequency bands, MIMO technology is considered as a key component in the race towards higher data rates in 5G/B5G networks [261–263]. MIMO is usually used to increase *spatial diversity* and combat channel fading, which enhances the reliability of the reception. Alternatively, fading can be seen as a source of increasing the degrees of freedom in MIMO systems. That is, the receiving antenna array can retrieve independent information streams with sufficiently different spatial signatures, which helps improve data rate. This technique is referred to as *spatial multiplexing*. The third popular use case of MIMO is *precoding or multi-flow beamforming*, wherein the same information symbol is sent by each of the transmitting antennas with appropriate phase and gain weighting, so

that the signal power is maximized at the receiver by constructively adding signals emitted by different antennas. Accordingly, channel estimation and symbol detection is a key challenge in MIMO systems.

Benchmarking system-level performance of MIMO techniques with conventional single-antenna channels is an another important concern in the state-of-the-art research works. For instance, MIMO spatial multiplexing technique in the case of a single-tier network is studied in [275]. The analysis of MIMO in the context of HetNets can be found in [203, 228, 240, 276, 277]. MIMO for uplink cellular networks is investigated in [245, 278]. The interplay between cell selection bias and MIMO in the context of load-aware networks is analyzed in [226, 228, 279]. Interference mitigation in a co-channel deployment of small cells is studied in [280] through spatial blanking, i.e., tuning the directionality of MIMO channel vectors. Interestingly, the contribution of combining MIMO with the merits of other efficient technologies is investigated in [281] for IBFD communications, in [282] for NOMA systems, and in [283] for mmWave cellular networks .

Multi-hop relays

One practical limitation of densifying HetNets via fully-functioning new cells is the complexity of provisioning all new cells with a dedicated wired backhaul connection. One proposed solution is to consider the deployment of RNs between BSs and cell-edge UEs [285]. That is, several relaying protocols have been investigated by the research community. For instance, amplify-and-forward (AF) RN, decode-and-forward (DF) RN, also known as L2 relay, and L3 RN, envisioned to support almost similar capabilities as small cells but without the need of a wired backhaul connection. Several use cases of RNs are assessed in the literature. For instance, RN with IBFD capability is surveyed in [286]. Cooperative RNs to create spatial diversity are investigated in [287]. In [288], cooperative RNs can be equipped with buffers to store received packets and resend them when optimal connectivity conditions are met.

Using methods from SG, several research works have considered analytical performance evaluation of relay-aided wireless networks. For instance, a novel analytical framework for the analysis of outage probability in the regime of high SNR and low BS density is proposed in [289]. The paradigm of SWIPT with cooperative relaying is investigated in [290, 291]. Quantifying the performance gain achieved when using RNs in HetNets is studied in [292]. In [293], a flexible cell association scheme is proposed, where some bias coefficients are introduced to prioritize the association of the typical UE with single- or multi-hop links, and then optimize the overall end-to-end coverage and rate. Interestingly, the performance of IBFD relay-aided cellular networks where BSs and RNs are equipped with MIMO antennas, is investigated in [294].

The promising approach of metasurfaces

Despite relatively lower costs and easy deployment of RNs as compared to macro and small cells, extensive deployment of RNs in UDNs can increase costs in view of their inherent power consumption and OPEX costs. Recently, a radically new wireless communication paradigm has been proposed [30,295,296], wherein some software-controlled metallic reflectors made of low-cost passive elements, i.e., metasurfaces, are judiciously placed in environment objects and controlled in order to minimize the multi-path profile, and then enhance the performance of edge users. Metasurfaces are actually equipped with atomic elements exhibiting a periodic texture, namely meta-atom patterns, where the control of their geometrical characteristics allows re-engineering the direction of impinging EM waves. In other words, the channel model is no longer treated as a probabilistic process, but as a software-defined measure due to programmable wireless environment via metasurfaces [296].

Quantifying the performance gain of a wireless network with software-driven metasurfaces is particularly done through extensive simulations (see [296–298] and the references therein). However, analytical evaluation based for example on SG and the theory of PPs is not available. Some initial efforts are actually considered in the literature [298], where objects coated with reconfigurable metasurfaces are uniformly and randomly scattered in the 2D plane. Next, the probability that the typical object can act as a reflector is derived consistently with the Snell’s law of reflection. The analytical framework is promising and may constitute the workhorse to develop a more general tractable approach that enables to derive performance metrics (e.g., coverage probability, ergodic rate) of a metasurface-aware wireless network.

Device-to-device communications

Cooperative communications via fixed terminal relaying can bring substantial improvements in wireless networks [287]. However, with the drastic growth in UE’s density and their unpredictable complex movement [178], the paradigm of cooperative communications via D2D communications is considered. Comprehensive surveys about D2D communications underlying cellular networks can be found in [299,300].

SG has been extensively explored in modeling and analysis of D2D communications. For instance, the crucial question of spectrum sharing in D2D communications is investigated in [301,302]. Also, since neighbor D2D UEs are more likely to be in prominent LOS transmissions, the authors of [303] evaluated network performance under Rician small-scale fading. Due to many technical challenges when deploying D2D communications in licensed bands, traffic offloading

via D2D in unlicensed bands is considered in [304]. The tendency of D2D UEs towards clustering is captured via PCP in [154, 155], where coverage probability and area spectral efficiency are next derived under several content availability scenarios. Last but not least, uplink analysis of D2D communications is provided in [305], the benefits of combining IBFD with the merit of underlaid D2D communications are evaluated in [306], the impact of massive MIMO on reducing D2D-to-cellular interference is studied in [284], and the performance of D2D communications when considering aerial access points is available in [255].

3.1.4 Cloud Radio Access Networks

Albeit the expected benefits of infrastructure densification, there are still many notable limitations. For instance, CAPEX and OPEX costs are steadily growing with densification [45]. Also, interference is expected to be more critical, which demands an aggressive frequency reuse. The question of mobility is also crucial due to reduced cells size and heterogeneity in neighboring cells, which requires proper load balancing and smooth handover schemes. An innovative paradigm to address such challenges, is to consider C-RAN architecture, in which the baseband units (BBUs), responsible of scheduling and data processing, are separated from radio units, and pooled farther away in a centralized data center equipped with the potential of cloud computing. Remote radio heads (RRHs) are connected to BBUs via a dedicated high-speed and low-latency links, e.g., radio over fiber, namely the fronthaul link. C-RAN can therefore manage simultaneously the BBU processing of a large geographical zone, which reduces costs (e.g., about 15% in CAPEX and 50% in OPEX [45]), facilitates load balancing, and enables the use of ICIC techniques and coordinated multipoint (CoMP) transmission and reception, considered as potential solutions in C-RAN [46]. One important variant of C-RAN is distributed antenna system (DAS), in which BS antennas and inherent radio frequency (RF) components are deployed far away from the BS to form a distributed antenna array, while the central intelligence is kept at the BS level. A typical application of DAS is the reinforcement of indoor coverage as aimed by the baseline work in [271].

Using tools from SG, the dynamics on the location of nodes in a C-RAN architecture, are captured for analytical evaluation of network performance. For instance, a model of 4-layers of nodes (UEs, RRHs, backhaul nodes, and data centers), modeled by independent PPPs is considered in [307], where by assuming various representative costs (cost of nodes, processing, and backhaul technology), the authors demonstrated that C-RAN based architectures can reduce costs by at least 10%. In [308], the performance of a C-RAN with multiple antenna RRHs is evaluated when assuming three degrees of collaboration between RRHs and their associated BS.

In [309], the authors considered MHPP II to capture the repulsion behavior in RRHs location. Interestingly, the contributions of some emerging techniques in the context of C-RAN is also studied. Representative works can be found in [310] for C-RAN with ICIC techniques, in [311] for C-RAN as an enabler for CoMP protocols, in [312] for IBFD transmissions, and in [313] for NOMA-based communications. As for the DAS variant of C-RAN, outage probability is investigated in [272], while spectral efficiency is studied in [273,274].

3.1.5 Virtualized Radio Access Networks

Increased network densification, as well as the use of CoMP and ICIC techniques in a C-RAN architecture, are expected to boost the overall network performance. However, they can amplify the signaling and control overhead, which is expected to generate a critical burden at the fronthaul level. One promising approach to alleviate the fronthaul bottleneck is by splitting the control plane (C-plane) and the user plane (U-plane) of the radio link via *RAN virtualization*. This capability is particularly supported by the software-defined networking (SDN) [314] where U-plane (message forwarding) is deployed in a decentralized fashion, while C-plane (control and radio resource management) is centralized in a controller. Typically, the C-plane can be provided by high-power nodes operating at sub-6 GHz bands to guarantee large coverage and efficient mobility schemes, while the U-plane can be provided by low-power nodes, namely *phantom cells*, operating at higher-frequency bands [315,316]. Such low/high-frequency bands operation helps actually to pave the way for joint URLLC and eMBB communications [317], which generally requires a prior combining of the C-RAN paradigm with HetNets, also known as H-CRAN [318].

Based on the tractability of SG, several recent works have investigated the performance gain under the setup of C-plane/U-plane split architecture. For instance, the authors of [319] evaluated EE improvements under the phantom cell paradigm as compared to a macro-only deployment. In [320], the authors studied offloading of the macrocellular layer through small cells CoMP transmissions in a virtualized RAN architecture. In [321], a tractable mobility-aware model is considered to quantify the expected performance gain with C-plane/U-plane split. Further extensions of the analysis are considered in [322] by taking into account mmWave sensitivity to LOS and NLOS transmissions, and in [323] by considering UAV-aided cellular networks.

3.1.6 Fog Radio Access Networks

Another promising paradigm to alleviate the fronthaul burden in H-CRAN is F-RAN architecture, in which a considerable fraction of the cloud is deployed in close proximity to UEs, which can be done through endowing edge terminals or third-party entities (e.g., parks, shopping centers) with computing and storage capabilities [324]. There are generally two typical applications of such promising paradigm. i) *Storing and computing capabilities*, wherein computation-intensive tasks are processed at the level of nearby fog servers and the result will be forwarded back to end UEs, which enables using the released memory space at UEs to process other services, and then enhance users QoE. ii) *Content delivery and caching*, wherein close fog servers, also known in this context as helper nodes, are endowed with high capacity caches in order to proactively cache popular internet content requested by end UEs [32].

Using tools from SG, most literature works on the analysis of F-RAN architectures, are typically focused on quantifying the benefits of the caching capability of helper nodes when assuming a network with limited backhaul [266] or fronthaul link capacity [325]. Typically, the SG generative setup is to consider the location of helper nodes as modeled according to some PP (e.g., PPP [266], β -GPP [325], MHPP II [326], PCP [155]), each node has a finite cache capacity, wherein files are placed according to some popularity distribution function (e.g., Zipf), and each cached file requires a minimum bitrate to meet the requirements of users QoE. That is, the performance of a cache-enabled network is quantified by the average delivery rate, defined as the probability that the typical UE can receive a downlink rate greater than the file bitrate threshold, and also the requested file can be found in the local cache of the tagged helper node. Otherwise, the file will be requested from the core network, and the average delivery rate of files will be constrained by the backhaul/fronthaul link capacity.

Accordingly, two lines of research are adopted in the literature. The first, is related to *the content placement strategy*, in which the problem can be stated as, how should we place the files in the helper caches to optimize some performance metrics (e.g., the hit probability defined as the probability that the typical UE may find the requested file at the tagged helper node)? Representative works can be found in [327] for single-tier cellular networks, in [326] for D2D communications, and in [328] for content placement policy in large-scale HetNets. The second direction of research is related to *the optimal delivery strategy*, wherein the analysis is focused on how to deliver the cache content at the user request in order to boost some performance metrics (e.g., the average delivery rate). For instance, the average delivery rate is considered in [266] to evaluate the question of adding more BSs or increasing the caching capability of already deployed BSs. In [329], the content delivery protocol is studied in a HetNet scenario where the

typical UE can request content from the nearest BS, RN, or cache-enabled UE. Interestingly, the joint analysis of placement and delivery techniques is brought in [330, 331].

3.2 Stochastic Geometry in Higher-Frequency Bands

With the severe spectrum scarcity in commercial wireless networks running generally at sub-6GHz frequency bands, researchers are steering new opportunities in higher frequency bands to conceive a sufficiently higher bandwidth and hence meet the increased data rate requirements for eMBB services [262]. In the following, we will outline the key aspects and challenges of using SG to evaluate communications in typical higher frequency bands.

3.2.1 mmWave Communications

With wavelengths from 1 to 10 mm and frequency range from 30 to 300 GHz, mmWave combined with advances in integrated circuit technologies enable to concentrate tens of miniaturized and high gain antennas in small areas, which permits directional beamforming alignment [27, 69, 166]. That is, several changes need to be considered w.r.t. conventional mathematical SG frameworks available for modeling and analysis of μ Wave wireless networks. Typically, i) nodes are equipped with directional antennas such that the antenna gain is maximized when the steering angle is inside a given main lobe width [158, 159], ii) the vulnerability of mmWaves to blockages is captured by considering LOS and NLOS transmissions in addition eventually to an outage state, in which the path loss is approximately infinite [83, 159, 332], and iii) the primacy of the thermal noise w.r.t. the interference in mmWave communications [332], is captured by assuming the noise-limited regime, i.e., $\text{SINR} \simeq \text{SNR}$.

Several representative research works are considered in the literature. For instance, coverage probability and average rate in a single-tier mmWave network is studied in [69], where the blockage effect is captured by a simplified LOS ball approximation (see Table 2). In [159], the previous seminal work is further generalized by considering an outage state of the blockage model, with emphasis on the noise-limited regime. The obtained theoretical results are also extended by taking into account beamforming alignment errors and a multi-tier mmWave cellular deployment. In [38, 333], DUDA is investigated in the context of a HetNet where μ Wave macrocells are overlaid by mmWave small cells. In [335], the feasibility of a backhaul based on multi-hop mmWave transmissions in the context of UDNs is compared with other concurrent technologies of wired and wireless backhails. Also, the performance of a mmWave cellular network under

various MIMO techniques is studied in [336].

3.2.2 TeraHertz Communications

Compared to mmWaves, directional beamforming alignment in teraHertz frequencies (from 300 GHz to 3 THz and wavelengths from 100 μm to 1 mm) is considerably more feasible due to shorter wavelength, which suggests roughly the same system model changes as those previously discussed in mmWave. One key exception is the increased propagation losses in the teraHertz bands due to severe sensitivity to rain and resonant absorption in water molecules [28]. Accordingly, the path loss function in the case of a teraHertz propagation is generally revisited by frequency-dependent molecular absorption effect with an emphasis on the LOS link as [160, Theorem 4] [337]

$$\ell(r) \simeq \left(\frac{c}{4\pi f} \right)^2 r^{-\alpha_{\text{LOS}}} e^{-k(f)r}, \quad (95)$$

where $k(f)$ is the medium absorption coefficient at frequency f , α_{LOS} is the path loss exponent in the LOS region, and c is the speed of light.

Using tools from SG, couple of works are considered for modeling and analysis of systems operating in teraHertz frequencies. For instance, the authors of [338, 339] studied the mean interference and next the SINR by considering the key aspects that affect signal propagation in teraHertz bands, e.g., high beamforming directivity and molecular absorption. In [340], coverage probability and average rate are derived in a teraHertz-aided network, where it has been shown the existence of a certain tradeoff between decreased coverage probability and improved average rate.

3.2.3 Visible Light Communications

Using light-emitting diodes (LEDs) in license-free visible light spectrum from 400 to 800 THz and wavelengths from 375 to 780 nm, VLC can offer simultaneous high brightness illumination and high indoor data rate [29]. That is, information bits are modulated onto the intensity of the emitted light, where the path loss function is expressed under the form #4 in Table 2, such that the path loss exponent is mapped to the Lambertian emission order of the LED light [341, Equation 11]. Also, given the reduced VLC wavelength combined with the vicinity of receivers detection area, multipath fading is generally ignored in VLC networks.

Based on SG frameworks, we can discern three typical lines of research in the literature.

i) *Performance evaluation of multiuser VLC networks* where the SINR statistics are evaluated under the setup of a VLC-only system. For instance, the authors of [341] evaluated the down-link performance of a VLC network under two extreme deployments of LED APs in the ceiling, namely PPP and regular lattice. The analytical framework is promising but remains intractable since the SINR distribution is expressed as a function of the Gram-Charlier series and Laguerre polynomials requiring efficient numerical computation. In [342], a novel SG framework is developed by considering a 3D model and idle mode capability at VLC APs. Coverage probability is next derived based on successive statistical equivalences of SINR, but the approach requires fundamental revisions in the way to address the lack of a fading term in VLC networks. ii) *Optimizing hybrid VLC/RF networks* such that a joint operation of both technologies is evaluated. For instance, the authors of [343] considered a setup of several configurations of coexisting RF/VLC networks to derive coverage probability based on techniques #5 and #8 in Tab 3. In [344], the outage probability is first derived in a VLC/RF system by approximating the interference as a sum of gamma distributions (technique #10 in Tab 3), and an optimization problem is next formulated to optimize the density of VLC/RF nodes enabling higher EE under an outage probability constraint. Furthermore, due to the inherent broadcast nature of VLC networks, data transfer may be subject to fraudulent eavesdropping. Several arts have considered iii) *secrecy enhancement in VLC networks*, where the physical layer (PHY) is exploited to prevent the information-theoretic security from interception [345–347].

3.2.4 Free-Space Optical Communications

Using signals with wavelength range in 785-1550 nm, free-space optical (FSO) communication is a laser beam communication technology for high data rate transmissions in a point-to-point free space setup, where it can serve as a promising backhaul solution to avoid expensive or not feasible deployments of wired connections [37, 348].

Despite the potential benefits of FSO communications, SG as a powerful analytical tool has not been sufficiently leveraged in the evaluation of FSO networks due to several major modeling challenges. To the authors' knowledge, it is only recently that the first PPP abstraction model has been leveraged in performance evaluation of FSO networks [349], where a scenario of SWIPT through laser beams emitted from the ground to UAV-mounted BSs is considered. In fact, i) FSO narrow beams require a perfect alignment of the LOS path, which can be problematic due to building sway generated by some environmental factors. such feature needs to be captured by a random process to be introduced into performance analysis [37]. ii) Urban FSO is very

sensitive to weather conditions¹, which can be typically captured by an attenuation function dependent on distance, rain, and snowfall rate [350,351]. iii) The FSO signal is also attenuated by atmosphere molecular absorption dependent on the wavelength of the transmitted signal. iv) Such signal can also be constrained by fluctuations in temperature and humidity gradients over time, also known as scintillation or turbulence-induced fading. The universal model to capture such turbulence conditions is to consider doubly stochastic fading models [37, 348, 352]. Last but not least v) the FSO link is also subject to undesirable ambient noise caused by photons radiations of sunlight [353].

3.3 Stochastic Geometry and 5G/B5G Enabling Technologies

3.3.1 Cognitive Wireless Networks

Cognitive radio (CR) is a promising technology to address the scarcity of the licensed spectrum. CR techniques ensure actually an opportunistic allocation of the available spectrum where secondary users, also known as cognitive users, can scan and access the unused spectrum portions at specific time or place without impairing existing primary users [354]. The literature is rich in contributions dealing with the use of SG to evaluate the benefits of various spectrum sharing schemes. The fundamental challenge actually is how to use SG tools to capture the availability of unused licensed spectrum portions. One key approach is to consider geographical regions where cognitive users are less likely to impair the performance of primary users.

The analysis of the literature shows that there are generally three generative ways to capture such event: i) *The guard zone approach* [101, 355], in which the secondary user is allowed to transmit as long as it is outside an exclusion region around primary users. The locations of active cognitive users can be modeled for example by a PHP [101], or a MHP [355]. Such coupling in the locations of active cognitive and primary users via exclusion regions renders the analysis of interference very challenging as no tractable expression of the PGFL is available, and then only some estimates of the aggregate interference are obtained. ii) *The max-received power approach* [356], in which the process of active cognitive users is derived as an independent thinning based on the probability that the maximum instantaneous signal power at the level of a random secondary user and sent by active primary users is below a certain threshold. iii) *The outage probability approach* [357], in which the location of active cognitive users follow a PPP with a specific density in such a way to guarantee that the induced outage probability at the

1. Several techniques are considered to overcome such impairments, for example using a mmWave backup link to supplement the FSO main link during adverse weather conditions [350], or using relay-assisted transmissions where the overall FSO path is splitted into small paths with reduced losses [351].

level of the primary network will not exceed a predefined threshold.

Furthermore, CR capability can be used beyond the conventional primary/secondary users setup, typically as a promising technique for distributed interference mitigation in co-channel deployments of HetNets [358]. That is, Femto BSs equipped with CR abilities, can sense the spectrum usage in intra-tier and cross-tier layers and hence select the appropriate spectrum sharing policy to avoid severe interference.

3.3.2 Non-Orthogonal Multiple Access Techniques

Compared to conventional orthogonal multiple access techniques where UEs are served in orthogonal resource blocks, NOMA is introduced as an emerging technology enabling multiple UEs to share the same time-frequency resource block [359]. One key variant is actually power-domain NOMA [47], in which multiple UEs can use the same resource block but at different power levels. That is, UEs are first ordered according to a measure of link quality. Next, the BS superposes the UEs in the same resource block by allocating a fraction of the BS transmit power to each UE so that the worst UE in terms of link quality is assigned the highest power coefficient. In downlink² NOMA reception, successive interference cancellation (SIC) is implemented at each UE in such a way that signals of weaker UEs are decoded and canceled from the observation, while signals of stronger UEs are treated as noise.

Based on such key components of power-domain NOMA, several research works have leveraged SG for performance analysis of NOMA wireless networks. The key modeling choices are: i) how to capture the cluster of UEs to be simultaneously served in the same resource block. Several setups are considered in the literature, for example, consider only the case of two UEs, typically two random UEs in the voronoi tessellation of the serving BS, i.e., random pairing [361, 362, 364, 367], or selective pairing of a cell-center and a cell-edge UE [361–363, 368]. Some works assume a more general setup where the cluster is a constant number of UEs (> 2) [370, 371], a bounded random number of UEs modeled as PPP [365] or as PCP [360, 369], or even two layers of user group in a NOMA-based multicast setup [366]. ii) Which measure of link quality to use in served UEs ordering. Due to its tractability, the common metric is to classify UEs based on their distance to the serving transmitter [360, 361, 365, 370, 371]. Other metrics is to consider the fading gain [362, 368], the instantaneous signal power based on fading and the path loss function [369], or the instantaneous signal power normalized by noise and inter-cell interference power [369]. Also, iii) how to introduce the effect of SIC in the SINR formulation. The generative approach is to introduce a fraction parameter ($\in [0, 1]$) that reflects

2. In uplink NOMA, SIC is implemented at the level of the serving BS, where signals from strong UEs are decoded and cancelled successively, while signals from weak UEs are considered as noise [47, 360].

the accuracy of SIC [369].

3.3.3 In-Band Full-Duplex Technology

IBFD wireless nodes can transmit and receive data simultaneously at the same time/frequency channel. Such capability is expected to double the spectrum efficiency at the expense of increased residual self-interference (SI) between uplink and downlink [48]. SG has been extensively used in the literature to quantify the performance gains achieved by IBFD capability [372–379]. The key model change is actually to account for the SI power after performing cancellation, which can be perfect, imperfect, or without prior knowledge of its effect.

Several models have been considered in the literature to capture such residual SI power gain. The common practice is to consider a constant value dependent on the transmit power, which is a typical scenario in digital cancellation techniques, where the SI intensity after cancellation can be estimated [372–374, 379]. However, in the context of other cancellation techniques where an estimation of the residual SI is not feasible, e.g., analog-domain or propagation-domain schemes as pointed out in [372], the residual SI channel is generally modeled by a random variable, e.g., Rician fading [377, 378], Nakagami- m fading [376]. For instance, modeling and analysis of a wireless network with random combination of HD and IBFD nodes is studied in [373], where it has been shown an enhanced success probability in HD-only networks, even under perfect SI cancellation. However, IBFD-only networks, can outperform their HD peers in terms of throughput due to higher resource utilization.

It is worth noting that the benefits of dense HetNets in terms of capacity improvements are generally limited by the spectrum scarcity. Typically, IBFD as a frequency reuse technique has been investigated in HetNets setup, where it has been reported that network throughput can be maximized under HD-only or IBFD-only HetNets rather than using a combination of them [372]. The problem of optimizing user association policy in IBFD HetNets with DUDA scheme is evaluated in [376]. Also, due to less viable wired backhaul for small cells, IBFD is investigated in [374, 378] as a promising solution for wireless backhaul of small cells. Last but not least, the potential of MIMO antennas to mitigate the extra interference introduced by IBFD is analyzed in [377, 379], while the impact of equipping MIMO RNs with IBFD capability in a cellular network with MIMO BSs is quantified in [375]. A common result is that BSs and IBFD RNs need to be equipped with sufficiently large number of antennas to achieve the expected benefits of IBFD capability.

3.3.4 Physical Layer Security

The usual bit-level cryptographic protocols, requiring heavy overheads and intense coordination, can be generally compromised if eavesdroppers are equipped with convenient computing capabilities. An alternative promising approach is to consider physical layer security besides the conventional error correction mechanisms in such a way to impair the channel capacity of eavesdroppers with limited impact on the QoS of legitimate users [49]. In fact, based on the Wyner's encoding scheme, a transmitter selects two rates, namely, the rate of codewords R_t and the rate of confidential messages R_s , i.e., the secrecy rate. Reliable connection is actually achieved when the instantaneous capacity at the intended receivers is greater than R_t , while a secrecy failure event occurs when the instantaneous capacity at eavesdroppers is above $R_t - R_s$ [380].

SG is typically harnessed to evaluate the impact of key system parameters on the physical layer security of large-scale wireless networks. That is, the interplay between cell association policy and the secrecy capability is investigated in [381–383]. Physical layer security in the context of large-scale networks with NOMA is studied in [384], with MIMO in [385], and with D2D communications in [386]. The sensitivity of mmWave communications to blockages is explored in [387] to establish a trade-off between higher data rates and enhanced secrecy. The question of secure communications in the context of a multiuser VLC network deployed in public areas under a broadcast topology is investigated in [345–347]. There are generally four popular techniques considered in the literature to enhance physical layer security. For instance, i) *the artificial noise approach* in which some artificial noise is added to secret messages in order to make decoding harder to eavesdroppers [385, 388]. ii) *The secrecy guard zone approach* in which confidential messages are transmitted only if eavesdroppers are outside an exclusion region around legitimate nodes [346, 380, 384]. iii) *The friendly interference approach* in which a friendly interference is generated to jam the channel capacity of eavesdroppers with controlled impact on the QoS of legitimate users, e.g., exploit the generated interference by D2D communications [386] or by a set of friendly jammers [389, 390]. iv) *The sectorized transmission approach* where confidential messages are transmitted via directional antennas in order to reduce the likelihood of being intercepted by eavesdroppers [380].

3.4 Chapter Summary

In this chapter, we outlined how SG has been considered to capture the properties of new RANs and quantified the benefits of a number of 5G/B5G enabling technologies. The main goal is to review the milestones established in the past decade in the usage of SG for wireless networks and to predict the challenges in the upcoming decade in the light of 5G/B5G emerging

paradigms.

A STOCHASTIC GEOMETRY BASED APPROACH TO TRACTABLE 5G RNPO

We consider a 3D cellular network in which generalized shadowing and RNPO parameters (antenna height, antenna tilt/azimuth, range expansion (RE)...) are incorporated into the cell-selection model. Using tools from SG, we derive an equivalent 2D network in which no shadowing and RNPO parameters are considered. Next, we derive coverage probability for a tractable case-study network, and the regimes where coverage probability is maximized in addition to the interference-limited one are investigated. An intermediary result is a closed-form expression generator encompassing the Q -function based-expression in [17]. Numerical results confirm the accuracy of our approximations.

4.1 Introduction

With the ongoing proliferation of data-hungry devices and applications, data traffic volumes in the coming years are expected to be multi-fold higher compared to today's levels. One way to tackle this challenge is by deploying UDNs [261]. However, densification will result in large coverage overlap areas, which increases the risk of other-cell interference and then reduces the network performance and system capacity. Consequently, environment characteristics such as shadowing, and RNPO parameters such as antenna height [71], antenna tilt/azimuth angle [391]- [393] and transmit power biasing [19] are strongly required for the analysis of UDNs performance since they affect directly the probability of LOS and NLOS connections and then cells overlapping.

4.1.1 Related Works

Due to its tractability and ability to capture spatial averages, SG has emerged as a potential mathematical tool for modeling cellular networks [17]. In fact, by ignoring shadowing and any

RNPO parameter effect, the seminal work in [17] provides comprehensive understanding about the behavior of UDNs performance. An important outcome is the SINR invariance property, which states that the BS density increases to the point where the noise becomes negligible, after which the SINR remains stable and independent of the BS density. However, using standard path-loss model and ignoring RNPO parameters in more realistic scenarios has raised some limitations [163], calling for an imperative revisitation of the model. Authors of [162] proved that the SINR invariance property is no longer valid when using the dual-slope path-loss model. A similar effect is reported in [71] for elevated BSs, and in [391] for a network using non-directional antennas.

4.1.2 Motivation and Contribution

The motivation behind this analysis is then to find a tractable manner to study UDNs performance when incorporating generalized shadowing and RNPO parameters into the cell-selection model. Using tools from SG, we first *i)* develop a 3D-2D *network equivalence* where a 3D random cellular network with shadowing and RNPO parameters is *stochastically equivalent* to a 2D network in which they are not considered. Next, for mathematical convenience, *ii)* we focus on a case-study based on a *H-LOS* probability model. *iii)* The coverage probability is then computed confirming that our expression is general enough to accommodate several previous expressions. Next, *iv)* we investigate the scaling law of the optimal BS density that maximizes the coverage probability. And finally, *v)* we develop a generator of closed-form expressions for coverage probability under the standard path-loss model, encompassing the \mathcal{Q} -function based results in [17].

4.2 System Model and Assumptions

We consider a downlink cellular network, in which BSs are scattered randomly according to a homogeneous PPP $\Phi_b \subset \mathbb{R}^3$ with density λ_b in [BSs/m²]. We assume that each BS is equipped with directional antennas, has at least one connected user and transmits with a fixed power P_{tx} . Denote σ^2 the variance of the additive noise and $\text{SNR} = P_{\text{tx}}/\sigma^2$. We consider a realization of RNPO parameters of interest: BS antenna elevation height measured in [m] and parametrized by ξ_{x_h} , electrical/mechanical antenna tilt angle by ξ_{x_t} , antenna azimuth angle by ξ_{x_a} and RE by ξ_{x_b} . For each BS $x \in \Phi_b$, we add independent¹ marks $(h_x, \chi_x, \xi_x, \alpha_x, T_x)$, where for the link

1. We omit the dependence scenario here, e.g., ξ_x and α_x may be correlated when a tuning of the RNPO parameters ξ_x can impact α_x by determining the link nature (LOS or NLOS) between a BS and the typical user.

between x and the typical user located at O , h_x denote the small scale fading assumed to be exponentially distributed with unit mean, χ_x is the shadowing effect assumed to be arbitrarily distributed, α_x is the path-loss exponent, T_x is the SINR threshold of x , and ξ_x is the vector $\xi_x = (\xi_{x_h}, \xi_{x_t}, \xi_{x_a}, \xi_{x_b})$ of RNPO parameters, such as the received power at O from the BS $x \in \Phi_b$ is

$$P_{rx} = \frac{\chi_x h_x P_{tx}}{(\Psi(r_x; \alpha_x; \xi_x))^{\alpha_x}}, \quad (96)$$

where r_x is the horizontal distance between x and O measured in [m], and $\Psi(\cdot)$ is a generalized function to capture RNPO parameters combined with the path-loss function. If there is such a function, it is reasonable to require of it the following properties: (i) monotonically increasing such as $\Psi(0, \cdot, \xi_{x_h} = 0^2) = \Psi_0 \geq 1$ at the origin O , this is in order to cover realistic bounded path-loss models and ensure that the received power cannot exceed the transmitted one, (ii) $\Psi(r_x; \cdot; \xi_x) \equiv \Psi(r; \cdot; \xi'_x)$ such as $r = \sqrt{r_x^2 + \xi_{x_h}^2}$ and ξ'_x is the vector $\xi'_x = (\xi_{x_t}, \xi_{x_a}, \xi_{x_b})$, (iii) the mean value of the shot noise process is finite, i.e., from the Campbell's theorem [4, Corollary 1.4.6.], we have

$$\mathbb{E} \left\{ \sum_{x \in \Phi_b} P_{rx} \right\} = \lambda_b P_{tx} \int_{\mathbb{R}^3} \frac{\mathbb{E} \{ \chi_x \} dx}{(\Psi(r_x; \alpha_x; \xi_x))^{\alpha_x}} < \infty, \quad (97)$$

The marked PPP, will be denoted, with a slight abuse of notation, also as Φ_b .

The proposed model is general enough to accommodate various choices of RNPO parameters and path-loss models, e.g., if the power law path-loss is adopted and BS height is the only RNPO parameter considered [71], $\xi_x = \xi_{x_h}$ captures BSs height and $\Psi(r_x; \cdot; \xi_x) = \sqrt{r_x^2 + \xi_x^2}$. When considering also tilt angle [392], azimuth angle [393] and RE bias [19], we have $\Psi(r_x, \alpha_x, \xi_x) = \sqrt{r_x^2 + \xi_{x_h}^2} [G_{\text{tilt}}(\xi_{x_t}) G_{\text{azimut}}(\xi_{x_a}) B(\xi_{x_b})]^{\frac{-1}{\alpha_x}}$, where $G_{\text{tilt}}(\cdot)$ is the antenna vertical radiation pattern parametrized by ξ_{x_t} , $G_{\text{azimut}}(\cdot)$ is the antenna horizontal radiation pattern parametrized by ξ_{x_a} and $B(\cdot)$ is the association bias parametrized by ξ_{x_b} .

2. $\xi_x \equiv 0$ is equivalent to no RNPO parameter considered on x , i.e., BS antenna is omnidirectional with 0 meter elevation and $B(\xi_b) \equiv 1$.

4.2.1 Path Loss process with shadowing and RNPO parameters

We define the path-loss process with shadowing and RNPO parameters (PLPSR) of Φ_b , the point process mapped from Φ_b on \mathbb{R}^+ , as

$$\Sigma = \left\{ y = \chi_x^{-1/\alpha_x} \Psi(r_x, \alpha_x, \xi_x), x \in \Phi_b \right\}. \quad (98)$$

Moreover, in order to capture the SINR threshold distribution we consider the following independently marked PLPSR

$$\Delta = \{(\Sigma, T_x), x \in \Phi_b\}. \quad (99)$$

The following lemma gives the intensity measure of Δ , which generalizes several previous results in [394] [86].

Lemma 1. *The point process Δ is a 1D independently marked PPP on \mathbb{R}^+ with intensity measure*

$$\Lambda_\Delta(s, t) = \frac{4\pi\lambda_b}{3} \mathbb{E} \left\{ \left[\Psi^{-1}(s\chi_x^{\frac{1}{\alpha_x}}; \alpha_x; \xi'_x) \right]^3 \mathbf{1}(T_x \leq t) \right\}, \quad (100)$$

where Ψ^{-1} is the inverse function of Ψ w.r.t. the first argument.

Proof. By the displacement theorem [4, Theorem 1.3.9] and the Campbell's theorem, Δ is a PPP with intensity measure \square

$$\Lambda_\Delta(s, t) = \lambda_b \mathbb{E} \left\{ \int_{\mathbb{R}^3} \mathbf{1} \left(\frac{\Psi(r_x; \alpha_x; \xi_x)}{\chi_x^{\frac{1}{\alpha_x}}} \leq s, T_x \leq t \right) dx \right\} \quad (101)$$

$$\stackrel{(a)}{=} 4\pi\lambda_b \mathbb{E} \left\{ \int_{\mathbb{R}^+} \mathbf{1} \left(\frac{\Psi(r; \alpha_x; \xi'_x)}{\chi_x^{\frac{1}{\alpha_x}}} \leq s \right) \mathbf{1}(T_x \leq t) r^2 dr \right\} \quad (102)$$

$$= \frac{4\pi\lambda_b}{3} \mathbb{E} \left\{ \int_{\mathbb{R}^+} \left[\Psi^{-1}(su^{\frac{1}{\alpha_x}}; \alpha_x; \xi'_x) \right]^3 \mathbf{1}(T_x \leq t) \mathbb{P}_{\chi_x} \{du\} \right\} \quad (103)$$

$$= \frac{4\pi\lambda_b}{3} \mathbb{E} \left\{ \left[\Psi^{-1}(s\chi_x^{\frac{1}{\alpha_x}}; \alpha_x; \xi'_x) \right]^3 \mathbf{1}(T_x \leq t) \right\}, \quad (104)$$

where (a) follows from the marks independence of the process Δ and property (ii) of $\Psi(\cdot)$.

If we assume that $T_x \equiv T$ is constant over all BSs of Φ_b . It is easy to mention from lemma 1 that for the defined RNPO parameters, Δ is generally a homogeneous PPP with density

$$\lambda_\Delta(s) = \lim_{t \rightarrow \infty} \frac{1}{4\pi s^2} \frac{\partial \Lambda_\Delta(s, t)}{\partial s}, \quad (105)$$

independent from s and proportionally related to $\mathbb{E} \left\{ \chi_x^{3/\alpha_x} \right\}$, e.g., when considering only height ($\xi_x \equiv \xi_{x_h}$), we have $\lambda_\Delta = \lambda_b \mathbb{E} \left\{ \chi_x^{3/\alpha_x} \right\} < \infty$.

Definition 1. Similarly to [394, definition 1] and [86, definition 2], a 3D marked PPP Φ_b is said to be equivalent in distribution to a 2D marked PPP Φ'_b if they generate the same 1D marked PPP Δ with the intensity measure $\Lambda(s, t)$.

Proposition 1. The marked process $\Phi_b \in \mathbb{R}^3$ is stochastically equivalent to a marked PPP $\Phi'_b \in \mathbb{R}^2$ in which shadowing and RNPO parameters are not considered, i.e., $\chi'_x \equiv 1$ and $\xi'_x \equiv 0$, and endowed with marks $T'_x \equiv T_x$ whose distribution is

$$G'_s(t) = \frac{1}{4\pi s^2 \lambda_\Delta(s)} \frac{\partial \Lambda_\Delta(s, t)}{\partial s}, \quad (106)$$

and, the density of Φ'_b is expressed as

$$\lambda'_b(s) = 2s \lambda_\Delta(s). \quad (107)$$

Proof. The proof of proposition 1 is analogous to that of [394, proposition 4]. In fact, the intensity measure of Δ' – the independently marked PLPSR of Φ'_b – when $\chi'_x \equiv 1$ and $\xi'_x \equiv 0$ is

$$\Lambda_{\Delta'}(v, t) = 2\pi \mathbb{E} \left\{ \int_{\mathbb{R}^+} \mathbf{1}(u \leq v) \mathbf{1}(T'_x \leq t) \lambda'_b(u) u du \right\} = 2\pi \int_0^v G'_u(t) \lambda'_b(u) u du \stackrel{(a)}{=} \Lambda_\Delta(v, t), \quad (108)$$

where (a) holds if equations (106) and (107) are met. \square

If noise, small scale fading, and path-loss exponent are the same, we have then

$$\text{SINR}(x_0) = \frac{\frac{h_{x_0} \chi_{x_0}}{(\Psi(\|x_0\|, \alpha_{x_0}, \xi_{x_0}))^{\alpha_{x_0}}}}{\sum_{x \in \Phi_b \setminus \{x_0\}} \frac{h_x \chi_x}{(\Psi(\|x\|, \alpha_x, \xi_x))^{\alpha_x}} + \left(\frac{1}{\text{SNR}}\right)} \Bigg|_{\lambda_b} \stackrel{(d)}{=} \frac{h_{y_0} y_0^{-\alpha_{y_0}}}{\sum_{y \in \Phi'_b \setminus \{y_0\}} h_y y^{-\alpha_y} + \frac{1}{\text{SNR}}} \Bigg|_{\lambda'_b} = \text{SINR}(y_0), \quad (109)$$

where $\stackrel{(d)}{=}$ denotes equivalence in distribution, $x_0 = \arg \max_{x \in \Phi_b} \left\{ \chi_x (\Psi(\|x\|, \alpha_x, \xi_x))^{-\alpha_x} \right\}$ and $y_0 = \arg \max_{y \in \Phi'_b} \left\{ y^{-\alpha_y} \right\}$.

4.3 Coverage Probability Analysis

Now, for mathematical convenience and model tractability, we take a minor detour from studying the stochastic equivalence between a 3D network with shadowing and RNPO parameters and a 2D network where they are absorbed into the model. In fact, we assume that the equivalent PPP $\Phi'_b \in \mathbb{R}^2$ is homogeneous $\lambda'_b = \lambda$, the SINR target is constant over all BSs $T'_x = \mathsf{T}$, and the path-loss exponent α'_x is distance-dependent according to the transmission path (LOS or NLOS) between BSs and the typical user, i.e., $\alpha'_x \in \{\alpha_{\text{los}}, \alpha_{\text{nlos}}\}$ such as $\eta = \alpha_{\text{nlos}}/\alpha_{\text{los}} \geq 1$. We consider that each BS $x \in \Phi'_b$ has a LOS path towards the typical user with a LOS probability denoted by P_{los} .

4.3.1 Association Policy Under the H-LOS Probability Model

Since common LOS probability functions are build upon exponentially decreasing functions [395] rendering analysis less tractable, we propose to approximate them by the following piecewise linear model, consistent with the models adopted by 3GPP [70] and dubbed here the *H-LOS* model,

$$P_{\text{los}}(r_x) = \begin{cases} 1 & \text{if } 0 \leq r_x \leq R_{\text{los}} \\ 1 - \frac{r_x - R_{\text{los}}}{R_{\text{nlos}} - R_{\text{los}}} & \text{if } R_{\text{los}} \leq r_x \leq R_{\text{nlos}} \\ 0 & \text{if } r_x > R_{\text{nlos}} \end{cases}, \quad (110)$$

where R_{los} is the maximum link distance between a LOS BS and the typical user such as there are no nearer NLOS BS to the typical user, while R_{nlos} is the minimum link distance between a NLOS BS and the typical user such as there are no farther LOS BS. Mathematically,

$$R_{\text{los}} = \max_{x \in \Phi_{\text{los}}} \{r_x; r_x < r_y, \forall y \in \Phi_{\text{nlos}}\}, R_{\text{nlos}} = \min_{y \in \Phi_{\text{nlos}}} \{r_y; r_x < r_y, \forall x \in \Phi_{\text{los}}\}, \quad (111)$$

such as Φ_{los} and Φ_{nlos} are the PPPs of LOS and NLOS BSs of Φ'_b respectively.

Fig. 18 shows the three regions of the network generated by the *H-LOS* probability model. Note that R_{los} and R_{nlos} are expanded by low shadowing effect and/or RNPO actions that expand cells size (uptilt, increasing association bias, azimuth that avoid blockages...). Shadowing and RNPO parameters are therefore absorbed into the 2D PPP but their effect is still captured via the fluctuation of aggregated parameters R_{los} and R_{nlos} .

The NLOS probability is obtained as $P_{\text{nlos}}(r_x) = 1 - P_{\text{los}}(r_x)$, $\forall x \in \Phi'_b$, and the path-loss

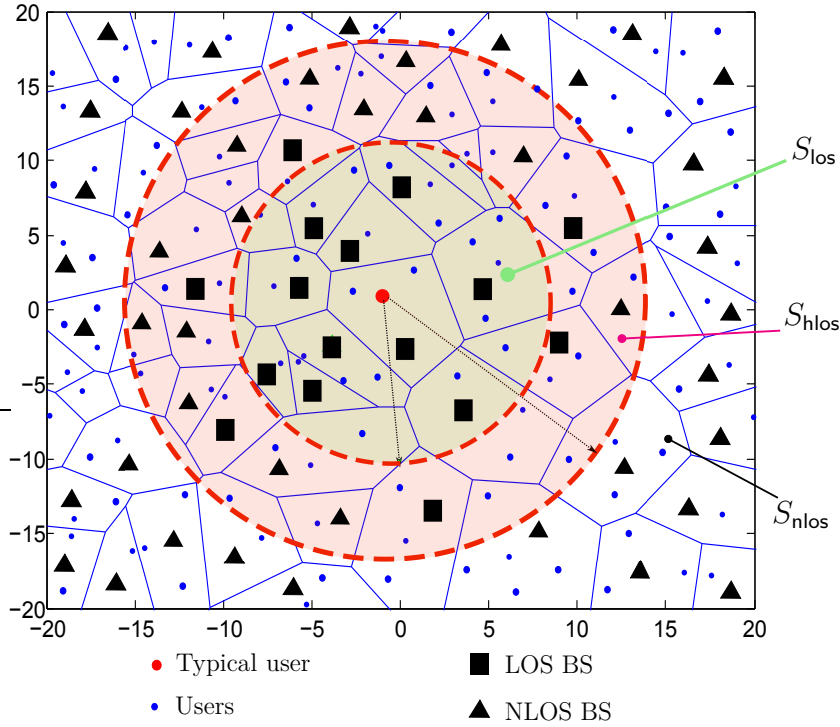


Figure 12 – S_{los} and S_{nlos} regions contain only LOS and NLOS BSs respectively, while S_{hlos} contains a mixture of the two with probability $p(r) = 1 - \frac{r - R_{\text{los}}}{R_{\text{nlos}} - R_{\text{los}}}$ for LOS BSs and $1 - p(r) = \frac{r - R_{\text{los}}}{R_{\text{nlos}} - R_{\text{los}}}$ for NLOS BSs.

function as

$$\ell(r_x) = \begin{cases} r_x^{-\alpha_{\text{los}}} & \text{with probability } P_{\text{los}}(r_x) \\ K r_x^{-\alpha_{\text{nlos}}} & \text{with probability } P_{\text{nlos}}(r_x), \end{cases} \quad (112)$$

where $K \triangleq R_{\text{los}}^{\alpha_{\text{nlos}} - \alpha_{\text{los}}}$ is a parameter to ensure the continuity of the path-loss function as in [162].

For positive reals m and R , we consider the following path-loss functions of interest³

$$\ell_1(m; r_x) = r_x^{-m} \text{ and } \ell_2(R; r_x) = \begin{cases} r_x^{-\alpha_{\text{los}}} & \text{if } r_x \leq R \\ K r_x^{-\alpha_{\text{nlos}}} & \text{if } r_x > R. \end{cases} \quad (113)$$

We consider the average power-based cell association policy. Since $\eta = \alpha_{\text{nlos}}/\alpha_{\text{los}} \geq 1$ and the H -LOS probability model is adopted, the strongest BS is the nearest one in the regions S_{los} and

3. Note that $\ell(\cdot) \equiv \ell_1(\alpha_{\text{los}}; \cdot)$ when $\alpha_{\text{los}} = \alpha_{\text{nlos}}$, i.e., $R_{\text{los}} \rightarrow \infty$ or $R_{\text{nlos}} \rightarrow 0$, and $\ell(\cdot) \equiv \ell_2(R_{\text{los}}; \cdot)$ when $R_{\text{los}} = R_{\text{nlos}}$.

S_{nlos} , while it is not necessarily the case in the transitional region S_{hlos} . To address this issue, we then examine the distribution of distances between the typical user and the serving BS as a result of two events: the transmission link type (LOS or NLOS), and the region to which the serving BS belongs (S_{los} , S_{nlos} or S_{hlos}). For $i \in \{\text{los}, \text{nlos}\}$, denote by S_{1i} the LOS and NLOS BSs of the S_{hlos} region, respectively, by D_i the link distance from the typical user to B_i , the nearest BS of LOS and NLOS BSs respectively, and by S the serving region, i.e., the region that contains the serving BS. For BSs in Φ_i , the PDF of the horizontal distance D_i is then expressed as

$$f_{D_i}(r) = 2\pi\lambda r P_i(r) \exp\left(-2\pi\lambda \int_0^r u P_i(u) du\right) \quad (114)$$

Conditioned on $D_i = r$ and B_i belongs to the S_{hlos} region, B_i is the serving BS if it verifies the following constraints:

$$\begin{cases} D_i^{-\alpha_{\text{los}}} > K D_{\text{nlos}}^{-\alpha_{\text{nlos}}} \Rightarrow D_{\text{nlos}} > r_0 & ; \text{ for } i = \text{los} \\ K D_i^{-\alpha_{\text{nlos}}} > D_{\text{los}}^{-\alpha_{\text{los}}} \Rightarrow D_{\text{los}} > r_1 & ; \text{ for } i = \text{nlos}, \end{cases} \quad (115)$$

where $r_0 = R_{\text{los}}^{1-\frac{1}{\eta}} r^{\frac{1}{\eta}}$ and $r_1 = \text{Min}(R_{\text{nlos}}, r^\eta / R_{\text{los}}^{\eta-1})$ holds since S_{nlos} contains no LOS BS.

Conditioned on $D_i = r$, the probability that the typical user will be connected to B_i is then given by

$$\Pi_i(r_x) = \begin{cases} 1 & \text{if } 0 \leq r \leq R_{\text{los}} \\ \mathbb{P}(D_{\text{nlos}} > r_0) \text{ for } i = \text{los} \\ \mathbb{P}(D_{\text{los}} > r_1) \text{ for } i = \text{nlos} \end{cases} \text{ if } R_{\text{los}} \leq r \leq R_{\text{nlos}}, \quad (116)$$

$$1 \quad \text{if } r \geq R_{\text{nlos}}$$

while $\mathbb{P}(D_{\text{nlos}} > r_0)$ and $\mathbb{P}(D_{\text{los}} > r_1)$ are computed using (191).

For $j \in \mathcal{J} = \{\text{los}, 1\text{los}, 1\text{nlos}, \text{nlos}\}$, The association probability $\mathcal{A}_j = \mathbb{P}(S = S_j)$ that the typical user connects to a BS from S_j , can be computed by integrating $\Pi_i(r) f_{D_i}(r)$ over each region radius interval. An interesting observation for the S_{los} region, is that for fixed parameter R_{los} , $\mathcal{A}_{\text{los}} = 1 - \exp(-\pi\lambda R_{\text{los}}^2)$ increases with λ , while the average number of users connected to S_{los} —expressed as $\widetilde{\mathcal{N}}_{\text{los}} = (\lambda_u / \lambda) \mathcal{A}_{\text{los}}$, where λ_u is the density of the users PPP—decreases. However, for fixed λ , expanding R_{los} leads to an increase in \mathcal{A}_{los} and $\widetilde{\mathcal{N}}_{\text{los}}$ simultaneously. More discussions are provided in the simulation section.

4.3.2 Coverage probability

We define the coverage probability under the path-loss function defined in (112) , as the probability $\mathcal{P}_\ell^{\text{SINR}}(\cdot)$ that the received SINR is greater than the threshold T when the serving BS belongs to one of the four sets S_{los} , $S_{1\text{los}}$, $S_{1\text{nlos}}$ or S_{nlos} .

Theorem 1. *The coverage probability under the path-loss function (112) is given by*

$$\mathcal{P}_\ell^{\text{SINR}}(\cdot) = \mathcal{P}_{\text{los}}^{\text{SINR}} + \mathcal{P}_{1\text{los}}^{\text{SINR}} + \mathcal{P}_{1\text{nlos}}^{\text{SINR}} + \mathcal{P}_{\text{nlos}}^{\text{SINR}}, \quad (117)$$

where for $j \in \mathcal{J} = \{\text{los}, 1\text{los}, 1\text{nlos}, \text{nlos}\}$, $\mathcal{P}_j^{\text{SINR}}$ stands for the coverage probability when the serving BS belongs to S_j and the supplementary equations are listed in the top of the next page such as $a = -1/(R_{\text{nlos}} - R_{\text{los}})$, $b = -R_{\text{nlos}}/(R_{\text{nlos}} - R_{\text{los}})$, $\rho_m = (R_{\text{nlos}}/R_{\text{los}})^m$ for $m \in \mathbb{R}$, $\delta_{p0} = p/\alpha_{\text{los}}$ and $\delta_{p1} = p/\alpha_{\text{nlos}}$ for $p = 2$ or 3 .

Proof. The sketch of the proof is as follows: The coverage probability is expressed as $\mathcal{P}_\ell^{\text{SINR}}(\cdot) = \sum_{j \in \mathcal{J}} \mathcal{P}_j^{\text{SINR}}(\cdot) = \sum_{j \in \mathcal{J}} \mathcal{A}_j \mathbb{P}(\text{SINR} > \mathsf{T} | S = S_j)$, and each component of $\mathcal{P}_\ell^{\text{SINR}}(\cdot)$ will be computed with the following similar steps

$$\mathcal{P}_{\text{los}}^{\text{SINR}} = \mathcal{A}_{\text{los}} \int_0^{R_{\text{los}}} \mathbb{P}(\text{SINR} > \mathsf{T} | u, S = S_{\text{los}}) f_{D_{\text{los}}}(u | S = S_{\text{los}}) du \quad (122)$$

$$\stackrel{(a)}{=} \int_0^{R_{\text{los}}} \mathbb{P}(\text{SINR} > \mathsf{T} | u, S_{\text{los}}) \Pi_{\text{los}}(u) f_{D_{\text{los}}}(u) du \quad (123)$$

$$\stackrel{(b)}{=} 2\pi\lambda \int_0^{R_{\text{los}}} u \exp\left(-\frac{\mathsf{T}}{\text{SNR}} u^{\alpha_{\text{los}}} - \pi\lambda u^2\right) \mathcal{L}_{I_{S_{\text{los}} \setminus \{B_{\text{los}}\}}}(s) \mathcal{L}_{I_{S_{1\text{los}}}}(s) \mathcal{L}_{I_{S_{1\text{nlos}}}}(s) \mathcal{L}_{I_{S_{\text{nlos}}}}(s) du, \quad (124)$$

where $s = \mathsf{T}u^{\alpha_{\text{los}}}$, (a) follows from $f_{D_{\text{los}}}(u | S = S_{\text{los}}) = \frac{d}{du} \frac{\mathbb{P}(D_{\text{los}} \leq u, S = S_{\text{los}})}{\mathbb{P}(S = S_{\text{los}})} = \frac{\Pi_{\text{los}}(u) f_{D_{\text{los}}}(u)}{\mathcal{A}_{\text{los}}}$, (b) holds since $h_{B_{\text{los}}} \sim \exp(1)$ and the aggregated interference $I_{\text{agg}} = \sum_{x \in \Phi'_b \setminus \{B_{\text{los}}\}} h_x \ell(r_x)$ is seen as the summation of the interference power (normalized by P_{tx}) from each set $U \in \{S_{\text{los}} \setminus \{B_{\text{los}}\}, S_{1\text{los}}, S_{1\text{nlos}}, S_{\text{nlos}}\}$, i.e.,

$$\mathcal{L}_{I_{\text{agg}}}(s) = \mathcal{L}_{I_{S_{\text{los}} \setminus \{B_{\text{los}}\}}}(s) \mathcal{L}_{I_{S_{1\text{los}}}}(s) \mathcal{L}_{I_{S_{1\text{nlos}}}}(s) \mathcal{L}_{I_{S_{\text{nlos}}}}(s). \quad (125)$$

We get the desired result for $\mathcal{P}_{\text{los}}^{\text{SINR}}(\cdot)$ in (118) by using the PGFL theorem to compute the Laplace transforms $\mathcal{L}_{I_U}(\cdot)$ and some variable changes. \square

Although the expression of coverage probability under the H -LOS model is in complicated form, it instigates an intuitive algorithmic development. Moreover, the expression is general enough to accommodate several previous expressions. For example, it reflects the 3GPP case 1

$$\mathcal{P}_{\text{los}}^{\text{SINR}}(\mathsf{T}) = \pi\lambda R_{\text{los}}^2 \int_0^1 \exp\left(-\frac{\mathsf{T}R_{\text{los}}^{\alpha_{\text{los}}}}{\text{SNR}}x^{\frac{\alpha_{\text{los}}}{2}} - \pi\lambda R_{\text{los}}^2 \left[A_{\text{los}}^{(1)}(x) + \rho_2 A_{\text{los}}^{(2)}(x) + \frac{2a}{3}R_{\text{los}}A_{\text{los}}^{(3)}(x) + bA_{\text{los}}^{(4)}(x)\right]\right) dx, \quad (118)$$

$$\mathcal{P}_{1\text{los}}^{\text{SINR}}(\mathsf{T}) = 2\pi\lambda \int_{R_{\text{los}}}^{R_{\text{nlos}}} (ar^2 + br) \exp\left(-\frac{\mathsf{T}}{\text{SNR}}r^{\alpha_{\text{los}}} - \pi\lambda \left[r_0^2 A_{1\text{los}}^{(1)}(r) + R_{\text{nlos}}^2 A_{1\text{los}}^{(2)}(r) + \frac{2a}{3}A_{1\text{los}}^{(3)}(r) + bA_{1\text{los}}^{(4)}(r)\right]\right) dr, \quad (119)$$

$$\mathcal{P}_{1\text{nlos}}^{\text{SINR}}(\mathsf{T}) = 2\pi\lambda \int_{R_{\text{los}}}^{R_{\text{nlos}}} ([1-b]r - ar^2) \exp\left(\frac{-\mathsf{T}r^{\alpha_{\text{nlos}}}}{K\text{SNR}} - \pi\lambda \left[r^2 A_{1\text{nlos}}^{(1)}(r) + R_{\text{nlos}}^2 A_{1\text{nlos}}^{(2)}(r) + \frac{2a}{3}A_{1\text{nlos}}^{(3)}(r) + bA_{1\text{nlos}}^{(4)}(r)\right]\right) dr, \quad (120)$$

$$\mathcal{P}_{\text{nlos}}^{\text{SINR}}(\mathsf{T}) = \pi\lambda R_{\text{nlos}}^2 \int_1^\infty \exp\left(-\frac{\mathsf{T}R_{\text{los}}^{\alpha_{\text{los}}}\rho_{\alpha_{\text{nlos}}}}{\text{SNR}}x^{\frac{\alpha_{\text{nlos}}}{2}} - \pi\lambda R_{\text{nlos}}^2 x F_{-\delta_{21}}(\mathsf{T})\right) dx, \quad (121)$$

$$A_{\text{los}}^{(1)}(x) = x \left[1 - F_{\delta_{20}}\left(\frac{1}{\mathsf{T}}\right)\right] + \rho_2 F_{\delta_{21}}\left(\frac{\rho_{\alpha_{\text{nlos}}}}{\mathsf{T}x^{\frac{1}{\delta_{20}}}}\right) + \left[F_{\delta_{20}}\left(\frac{1}{\mathsf{T}x^{\frac{1}{\delta_{20}}}}\right) - F_{\delta_{21}}\left(\frac{1}{\mathsf{T}x^{\frac{1}{\delta_{20}}}}\right)\right], \quad A_{\text{los}}^{(2)}(x) = F_{-\delta_{21}}\left(\frac{\mathsf{T}}{\rho_{\alpha_{\text{nlos}}}}x^{\frac{1}{\delta_{20}}}\right) - 1,$$

$$A_{\text{los}}^{(3)}(x) = \rho_3 \left[F_{\delta_{30}}\left(\frac{\rho_{\alpha_{\text{los}}}}{\mathsf{T}x^{\frac{1}{\delta_{20}}}}\right) - F_{\delta_{31}}\left(\frac{\rho_{\alpha_{\text{nlos}}}}{\mathsf{T}x^{\frac{1}{\delta_{20}}}}\right)\right] - \left[F_{\delta_{30}}\left(\frac{1}{\mathsf{T}x^{\frac{1}{\delta_{20}}}}\right) - F_{\delta_{31}}\left(\frac{1}{\mathsf{T}x^{\frac{1}{\delta_{20}}}}\right)\right],$$

$$A_{\text{los}}^{(4)}(x) = \rho_2 \left[F_{\delta_{20}}\left(\frac{\rho_{\alpha_{\text{los}}}}{\mathsf{T}x^{\frac{1}{\delta_{20}}}}\right) - F_{\delta_{21}}\left(\frac{\rho_{\alpha_{\text{nlos}}}}{\mathsf{T}x^{\frac{1}{\delta_{20}}}}\right)\right] - \left[F_{\delta_{20}}\left(\frac{1}{\mathsf{T}x^{\frac{1}{\delta_{20}}}}\right) - F_{\delta_{21}}\left(\frac{1}{\mathsf{T}x^{\frac{1}{\delta_{20}}}}\right)\right],$$

$$A_{1\text{los}}^{(1)}(r) = 1 - F_{\delta_{21}}\left(\frac{1}{\mathsf{T}}\right), \quad A_{1\text{los}}^{(2)}(r) = F_{\delta_{21}}\left(\frac{\rho_{\alpha_{\text{nlos}}}R_{\text{los}}^{\alpha_{\text{los}}}}{\mathsf{T}r^{\alpha_{\text{los}}}}\right) + F_{-\delta_{21}}\left(\frac{\mathsf{T}r^{\alpha_{\text{los}}}}{\rho_{\alpha_{\text{nlos}}}R_{\text{los}}^{\alpha_{\text{los}}}}\right) - 1,$$

$$A_{1\text{los}}^{(3)}(r) = r_0^3 \left[F_{\delta_{31}}\left(\frac{1}{\mathsf{T}}\right) - 1\right] - r^3 \left[F_{\delta_{30}}\left(\frac{1}{\mathsf{T}}\right) - 1\right] + R_{\text{nlos}}^3 \left[F_{\delta_{30}}\left(\frac{R_{\text{nlos}}^{\alpha_{\text{los}}}}{\mathsf{T}r^{\alpha_{\text{los}}}}\right) - F_{\delta_{31}}\left(\frac{\rho_{\alpha_{\text{nlos}}}R_{\text{los}}^{\alpha_{\text{los}}}}{\mathsf{T}r^{\alpha_{\text{los}}}}\right)\right],$$

$$A_{1\text{los}}^{(4)}(r) = r_0^2 \left[F_{\delta_{21}}\left(\frac{1}{\mathsf{T}}\right) - 1\right] - r^2 \left[F_{\delta_{20}}\left(\frac{1}{\mathsf{T}}\right) - 1\right] + R_{\text{nlos}}^2 \left[F_{\delta_{20}}\left(\frac{R_{\text{nlos}}^{\alpha_{\text{los}}}}{\mathsf{T}r^{\alpha_{\text{los}}}}\right) - F_{\delta_{21}}\left(\frac{\rho_{\alpha_{\text{nlos}}}R_{\text{los}}^{\alpha_{\text{los}}}}{\mathsf{T}r^{\alpha_{\text{los}}}}\right)\right],$$

$$A_{1\text{nlos}}^{(1)}(r) = 1 - F_{\delta_{21}}\left(\frac{1}{\mathsf{T}}\right), \quad A_{1\text{nlos}}^{(2)}(r) = F_{\delta_{21}}\left(\frac{R_{\text{nlos}}^{\alpha_{\text{nlos}}}}{\mathsf{T}r^{\alpha_{\text{nlos}}}}\right) + F_{-\delta_{21}}\left(\frac{\mathsf{T}r^{\alpha_{\text{nlos}}}}{R_{\text{nlos}}^{\alpha_{\text{nlos}}}}\right) - 1,$$

$$A_{1\text{nlos}}^{(3)}(r) = r^3 \left[F_{\delta_{31}}\left(\frac{1}{\mathsf{T}}\right) - 1\right] - r_1^3 \left[F_{\delta_{30}}\left(\frac{K r_1^{\alpha_{\text{los}}}}{\mathsf{T}r^{\alpha_{\text{nlos}}}}\right) - 1\right] + R_{\text{nlos}}^3 \left[F_{\delta_{30}}\left(\frac{\rho_{\alpha_{\text{los}}}R_{\text{los}}^{\alpha_{\text{nlos}}}}{\mathsf{T}r^{\alpha_{\text{nlos}}}}\right) - F_{\delta_{31}}\left(\frac{R_{\text{nlos}}^{\alpha_{\text{nlos}}}}{\mathsf{T}r^{\alpha_{\text{nlos}}}}\right)\right],$$

$$A_{1\text{nlos}}^{(4)}(r) = r^2 \left[F_{\delta_{21}}\left(\frac{1}{\mathsf{T}}\right) - 1\right] - r_1^2 \left[F_{\delta_{20}}\left(\frac{K r_1^{\alpha_{\text{los}}}}{\mathsf{T}r^{\alpha_{\text{nlos}}}}\right) - 1\right] + R_{\text{nlos}}^2 \left[F_{\delta_{20}}\left(\frac{\rho_{\alpha_{\text{los}}}R_{\text{los}}^{\alpha_{\text{nlos}}}}{\mathsf{T}r^{\alpha_{\text{nlos}}}}\right) - F_{\delta_{21}}\left(\frac{R_{\text{nlos}}^{\alpha_{\text{nlos}}}}{\mathsf{T}r^{\alpha_{\text{nlos}}}}\right)\right].$$

study in [70] when $R_{\text{los}} \rightarrow 0$, and approximates the 3GPP case 2 study when $R_{\text{los}} \rightarrow \epsilon d_1$ and $R_{\text{nlos}} \rightarrow d_1/\epsilon$ where $0 < \epsilon < 1$ is to adjust the approximation's error. More precisely, (117) generally approximates the coverage analysis under the models in [395] by simply adjusting the parameters a and b . Furthermore, when $R_{\text{nlos}} \simeq R_{\text{los}}$, ℓ becomes a dual-slope path-loss model ℓ_2 and (117) is simplified under the expression in [3, Th. 1]. If $\alpha_{\text{nlos}} \simeq \alpha_{\text{los}}$, (117) will be the same expression as [2, Th. 2].

4.3.3 The Regime of UDNs

We consider the scenario of ultra-dense networks [261], where the interference I_{agg} dominates the noise normalized by the transmit power (σ^2/P_{tx}). SINR is then approximated by $\text{SIR}_\ell \triangleq \text{SINR}_\ell |_{\frac{\sigma^2}{P_{\text{tx}}}=0}$

Remark 1. *In the interference-limited regime, the coverage probability in (117) remains invariant as long as λR_{los}^2 and $\lambda R_{\text{nlos}}^2$ are invariant. In other words, the impact on coverage probability of increasing/decreasing λ is analogous to increasing/decreasing $(R_{\text{los}}, R_{\text{nlos}})$ simultaneously, which is a generalization of [162, Fact 1].*

In the following proposition, comparisons are made for \mathcal{P}^{SIR} under ℓ_1 , ℓ_2 and ℓ .

Proposition 2. *The following SIR coverage ordering holds for arbitrary $0 < \alpha_{\text{los}} \leq \alpha_{\text{nlos}}$ and $R_{\text{los}} \leq R_{\text{nlos}}$*

$$(i) \mathcal{P}_{\ell(\cdot)}^{\text{SIR}} > \mathcal{P}_{\ell_2(R_{\text{nlos}};\cdot)}^{\text{SIR}} > \mathcal{P}_{\ell_1(\alpha_{\text{los}};\cdot)}^{\text{SIR}}. \quad (126)$$

$$(ii) \mathcal{P}_{\ell(\cdot)}^{\text{SIR}} < \mathcal{P}_{\ell_2(R_{\text{los}};\cdot)}^{\text{SIR}} < \mathcal{P}_{\ell_1(\alpha_{\text{nlos}};\cdot)}^{\text{SIR}}. \quad (127)$$

$$(iii) \lim_{\lambda \rightarrow \infty} \mathcal{P}_{\ell(\cdot)}^{\text{SINR}} = \lim_{\lambda \rightarrow \infty} \mathcal{P}_{\ell(\cdot)}^{\text{SIR}} = \mathcal{P}_{\ell_1(\alpha_{\text{los}};\cdot)}^{\text{SIR}}. \quad (128)$$

$$(iv) \lim_{\lambda \rightarrow \infty} \mathcal{P}_{\ell(\cdot)}^{\text{SINR}} = \lim_{\lambda \rightarrow \infty} \mathcal{P}_{\ell(\cdot)}^{\text{SIR}}(\cdot) = 0 \text{ when } \alpha_{\text{los}} \leq 2. \quad (129)$$

$$(v) \lim_{\lambda \rightarrow 0} \mathcal{P}_{\ell(\cdot)}^{\text{SIR}} = \mathcal{P}_{\ell_1(\alpha_{\text{nlos}};\cdot)}^{\text{SIR}}. \quad (130)$$

Proof. The proof of (i) and (ii) is similar to that of [162, Lemma 2], the main change is to proceed by considering the two cases when the serving BS $x_0 \in (S_{\text{los}} \cup S_{\text{nlos}})$ (where $\ell \equiv \ell_2$) and $x_0 \in S_{\text{hlos}}$. (iii) and (v) follows from the observation of Remark 1 where $\lambda \rightarrow \infty \equiv (R_{\text{los}}, R_{\text{nlos}}) \rightarrow \infty$ and $\lambda \rightarrow 0 \equiv (R_{\text{los}}, R_{\text{nlos}}) \rightarrow 0$. Such scaling in the definition of $\ell(\cdot)$ results in $\ell_1(\alpha_{\text{los}};\cdot)$ or $\ell_1(\alpha_{\text{nlos}};\cdot)$. (iv) follows from combining (ii) and [162, Proposition 1]. The proof is completed by the observation that $\mathcal{P}_{\ell(\cdot)}^{\text{SINR}} \rightarrow \mathcal{P}_{\ell(\cdot)}^{\text{SIR}}$ as $\lambda \rightarrow \infty$. \square

4.3.4 The Regime of Optimal Network Density

We define the optimal BS density $\lambda_\ell^{\text{opt}}$ as the specific λ that maximizes the coverage probability under the path-loss function ℓ . Mathematically,

$$\lambda_\ell^{\text{opt}}(\cdot) = \arg_{\lambda} \left(\frac{\partial \mathcal{P}_{\ell}^{\text{SINR}}(\cdot)}{\partial \lambda} = 0 \right). \quad (131)$$

Using a combination of proposition 2 and [162, lemma 4], $\mathcal{P}_\ell^{\text{SINR}}(\lambda)$ is a decreasing function when $\lambda > \lambda_\ell^{\text{opt}}$ and $\text{SINR} \simeq \text{SIR}$. $\lambda_\ell^{\text{opt}}$ can then be seen as the BS density to enter the SIR regime. We define *the optimal regime* under ℓ , the regime where the BS density $\lambda \simeq \lambda_\ell^{\text{opt}}$. In this regime, the noise normalized by the transmit power is small w.r.t. the aggregated interference but it is non-zero. Consequently, (i)-(ii) of proposition 2 are at first stages to be met. We have then

$$\mathcal{P}_{\ell_1(\alpha_{\text{los};\cdot})}^{\text{SINR}} < \mathcal{P}_{\ell(\cdot)}^{\text{SINR}} < \mathcal{P}_{\ell_1(\alpha_{\text{nlos};\cdot})}^{\text{SINR}}. \quad (132)$$

$$\lambda_{\ell_2(\text{R}_{\text{nlos};\cdot})}^{\text{opt}} < \lambda_\ell^{\text{opt}} < \lambda_{\ell_2(\text{R}_{\text{los};\cdot})}^{\text{opt}}. \quad (133)$$

Due to the lack of general closed-form expression for $\mathcal{P}_{\ell_1(\alpha;\cdot)}^{\text{SINR}}$ that would avoid the computation of a two-fold numerical integral in [17, theorem 1], almost all literature works focus on the \mathcal{Q} -function based expression when the path-loss exponent $\alpha = 4$, which is only typical for terrestrial propagation at moderate to large distances. The following proposition overcome this limitation by developing closed-form expressions for $\mathcal{P}_{\ell_1(\alpha;\cdot)}^{\text{SINR}}$ considering all integer $\alpha > 2$ (not only $\alpha = 4$) and then conclude closed-form bounds for $\mathcal{P}_{\ell(\cdot)}^{\text{SINR}}$ in the optimal regime.

Proposition 3. *For integer path-loss exponents α_{los} and α_{nlos} such as $2 < \alpha_{\text{los}} < \alpha_{\text{nlos}}$. $\mathcal{P}_\ell^{\text{SINR}}$ is bounded in the optimal regime as follows $\mathcal{P}_{\ell_1(\alpha_{\text{los};\cdot})}^{\text{SINR}} < \mathcal{P}_{\ell(\cdot)}^{\text{SINR}} < \mathcal{P}_{\ell_1(\alpha_{\text{nlos};\cdot})}^{\text{SINR}}$ such as the lower and upper bounds are achievable by respectively increasing R_{los} and decreasing R_{nlos} , and where for even and odd values of α , respectively*

$$\mathcal{P}_{\ell_1(\alpha;\cdot)}^{\text{SINR}} = \frac{2\pi\lambda}{\alpha (\text{T}/\text{SNR})^{\frac{2}{\alpha}}} \sum_{k=0}^{\frac{\alpha}{2}-1} \frac{(-1)^k \kappa^k}{k!} \Gamma\left(\frac{2+2k}{\alpha}\right) {}_1F_{\frac{\alpha-2}{2}}\left(\begin{matrix} 1 \\ \frac{4+2k}{\alpha}, \dots, \frac{\alpha+2k}{\alpha} \end{matrix} \middle| \frac{(-\kappa)^{\frac{\alpha}{2}}}{\left(\frac{\alpha}{2}\right)^{\frac{\alpha}{2}}}\right), \quad (134)$$

$$\mathcal{P}_{\ell_1(\alpha;\cdot)}^{\text{SINR}} = \frac{2\pi\lambda}{\alpha (\text{T}/\text{SNR})^{\frac{2}{\alpha}}} \sum_{k=0}^{\alpha-1} \frac{(-1)^k \kappa^k}{k!} \Gamma\left(\frac{2+2k}{\alpha}\right) {}_2F_{\alpha-1}\left(\begin{matrix} 1, \frac{1}{2} + \frac{k+1}{\alpha} \\ \frac{2+k}{\alpha}, \dots, \frac{\alpha+k}{\alpha} \end{matrix} \middle| \frac{4(-\kappa)^\alpha}{\alpha^\alpha}\right), \quad (135)$$

such as $\kappa = \frac{\pi\lambda F_{-\delta}(\text{T})}{(\text{T}/\text{SNR})^\delta}$, $\delta = \frac{2}{\alpha}$, $\Gamma(\cdot)$ is the complete gamma function and ${}_pF_q(\cdot)$ is the generalized hypergeometric function.

Proof. By the variable change $(\text{T}/\text{SNR})x^{\alpha/2} \rightarrow x$, the expression of $\mathcal{P}_{\ell_1(\alpha;\cdot)}^{\text{SINR}}$ in [17, Theorem 2] can be rewritten as

$$\mathcal{P}_{\ell_1(\alpha;\cdot)}^{\text{SINR}} = \frac{2\pi\lambda}{\alpha (\text{T}/\text{SNR})^{\frac{2}{\alpha}}} \int_0^\infty x^{\frac{2}{\alpha}-1} e^{-x} e^{-\kappa x^{2/\alpha}} dx = \frac{2\pi\lambda}{\alpha (\text{T}/\text{SNR})^{\frac{2}{\alpha}}} \int_0^\infty x^{\frac{2}{\alpha}-1} e^{-x} {}_0F_0(\cdot; \cdot; -\kappa x^{2/\alpha}) dx.$$

Depending on the parity of α , we use [396, Eq. (43)] (with $\alpha/2$ order for the even case and α order for the odd one). Next, we explore the integral transformation of hypergeometric functions in [397, (1.7.525)]. The proof is completed by combining (132) with Remark 1. \square

Based on proposition 3, the \mathcal{Q} -function based expression for $\alpha = 4$ in [17], can be rewritten as

$$\mathcal{P}_{\ell_1(4; \cdot)}^{\text{SINR}} = \frac{\pi^{\frac{3}{2}} \lambda}{2\sqrt{\mathbb{T}/\text{SNR}}} \left[{}_0F_0\left(-; - \middle| \frac{\kappa^2}{4}\right) - \frac{\kappa}{\sqrt{\pi}} {}_1F_1\left(1; \frac{3}{2} \middle| \frac{\kappa^2}{4}\right) \right] = \frac{\pi^{\frac{3}{2}} \lambda}{\sqrt{\mathbb{T}/\text{SNR}}} \mathcal{Q}\left(\frac{\kappa}{\sqrt{2}}\right) \exp\left(\frac{\kappa^2}{4}\right).$$

While proposition 3 gives a complete characterization of \mathcal{P}_ℓ in the optimal regime. The following proposition gives the scaling law of $\lambda_\ell^{\text{opt}}$ as $R_{\text{los}} \rightarrow \infty$ and $R_{\text{nlos}} \rightarrow 0$.

Proposition 4. *Under the H-LOS probability model such as $2 < \alpha_{\text{los}} < \alpha_{\text{nlos}}$, the optimal BS density scales as follows*

$$(i) \lambda_\ell^{\text{opt}} = \Omega\left(\left(\frac{\mathbb{T}}{\text{SNR}}\right)^{\delta_{20}} \frac{1}{\pi F_{-\delta_{20}}(\mathbb{T})}\right) \text{ if } R_{\text{los}} \rightarrow \infty. \quad (136)$$

$$(ii) \lambda_\ell^{\text{opt}} = O\left(\left(\frac{\mathbb{T}}{\text{SNR}}\right)^{\delta_{21}} \frac{1}{\pi F_{-\delta_{21}}(\mathbb{T})}\right) \text{ if } R_{\text{nlos}} \rightarrow 0. \quad (137)$$

Proof. Using [162, Theorem 1], $\mathcal{P}_{\ell_2(\mathbb{R}_{c; \cdot})}^{\text{SINR}}$ is expressed for a given radius R_c as

$$\mathcal{P}_{\ell_2}^{\text{SINR}} = \underbrace{\lambda\pi R_c^2 \int_0^1 e^{-I_f(x) - W_f(x)} dx}_{f(\cdot)} + \underbrace{\lambda\pi R_c^2 \int_1^\infty e^{-I_g(x) - W_g(x)} dx}_{g(\cdot)}, \quad (138)$$

$$\text{where } I_f(x) = \lambda\pi R_c^2 \left(F_{\delta_{20}}\left(\frac{1}{\mathbb{T}x^{\frac{1}{\delta_{20}}}}\right) + F_{-\delta_{20}}\left(\mathbb{T}x^{\frac{1}{\delta_{20}}}\right) \right) + \lambda\pi R_c^2 x \left(1 - F_{\delta_{20}}\left(\frac{1}{\mathbb{T}}\right) \right) - \lambda\pi R_c^2,$$

$$W_f(x) = \frac{\mathbb{T}}{\text{SNR}} R_c^{\alpha_{\text{los}}} x^{\frac{\alpha_{\text{los}}}{2}}, \quad I_g(x) = \pi\lambda R_c^2 x F_{-\delta_{21}}(\mathbb{T}), \quad \text{and } W_g(x) = \frac{\mathbb{T}}{\text{SNR}} R_c^{\alpha_{\text{los}}} x^{\frac{\alpha_{\text{nlos}}}{2}}.$$

We note that I_f and I_g are the terms reflecting interference while W_f and W_g are those capturing noise. In the optimal regime under ℓ_2 , i.e., $\lambda \simeq \lambda_{\ell_2(\mathbb{R}_{c; \cdot})}^{\text{opt}}$, W_f and W_g are respectively negligible w.r.t. I_f and I_g but non zero. We expand then the terms $e^{-W_f(x)}$ and $e^{-W_g(x)}$ as $e^{-\mu} = \sum_{k=0}^n \frac{(-\mu)^k}{k!} + E_n(\mu)$, where E_n is the error of approximation such as $E_n(\mu) \leq \frac{|\mu|^{n+1}}{(n+1)!}$. The

error of approximation of $\mathcal{P}_{\ell_2}^{\text{SINR}}$ in the optimal regime is then upper bounded as

$$|E_n| \leq \lambda \pi R_c^2 A^{n+1} U_n + \lambda \pi R_c^2 B^{n+1} V_n, \quad (139)$$

$$\text{where } A \simeq \frac{\mathbb{T}}{(\lambda \pi F_{-\delta_{20}}(\mathbb{T}))^{\frac{\alpha_{\text{los}}}{2}} \text{SNR}}, B = \frac{\mathbb{T} R_c^{\alpha_{\text{los}}}}{(\lambda \pi R_c^2 F_{-\delta_{21}}(\mathbb{T}))^{\frac{\alpha_{\text{nos}}}{2}} \text{SNR}}, U_n = \frac{\gamma((n+1)^{\frac{\alpha_{\text{los}}}{2}} + 1, \pi \lambda R_c^2 F_{-\delta_{20}}(\mathbb{T}))}{(n+1)!},$$

$$\text{and } V_n = \frac{\Gamma((n+1)^{\frac{\alpha_{\text{nos}}}{2}} + 1, \pi \lambda R_c^2 F_{-\delta_{21}}(\mathbb{T}))}{(n+1)!}.$$

For any given error tolerance ϵ , the bound (139) gives

$$A \leq \left(\frac{\epsilon}{\lambda \pi R_c^2 2U_n} \right)^{\frac{1}{n+1}}, \quad B \leq \left(\frac{\epsilon}{\lambda \pi R_c^2 2V_n} \right)^{\frac{1}{n+1}}. \quad (140)$$

If $R_c \rightarrow \infty$ and since $\alpha_{\text{los}} > 2$, $U_n \rightarrow \infty$ as $n \rightarrow \infty$ and then $\left(\frac{\epsilon}{\lambda \pi R_c^2 2U_n} \right)^{\frac{1}{n+1}} \rightarrow 1$ as $n \rightarrow \infty$. (140).1 simplifies as

$$\lambda \geq \left(\frac{\mathbb{T}}{\text{SNR}} \right)^{\delta_{20}} \frac{1}{\pi F_{-\delta_{20}}(\mathbb{T})} \Rightarrow \exists \omega_f \geq 1 \text{ such as } \lambda_{\ell_2(\mathbf{R}_{c;\cdot})}^{\text{opt}} = \left(\frac{\mathbb{T}}{\text{SNR}} \right)^{\delta_{20}} \frac{\omega_f}{\pi F_{-\delta_{20}}(\mathbb{T})}. \quad (141)$$

If $R_c \rightarrow 0$ and since $\alpha_{\text{nos}} > 2$, $V_n \rightarrow \infty$ as $n \rightarrow \infty$ and then $\left(\frac{\epsilon}{\lambda \pi R_c^2 2V_n} \right)^{\frac{1}{n+1}} \rightarrow 1$ as $n \rightarrow \infty$. (140).2 simplifies as

$$\lambda \geq \left(\frac{\mathbb{T}}{\text{SNR}} \right)^{\delta_{21}} \frac{1}{\pi F_{-\delta_{21}}(\mathbb{T})}, \Rightarrow \exists \omega_g \geq 1 \text{ such as } \lambda_{\ell_2(\mathbf{R}_{c;\cdot})}^{\text{opt}} = \left(\frac{\mathbb{T}}{\text{SNR}} \right)^{\delta_{21}} \frac{\omega_g}{\pi F_{-\delta_{21}}(\mathbb{T})}. \quad (142)$$

The proof is completed by combining (141) and (142) with (133). \square

By varying one parameter and fixing the others in (136) and (137), $\lambda_{\ell}^{\text{opt}}$ is monotonically increasing with the SINR target \mathbb{T} , the noise variance σ^2 and the path-loss exponents, while it is decreasing with the transmit power P_{tx} (intuitively, the higher you increase P_{tx} the less you will need more BSs). Besides, $\lambda_{\ell}^{\text{opt}}$ cannot be increased indefinitely with \mathbb{T} . In fact, for a real $0 < m < 1$, $\psi_m : \mathbb{T} \rightarrow \mathbb{T}^m / F_{-m}(\mathbb{T})$ is an increasing function bounded as $\psi_m(\mathbb{T}) \leq \lim_{\mathbb{T} \rightarrow \infty} \psi_m(\mathbb{T}) = \frac{1}{\varphi(m)}$, where $\varphi(m) = \int_0^\infty \frac{du}{1+u^{\frac{1}{m}}}$ is finite (Riemann integral).

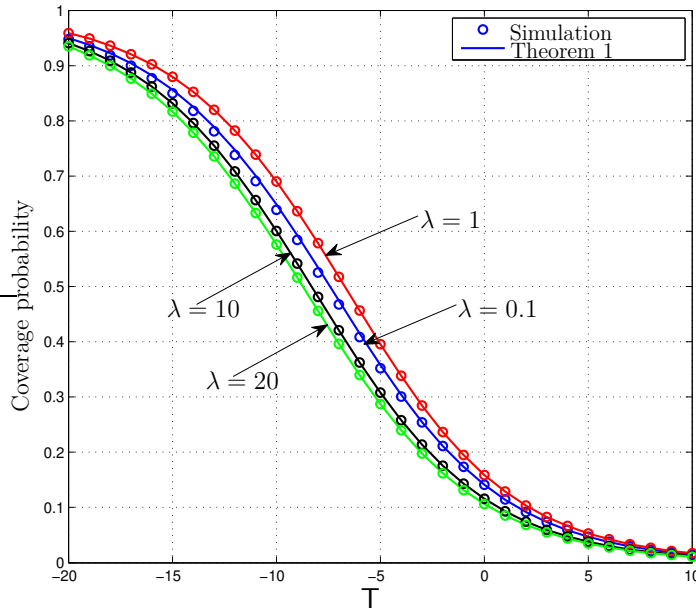


Figure 13 – Coverage probability from both Theorem 1 and simulation results. $\alpha_{\text{los}} = 2$, $\alpha_{\text{nlos}} = 4$, $R_{\text{los}} = 1$ and $R_{\text{nlos}} = 10$.

4.4 Numerical Results

In this section, we present numerical results to assess our theoretical analysis. In the following, $\text{SNR} = 0$ dB, integral expressions are evaluated using Matlab and Monte carlo simulations are performed with 10^6 iterations.

4.4.1 Validation of the Model

The expression of coverage probability in (117) configured with path-loss exponents $\alpha_{\text{los}} = 2$, $\alpha_{\text{nlos}} = 4$ and a given realization of BSs, shadowing and RNPO actions such as $R_{\text{los}} = 1$ and $R_{\text{nlos}} = 10$, is plotted in Fig. 13. The plots show that the analytical expression match the simulation results well, and hence the accuracy of our theoretical analysis is validated. In particular, Fig. 13 shows that the coverage probability increases at first with network density λ until achieving the optimal value $\lambda_{\ell}^{\text{opt}}$, after that $\mathcal{P}_{\ell}^{\text{SINR}}$ shrinks down as densification continue.

4.4.2 Operational Regimes

A combination of Fig. 16 (a) and (b), reveals that when $\lambda \ll 1$ ($\lambda < 0.002$ BSs/m²), the serving BS is potentially to be a BS from the S_{nlos} set and the operational regime is the noise-limited regime where $I_{\text{agg}} \ll (\sigma^2/P_{\text{tx}})$; this is due to the observation that the network will be more sparse and the inter-distance between BSs is high enough such that I_{agg} can be ignored. As λ slightly increases ($\lambda \rightarrow 0.002$ BSs/m²), the typical user is more likely to connect unsteadily to

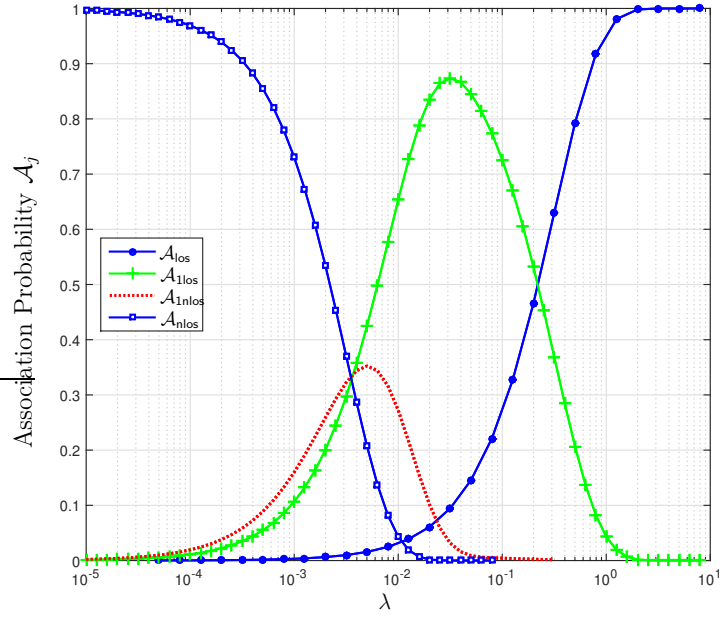


Figure 14 – Association probability scaling with BS density λ for $R_{\text{los}} = 1$ and $R_{\text{nlos}} = 10$.

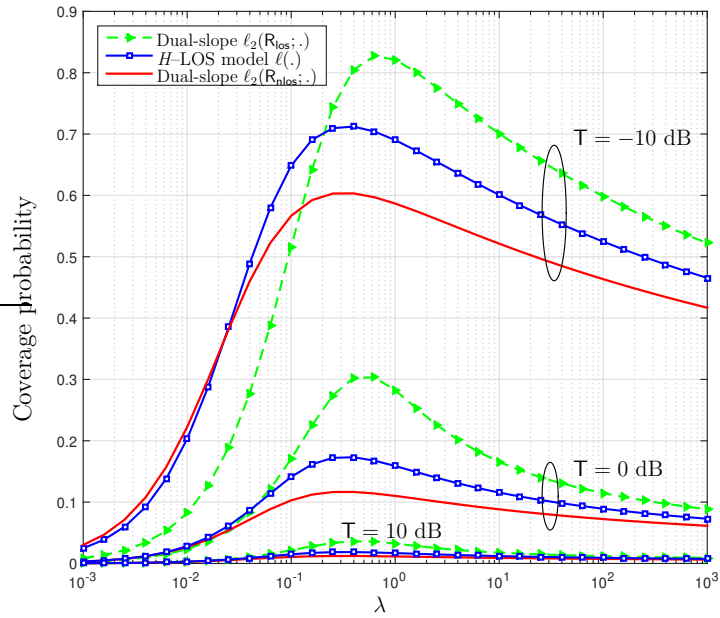
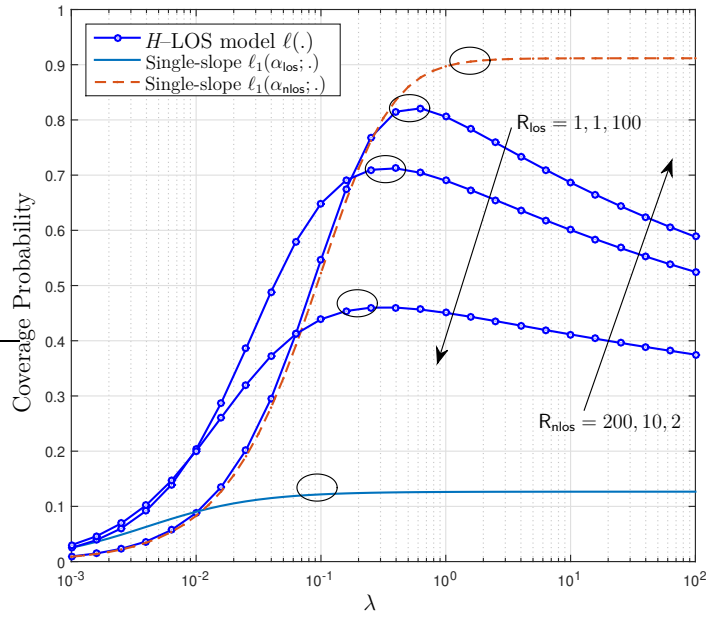
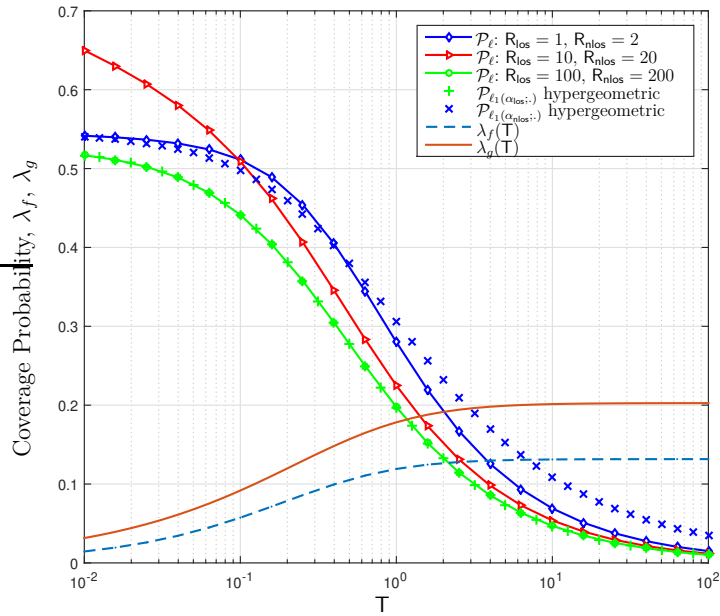


Figure 15 – Coverage probability scaling with λ under ℓ and ℓ_2 path-loss models, $R_{\text{los}} = 1$ and $R_{\text{nlos}} = 10$, $\alpha_{\text{los}} = 2$ and $\alpha_{\text{nlos}} = 4$.


 Figure 16 – Scaling of $\lambda_{\ell}^{\text{opt}}$ with R_{los} and R_{nlos} variations, $\alpha_{\text{los}} = 2.03$, $\alpha_{\text{nlos}} = 4$ and $T = -10$ dB.

 Figure 17 – Coverage probability scaling with network density λ for ℓ and ℓ_2 path-loss models. $R_{\text{los}} = 1$ and $R_{\text{nlos}} = 10$ and path-loss exponents $\alpha_{\text{los}} = 2$ and $\alpha_{\text{nlos}} = 4$.

an NLOS BS from the hybrid region S_{hlos} . By continuously adding more BSs ($0.002 \text{ BSs/m}^2 < \lambda < 0.2 \text{ BSs/m}^2$), the serving BS crosses to be a LOS BS from S_{hlos} . Once λ is large enough ($\lambda > 0.2 \text{ BSs/m}^2$), the typical user is most likely to connect to a BS from S_{los} and thus the coverage probability continues to increase until λ achieves a specific value $\lambda_\ell^{\text{opt}} \simeq 400 \text{ BSs/km}^2$. At that level, $\mathcal{P}_{\ell_3}^{\text{SIR}}$ achieves its maximum value and follows the regression driven by interference I_{agg} as λ continue to increase.

4.4.3 Optimal Network Density

Fig. 16 (b) and (c) verifies Proposition 2 in the optimal regime as the coverage probability $\mathcal{P}_\ell^{\text{SINR}}$ and optimal BS density $\lambda_\ell^{\text{opt}}$ remain bounded between those achieved under the standard and dual-slope path-loss functions. Numerically, $0.12 < \mathcal{P}_\ell^{\text{SINR}} < 0.9$ and $0.1 \text{ BSs/m}^2 < \lambda_\ell^{\text{opt}} < 1 \text{ BSs/m}^2$ and in particular, the lower and upper bounds are achievable for sufficient expansion and shrinking on R_{los} and R_{nlos} respectively.

Fig. 17 is consistent with Proposition 3 and 4. In fact, for the purpose to assess the accuracy of \mathcal{P}_ℓ bounds approximation in the optimal regime, we limit first the scaling of \mathcal{P}_ℓ with T into this regime by considering the combinations $(\lambda = \lambda_g; R_{\text{los}} = 1; R_{\text{nlos}} = 2)$, $(\lambda = \frac{\lambda_f + \lambda_g}{2}; R_{\text{los}} = 10; R_{\text{nlos}} = 20)$ and $(\lambda = \lambda_f; R_{\text{los}} = 100; R_{\text{nlos}} = 200)$, where $\lambda_f = \frac{T^{\delta_{20}}}{\pi F_{-\delta_{20}}(T)}$ and $\lambda_g = \frac{T^{\delta_{21}}}{\pi F_{-\delta_{21}}(T)}$. As can be observed from Fig. 17 for $\alpha_{\text{los}} = 3$ and $\alpha_{\text{nlos}} = 4$, λ_f and λ_g are increasing with the SINR target T until a stage where they become stable and independent from T . Moreover, $\mathcal{P}_\ell^{\text{SINR}}$ remains bounded by the hypergeometric closed-form expression of $\mathcal{P}_{\ell_1}^{\text{SINR}}(\alpha_{\text{los}}; T)$ for $\lambda = \lambda_f$ and $\mathcal{P}_{\ell_1}^{\text{SINR}}(\alpha_{\text{nlos}}; T)$ for $\lambda = \lambda_g$.

4.5 Chapter Summary

In this chapter, we investigated the impact of conventional radio planning and optimization actions on the network performance as BS density increases. An equivalent PPP that absorbs the effect of actions has been derived, and a tractable LOS probability model was introduced where the actions impact is translated by the fluctuation of aggregated parameters. Under these assumptions, the coverage probability under our path loss model generalizes several previous expressions, and it is bounded by the coverage probability under the single-slope and the dual-slope path loss models.

Our results suggest that network performance will be maximized when implementing the class of optimization actions that reduce the cells sizes. In addition, the critical network density that maximizes the network performance has been approximated using Taylor series expansion. The work gives practical guidelines for operators and vendors considering the deployment of

ultra-dense 5G networks.

STOCHASTIC ANALYSIS OF UDNs WITH RESOURCE CAPACITY AND USER SCHEDULING

In this chapter we investigate the impact of antenna elevation, resource capacity and user scheduling on the performance of UDNs. Using tools from SG, we extend a recently introduced definition of coverage probability by inducing a generic thinning that can capture BSs with available resource capacity to transmit users data. Analytical results are then derived for the coverage probability and the average achievable rate, where we obtain closed-form expressions allowing to assess UDNs performance in a more tractable and meaningful fashion compared to the conventional definition of coverage probability. Moreover, we show that the average rate under the new definition requires only the computation of a two-fold numerical integral rather than a four-fold integral in the previous works, which is expected to significantly reduce computational complexity. Comparing the obtained results, we find that the impact of parameters, such as resource capacity, BS transmit power as well as the implementation complexity of scheduling schemes are irrelevant as network density increases, which suggests new insights into the role of these parameters in UDNs.

5.1 Introduction

With the rapidly growing interest in smart-phones and their data-hungry applications, modern cellular networks are increasingly characterized by opportunistic deployment to address end-user specific demands and improve QoS perceptions [39]. Particularly, UDNs based on huge deployment of small-cell BSs are envisioned as the workhorse of capacity improvement in 5G networks [262].

Accordingly, the analysis and modeling of UDNs require generally powerful mathematical tools and new concepts in order to capture key system parameters that impact the *equilibrium*

of the utility function incorporating users QoS and operators investment. The key challenge in fact, is *to develop sufficiently tractable models inducing physically meaningful performance trends*. Recently, SG has shown success as a powerful mathematical tool allowing to derive spatial averages of network performance metrics (e.g. coverage probability, average rate,...), and thereby prevents the use of time-consuming computer simulations [4, 17].

5.1.1 Related Works

Almost all previous studies based on SG models considered the conventional received signal-to-interference-plus-noise ratio (SINR) as the key driver for user's QoE. Hence, the CCDF of SINR, i.e., coverage probability, is in general expressed under an improper integral [4, 17, 18, 162], requiring efficient and arduous numerical integration [204], except for some special cases where closed-form expressions can be obtained (e.g. path-loss exponent equals four, the interference-limited regime,...). Furthermore, almost all SG based studies derive the ergodic rate by integrating the coverage probability over the positive real axis, which resorts to a four-fold integral [17, Appendix C], except the Hamdi's lemma based approach presented in [68], which requires only the computation of a two-fold numerical integral but needs however the use of Meijer G-function [68, Corollary 1].

To overcome the aforementioned shortcomings, authors of [204, 205] introduced a new definition of coverage probability, where the typical user is in coverage when, i) the user receives a sufficiently good signal strength without any over-provision of the BS transmit power, i.e., the short-term average Signal-to-Noise-Ratio ($\overline{\text{SNR}}$) is greater than a certain threshold, ii) the user receives a good signal quality, i.e., the Signal-to-Interference-Ratio (SIR) is greater than another threshold. Interestingly, the new framework captures more system-level parameters than the available definition, and enables deriving general closed-form expressions of coverage probability, which is not allowed by the conventional definition.

However, in realistic networks, the user may experience voice/data drops due to congestion at peak demand, regardless of the received signal strength or quality. The critical missing piece in the framework introduced in [204, 205], is then a measure of physical and logical resource capacity on active BSs (e.g., channel resource elements grouped into physical resource blocks (PRB) in 5G New Radio (NR), or the common power channel resource like the P-CPICH channels in UMTS,...).

5.1.2 Motivation and Contribution

In this chapter, we extend the framework of [204, 205] by tractably capturing BS resource capacity. In this context, we introduce into analysis a generic thinning that can reflect BSs with available capacity. Next, we address for the first time the analysis of UDNs under the new revisited framework of [204, 205]. Typically, we incorporate into analysis three representative scheduling schemes in terms of fairness and implementation complexity. The rationale is to compare their performance in UDNs. We also incorporate the BS height since i) its effect is critical in UDNs [398] and ii) to avoid the occurrence of the less-realistic SINR invariance property [17, 162].

5.2 System Model and Assumptions

5.2.1 Cellular Network and Channel Model

We consider a downlink cellular network, in which the location of BSs and users is modeled with two independent homogeneous PPPs Ψ_b and Ψ_u in the plane \mathbb{R}^2 , with respective densities λ_b and λ_u measured in [BSs/m²] and [Users/m²], respectively. Without loss of generality, and as permitted by the Slivnyak-Mecke's theorem [4, vol. 1, Theorem 1.4.5], the typical user y_0 at the origin O , is taken as the object of the analysis.

We assume that all BSs transmit with the same transmit power P_{tx} , and that multipath fading of the link between a BS located at $x_k \in \Psi_b$ and the typical user located at O , is incorporated by a positive and i.i.d. exponential fading g_k with unit mean, while $r_k \triangleq \|x_k\|$ denotes the horizontal distance between x_k and the typical user such that the subscript 0 and i are used to identify the desired and interfering links, respectively. The radio channel attenuation is dependent on a path-loss function $\ell(\cdot)$, such that the received power at O from a BS x_k is $P_{rx} = P_{tx}g_k/\ell(x_k)$. The path-loss function $\ell(\cdot)$ is assumed to: i) accept an inverse function $\ell^{-1}(\cdot)$, ii) validate the dependency condition of $\ell(\sqrt{xy})/\ell(\sqrt{x})$ on $x \in \mathbb{R}$ for $y \geq 1$ [162, Lemma 1], assumed to avoid the scenario of the SINR invariance property, and iii) $\ell(\cdot)$ is a monotonically increasing function with distance from the origin, to ensure that the received power cannot exceed the transmitted one. σ^2 denote the variance of the additive noise such that $\text{SNR} = P_{tx}/\sigma^2$.

5.2.2 Cell Association Model

We assume the association criterion of the highest average received power, where the typical user is assigned to a unique BS $\{x_0\}$ from Ψ_b such that

$$x_0 = \arg \max_{x_k \in \Psi_b} \{P_{\text{tx}}/\ell(r_k)\} \stackrel{(a)}{=} \arg \min_{x_k \in \Psi_b} \{r_k\}. \quad (143)$$

where (a) follows from the property (iii) of $\ell(\cdot)$. The plane \mathbb{R}^2 seen from BSs is then divided into cells corresponding to the spatially nearest points to each BS than to any other BSs of Ψ_b , namely the *Poisson Voronoi tessellation*. We denote by C_0 , the Voronoi cell containing the typical user and the intended BS x_0 , formally named, the 0-cell [204].

In realistic networks, x_0 needs to be endowed with available resource capacity to carry the typical user's data. Actually, insufficient capacity is likely due to a bottleneck at the backhaul level and/or the scarcity of traffic channels as a result of high data demand or as a result of maintenance failures (e.g., some channel physical modules are down). At a given time, we denote by p_Θ the probability that the typical has sufficient resource capacity to carry the data of a user requesting connection to the typical BS. By construction, p_Θ should differ from the probability p_Δ of having no user associated to the typical BS, since the event of the former covers generally that of the latter, and given p_Θ also depends on a parameter η , correlated to the average inherent resource capacity over all BSs when no user is served. However, both p_Θ and p_Δ need to increase with BS density and shrink with users density. For tractability, we assume that the process Θ_b of BSs with sufficient capacity, is an independent thinning of Ψ_b with density $\lambda_\Theta = p_\Theta \lambda_b$, where p_Θ will be approximated in the next section.

5.2.3 Scheduling Modeling

BSs not serving any user are assumed to be in idle mode in order to mitigate the other-cell interference and improve the energy efficiency. Let Δ_b be the process of BSs in idle mode. The density of Δ_b is $\lambda_\Delta = p_\Delta \lambda_b$ where p_Δ is approximated as [399, Proposition 1],

$$p_\Delta \approx \left(1 + \frac{\lambda_u}{3.5\lambda_b}\right)^{-3.5}. \quad (144)$$

However, on the other hand, when multiple competing users simultaneously need to access the same BS x_0 , three representative scheduling schemes will be considered and investigated to assess the impact on performance in the context of sparse networks and UDNs. An important quantity is the probability mass function (PMF) of the number of competing users inside C_0 .

Let \mathcal{N}_u be the random variable that denotes the number of users in $C_0 \setminus \{y_0\}$. The PMF of \mathcal{N}_u is approximated as [399, Proposition 2],

$$\mathbb{P}\{\mathcal{N}_u = n\} \approx \frac{3.5^{4.5} \Gamma(n + 4.5) (\lambda_u / \lambda_b)^n}{\Gamma(4.5) \Gamma(n + 1) (3.5 + \lambda_u / \lambda_b)^{n+4.5}}. \quad (145)$$

Hereafter, the three scheduling schemes considered:

Scheduling Model 1 (Non-orthogonal Scheduling): Each BS simultaneously serves multiple users associated with it on the same resource block, this is feasible for example when only the typical user that is associated to x_0 ($\mathbb{P}\{\mathcal{N}_u = 0\} = 1$), or when using a NOMA technique such as power-based NOMA, but at the cost of increased intra-cell interference that may be mitigated by SIC at the receivers.

Scheduling Model 2 (Round-Robin (RR) Scheduling): Simultaneous users are scheduled with equal probability regardless of their channel qualities, which enhance temporal fairness among users and reduce implementation complexity.

Scheduling Model 3 (Proportional Fair (PF) Scheduling): Users are scheduled by leveraging their spatial diversity based on the channel quality indicators (CQI), which will increase system throughput at the cost of fairness. *For tractability, we assume that the selection of users for downlink transmission based on maximum PF metric is closely reflected by the largest fading gain g_k , as was endorsed by [400].*

5.3 Coverage Probability and Ergodic Rate Analysis

Following the limitations mentioned in [204] of the commonly available definition of coverage probability P_{cov} , i.e., the SINR of the typical user is above a certain threshold, we consider the new definition adopted in [204, 205], such that the typical user is in coverage when: (i) it receives a sufficiently good signal strength from the nearest BS without any over-provision of the transmitting power P_{tx} , i.e., the average $\overline{\text{SNR}} = P_{\text{tx}} / (\sigma^2 \ell(r_0)) = \text{SNR} / \ell(r_0)$ is greater than a threshold T_s , ii) the $\text{SIR} = g_0 P_{\text{tx}} / (\ell(r_0) I) = g_0 / \sum_i g_i (\ell(r_0) / \ell(r_i))$ is greater than a threshold T_q , where I is the other-cell interference. The coverage probability will then be expressed as

$$P_{\text{cov}}^{(j)}(T_q, T_s) = \sum_{n=0}^{\infty} \mathbb{P}\{\text{SIR} \geq T_q, \overline{\text{SNR}} \geq T_s, \mathcal{N}_u = n\}, \quad (146)$$

where the superscript $j = 1, 2$ or 3 indexes the adopted scheduling model, and we commonly consider that $P_{\text{cov}}^{(1)} = \mathbb{P}\{\text{SIR} \geq T_q, \overline{\text{SNR}} \geq T_s\}$, i.e., each BS serves one user.

5.3.1 Approximation of the Process of BSs with Available Resource Capacity

The resource capacity of the typical BS is closely dependent on the traffic demand from high priority users, which may be the ones with greatest CQI or those privileged through system configuration to access traffic channels (very important users or services). This observation makes it less tractable to derive p_{Θ} since we do not have *a priori* knowledge about the distribution of traffic demand from high priority users. To overcome this limitation and approximate p_{Θ} , we assume that the high priority traffic demand is related to the number of users located inside a disc D_c centered at x_0 and containing: i) sufficiently closest users to x_0 , ii) the closest users from other cells with high probability to make a handover towards x_0 , i.e., the nearest users from the nearest neighboring cell.

Let ξ_M denote the random variable of the radius of the minimal disc D_M centered at x_0 and containing C_0 , and ξ_m as the radius of the maximal disc D_m centered at x_0 and contained by C_0 (see Fig. 18). To the authors knowledge, the distribution of the former does not exist except for some lower bounds as in [401, equation 10] or intractable mathematical expressions as in [402], while the distribution of the latter is totally known as in [401, equation 9]. For analytical tractability, *we consider that the radius ξ_c of D_c is somewhere bounded between ξ_m and ξ_M such that the disc of radius $\sqrt{\eta}\xi_c$ and centered at x_0 contains at most the nearest BS to x_0 .* Formally expressed, we have

$$\mathbb{P}(\xi_c > r) = (1 + \pi\lambda_b\eta r^2)e^{-\pi\lambda_b\eta r^2}. \quad (147)$$

The PDF of ξ_c is then derived as

$$f_{\xi_c}(r) = 2\eta^2 (\pi\lambda_b)^2 r^3 e^{-\pi\lambda_b\eta r^2}, \quad (148)$$

and p_{Θ} is approximated by averaging $\exp(-\pi\lambda_u\xi_c^2)$ over the distribution of ξ_c , as

$$p_{\Theta} \approx \mathbb{E}_{\xi_c} \left\{ \exp(-\pi\lambda_u\xi_c^2) \right\} = \left(1 + \frac{\lambda_u}{\eta\lambda_b} \right)^{-2}. \quad (149)$$

Remark 2. *The expression of p_{Θ} in (149) confirms our initial intuition in Section 7.2. In fact, p_{Θ} can be increased by acting on the network macroscopic resource capacity via densification with new BSs, or by improving the average intrinsic resource capacity of existing BSs via η . Besides, increasing users density, will decrease p_{Θ} and then the availability of BSs to carry users traffic.*

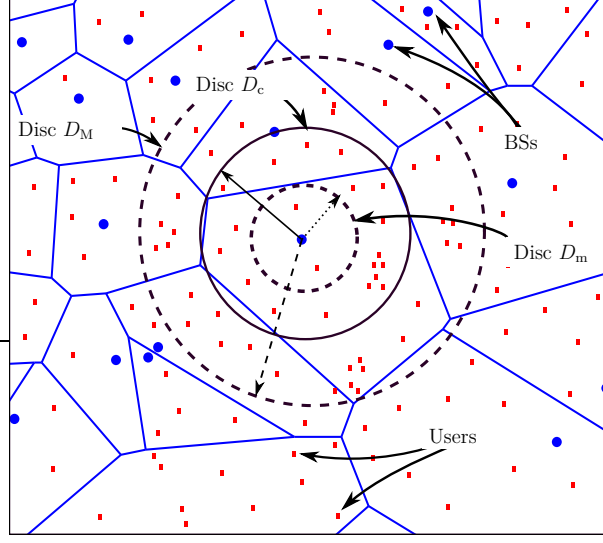


Figure 18 – A PPP realization of BSs and users ($\lambda_u > \lambda_b$) where the boundaries of D_M , D_m and D_c are illustrated.

For fixed densities λ_b and λ_u , it is obvious to mention from (149) and (144) that, if η becomes greater than a threshold $\eta_0 = \mu(\lambda_u/\lambda_b)$, where $\mu(x) = x/[(1+x)^{1.75} - 1]$, the tendency of having more BSs with sufficient capacity increases at the expense of idle mode BSs, which sheds light on the interplay between p_Δ and p_Θ . We note also that $\frac{\lambda_b}{\lambda_u} p_\Theta (1 - p_\Delta) \rightarrow 1$ as $\lambda_b \gg \lambda_u$, while $\frac{\lambda_b}{\lambda_u} p_\Theta (1 - p_\Delta) \rightarrow 0$ as $\lambda_u \gg \lambda_b$.

The following lemma describes the scaling law with λ_b and λ_u of useful combinations of p_Θ and p_Δ .

Lemma 2. Under the previous approximations of p_θ and p_Δ , we have the following properties:

i) $\frac{\lambda_b}{\lambda_u} p_\Theta (1 - p_\Delta)$ scales with $\frac{\lambda_b}{\lambda_b + \lambda_u} \exp\left(-\frac{\theta(\eta)\lambda_u}{\lambda_b + \lambda_u}\right)$, where $\theta(x)$ is a monotonically decreasing function for $x \geq 1$.

ii) For every reals $M, N \geq 0$, $\frac{1 - \exp(-M[p_\Theta + N(1 - p_\Delta)])}{p_\Theta + N(1 - p_\Delta)}$ scales with $p_\Theta^{-1} \exp(-\beta p_\Theta^{-1})$, where β is a constant.

Proof. For a given users density $\lambda_u \geq 0$ and a real $q > 1$, $\exists \lambda_b^0 = \frac{1}{q-1} \lambda_u$ such that: $\forall \lambda_b > \lambda_b^0$, $p_\Theta^{-1} \leq \left(1 + \frac{q\lambda_u}{\eta(\lambda_b + \lambda_u)}\right)^2$. Using the observation that $\exp(-x) < (1 + \frac{x}{y})^{-y} < \exp(\frac{-xy}{x+y})$ for every reals $x, y > 0$, we get

$$\exp\left(\frac{-2q\lambda_u}{\eta(\lambda_b + \lambda_u)}\right) \leq p_\Theta \leq \exp\left(\frac{-2\lambda_u}{\max(1, \eta)(\lambda_b + \lambda_u)}\right), \quad (150)$$

$$1 - \exp\left(\frac{-\lambda_u}{\lambda_b + \lambda_u}\right) \leq 1 - p_\Delta \leq 1 - \exp\left(\frac{-\lambda_u}{\lambda_b}\right) \quad (151)$$

Moreover, using the observation that $\exists 0 < m < 1$ such that for every real $x > 0$

$$\exp\left(-\frac{1}{x}\right) < \frac{x}{x+1} < 1 - \exp(-x) < \exp\left(\frac{-m}{x}\right) < \frac{x}{m(x+1)}, \quad (152)$$

we then get,

$$\frac{\lambda_u}{2(\lambda_b + \lambda_u)} \leq 1 - p_\Delta \leq \frac{\lambda_u}{m(\lambda_b + \lambda_u)}. \quad (153)$$

The proof of i) is then completed by combining (150) and (153).

For every real M and $N \geq 0$, we have $p_\Theta \leq p_\Theta + N(1 - p_\Delta) \leq N + (N + 1)p_\Theta$, and by applying (152), we can see that for a given users density λ_u , $\exists \lambda_b^1 = \lambda_u / \left(\eta \left[\sqrt{(N + 1)/N} - 1\right]\right)$ such that: $\forall \lambda_b \geq \lambda_b^1$, $(1 - \exp(-M[p_\Theta + N(1 - p_\Delta)])) / [p_\Theta + N(1 - p_\Delta)]$ is bounded between $\frac{1}{2(N+1)}p_\Theta^{-1} \exp\left(-\frac{p_\Theta^{-1}}{M}\right)$ and $p_\Theta^{-1} \exp\left(-\frac{mp_\Theta^{-1}}{[2M(N + 1)]}\right)$, which completes the proof of (ii). \square

5.3.2 Coverage probability

The following lemma derives the coverage probability under the path-loss function $\ell(\cdot)$ and the scheduling model 1.

Lemma 3. *The coverage probability under the scheduling model 1 and a path-loss function $\ell(\cdot)$ validating the dependency condition is expressed as*

$$\mathbf{P}_{cov}^{(1)}(T_q, T_s) \approx \pi \lambda_b p_\Theta \int_0^\gamma \exp\left\{-\pi \lambda_b x \left(p_\Theta + (1 - p_\Delta) \int_1^\infty \frac{dy}{1 + \frac{\ell(\sqrt{xy})}{T_q \ell(\sqrt{x})}}\right)\right\} dx, \quad (154)$$

where $\gamma = \max\left(0, [\ell^{-1}(\text{SNR}/T_s)]^2\right)$.

Proof. The coverage probability in (146), is expressed under the scheduling model 1 as:

$$\mathbf{P}_{cov}^{(1)}(T_q, T_s) = \mathbb{P}\left\{\text{SIR} \geq T_q, \overline{\text{SNR}} \geq T_s, \mathcal{N}_u = 0\right\} \quad (155)$$

$$\approx 2\pi \lambda_\Theta \int_0^\infty e^{-\pi \lambda_\Theta r^2} \mathbb{E}_I \left\{ \mathbb{P}\left\{\text{SIR} \geq T_q, \overline{\text{SNR}} \geq T_s | I, r\right\}\right\} r dr \quad (156)$$

$$\stackrel{(a)}{=} 2\pi \lambda_\Theta \int_0^\infty e^{-\pi \lambda_\Theta r^2} \mathbf{1}\left\{\ell(r) \leq \frac{\text{SNR}}{T_s}\right\} \mathbb{E}_I \left\{ \mathbb{P}\left\{\text{SIR} \geq T_q | I, r\right\}\right\} r dr \quad (157)$$

$$= 2\pi \lambda_\Theta \int_0^{\sqrt{\gamma}} e^{-\pi \lambda_\Theta r^2} \underbrace{\mathbb{E}_I \left\{ \mathbb{P}\left\{\text{SIR} \geq T_q | I, r\right\}\right\}}_{\chi(T_q, T_s)} r dr, \quad (158)$$

and the expectation term, $\chi(T_q, T_s)$, in the integrand function, can be computed as follows:

$$\chi(T_q, T_s) = \mathbb{L}_I \left\{ \frac{T_q \ell(r)}{P_{\text{tx}}} \right\} = \mathbb{E}_{\Psi_b \setminus \Delta, \{g_i\}} \left\{ \prod_{x_i \in \Psi_b \setminus \Delta} \frac{\ell(r_i)}{\ell(r_i) + T_q \ell(r)} \right\} \quad (159)$$

$$\stackrel{(b)}{=} \exp \left(-2\pi(\lambda_b - \lambda_\Delta) \int_r^\infty \frac{T_q \ell(r) u du}{\ell(u) + T_q \ell(r)} \right) \quad (160)$$

$$\stackrel{(c)}{=} \exp \left(-\pi \lambda_b (1 - p_\Delta) r^2 \int_1^\infty \frac{du}{1 + \frac{\ell(r\sqrt{u})}{T_q \ell(r)}} \right), \quad (161)$$

where (a) follows from the independence of $\overline{\text{SNR}}$ from the cumulative other-cell interference I . (b) follows from the PGFL theorem and (c) from the variable change $u^2/r^2 \rightarrow u$. Plugging (161) into (158) with $r^2 \rightarrow x$ gives the desired result. \square

For the remainder, we adopt the standard power-law path-loss model with elevated BSs of height $h \geq 0$ measured in [m], i.e., $\ell(r_k) = (r_k^2 + h^2)^{\frac{\alpha}{2}}$ for all $x_k \in \Psi_b$, where α is the path-loss exponent assumed to be $\alpha > 2$, and let $\delta = 2/\alpha$. Generalizing our work to other relevant path-loss models such that the dual-slope [162] and stretched path-loss models, is left to future works.

The following theorem in the bottom of this page, gives the coverage probability under the considered path-loss model and the three scheduling models.

Theorem 2. *The coverage probability under the considered path-loss model and the three scheduling models is expressed as*

$$\mathbf{P}_{\text{cov}}^{(1)}(T_q, T_s) \approx p_\Theta \frac{1 - \exp(-\pi \lambda_b \mathcal{A} \mathcal{Q}(\lambda_u, \lambda_b, \delta, T_q))}{\mathcal{Q}(\lambda_u, \lambda_b, \delta, T_q)} \exp(-\pi \lambda_b h^2 (\mathcal{Q}(\lambda_u, \lambda_b, \delta, T_q) - p_\Theta)), \quad (162)$$

$$\mathbf{P}_{\text{cov}}^{(2)}(T_q, T_s) \approx \frac{\lambda_b}{\lambda_u} (1 - p_\Delta) \mathbf{P}_{\text{cov}}^{(1)}(T_q, T_s), \quad (163)$$

$$\mathbf{P}_{\text{cov}}^{(3)}(T_q, T_s) \approx \sum_{n=0}^{\infty} \mathbb{P}\{\mathcal{N}_u = n\} \left[\sum_{k=1}^{n+1} \binom{n+1}{k} (-1)^{k+1} \mathbf{P}_{\text{cov}}^{(1)}(kT_q, T_s) \right] \quad (164)$$

where $\mathcal{Q}(\lambda_u, \lambda_b, m, T_q) = p_\Theta + (1 - p_\Delta) (F_m(T_q) - 1)$, and $\mathcal{A} = \max \left(0, \left(\frac{\text{SNR}}{T_s} \right)^\delta - h^2 \right)$.

Proof. The proof of the expression of $P_{\text{cov}}^{(1)}$ in Theorem 2 follows directly from Lemma 3 where $\gamma = \mathcal{A}^2$, and (161) is derived as

$$\chi(T_q, T_s) = \exp\left(-\pi\lambda_b(1-p_\Delta)(r^2+h^2)T_q^{\frac{2}{\alpha}}\int_{T_q^{-\frac{2}{\alpha}}}^{\infty}\frac{du}{1+u^{\frac{\alpha}{2}}}\right), \quad (165)$$

where $T_q^{\frac{2}{\alpha}}\int_{T_q^{-\frac{2}{\alpha}}}^{\infty}\frac{du}{1+u^{\frac{\alpha}{2}}}+1 = F_\delta(T_q)$.

The coverage probability under the scheduling model 2, $P_{\text{cov}}^{(2)}$, is expressed as

$$P_{\text{cov}}^{(2)}(T_q, T_s) = \sum_{n=0}^{\infty} \mathbb{P}\left\{\text{SIR} \geq T_q, \overline{\text{SNR}} \geq T_s, \mathcal{N}_u = n\right\} \quad (166)$$

$$= \sum_{n=0}^{\infty} \mathbb{P}\left\{\text{SIR} \geq T_q, \overline{\text{SNR}} \geq T_s | \mathcal{N}_u = n\right\} \mathbb{P}\left\{\mathcal{N}_u = n\right\} \quad (167)$$

$$\stackrel{(a)}{=} \mathbb{P}\left\{\text{SIR} \geq T_q, \overline{\text{SNR}} \geq T_s\right\} \sum_{k=0}^{\infty} \frac{\mathbb{P}\left\{\mathcal{N}_u = n\right\}}{k+1} \quad (168)$$

$$\stackrel{(b)}{\approx} \frac{\lambda_b}{\lambda_u} (1-p_\Delta) \mathbb{P}\left\{\text{SIR} \geq T_q, \overline{\text{SNR}} \geq T_s\right\}, \quad (169)$$

where (a) follows by assuming the independence of the events $\mathcal{E} = (\text{SIR} \geq T_q, \overline{\text{SNR}} \geq T_s)$ and $\mathcal{F}_n = \{\mathcal{N}_u = n\}$ as in [204, 205], in addition to the properties of the RR scheduling where each user is selected with the same probability. (b) follows from [399, Proposition 2] where $\sum_{n=0}^{\infty} (n+1)^{-1} \mathbb{P}(\mathcal{N}_u = n) = (\lambda_b/\lambda_u)(1-p_\Delta)$.

The coverage probability under the scheduling model 3, $P_{\text{cov}}^{(3)}$, is expressed from (167) as

$$P_{\text{cov}}^{(3)}(T_q, T_s) = \sum_{n=0}^{\infty} \underbrace{\mathbb{P}\left\{\frac{\max(g_0, \dots, g_n)P_{\text{tx}}}{\ell(r_0)I} \geq T_q, \overline{\text{SNR}} \geq T_s\right\}}_{\varphi(T_q, T_s)} \mathbb{P}\left\{\mathcal{N}_u = n\right\}, \quad (170)$$

where the probability term, $\varphi(T_q, T_s)$, is derived as

$$\varphi(T_q, T_s) = \mathbb{E}_{r_0, I} \left\{ \mathbb{P}\left\{\max(g_0, \dots, g_n) \geq \frac{T_q \ell(r_0) I}{P_{\text{tx}}}, \overline{\text{SNR}} \geq T_s \mid I, r_0\right\} \right\} \quad (171)$$

$$\stackrel{(a)}{=} \mathbb{E}_{r_0, I} \left\{ \mathbb{1}\left\{\ell(r_0) \leq \frac{\text{SNR}}{T_s}\right\} \left[1 - \left(1 - \exp\left(-\frac{T_q \ell(r_0) I}{P_{\text{tx}}}\right)\right)^{n+1}\right] \right\} \quad (172)$$

$$\stackrel{(b)}{=} \sum_{k=1}^{n+1} \binom{n+1}{k} (-1)^{k+1} \mathbb{E}_{r_0} \left\{ \mathbb{1}\left\{\ell(r_0) \leq \frac{\text{SNR}}{T_s}\right\} \mathbb{L}_I \left\{-\frac{k T_q \ell(r_0)}{P_{\text{tx}}}\right\} \right\}, \quad (173)$$

where (a) holds since the random variables $g_k, k = 0, \dots, n$ are i.i.d. exponential RVs with mean 1, and the cumulative function (CDF) of $\max(g_0, \dots, g_n)$ is expressed as

$$\mathbb{P} \{ \max(g_0, \dots, g_n) \leq u \} = (1 - e^{-u})^{n+1}, \quad (174)$$

(b) follows from the binomial theorem. We get the desired result by combining the last expression with (158). \square

Remark 3. *The main strength of Theorem 2 is that the expressions of $\mathbf{P}_{cov}^{(1)}$ and $\mathbf{P}_{cov}^{(2)}$ are written under closed-form expressions, which is very helpful for performance evaluation as it reduces computational complexity and time-consuming processing. Moreover, the expression of $\mathbf{P}_{cov}^{(3)}$ is an infinite sum that can be further simplified by assuming that the cell has exactly n_0 points, where $n_0 = \lceil \mathbb{E} \{ \mathcal{N}_u \} \rceil$ and $\mathbb{E} \{ \mathcal{N}_u \} \approx 1 + 1.28(\lambda_u/\lambda_b)$ [403, Lemma 4]. The coverage probability under the scheduling model 3 is then approximated as*

$$\mathbf{P}_{cov}^{(3)}(T_q, T_s) \approx \sum_{k=1}^{n_0+1} \binom{n_0+1}{k} (-1)^{k+1} \mathbf{P}_{cov}^{(1)}(kT_q, T_s). \quad (175)$$

The accuracy of this approximation will be discussed in Section 5.4.

Remark 4. *Theorem 2 reveals that the coverage probability under the scheduling models 2 and 3 is based on its computation under the scheduling model 1. In other words, $\mathbf{P}_{cov}^{(2)}$ and $\mathbf{P}_{cov}^{(3)}$ can be expressed on the basis $(\mathbf{P}_{cov}^{(1)}(kT_q, T_s))_{k=1, \dots, n+1}$, where n is an integer ≥ 1 . As a result, we can focus the analysis on the building block component $\mathbf{P}_{cov}^{(1)}$.*

Remark 5. *The scaling law of $\mathbf{P}_{cov}^{(j)}$ with λ_b and λ_u is completely defined. In fact, Lemma 2 determines the scaling law of $(\lambda_b/\lambda_u)p_\Theta(1 - p_\Delta)$ and $(1 - \exp(-\pi\lambda_b\mathcal{A}\mathcal{Q}(\lambda_u, \lambda_b, \delta, T_q)))/\mathcal{Q}(\lambda_u, \lambda_b, \delta, T_q)$, while (153) confirms that $\exp(-\pi\lambda_b h^2(\mathcal{Q}(\lambda_u, \lambda_b, \delta, T_q) - p_\Theta))$ scales with $\exp(-\kappa h^2(F_\delta(T_q) - 1)\frac{\lambda_b\lambda_u}{\lambda_b + \lambda_u})$, where κ is a constant.*

We now investigate the asymptotic behavior of $\mathbf{P}_{cov}^{(j)}$, where the rationale is to understand the interplay between coverage probability and the parameters \mathbf{P}_{tx} , λ_b , λ_u and antennas height h , assuming that when acting on specific parameters, the others are supposed to be constant. The results are summarized in the following three propositions.

Proposition 5. *The coverage probability under the considered path-loss function $\ell(\cdot)$ and the three scheduling models, tends towards a surely "universal outage" in the following asymptotic*

cases

$$\lim_{\lambda_u \rightarrow \infty} \mathbf{P}_{cov}^{(j)}(T_q, T_s) = \lim_{\mathcal{A} \rightarrow 0} \mathbf{P}_{cov}^{(j)}(T_q, T_s) = 0. \quad (176)$$

Proof. The proof follows by a direct inspection of Theorem 2. \square

Remark 6. Proposition 5 shows that the intended BS needs to check the primary constraint $P_{tx} > h^\alpha T_s \sigma^2$ in order to generate the earliest samples of users or areas with a correct coverage. Moreover, it identifies the detrimental effect of increasing users density on BS resource capacity ($p_\Theta \rightarrow 0$) and then on the network overall coverage probability.

Proposition 6. The coverage probability under the PF and RR schedulers converges to that of the non-orthogonal scheduler as $\lambda_b \rightarrow \infty$ or $\lambda_u \rightarrow 0$. Hence, $\mathbf{P}_{cov}^{(j)}(T_q, T_s)$ tends towards a limit conditioned on other parameters, as

$$i) \lim_{\lambda_b \rightarrow \infty} \mathbf{P}_{cov}^{(j)}(T_q, T_s) = \exp\left(-\pi \lambda_u h^2 (F_\delta(T_q) - 1)\right), \quad (177)$$

$$ii) \lim_{\lambda_u \rightarrow 0} \mathbf{P}_{cov}^{(j)}(T_q, T_s) = 1 - \exp(-\pi \lambda_b \mathcal{A}). \quad (178)$$

Proof. The sketch of the proof stems from Remark 2, and the observation that

$$\lim_{\lambda_b \rightarrow \infty} \mathbb{P}\{\mathcal{N}_u = n\} = \lim_{\lambda_u \rightarrow 0} \mathbb{P}\{\mathcal{N}_u = n\} = \begin{cases} 1 & \text{if } n = 0 \\ 0 & \text{if } n \geq 1. \end{cases} \quad (179)$$

\square

Remark 7. Several earlier works suggested that the tendency of coverage probability in UDNs is either towards 0 [162] or 1 [404], which involves that the performance of different networks will be the same in the regime of high BS density. However, we show in (177) a more precise result, where the performance of several UDNs will be different as well as their respective users density, average BS height, path-loss exponent and the threshold T_q are different. We note moreover from Prop.6 that $\lim_{\lambda_b \rightarrow \infty} \mathbf{P}_{cov}^{(j)}(T_q, T_s)$ is independent of T_s (more generally of SNR), while $\lim_{\lambda_u \rightarrow 0} \mathbf{P}_{cov}^{(j)}(T_q, T_s)$ is independent of T_q , which is due to the idle mode capability that mitigates interference as $\lambda_b \rightarrow \infty$ and/or $\lambda_u \rightarrow 0$.

Proposition 7. Considering the reduced height and high SNR scenarios, the coverage probability

under the Non-orthogonal scheduling is expressed as

$$i) \lim_{h \rightarrow 0} P_{cov}^{(1)}(T_q, T_s) = p_\Theta \frac{1 - e^{-\pi \lambda_b \left(\frac{\text{SNR}}{T_s}\right)^\delta \mathcal{Q}(\lambda_u, \lambda_b, \delta, T_q)}}{\mathcal{Q}(\lambda_u, \lambda_b, \delta, T_q)} \quad (180)$$

$$ii) \lim_{\text{SNR} \rightarrow \infty} P_{cov}^{(1)}(T_q, T_s) = p_\Theta \frac{e^{-\pi \lambda_b h^2 (\mathcal{Q}(\lambda_u, \lambda_b, \delta, T_q) - p_\Theta)}}{\mathcal{Q}(\lambda_u, \lambda_b, \delta, T_q)} \quad (181)$$

Proof. The sketch of the proof follows by a direct inspection of Theorem 2. \square

We now assume that we have previously identified the parameters T_q and T_s required to access the system, the parameter α defined by the propagation environment, the parameter λ_u expected from end-users behavior. The following proposition gives the correlation constraint that needs to be established between the pre-defined parameters and the commonly used parameters for cellular network optimization, namely λ_b , h and P_{tx} , in order to meet a given coverage probability $0 < P^{(1)} < 1$ under the baseline scheduling model.

Corollary 1. *For pre-defined parameters T_q , T_s , λ_u and δ , the following constraint needs to be verified to meet a required coverage probability $0 < P^{(1)} < 1$ under the Non-orthogonal scheduling model,*

$$P^{(1)} \leq \frac{p_\Theta}{\mathcal{Q}(\lambda_u, \lambda_b, \delta, T_q)} \varrho(\lambda_b, h, P_{tx}), \quad (182)$$

where

$$\varrho(\lambda_b, h, P_{tx}) = \min \left(e^{-\pi \lambda_b h^2 (\mathcal{Q}(\lambda_u, \lambda_b, \delta, T_q) - p_\Theta)}; 1 - e^{-\pi \lambda_b \mathcal{A} \mathcal{Q}(\lambda_u, \lambda_b, \delta, T_q)} \right). \quad (183)$$

Proof. The sketch of the proof is as follows: For fixed parameters T_q , T_s , λ_u , δ and coverage probability $P^{(1)}$. Equation (162) can be expressed as $P_{cov}^{(1)}(T_q, T_s) = u(\lambda_b) e^{-v(\lambda_b, h)} (1 - e^{-w(\lambda_b, h, P_{tx})})$, where $u(\lambda_b) = p_\Theta (\mathcal{Q}(\lambda_u, \lambda_b, \delta, T_q))^{-1}$, $v(\lambda_b, h) = \pi \lambda_b h^2 (\mathcal{Q}(\lambda_u, \lambda_b, \delta, T_q) - p_\Theta)$ and $w(\lambda_b, h, P_{tx}) = \pi \lambda_b \mathcal{A} \mathcal{Q}(\lambda_u, \lambda_b, \delta, T_q)$. However, since $\mathcal{A} > 0$ and $T_q \mapsto F_\delta(T_q)$ is a monotonically increasing function with $T_q \geq 0$ and $0 \leq \delta < 1$, where $F_\delta(0) = F_0(T_q) = 1$; the functions u , v and w are then positive for every parameters λ_b , h and P_{tx} . The constraint (182) is then true for $P^{(1)}$ chosen such that $0 < e^{-v(\lambda_b, h)} < 1$ and $0 < e^{-w(\lambda_b, h, P_{tx})} < 1$ in (162), which completes the proof. \square

Remark 8. *A direct inspection of (182) confirms that the achievable coverage probability will be maximized if the following intuitive adjustments are established: On the one hand: increase the ratio $\lambda_b/\lambda_u \gg 1$, P_{tx} , and α . On the other hand, decrease h , σ^2 , T_q , and T_s .*

5.3.3 Average Achievable Rate

We also investigate the mean data rate achievable over a cell in units of nats/Hz, and verify how it is impacted with network parameters when considering the three scheduling models. Consistently with our adopted model of coverage probability (146) [204], we introduce the following definition of the ergodic rate of the typical user associated to x_0 ,

$$\tau_c^{(j)}(.) = \mathbb{E} \left\{ \mathbb{1} \left\{ \ell(r_0) \leq \frac{\text{SNR}}{T_s} \right\} \ln(1 + \text{SIR}) \right\} \stackrel{(a)}{=} \int_{t>0} \mathbf{P}_{\text{cov}}^{(j)}(e^t - 1, T_s) dt, \quad (184)$$

where j refers to the scheduling model, and (a) follows from similar steps in [17, Theorem 3].

We have then; from Theorem 2 and some variable changes,

$$\tau_c^{(2)}(.) \approx \frac{\lambda_b}{\lambda_u} (1 - p_\Delta) \tau_c^{(1)}(.), \quad (185)$$

$$\tau_c^{(3)} = \sum_{n=0}^{\infty} \mathbb{P} \{ \mathcal{N}_u = n \} \left[\sum_{k=1}^{n+1} \binom{n+1}{k} (-1)^{k+1} \int_{x>0} \frac{\mathbf{P}_{\text{cov}}^{(1)}(kx, T_s)}{x+1} dx \right]. \quad (186)$$

Note that the expression of ergodic rate in [17, Theorem 3], needs generally, the computation of a four-fold numerical integral, whereas the expression in (184), requires only the computation of a two-fold integral, which is expected to be more computationally efficient.

5.4 Numerical Results

In this section, we present numerical results to validate our theoretical analysis and assess the network performance trend as a function of several key parameters adjustment. We consider in the following, $\sigma^2 = 0$ dB, $\alpha = 4$, T_s is mapped with T_q by the expression $T_s = T_q \Gamma(1+\delta)^{-1/\delta}$ [205, Eq. (5)], where $\Gamma(\cdot)$ denotes the complete gamma function. Integral expressions are evaluated using Matlab, and Monte Carlo simulations are performed with 10^4 iterations.

Fig. 19 shows that the simulation results of coverage probability under the baseline scheduling model, match perfectly with the analytical expression, which validates the accuracy of our analytical model. Moreover, and consistently with previous results considering the conventional definition of coverage probability [400], Fig. 19 shows that under the new coverage probability framework [204], the PF scheduler is the model that best improves the coverage probability, due to the multi-user diversity gain. However, the RR scheduler [399], reduces the coverage probability due to the equal probability scheduling process, particularly for large users density. Besides, Fig. 19 shows that the approximation expression (175), is generally a sufficient tight

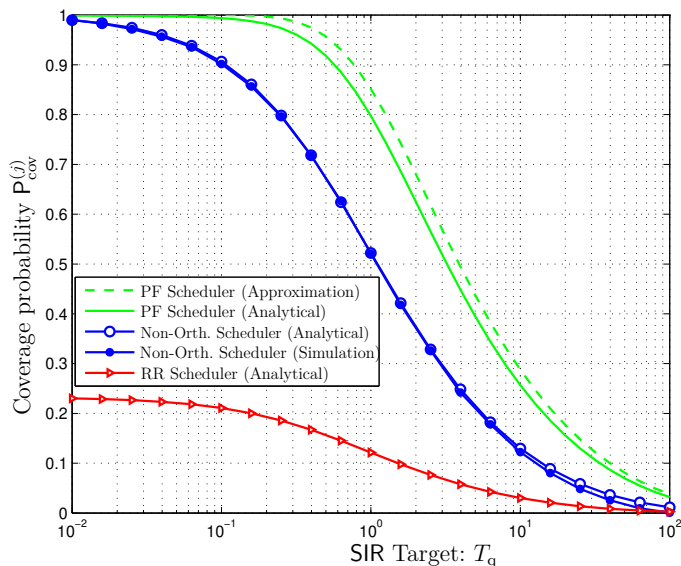


Figure 19 – The scaling of coverage probability $P_{\text{cov}}^{(j)}$ with SIR target T_q , for $\lambda_b = \lambda_u/4 = 0.25$ BS/m², $\eta = 10^3$, $h = 0.4$ m, and $P_{\text{tx}} = 43$ dBm.

upper-bound of $P_{\text{cov}}^{(3)}$, reflecting the main trends of $P_{\text{cov}}^{(3)}$.

Fig. 20 shows that for constant P_{tx} , T_q , η and h , the behavior of coverage probability in UDNs scales with user and BS densities, λ_u and λ_b , respectively. More generally, for large λ_b , the coverage probability under the three representative scheduling schemes scales with $\exp(-\pi\lambda_u h^2 (F_\delta(T_q) - 1))$ consistently with Eq. (177).

Fig. 21 shows the scaling trend of $P_{\text{cov}}^{(j)}$ with BS density λ_b as a function of η , P_{tx} and h . The figure confirms Proposition 6, where the three scheduling models are equivalent in UDNs. Consequently, we recommend to deploy a scheduling strategy with the most reduced implementation complexity in UDNs. Moreover, we mention the limited impact of inherent resource capacity η and the BS transmit power P_{tx} as network density increases. In other words, η and P_{tx} need to scale with nearly a $1/\lambda_b$ rate to reduce infrastructure power consumption and the cost of acquired resource capacity. In this context, investigating the optimum scaling law of P_{tx} and η with λ_b as part of an energy efficiency setup, in addition to approximating the BS density that maximizes the network performance will be left to future work.

Fig. 22 evaluates expression (184), where it confirms the detrimental effect of BS height h and users density λ_u on the network average rate. In addition, and in agreement with our previous results, we conclude the limited impact of inherent resource capacity η and the transmit power P_{tx} as λ_b increases.

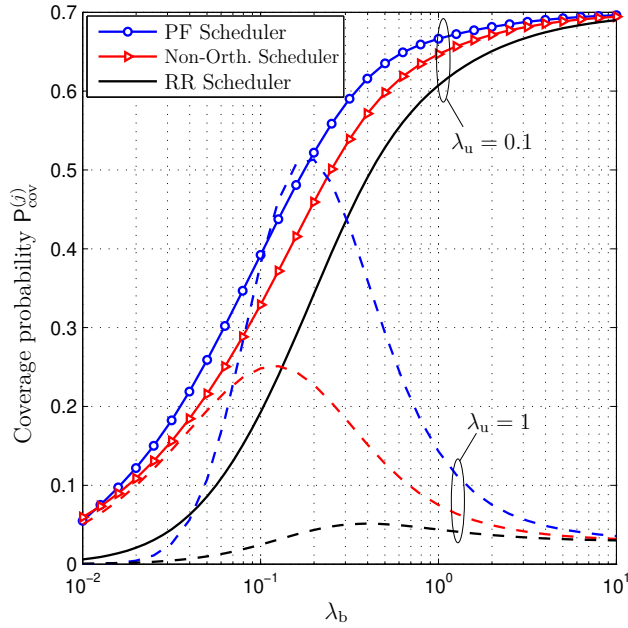


Figure 20 – The scaling of coverage probability $P_{\text{cov}}^{(j)}$ with network density λ_b and users density λ_u . The other parameters are fixed as: $P_{\text{tx}} = 43$ dBm, $T_q = 2$ dB, $\eta = 10^3$, $h = 1$ m.

5.5 Chapter Summary

Considering a revisited version of the coverage probability recent definition, introduced in [204], this chapter derived the coverage probability and the average data rate for a downlink cellular network with elevated BSs and three representative scheduling models. The network performance under a given scheduling model is shown to be expressed on the basis of that under non-orthogonal scheduling, where competing users are served on the same resource block. In addition, it is revealed that the PF scheduler gives the best network performance due to multi-user diversity gain, while the RR scheduling is impaired by users density due to the equal probability selection process. However, the three scheduling models are equivalent in the context of UDNs, where we recommend to deploy the scheduling model with the most reduced implementation complexity.

Besides, our results showed that BS height and user density are so detrimental to coverage probability and average rate in UDNs, while inherent resource capacity and the transmit power have reduced impact as network density increases, which suggests new insights into the role of these parameters in UDNs.

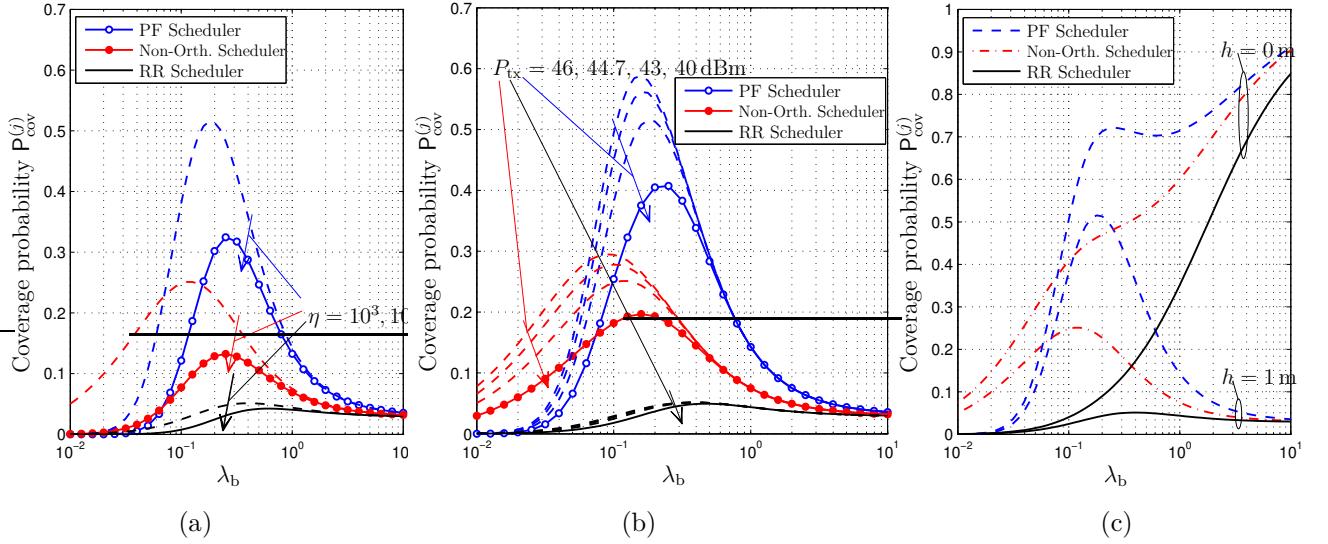


Figure 21 – For $\lambda_u = 1$ user/m² and $T_q = 2$ dB, we plot the scaling of coverage probability $P_{\text{cov}}^{(j)}$ with network density λ_b as a function of: (a) The resource capacity η when $P_{\text{tx}} = 43$ dBm, $h = 1$ m, (b) The transmit power P_{tx} when $\eta = 10^3$ and $h = 1$ m, (c) The BS height h when $\eta = 10^3$ and $P_{\text{tx}} = 43$ dBm.

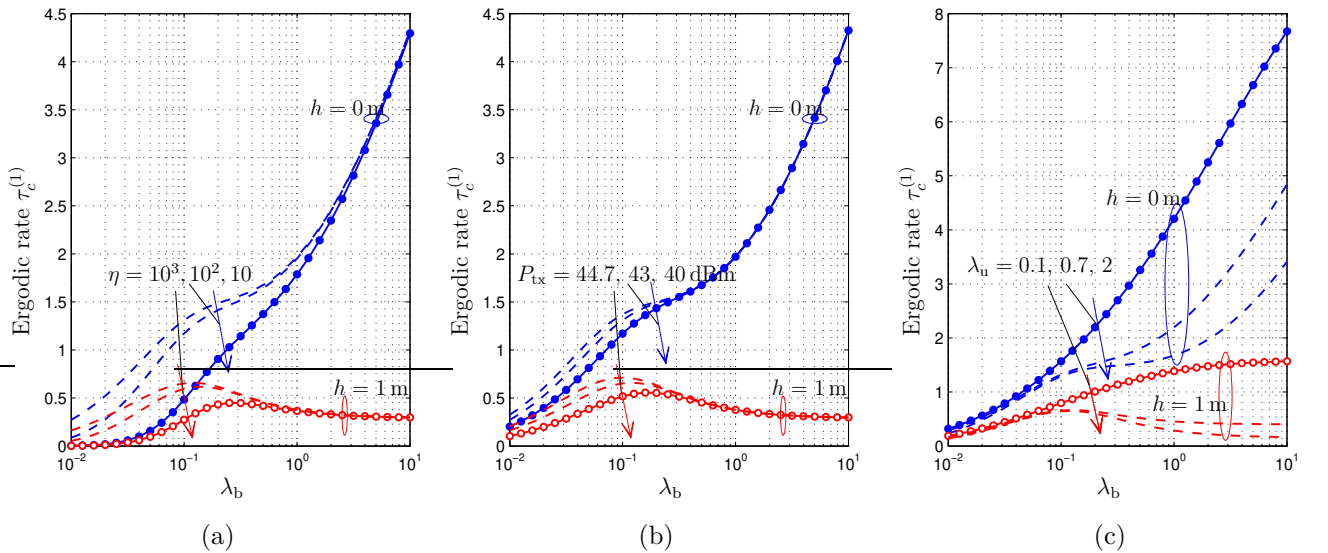


Figure 22 – The scaling of the average rate under the non-orthogonal scheduling, $\tau_c^{(1)}$, with network density λ_b , as a function of: (a) The resource capacity η and BS height h when $\lambda_u = 1$ user/m² and $P_{\text{tx}} = 43$ dBm, (b) The transmit power P_{tx} and BS height h when $\lambda_u = 1$ user/m² and $\eta = 10^3$, (c) The user density λ_u and BS height h when $\eta = 10^3$ and $P_{\text{tx}} = 43$ dBm.

UPLINK COVERAGE AND HANDOFF RATE WITH REALISTIC POWER CONTROL MODELS

In this chapter, we characterize, based on stochastic geometry, the uplink coverage probability with a unified power control scheme built upon realistic path loss models and UE constrained transmit power. To improve their uplink connectivity, active UEs are next assumed to move in a random direction without prior knowledge of their nearest base station location, namely the BCS movement. A tractable expression of the uplink handoff rate is then derived and the induced uplink coverage probability following the BCS movement is evaluated. The results show different echoes of the uplink coverage probability depending on the serving UE profile (stationary or mobile) and the considered path loss model, which suggests new insights into the design of uplink system parameters.

6.1 Introduction

With the exponential growth of mobile-broadband data usage, driven essentially by means of enhanced device capabilities and emerging data-hungry applications, operators are in a steady race to provide optimal QoE. One key measure to quantify the users' QoE is the TTC metric, defined as the period time from requesting to receiving online content on the UE display. Typically, it has been observed that users need generally to feel a TTC below 6 seconds to report a positive QoE feedback [405]. Also, downlink performance is commonly known as the first factor affecting the overall TTC since most popular applications download more data than they upload. However, recent measurements have shown that a reduced uplink speed of fewer than 300 kbps, may be systematically the bottleneck of a delayed TTC of more than 4 seconds [405]. Hence, the ever-increasing importance of improving uplink coverage.

One effective way for uplink coverage enhancement is by deploying UDNs, envisioned as

the workhorse of ubiquitous coverage in 5G networks and B5G [263]. That is, real deployment of nodes in the context of UDNs is opportunistic due to several socio-economic factors, and analytical tools such as SG and the theory of point processes are more efficient to capture such spatial variability of nodes [4, 24].

6.1.1 Related Works

To the authors' knowledge, the work in [20] is the first to consider a tractable SG-based model to evaluate the uplink coverage probability at the level of the typical BS, uniformly and randomly deployed in the Voronoi cell of the serving UE. In [24], the previous work is slightly extended, where the assumption of modelling the active uplink UEs with a PPP having the same density as the PPP of BSs, is particularly validated via simulations. In [245], uplink heterogeneous cellular networks based on fractional power control with maximum transmit power at UEs are investigated. In [148], the UEs transmit power is conceived as a random variable mapped via a truncated channel inversion power control to the distribution of the desired link distance. However, the question of uplink UDNs has not been explicitly addressed in the previous works, where all of them have considered the simplistic standard path loss model that has demonstrated less-realistic performance trends in the context of downlink UDNs [162, 164]. Interestingly, the authors of [406] addressed such limitation and evaluated the uplink coverage in UDNs with stationary UEs and a revisited path loss model related to a piecewise function. However, incorporating UEs mobility in the context of UDNs is so crucial given the reduced size of cells.

A review of SG mobility-aware models, shows that there are particularly two directions of analysis: i) *the trajectory-based handoff* wherein the handoff event occurs as long as the receiver crosses transmitters cell boundary, and hence, the handoff rate is biased by the efficiency of quantifying the statistical distribution of cells boundaries. A representative uplink analysis using such method is given in [148]. ii) *The association-based handoff* where the handoff event occurs as long as another BS verifies the association criterion better than the current serving BS [185]. To the authors' knowledge, this paper is the first work that extends the association-based handoff concept to the uplink analysis.

6.1.2 Motivation and Contribution

Typically, the contributions of this paper are threefold: i) We extend the frameworks in [20, 24, 148, 245] by evaluating the uplink coverage probability under a unified power control

scheme built upon realistic path loss models and constrained transmit power of UEs. ii) Inspired from the the 3GPP simulation mobility model [408], active UEs are assumed to intuitively engage in a linear movement with a random direction in order to improve their connectivity conditions. In such a context, we derive the uplink handoff rate as an extension of the tractable downlink analysis in [185]. iii) Using the obtained handoff rate, we also evaluate the induced uplink coverage probability following such mobility model. The analytical accuracy of our results is next validated via simulations and the interplay of system parameters with the uplink coverage probability and the handoff rate is assessed.

6.2 System Model and Assumptions

6.2.1 Cellular Network Model and Association Scheme

We consider the uplink of a cellular network, wherein the location of BSs and users is modeled with respective 2D homogeneous PPPs Ψ_b and Ψ_u , with respective densities λ_b and λ_u measured in [BSs/m²] and [Users/m²]. Without loss of generality, and as permitted by the Slivnyak-Mecke's theorem [4, Th. 1.4.5], the typical BS at the origin O , is taken as the object of the analysis.

We assume an orthogonal access scheme, e.g., OFDMA, where the typical BS schedules randomly one UE per resource block from the UEs located inside its Voronoi cell. We focus on the loaded regime where each BS is active in the uplink, i.e., $\lambda_u \gg \lambda_b$. That is, the process of active UEs (those scheduled to serve their own BS), denoted by $\Psi \subset \Psi_u$, is assumed to preserve the Poisson law as was endorsed via simulations in [24, Fig. 5]. Hence, it is reasonable to assume that the density of Ψ is λ_b due to the OFDMA property.

As illustrated in Fig. 28, the distance from each active UE $x \in \Psi$ to its nearest BS $y \in \Psi_b$ is denoted by r_x . Particularly, the distance from the typical BS y_0 to its serving UE x_0 is denoted by r . Besides, the distance from y_0 to the interfering UEs $x \in \Psi \setminus \{x_0\}$ is denoted by d_x .

6.2.2 Channel Model and Power Control Scheme

Multipath fading of the link between the typical BS y_0 and a UE x , is incorporated by a positive and i.i.d. Rayleigh fading g_x with unit mean, i.e., $g_x \sim \exp(1)$. We consider a more realistic path loss model $\ell(\cdot)$ that can i) avoid the singularity¹ at reduced transmit-receive

1. Holds when considering the standard path loss model of the form $r^{-\alpha}$.

distances [164] and ii) capture the subduction² effect of the path loss exponent [162], as

$$\ell(r_x) = \begin{cases} (\delta + r_x^{\alpha_0})^{-1} & , r_x \leq R_b \\ K r_x^{-\alpha_1} & , r_x > R_b \end{cases}, \quad (187)$$

where $\delta \in \{0, 1\}$, R_b is a baseline distance fitted from the propagation environment [162], $K = R_b^{\alpha_1} / (\delta + R_b^{\alpha_0})$ to ensure the continuity of $\ell(\cdot)$ in R_b , and α_0, α_1 are respectively the near- and far-field path loss exponents, such as $0 < \alpha_0 \leq \alpha_1$.

(187) as defined above, is a unified framework that can capture several popular models of the path loss. Typically,

- $\ell(\cdot)$ is the standard UPM when $\delta = 0$ and $\alpha_0 = \alpha_1 > 2$ [20, 24].
- $\ell(\cdot)$ is the BPM when $\delta = 1$ and $\alpha_0 = \alpha_1 > 2$ [164].
- $\ell(\cdot)$ is the DSPM when $\delta = 0$ and $\alpha_0 < \alpha_1$ [162].

Since UEs are battery-powered, each UE needs to tune its transmit power and compensate for the path loss effect in accordance with the distance to its associated BS. Also, UE transmit power cannot be increased indefinitely, but needs to be bounded by a maximum value P_{\max} . We then introduce a specific power control scheme, namely the DSBPC function $\psi(\cdot)$, as

$$\psi(r_x) = \begin{cases} \min \{ \hat{P}_{\max}; (\delta + r_x^{\alpha_0})^\epsilon \}, & r_x \leq R_b \\ \min \{ \hat{P}_{\max}; (r_x^{\alpha_1} / K)^\epsilon \}, & r_x > R_b \end{cases}, \quad (188)$$

where $\epsilon \in [0, \epsilon_d]$ is a parameter to tune the intensity of power control, such as $\epsilon_d \geq 1$ is a design upper allowed value of ϵ . \hat{P}_{\max} is the UE maximum transmit power, normalized by P_{ref} (UE reference transmit power when $\epsilon = 0$ or $r_x = 1 - \delta$).

Since most UDNs are interference-limited, we focus our analysis on the uplink SIR at the typical BS y_0 , expressed as

$$\text{SIR}(x_0; y_0) = \frac{g_{x_0} \ell(r) \psi(r)}{I_{x_0}}, \quad (189)$$

where I_{x_0} is the other-UE interference conditioned on a serving UE located at x_0 , and expressed as

$$I_{x_0} = \sum_{x \in \Psi \setminus \{x_0\}} g_x \ell(d_x) \psi(r_x). \quad (190)$$

2. It is the variation of the path loss exponent in multi-breakpoint between the transmitter and the receiver.

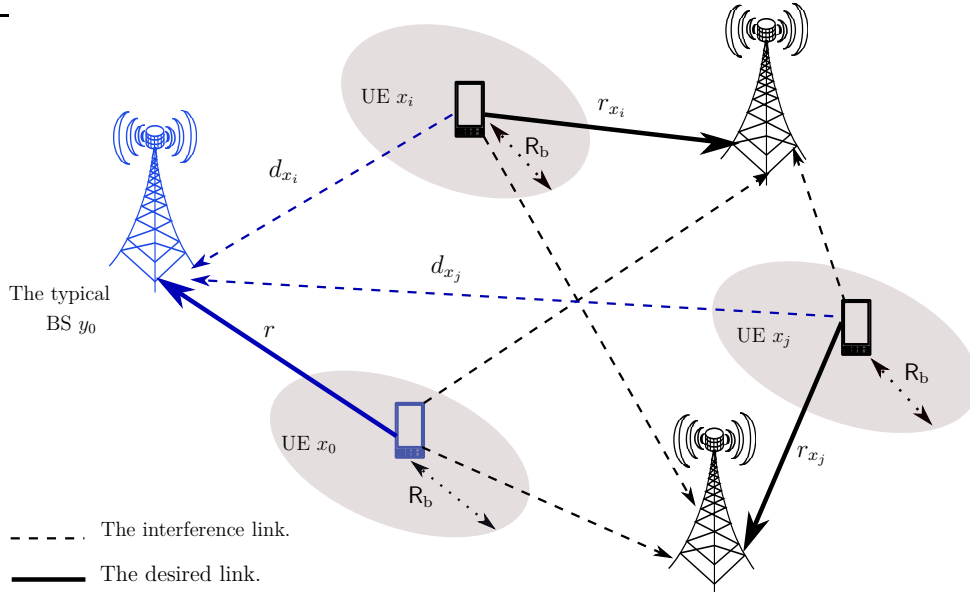


Figure 23 – The BS y_0 is served by x_0 and jammed by signals from the other active UEs. R_b is a parameter of the path loss model.

6.2.3 Distribution of Link Distances and the Process of the Interference Field

Approximating the distribution of key distances r and r_x , and characterizing the process of interfering UEs $\Psi \setminus \{x_0\}$, is generally challenging in uplink networks. This is in particular due to i) the coupling of active UEs location given the assumption of full-load uplink scenario combined with the OFDMA property, and ii) the coupling of active UEs location with that of BSs, due to the location dependent and power constrained DSBPC scheme.

A tight approximation of active UEs point process is proposed in [215], but with limited change to system design insights. Hence, for tractability, we adopt similar generative assumptions as those considered in [20, 24], where the PDF of r is expressed from the *void probability* as,

$$f_r(\xi) = 2\pi\lambda_b \exp(-\pi\lambda_b\xi^2), \quad (191)$$

and the distribution of r_x conditioned on d_x , expressed under a truncated version of (191), as

$$f_{r_x}(u|d_x) = \frac{f_r(u)}{1 - \exp(-\pi\lambda_b d_x^2)}, \quad 0 \leq u \leq d_x. \quad (192)$$

Furthermore, we model the location of interfering UEs by an inhomogeneous PPP outside an exclusion region of radius r . Its density is obtained as [24]

$$\lambda_{I_{x_0}}(d_x) = \lambda_b \left(1 - \exp(-\pi \lambda_b d_x^2)\right), \quad d_x > r. \quad (193)$$

6.2.4 Mobility Model

In realistic scenarios where users QoE is a crucial metric, active UEs are constantly on a quest for more advantageous locations enabling optimal uplink SIR such as openings, windows, and elevated points in obstructed areas. Accordingly, active UEs are assumed to simultaneously engage in a random movement in \mathbb{R}^2 without prior knowledge of their nearest BS location, namely the blind cell search (BCS) movement. For tractability, we adopt the 3GPP simulation mobility model introduced in [408], wherein the UE moves in a straight line with velocity v (distance per unit time), at angle θ w.r.t. the direction of connection. θ is randomly and uniformly distributed in $[0, \pi]$ due to symmetry.

6.3 Uplink Coverage Probability Analysis

In this section, we develop the baseline uplink framework under the DSBPC scheme (188). Typically, we consider two cases of analysis, i) the case of stationary active UEs and ii) the case of moving active UEs.

6.3.1 Case of Stationary Active UEs

When active UEs are randomly scattered but stationary, the uplink coverage probability is defined as the probability that the SIR at the typical BS located at the origin, exceeds a target T . Formally,

$$P_{cov}(\lambda_b, T) = \mathbb{P}(\text{SIR}(x_0; y_0) \geq T), \quad (194)$$

The following theorem derives the uplink coverage probability under the DSBPC scheme.

Theorem 3. *The uplink coverage probability under the DSBPC scheme is expressed as*

$$P_{cov}(\lambda_b, T) \approx 2\pi\lambda_b \int_0^{R_b} r \exp(-\pi\lambda_b r^2) \Omega(r) dr + 2\pi\lambda_b \int_{R_b}^{\infty} r \exp(-\pi\lambda_b r^2) \Theta(r) dr, \quad (195)$$

where the supplementary equations are listed in the top of the next page.

Proof. Given the formulation of SIR in (221), the definition of coverage probability in (194) is simplified as

$$P_{\text{cov}}(\lambda_b, \mathbb{T}) = \mathbb{E}_r \left\{ \mathcal{L}_{I_{x_0}} \left(\frac{\mathbb{T}}{\ell(r)\psi(r)} \middle| r \right) \right\}, \quad (199)$$

where the inner conditional Laplace function is derived as

$$\mathcal{L}_{I_{x_0}} \left(\frac{\mathbb{T}}{\ell(r)\psi(r)} \middle| r \right) = \mathbb{E} \left\{ \prod_{x \in \Psi \setminus \{x_0\}} \exp \left(- \frac{\mathbb{T} g_x \ell(d_x) \psi(r_x)}{\ell(r)\psi(r)} \right) \middle| r \right\} \quad (200)$$

$$\stackrel{\text{(a)}}{=} \mathbb{E}_{\Psi \setminus \{x_0\}} \left\{ \prod_{x \in \Psi \setminus \{x_0\}} \mathbb{E}_{r_x} \left\{ \frac{1}{1 + \frac{\mathbb{T} \ell(d_x) \psi(r_x)}{\ell(r)\psi(r)}} \middle| d_x, r \right\} \right\} \quad (201)$$

$$\stackrel{\text{(b)}}{=} \exp \left(-2\pi\lambda_b \int_r^\infty \mathbb{E}_{r_x} \left\{ \frac{1 - \exp(-\pi\lambda_b u^2)}{1 + \frac{\ell(r)\psi(r)}{\mathbb{T} \ell(u)\psi(r_x)}} \middle| r \right\} u du \right), \quad (202)$$

where (a) holds since $\Psi \setminus \{x_0\}$, r_x , and g_x are independent, in addition to $g_x \sim \exp(1)$, while (b) follows from the PGFL theorem [4, Prop. 1.2.2] and the expression of the interference process density in (193).

The remainder of the proof is obtained by first substituting (187) and (188) in (202), and next using PDFs (191) and (192) to average over r and r_x conditioned on d_x . \square

Although the expression of the uplink coverage probability under the DSBPC scheme in (195) is in complicated form, it is general enough to accommodate several previous expressions in [20, 24, 245]. Developing special closed form expressions of (195) is deferred to the journal version.

6.3.2 Case of Moving Active UEs

To quantify the contribution of the BCS mobility model on the statistics of the uplink coverage probability at the level of the typical BS y_0 , we introduce the induced³ uplink coverage probability, defined as the resultant uplink coverage probability following the BCS mobility

3. A dualism premise can be thought with the induced current in a coil following a random movement of the magnetic field inside it, i.e., the Faraday's law of electromagnetic induction.

$$\Omega(w) = \exp \left(-4\pi^2 \lambda_b^2 \left[\int_w^{R_b} h_1(u, w) u du + \int_{R_b}^{\infty} h_2(u, w) u du + \int_{R_b}^{\infty} h_3(u, w) u du \right] \right), \quad (196)$$

$$\Theta(w) = \exp \left(-4\pi^2 \lambda_b^2 \left[\int_w^{\infty} h_4(u, w) u du + \int_w^{\infty} h_5(u, w) u du \right] \right), \quad (197)$$

$$\begin{aligned} h_1(u, w) &= \int_0^u \frac{z \exp(-\pi \lambda_b z^2)}{1 + \frac{1}{T} \frac{\delta + u^{\alpha_0}}{\delta + w^{\alpha_0}} \frac{\min\{\hat{P}_{\max}; (\delta + w^{\alpha_0})^\epsilon\}}{\min\{\hat{P}_{\max}; (\delta + z^{\alpha_0})^\epsilon\}}} dz, & h_2(u, w) &= \int_0^{R_b} \frac{z \exp(-\pi \lambda_b z^2)}{1 + \frac{1}{TK} \frac{u^{\alpha_1}}{\delta + w^{\alpha_0}} \frac{\min\{\hat{P}_{\max}; (\delta + w^{\alpha_0})^\epsilon\}}{\min\{\hat{P}_{\max}; (\delta + z^{\alpha_0})^\epsilon\}}} dz, \\ h_3(u, w) &= \int_{R_b}^u \frac{z \exp(-\pi \lambda_b z^2)}{1 + \frac{1}{TK} \frac{u^{\alpha_1}}{\delta + w^{\alpha_0}} \frac{\min\{\hat{P}_{\max}; (\delta + w^{\alpha_0})^\epsilon\}}{\min\{\hat{P}_{\max}; z^{\epsilon \alpha_1} / K^\epsilon\}}} dz, & h_4(u, w) &= \int_0^{R_b} \frac{z \exp(-\pi \lambda_b z^2)}{1 + \frac{1}{T} \frac{u^{\alpha_1}}{w^{\alpha_1}} \frac{\min\{\hat{P}_{\max}; w^{\epsilon \alpha_1} / K^\epsilon\}}{\min\{\hat{P}_{\max}; (\delta + z^{\alpha_0})^\epsilon\}}} dz, \\ h_5(u, w) &= \int_{R_b}^u \frac{z \exp(-\pi \lambda_b z^2)}{1 + \frac{1}{T} \frac{u^{\alpha_1}}{w^{\alpha_1}} \frac{\min\{\hat{P}_{\max}; w^{\epsilon \alpha_1} / K^\epsilon\}}{\min\{\hat{P}_{\max}; z^{\epsilon \alpha_1} / K^\epsilon\}}} dz. \end{aligned} \quad (198)$$

model. Formally,

$$P_{\text{ind}}(\lambda_b, T, v) = \mathbb{E}_{r, \theta} \left(\mathbb{P} \left(\text{SIR}(x; y_0) \geq T, \bar{h} | r, \theta \right) \right) \quad (203)$$

$$= \mathbb{E}_{r, \theta} \left\{ \mathcal{L}_{I_x} \left(\frac{T}{\ell(\xi) \psi(\xi)} \middle| r, \theta \right) P_{\bar{h}}(\lambda_b, v | r, \theta) \right\}, \quad (204)$$

where x is the new location of the serving UE after the BCS such that $\xi = \|x - y_0\| = \sqrt{r^2 + v^2 + 2rv \cos(\theta)}$, \bar{h} denotes the event of no handover occurred where $P_{\bar{h}}(\lambda_b, v | r, \theta)$ is the probability that the handover does not occur given r and θ .

In the following, we will first evaluate the uplink handoff rate before deriving the induced uplink coverage probability.

The handoff rate abstraction

OFDMA is very sensitive to uplink interference [409], where the SIR achieved by a given UE may be severely limited by signals from closer UEs to the tagged BS. In such context, the serving UE is more likely to trigger a handoff towards another BS. Accordingly, we consider an association-based handoff rate as in [185], wherein the serving UE triggers immediately a handoff event as soon as another active UE becomes more closer to the typical BS.

Proposition 8 in the top of the following page, derives the uplink handoff rate conceived as the probability of generating a handoff event at the typical BS.

Proposition 8. *The uplink handoff rate for a serving UE moving according to the BCS mobility model is expressed as*

$$\begin{aligned} P_h(\lambda_b, v) &= 1 - \exp(-\pi\lambda_b v^2) + v\sqrt{\lambda_b} \int_{\pi/2}^{\pi} \cos(\theta) e^{-\pi\lambda_b v^2 \sin^2(\theta)} \operatorname{erf}\left(v\sqrt{\pi\lambda_b} \frac{\cos(2\theta)}{2\cos(\theta)}\right) d\theta \\ &+ v\sqrt{\lambda_b} \int_0^{\pi/2} \cos(\theta) e^{-\pi\lambda_b v^2 \sin^2(\theta)} d\theta - v\sqrt{\lambda_b} \int_0^{\pi} \cos(\theta) e^{-\pi\lambda_b v^2 \sin^2(\theta)} \operatorname{erf}\left(v\sqrt{\pi\lambda_b} \cos(\theta)\right) d\theta. \end{aligned} \quad (205)$$

Theorem 4. *The induced uplink coverage probability at the typical BS following the BCS mobility model of active UEs, is expressed when $v < R_b$, as*

$$\begin{aligned} P_{ind}(\lambda_b, T, v) &= 2\lambda_b \left[\int_0^{\frac{\pi}{2}} \int_0^{r_0} e^{-\pi\lambda_b \xi^2} \Omega(\xi) r dr d\theta + \int_{\frac{\pi}{2}}^{\pi} \int_0^{r_1} e^{-\pi\lambda_b \xi^2} \Omega(\xi) r dr d\theta + \int_{\frac{\pi}{2}}^{\pi} \int_{\frac{-v}{2\cos(\theta)}}^{r_2} e^{-\pi\lambda_b r^2} \Omega(\xi) r dr d\theta \right. \\ &\left. + \int_0^{\frac{\pi}{2}} \int_{r_0}^{\infty} e^{-\pi\lambda_b \xi^2} \Theta(\xi) r dr d\theta + \int_{\frac{\pi}{2}}^{\pi} \int_{r_1}^{\frac{-v}{2\cos(\theta)}} e^{-\pi\lambda_b \xi^2} \Theta(\xi) r dr d\theta + \int_{\frac{\pi}{2}}^{\pi} \int_{r_2}^{\infty} e^{-\pi\lambda_b r^2} \Theta(\xi) r dr d\theta \right], \end{aligned} \quad (206)$$

and when $v \geq R_b$, as

$$P_{ind}(\lambda_b, T, v) = 2\lambda_b \left[\int_0^{\frac{\pi}{2}} \int_0^{\infty} e^{-\pi\lambda_b \xi^2} \Theta(\xi) r dr d\theta + \int_{\frac{\pi}{2}}^{\pi} \int_0^{\frac{-v}{2\cos(\theta)}} e^{-\pi\lambda_b \xi^2} \Theta(\xi) r dr d\theta + \int_{\frac{\pi}{2}}^{\pi} \int_{\frac{-v}{2\cos(\theta)}}^{\infty} e^{-\pi\lambda_b r^2} \Theta(\xi) r dr d\theta \right], \quad (207)$$

where $r_0 = v\sqrt{\frac{R_b^2}{v^2} - \sin^2(\theta)} - v\cos(\theta)$, $r_1 = \min\left(r_0, \frac{-v}{2\cos(\theta)}\right)$, and $r_2 = \max\left(r_0, \frac{-v}{2\cos(\theta)}\right)$.

Proof. We will only give the outline of the proof. In fact, conditioned on r and θ , the probability that no handover occurs is expressed via the void probability, as

$$P_{\bar{h}}(\lambda_b, v|r, \theta) = \begin{cases} e^{-\pi\lambda_b(\xi^2 - r^2)}, & 0 \leq \theta \leq \frac{\pi}{2} \ \& \ r \geq 0 \\ 1, & \frac{\pi}{2} \leq \theta \leq \pi \ \& \ r \geq \frac{-v}{2\cos(\theta)} \\ e^{-\pi\lambda_b(\xi^2 - r^2)}, & \frac{\pi}{2} \leq \theta \leq \pi \ \& \ r \leq \frac{-v}{2\cos(\theta)}. \end{cases} \quad (208)$$

Next $P_{\bar{h}}(\lambda_b, v)$ is derived by averaging over the distribution of r in (191) and the distribution of θ , assumed to be uniformly distributed in $[0, \pi]$ due to symmetry. We have then

$$P_{\bar{h}}(\lambda_b, v) = \mathbb{E}_{r, \theta}(P_{\bar{h}}(\lambda_b, v|r, \theta)) \quad (209)$$

$$\begin{aligned} &= \frac{1}{\pi} \int_0^{\frac{\pi}{2}} \int_0^{\infty} 2\pi\lambda_b r e^{-\pi\lambda_b \xi^2} dr d\theta + \frac{1}{\pi} \int_{\frac{\pi}{2}}^{\pi} \int_{\frac{-v}{2\cos(\theta)}}^{\infty} 2\pi\lambda_b r e^{-\pi\lambda_b r^2} dr d\theta \\ &+ \frac{1}{\pi} \int_{\frac{\pi}{2}}^{\pi} \int_0^{\frac{-v}{2\cos(\theta)}} 2\pi\lambda_b r e^{-\pi\lambda_b \xi^2} dr d\theta. \end{aligned} \quad (210)$$

Table 4 – Comparing ξ and R_b based on the intervals of v , r , and θ .

	$v < R_b$	$v \geq R_b$
$\xi \leq R_b$	$0 \leq \theta \leq \frac{\pi}{2}, 0 \leq r \leq r_0$ $\frac{\pi}{2} \leq \theta \leq \pi, 0 \leq r \leq r_1$ $\frac{\pi}{2} \leq \theta \leq \pi, \frac{-v}{2\cos(\theta)} \leq r \leq r_2$	–
$\xi \geq R_b$	$0 \leq \theta \leq \frac{\pi}{2}, r \geq r_0$ $\frac{\pi}{2} \leq \theta \leq \pi, r_1 \leq r \leq \frac{-v}{2\cos(\theta)}$ $\frac{\pi}{2} \leq \theta \leq \pi, r \geq r_2$	$0 \leq \theta \leq \frac{\pi}{2}, r \geq 0$ $\frac{\pi}{2} \leq \theta \leq \pi, 0 \leq r \leq \frac{-v}{2\cos(\theta)}$ $\frac{\pi}{2} \leq \theta \leq \pi, r \geq \frac{-v}{2\cos(\theta)}$

The proof is finished by considering the definition of the error function $\text{erf}(\cdot)$ and deriving the handoff probability as $P_h(\lambda_b, v) = 1 - P_{\bar{h}}(\lambda_b, v)$. \square

The induced coverage probability

Theorem 4 in the top of next page, derives the induced uplink coverage probability following the BCS movement.

Proof. Given the properties of the BCS mobility model as described in Section II-D, it is quite obvious to mention that the process of active UEs Ψ remains a PPP. Also, given the expression of the induced uplink coverage probability in (204), we obtain

$$\begin{aligned}
P_{\text{ind}}(\cdot) &= \frac{1}{\pi} \int_0^\pi \int_0^\infty 2\pi\lambda_b r e^{-\pi\lambda_b r^2} P_{\bar{h}}(\lambda_b, v|r, \theta) \\
&\quad \times \exp\left(-2\pi\lambda_b \int_\xi^\infty \mathbb{E}_{r_x} \left\{ \frac{1 - \exp(-\pi\lambda_b u^2)}{1 + \frac{\ell(\xi)\psi(\xi)}{\Gamma\ell(u)\psi(r_x)}} \Big| r, \theta \right\} u du\right) dr d\theta. \quad (211)
\end{aligned}$$

Next, given the distance-dependence of the path loss model in (187) and the DSBPC in (188), splitting the expressions of $\ell(\xi)$ and $\psi(\xi)$ in (211) requires to previously identify the intervals of r and θ that yield a greater or lower ξ as compared to R_b , which comes to compare $\left(\frac{r}{v} + \cos(\theta)\right)^2 - \left(\frac{R_b^2}{v^2} - \sin^2(\theta)\right)$ with 0. Table 4 describes the effect of r , θ , and v intervals on the magnitude of ξ w.r.t. R_b . We conclude the proof by combining Table. 4 and Eq. (211). \square

6.4 Numerical Results

In this section, we present numerical results to assess our theoretical findings and quantify the interplay of system parameters. Numerical integration is evaluated using Matlab and Monte Carlo simulations are performed with 10^5 iterations.

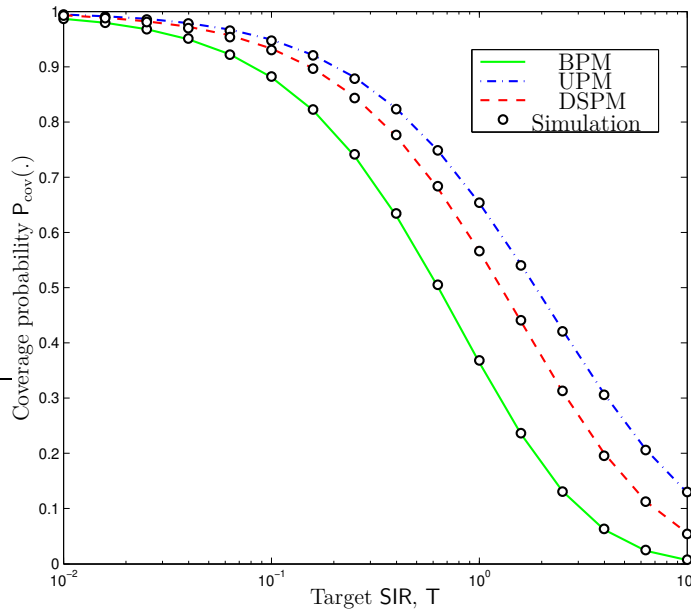


Figure 24 – The scaling of coverage probability with SIR threshold T under the BPM ($\delta = 1, \alpha_0 = \alpha_1 = 4$), the UPM ($\delta = 0, \alpha_0 = \alpha_1 = 4$), and the DSPM ($\delta = 0, R_b = 1, \alpha_0 = 2, \alpha_1 = 4$). We use the following common parameters, $\hat{P}_{\max} = 2, \lambda_b = 0.5$, and $\epsilon = 0.7$.

6.4.1 Validation of the Analytical results

Considering the three special cases of (187), namely the BPM, the UPM, and the DSPM, Fig. 24 describes the scaling of the uplink coverage probability with the SIR threshold T . The analytical curves (Theorem 3) match perfectly with the simulation results (eq. (194)), which validates the accuracy of our theoretical analysis. Typically, the UPM gives optimistic results of the uplink coverage probability as compared to BPM and DSPM, this is due in particular to the observation that the UPM amplifies the desired signal as $r \in [0, 1]$.

6.4.2 The DSBPC and the Uplink Performance of UDNs

Based on cells density λ_b , which implicitly reflects several loads of active uplink UEs, we can distinguish from Fig. 25, four operating regimes of OFDMA uplink networks.

The lightly loaded network regime

In such regime, e.g., $\lambda_b \leq 10^{-2}$ BSs/m² for $\hat{P}_{\max} = 2$ in Figs. 25-(a), (b), and (c), the uplink coverage for fixed \hat{P}_{\max} , is i) similar under the three path loss models and ii) λ_b -invariant regardless of ϵ (insensitive to power control). This is due to the observation that in such regime, UEs are more likely to be far from their nearest BS, and hence, the three path loss models are

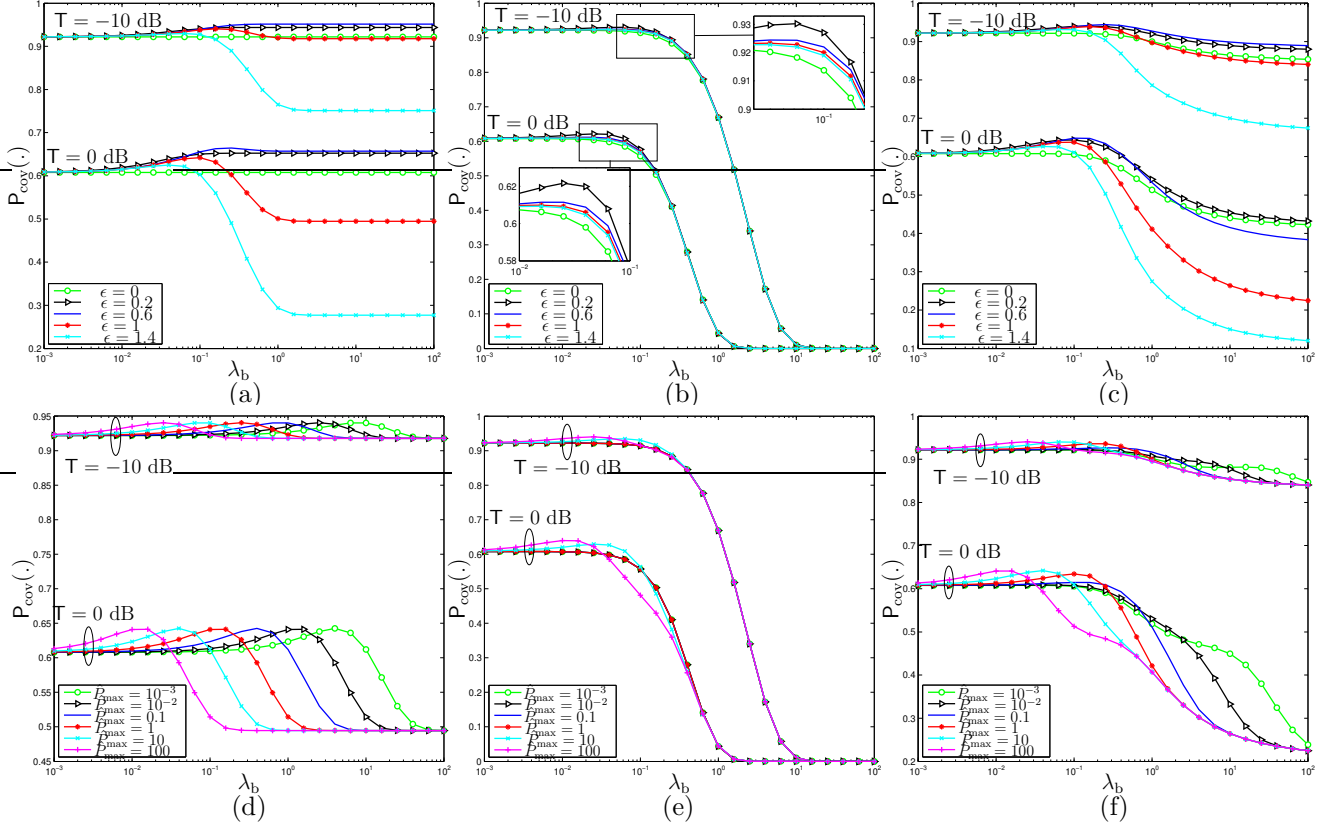


Figure 25 – The scaling of the uplink coverage probability $P_{\text{cov}}(\cdot)$ as a function of BS density λ_b and i) the power control exponent ϵ for $\hat{P}_{\text{max}} = 2$ in (a), (b) and (c). ii) the UE normalized maximum transmit power \hat{P}_{max} for $\epsilon = 1$ in (d), (e) and (f). Parameters for the UPM case in (a) and (d), are $\alpha_0 = \alpha_1 = 4$ and $\delta = 0$, for the BPM case in (b) and (e), are $\alpha_0 = \alpha_1 = 4$ and $\delta = 1$, and for the DSPM case in (c) and (f), are $\alpha_0 = 3$, $\alpha_1 = 4$, $R_b = 1$ and $\delta = 0$.

equivalent due to large transmitter-receiver distance. Also, UEs are more unlikely to benefit from the path loss compensation due to the \hat{P}_{max} constraint and hence the uplink interference power is counter-balanced by the serving signal power. We denote by $\lambda_b^{(1)}$ the width of this regime. Interestingly, Figs. 25-(d), (e), and (f) show that $\lambda_b^{(1)}$ scales with $1/\hat{P}_{\text{max}}$.

The affluent regime

As λ_b becomes greater than $\lambda_b^{(1)}$, we get into the affluent regime, wherein the uplink P_{cov} increases almost linearly with λ_b until a maximum value $P_{\text{cov}}^{\text{max}}$ when λ_b achieves some $\lambda_b^{(2)}$. This P_{cov} trend is particularly due to the increasing amount of active UEs that succeed to invert the path loss, while farther UEs (interferers) are still drastically constrained by \hat{P}_{max} . Interestingly, we can sense the effect of ϵ in this regime and the gap between UPM, BPM, and DSPM begins to emerge. Typically, P_{cov} remains almost unchanged from the previous regime if $\epsilon = 0$ and an increasing ϵ improves the rate of P_{cov} growth, until an optimum exponent $\epsilon_{\text{opt}} < 1$, after which the rate of P_{cov} growth shrinks down. Numerically, we obtain from Figs. 25-(a), (b), and (c),

that $\epsilon_{\text{opt}} \simeq 0.6$ under the UPM and DSPM, while $\epsilon_{\text{opt}} \simeq 0.2$ under the BPM.

The decay regime

when $\lambda_b > \lambda_b^{(2)}$, the average transmitter-receiver distance decreases, and hence the amount of farther (interfering) UEs that succeed to invert the path loss increases, while close UEs are increasingly reducing their transmit powers, particularly when $\epsilon \geq \epsilon_{\text{opt}}$, which results on the decay of the uplink coverage probability. However, when $\epsilon < \epsilon_{\text{opt}}$, the trend of uplink coverage probability is dependent on the considered path loss model. In fact, under the UPM, an increase in the interference power will be almost counter-balanced by an equivalent increase in the desired signal power due to singularity of the model, and hence the SIR remains almost invariant from the previous regime (Fig. 25-(a)). Conversely, the uplink coverage probability will decay under the BPM and the DSPM where the interference will be more powerful than the desired signal power given the non-singularity of the BPM, and the lower path loss exponent of the near-field region under the DSPM [162].

The UDNs regime

when λ_b is getting sufficiently large, e.g., $\lambda_b \geq 1$ BS/m² for $T = 0$ dB in Fig. 25, i.e., the context of UDNs, or heavily loaded OFDMA uplink networks. The gap between UPM, BPM and DSPM becomes evident. Typically, the SIR becomes λ_b -invariant under the UPM, due to the equilibrium between the interference and the desired signal powers. Conversely, the uplink P_{cov} under the BPM goes towards the near-universal outage as $\lambda_b \rightarrow \infty$, due to non-singularity at the transmitter [164]. Also, the uplink P_{cov} under the DSPM, goes towards 0 as $\lambda_b \rightarrow \infty$ if $\alpha_0 \leq 2$ (Fig. 25-(c)). Similar proof to [162, Prop. 1] is omitted here.

6.4.3 The Impact of Mobility on the Uplink Performance

Fig. 26 illustrates the scaling of the uplink handoff rate as a function of UE velocity v and network density λ_b . The analytical expression in Prop. 8 exactly matches the simulation results, which validate the accuracy of the theoretical analysis. Also, the curves in Fig. 26 show that the uplink handoff rate increases naturally with UE velocity v and cells density λ_b .

In Fig. 27, we assess the induced uplink coverage probability of Theorem. 4 conditioned on θ . Based on the parameter pair (v, θ) , We can identify the following key cases.

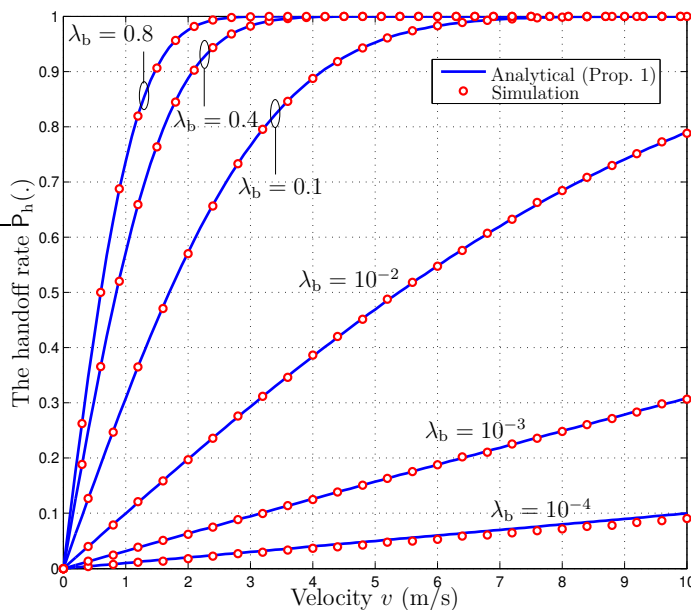


Figure 26 – The handoff rate as a function of the serving UE velocity v and the BS density λ_b .

A fleeing repulsive motion

it occurs when the serving UE moves away from y_0 at the earliest stage of its random movement, i.e., $0 \leq \theta \leq \pi/2$. That is, the serving UE movement is more likely to reduce the uplink P_{cov} under the UPM and BPM since it widens the desired link distance. Conversely, the DSPM enables to improve the induced coverage probability for low velocity of the serving UE, i.e., $0 < v < R_b$, due particularly to the observation that such random movement will reduce the desired signal power for low v and also the average number of interfering active UEs inside the near-field disk. However, when v is high enough, i.e., $v > R_b$, the uplink P_{cov} under DSPM converges to that under the UPM with α_1 .

A fleeing clustering motion

it occurs when the serving UE moves towards y_0 and next gets away from it given the amplitude of v , i.e., $\pi/2 < \theta \leq \pi$. In such a context, the uplink coverage probability under the UPM and the BPM, increases steadily with the serving UE mobility, until achieving the nearest allowed point to the typical BS. Next, the uplink P_{cov} shrinks down until a handover occurs. A different performance trend is reported under the DSPM, where the uplink coverage probability significantly increases for low user velocity, due to the interplay between of the desired signal and the interference powers with the near-field disk, next the P_{cov} curve converges to that under

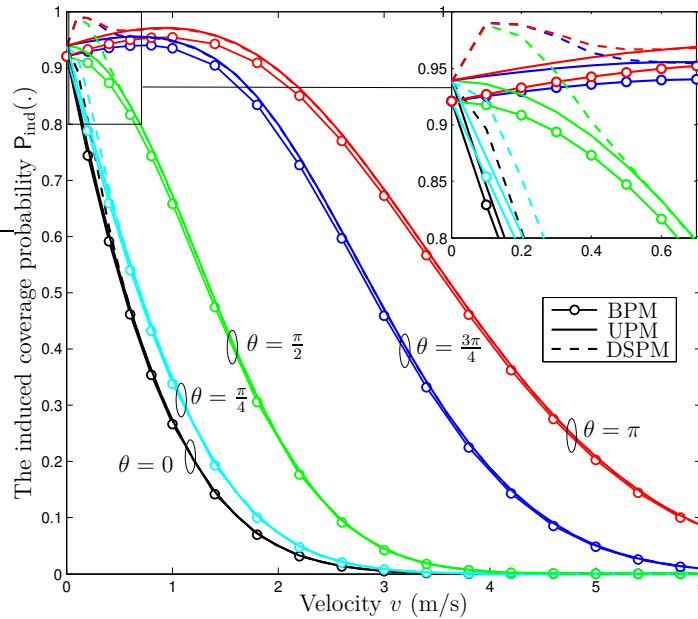


Figure 27 – The induced uplink coverage probability following the serving UE movement with velocity v , in the direction θ w.r.t. the link to the tagged BS. We use the following parameters: $\lambda_b = 10^{-3}$, $T = -10$ dB, $\hat{P}_{\max} = 2$, the BPM ($\delta = 1$, $\alpha_0 = \alpha_1 = 4$), the UPM ($\delta = 0$, $\alpha_0 = \alpha_1 = 4$), and the DSPM ($\delta = 0$, $R_b = 1$, $\alpha_0 = 3$, $\alpha_1 = 4$).

the UPM for sufficiently higher velocities

6.5 Chapter Summary

Considering a novel power control scheme built upon realistic path loss models and UEs constrained transmit power, we first develop a unified mathematical framework of the uplink coverage probability assuming a randomly but stationary active UEs. Next, and in order to improve their connectivity conditions, active UEs are assumed to engage in a linear random movement according to the 3GPP simulation mobility model. In such a context, we develop a tractable expression of the uplink handoff rate, which is necessary to derive the induced uplink coverage probability following mobility model. Analytical results are validated via simulations where we have identified four operating regimes of OFDMA uplink networks depending on system design parameters and the path loss model considered.

Typically, it has been shown that for sufficiently dense networks, the impact of power control on the uplink coverage is limited under the BPM, particularly for low SIR target, where farther UEs are more likely to jam the desired signal regardless of the path loss compensation. Conversely, the impact of power control is meaningful under the UPM and the DSPM due to

singularity at very low distances.

UPLINK ENERGY EFFICIENCY DISTRIBUTION WITH AERIAL USERS

The power consumption of future user equipments (UEs) will be affected by the projected growth in their computing capacity, while data throughput may be affected by emerging aerial UEs with specific radio propagation conditions compared to terrestrial UEs. In such a context, this letter evaluates a key metric of interest, namely the probability that the uplink energy efficiency (EE) at a typical ground base station will be higher than a predefined threshold. We first characterize the priority bias of each UE layer as a function of shadowing and system-level parameters to assess its penetration rate, i.e., the amount of active UEs from each tier among the total population of active UEs. Next, tractable approximations of the desired signal and the interference distribution are performed, enabling to derive the uplink EE. Our results demonstrate that an aggregation of the system-level parameters through the aerial priority bias needs to meet a given constraint to mitigate interference from aerial UEs and enhance the uplink EE of ground UEs. Monte-Carlo simulations validate the accuracy of our analytical results.

7.1 Introduction

Given their agility and flexible deployment, interest in unmanned aerial vehicles (UAVs) technology is rapidly growing, opening doors to various realms of application. The ongoing technological advances and upcoming generations of wireless networks such as fifth generation (5G) and beyond (B5G), will enable these equipments to be enhanced with many new sensors and seamless connectivity, making them more robust and more useful than their older versions.

Despite their expected benefits, UAVs as aerial user equipment (UE) in communication networks, can nevertheless have a detrimental impact on the performance of terrestrial UEs, which are often assigned more critical tasks than UAVs (e.g., monetary transactions, health-care services) [410]. The Third Generation Partnership Project (3GPP) has involved in Release 15 a technical study to assess the capability to serve aerial UEs through Long Term Evolution

(LTE) deployments where base station (BS) antennas are targeting terrestrial UEs [408]. It is particularly observed from simulations that an increased density¹ of aerial UEs will significantly increase the uplink interference on ground BSs. This is due to the observation that a typical aerial UE experiences line-of-sight propagation conditions with a higher probability to more cells as compared to a typical terrestrial UE. This increase in uplink interference would require a higher resource utilization level to maintain a similar level of throughput for ground UEs. On the other hand, increasing the resource utilization level further magnifies the uplink interference in the network, and hence further degrades the uplink throughput of both aerial and terrestrial UEs.

7.1.1 Related Works

Considering deterministic locations and fixed number of ground BSs, terrestrial UEs, and aerial UEs, most research efforts have generally leveraged field measurements and simulations [411], algorithmic analysis [412], and optimization theory [413] to evaluate the impact of aerial UEs on the performance of terrestrial LTE cellular networks. The above techniques are typically time-consuming, require customized setups for each experiment, and need complex and efficient algorithms. Hence, increasing need for tractable analytical models. To our knowledge, there is no analytical model available in the literature to capture the impact of UAVs system-level parameters (density, height, consumed power, and power control exponent) on uplink performance metrics of cellular networks.

Stochastic geometry and its inherent point process theory is considered as a powerful mathematical tool for the system-level analysis of wireless networks [17]. However, uplink analysis is highly challenging due to the coupling in active UEs locations following the use of orthogonal multiple access schemes such as orthogonal frequency-division multiple access (OFDMA), and also due to distance-dependent power control schemes inducing dependency between BSs and UEs locations. Several generative models have been developed in the literature to assess the uplink performance in terrestrial single-tier cellular networks [20], multi-tier wireless networks [414], and dense cellular networks [415]. Despite these analytical models, there are still important unexplored leads that need to be addressed. For instance, i) considering heterogeneity at the UE level (terrestrial and aerial UEs) as opposed to BS level (small cells, macro cells). The uplink analysis under the latter is revealed to be statistically equivalent to that under the single tier setup [414, Corollary 4]. Also, ii) previous works have only addressed typical perfor-

1. In this work, we consider an aggregated measure more general than aerial UE density, namely the aerial priority bias that we will discuss later.

mance metrics such as coverage probability and throughput. Adjusting system-level parameters to improve these metrics would however have a detrimental impact on other important metrics such as the power consumption at UEs interested in having longer battery autonomy.

7.1.2 Motivation and Contribution

In this chapter, our contributions can be summarized as follows:

- We consider two classes of terrestrial and aerial UEs with distinctive parameters in terms of shadowing, and system-level parameters, and introduce a measure of priority between UE tiers, namely the UE priority bias. The rationale is to evaluate the process of active uplink UEs from each tier and then derive the distribution of the distance to the serving UE in uplink.
- Deriving the process of interfering UEs is quite challenging in the uplink analysis. In our setup, we approximate it with an inhomogeneous Poisson point process (PPP) over an exclusion region defined by the tradeoff between interfering UEs and the serving UE average received power at the typical BS.
- Finally, we derive the distribution of the uplink energy efficiency (EE), enabling us to evaluate the amount of UEs with a good tradeoff between throughput and power consumption. Next, we illustrate the detrimental effect of increasing aerial priority bias on the EE. An analytical constraint based on the Lambert W function and mapping main system-level parameters is identified for proper operational regime of cellular networks with aerial UEs.

7.2 System Model

We consider the uplink of a cellular network made of terrestrial BSs modeled according to a 2D homogeneous PPP $\Psi_b \triangleq \{y_i\}$ with density λ_b in the plane $\mathcal{P} \subset \mathbb{R}^2$, and a vertical set of heterogeneous UEs (having data to transmit in uplink), comprising two classes of UEs; terrestrial UEs modeled according to a HPPP Ψ_t with density λ_t , and aerial UEs deployed at an average altitude h_a such that their projection in \mathcal{P} is modeled according to a homogeneous PPP Ψ_a with density λ_a . Without loss of generality, the typical BS y_0 at the origin O , is the object of the analysis.

We consider standard power-law path-loss between y_0 and UEs from Ψ_t and Ψ_a as $\ell_t(r) = \mathsf{K}r^{-\alpha}$ and $\ell_a(r) = \mathsf{K}(h_a^2 + r^2)^{-\frac{\alpha}{2}}$, respectively, where r is the horizontal distance between the UE

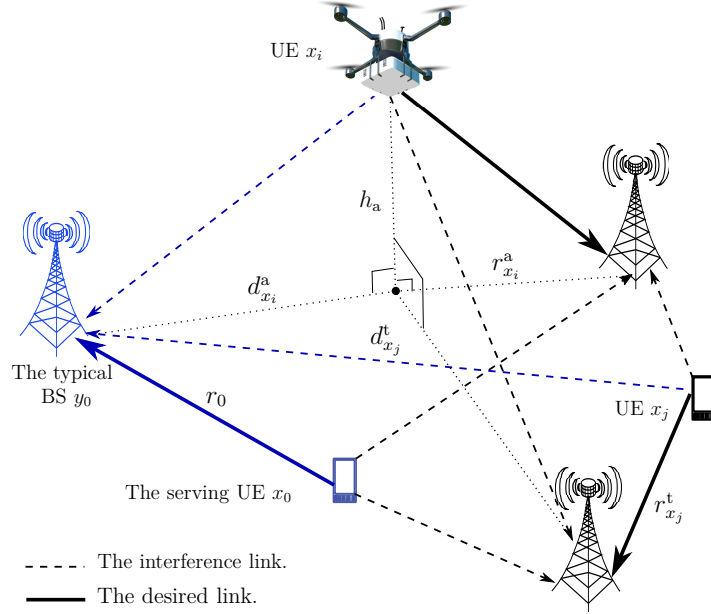


Figure 28 – PPP locations of BSs, terrestrial UEs, and aerial UEs. The BS y_0 is served by UE x_0 and jammed by signals from the other active UEs.

of interest and y_0 , $\alpha > 2$ is the path-loss exponent, and $K = \left(\frac{3 \cdot 10^8}{4\pi f}\right)^2$ is the free-space path-loss such that f is the transmission frequency. Multipath fading of the link between y_0 and a UE x , is incorporated by a positive independent and identically distributed (i.i.d.) exponential random variable (RV) g_x with unit average power, i.e., $g_x \sim \exp(1)$. Also, for $i \in \{t, a\}$, the link between y_0 and a UE from Ψ_i is subject to shadowing such that its power is modeled by log-normal RVs χ_i with mean μ_i (in dB) and standard deviation σ_i (in dB). Based on the displacement theorem, shadowing effect can be absorbed into the HPPP density. In this way, the displaced HPPP is still noted Ψ_i with density $\bar{\lambda}_i = \lambda_i \mathbb{E}(\chi_i^{2/\alpha}) < \infty$, where $\mathbb{E}(\chi_i^{2/\alpha}) = \exp\left(\frac{\ln(10)}{5} \frac{\mu_i}{\alpha} + \left(\frac{\ln(10)}{5\sqrt{2}} \frac{\sigma_i}{\alpha}\right)^2\right)$.

The total power usage for the uplink transmission of a UE from Ψ_i is $P_{\text{usage}}^i = P_{s,i} + P_{d,i}$, where $P_{s,i}$ and $P_{d,i}$ are, respectively, the static power consumed in UE's internal processes (e.g., signal processing, computing tasks, battery backup) and the dynamic power for wireless transmissions tuned in accordance with the distance to the associated BS since UEs are battery-powered. In this paper, we consider the fractional power control (FPC) such that $P_{d,i} = P_i (\ell_i(r))^{-\epsilon_i}$, where $\epsilon_i \in [0, 1]$ is the power control exponent and P_i is the UE transmit power when no power control is considered, i.e., $\epsilon_i = 0$. P_i can be seen as a selection bias to tune the uplink range of UEs. In a given time/frequency resource, the typical BS randomly selects a single active uplink UE

from all the UEs having a vertical projection inside its Voronoi cell², namely \mathcal{C}_0 . We focus on the loaded regime where each BS is active in the uplink. After associating only one UE per each BS, we have a network with a mixture of active terrestrial and aerial UEs. The amount of active UEs from each tier, i.e., the penetration rate, can be tuned by a knob of priority bias that naturally has to be designed as a function of shadowing and all system parameters (e.g., UE density, power bias, power control exponent, and altitude). For instance, we can increase the tendency of the typical BS to be connected to aerial UEs in uplink by lowering their altitude and/or increasing their density.

For tractability, we consider the following assumptions.

Assumption 1. *The class of UEs with higher priority bias is the one offering the best uplink average received power.*

Assumption 2. *The process of active uplink UEs (those scheduled to serve their own BS) is assumed to preserve the Poisson law as was endorsed by simulations in [24, Fig. 5].*

Given Assumptions 1 and 2, the priority bias measure can be used to characterize the process of active terrestrial and aerial UEs via independent thinning, respectively, denoted by $\tilde{\Psi}_t$ and $\tilde{\Psi}_a$ with respective densities $\tilde{\lambda}_t = \mathcal{A}_t \lambda_b$ and $\tilde{\lambda}_a = \mathcal{A}_a \lambda_b$, where \mathcal{A}_t and \mathcal{A}_a are the priority bias of terrestrial and aerial UEs, respectively. If terrestrial and aerial UEs are identical in terms of shadowing and system-level parameters, we naturally need to get $\mathcal{A}_t = \mathcal{A}_a = 0.5$. The following Lemma considers the general setup.

Lemma 4. *The priority bias of terrestrial and aerial UEs is, respectively, expressed as*

$$\begin{aligned} \mathcal{A}_t &= 1 - \exp\left(-\pi \bar{\lambda}_t \delta^2\right) \\ &+ 2\pi \bar{\lambda}_t e^{\pi \bar{\lambda}_a h_a^2} \int_{\delta}^{\infty} r \exp\left(-\pi \left(\bar{\lambda}_t r^2 + \bar{\lambda}_a \left(\mathsf{K}^{\epsilon_t - \epsilon_a} \frac{P_a}{P_t}\right)^{\frac{2}{\alpha(1-\epsilon_a)}} r^{\frac{2(1-\epsilon_t)}{1-\epsilon_a}}\right)\right) dr, \end{aligned} \quad (212)$$

$$\mathcal{A}_a = 2\pi \bar{\lambda}_a \int_0^{\infty} r \exp\left(-\pi \left(\bar{\lambda}_a r^2 + \bar{\lambda}_t \left(\mathsf{K}^{\epsilon_a - \epsilon_t} \frac{P_t}{P_a}\right)^{\frac{2}{\alpha(1-\epsilon_t)}} \left(r^2 + h_a^2\right)^{\frac{1-\epsilon_a}{1-\epsilon_t}}\right)\right) dr, \quad (213)$$

where $\delta = h_a^{\frac{1-\epsilon_a}{1-\epsilon_t}} \left(\mathsf{K}^{\epsilon_a - \epsilon_t} \frac{P_t}{P_a}\right)^{\frac{1}{\alpha(1-\epsilon_t)}}$.

Proof. For $i \in \{t, a\}$, the complementary cumulative distribution function (CCDF) of \bar{r}_i , the smallest distance to contact a UE from Ψ_i , is obtained from the null probability of the PPP Ψ_i

2. Hence, intra-cell interference is ignored, while inter-cell interference is present due to universal frequency reuse.

as

$$F_{\bar{r}_i}(u) = \mathbb{P}(\bar{r}_i > u) = \exp(-\pi \bar{\lambda}_i u^2). \quad (214)$$

From the abstraction of \mathcal{A}_t in Assumption 1, we get

$$\mathcal{A}_t = \mathbb{P}\left(\mathsf{K}^{1-\epsilon_t} P_t \bar{r}_t^{-\alpha(1-\epsilon_t)} \geq \mathsf{K}^{1-\epsilon_a} P_a \left(\bar{r}_a^2 + h_a^2\right)^{-\frac{\alpha(1-\epsilon_a)}{2}}\right) \quad (215)$$

$$= \mathbb{E}_{\bar{r}_t} \left(\mathbb{P}\left(\bar{r}_a^2 \geq \left(\mathsf{K}^{\epsilon_t - \epsilon_a} \frac{P_a}{P_t}\right)^{\frac{2}{\alpha(1-\epsilon_a)}} u^{\frac{2(1-\epsilon_t)}{1-\epsilon_a}} - h_a^2 \middle| \bar{r}_t = u\right) \right) \quad (216)$$

$$= - \int_0^\infty F_{\bar{r}_a} \left(\sqrt{\max\left(0, \left(\mathsf{K}^{\epsilon_t - \epsilon_a} \frac{P_a}{P_t}\right)^{\frac{2}{\alpha(1-\epsilon_a)}} u^{\frac{2(1-\epsilon_t)}{1-\epsilon_a}} - h_a^2\right)} \right) dF_{\bar{r}_t}(u). \quad (217)$$

Exact expression of \mathcal{A}_t is then obtained by using CCDFs in (214) and splitting the interval of integration based on δ . A similar approach is followed to derive \mathcal{A}_a . \square

Special cases: when $\epsilon_t = \epsilon_a = \epsilon$, Lemma 4 can be simplified under a closed-form expression as

$$\mathcal{A}_a = 1 - \mathcal{A}_t \quad (218)$$

$$= \frac{\bar{\lambda}_a P_a^{\frac{2}{\alpha(1-\epsilon)}}}{\bar{\lambda}_t P_t^{\frac{2}{\alpha(1-\epsilon)}} + \bar{\lambda}_a P_a^{\frac{2}{\alpha(1-\epsilon)}}} \exp\left(-\pi \bar{\lambda}_t h_a^2 \left(\frac{P_t}{P_a}\right)^{\frac{2}{\alpha(1-\epsilon)}}\right). \quad (219)$$

If we also have $P_a = P_t$, (219) can be further simplified as

$$\mathcal{A}_a = 1 - \mathcal{A}_t = \frac{\bar{\lambda}_a}{\bar{\lambda}_t + \bar{\lambda}_a} \exp\left(-\pi \bar{\lambda}_t h_a^2\right). \quad (220)$$

For $i \in \{t, a\}$, we denote by r_x^i the horizontal distance between a given UE $x \in \tilde{\Psi}_i$ and its nearest BS. Particularly, r_t and r_a are, respectively, the horizontal distance from y_0 to its nearest UE from $\tilde{\Psi}_t$ and $\tilde{\Psi}_a$. Also, we denote by \mathcal{S} the serving tier, i.e., $\mathcal{S} = \tilde{\Psi}_t$ or $\mathcal{S} = \tilde{\Psi}_a$, and by r_0 the horizontal distance from y_0 to its serving UE $x_0 \in \mathcal{S}$. The distance from y_0 to an interfering UE x from $\tilde{\Psi}_i \setminus \{x_0\}$ is denoted by d_x^i . Fig. 28 illustrates the setup of our system model.

For the sake of simplicity, we ignore thermal noise and focus our analysis on the interference-limited regime [20, 414]. In such a context, the signal-to-interference ratio (SIR) at y_0 is given

by

$$\text{SIR}(x_0 \in \tilde{\Psi}_i; y_0) = \frac{g_{x_0} P_i (\ell_i(r_0))^{1-\epsilon_i}}{I_{x_0,i}^t + I_{x_0,i}^a}, \quad (221)$$

where for $i, j \in \{t, a\}$, $I_{x_0,i}^j$ is the interference generated by UEs from $\tilde{\Psi}_j \setminus \{x_0\}$ conditioned on a serving UE $x_0 \in \tilde{\Psi}_i$. It is expressed as

$$I_{x_0,i}^j = \sum_{x \in \tilde{\Psi}_j \setminus \{x_0 \in \tilde{\Psi}_i\}} g_x P_j \ell_j(d_x^j) (\ell_j(r_x^j))^{-\epsilon_j}. \quad (222)$$

7.3 Uplink Energy Efficiency Distribution

In this section, we provide the key analytical framework to derive the uplink EE distribution under a setup with terrestrial and aerial UEs.

Definition 1. *The uplink rate (in bps) at the typical BS y_0 when it is served by $x_0 \in \tilde{\Psi}_i$ ($i \in \{t, a\}$) is*

$$\mathcal{R}_i = \frac{\mathbf{B}}{\mathbf{N} + 1} \log_2 \left(1 + \text{SIR}(x_0 \in \tilde{\Psi}_i; y_0) \right), \quad (223)$$

where \mathbf{B} is the total effective uplink bandwidth in Hz and \mathbf{N} is the total number of UEs from $\Psi_t \cup \Psi_a \setminus \{x_0 \in \tilde{\Psi}_i\}$ with orthogonal projection inside \mathcal{C}_0 .

Definition 2. *(Energy efficiency coverage). EE coverage \mathcal{E}_c is defined as the probability that the uplink EE measured at the typical BS is higher than a predefined threshold T . Formally,*

$$\mathcal{E}_c = \sum_{i \in \{t, a\}} \mathbb{P} \left(\frac{\mathcal{R}_i}{P_{s,i} + P_{d,i}} \geq \mathsf{T}, \mathcal{S} = \tilde{\Psi}_i \right). \quad (224)$$

The EE distribution is completely characterized by the EE coverage. Also, \mathbf{N} is a RV depending on the serving area of the typical BS y_0 , i.e., \mathcal{C}_0 , and the priority bias that governs the number of active terrestrial and aerial UEs in the uplink.

Assumption 3. *Given the orthogonal allocation of channel resources, it is reasonable to consider that the number \mathbf{N} of competing UEs is uncorrelated with SIR at y_0 .*

In this way, the EE coverage can be derived as

$$\mathcal{E}_c = \sum_{i \in \{t, a\}} \mathbb{P} \left(\frac{\log_2 \left(1 + \text{SIR}(x_0 \in \tilde{\Psi}_i; y_0) \right)}{P_{s,i} + P_{d,i}} \geq \frac{T(N+1)}{B}, \mathcal{S} = \tilde{\Psi}_i \right) \quad (225)$$

$$\stackrel{(a)}{=} \sum_{m \geq 0} \sum_{i \in \{t, a\}} \mathbb{P}(\mathbf{N} = m) \mathbb{P} \left(g_{x_0} \geq s_i(m, r_0) \left(I_{x_0, i}^t + I_{x_0, i}^a \right), \mathcal{S} = \tilde{\Psi}_i \right) \quad (226)$$

$$\stackrel{(b)}{=} \sum_{m \geq 0} \sum_{i \in \{t, a\}} \mathbb{P}(\mathbf{N} = m) \mathbb{E}_{r_0} \left(\mathcal{L}_{I_{x_0, i}^t} \left(s_i(m, r_0) \right) \mathcal{L}_{I_{x_0, i}^a} \left(s_i(m, r_0) \right) \right), \quad (227)$$

where (a) comes from the independence between the distribution of the number of competing UEs to x_0 and the received SIR from x_0 , (b) comes from $g_x \sim \exp(1)$ and the definition of the Laplace functional, where for $i \in \{t, a\}$, $s_i(m, r_0) = \frac{2^{\frac{T(m+1)}{B}} (P_{s,i} + P_i(\ell_i(r_0))^{-\epsilon_i}) - 1}{P_i(\ell_i(r_0))^{1-\epsilon_i}}$, and the probability mass function (PMF) of \mathbf{N} is [403]

$$\mathbb{P}(\mathbf{N} = m) \simeq \frac{3.5^{3.5}}{\Gamma(3.5)} \frac{\Gamma(m+4.5)}{m!} \left(\frac{\bar{\lambda}_t + \bar{\lambda}_a}{\lambda_b} \right)^m \left(3.5 + \frac{\bar{\lambda}_t + \bar{\lambda}_a}{\lambda_b} \right)^{-(m+4.5)}. \quad (228)$$

We derive next the supplementary terms for the computation of the uplink EE coverage.

7.3.1 Distribution of the serving UE

After associating one UE per each BS, the probability density function (PDF) of the horizontal distance between the typical BS y_0 and its serving UE x_0 from $\tilde{\Psi}_t$ is derived as

$$f_{r_0}(u, \mathcal{S} = \tilde{\Psi}_t) = f_{r_t}(u) \mathbb{P} \left(\mathbf{K}^{-\epsilon_t} P_t u^{-\alpha(1-\epsilon_t)} > \mathbf{K}^{-\epsilon_a} P_a \left(r_a^2 + h_a^2 \right)^{-\frac{\alpha(1-\epsilon_a)}{2}} \right) \quad (229)$$

$$= 2\pi \tilde{\lambda}_t u \exp(-\pi \tilde{\lambda}_t u^2) \times \begin{cases} 1, & u < \delta \\ \exp \left(-\pi \tilde{\lambda}_a \left(\left(\mathbf{K}^{\epsilon_t - \epsilon_a} \frac{P_a}{P_t} \right)^{\frac{2}{\alpha(1-\epsilon_a)}} u^{\frac{2(1-\epsilon_t)}{1-\epsilon_a}} - h_a^2 \right) \right), & \text{otherwise.} \end{cases} \quad (230)$$

Similarly, the PDF of the horizontal distance between the typical BS y_0 and its serving UE x_0 from $\tilde{\Psi}_a$ is

$$f_{r_0}(u, \mathcal{S} = \tilde{\Psi}_a) = f_{r_a}(u) \mathbb{P} \left(\mathsf{K}^{-\epsilon_a} P_a (u^2 + h_a^2)^{-\frac{\alpha(1-\epsilon_a)}{2}} > \mathsf{K}^{-\epsilon_t} P_t r_t^{-\alpha(1-\epsilon_t)} \right) \quad (231)$$

$$= 2\pi \tilde{\lambda}_a u \exp(-\pi \tilde{\lambda}_a u^2) \exp \left(-\pi \tilde{\lambda}_t \left(\left(\mathsf{K}^{\epsilon_a - \epsilon_t} \frac{P_t}{P_a} \right)^{\frac{2}{\alpha(1-\epsilon_t)}} (u^2 + h_a^2)^{\frac{1-\epsilon_a}{1-\epsilon_t}} \right) \right). \quad (232)$$

The above expressions of the serving distance PDF are different from those defined in [20, 414, 415], where only one homogeneous class of UEs is considered.

Approximating the process of interfering UEs is quite challenging due to coupling in UEs locations. For tractability, we adopt a similar abstraction as in [24, 414], where for $i \in \{t, a\}$,

Assumption 4. *The process of interferers from $\tilde{\Psi}_i$, conditioned on the serving UE, is modeled by an inhomogeneous PPP of density $\tilde{\lambda}_i (1 - \exp(-\pi \tilde{\lambda}_i v^2))$, where v is the horizontal distance to a given interferer.*

Assumption 5. *Conditioned on an interfering UE $x \in \tilde{\Psi}_i$, the PDF of r_x^i is expressed under a truncated version as*

$$f_{r_x^i}(w | d_x^i = v) = \frac{2\pi \tilde{\lambda}_i w \exp(-\pi \tilde{\lambda}_i w^2)}{1 - \exp(-\pi \tilde{\lambda}_i v^2)}, \forall w \leq v. \quad (233)$$

The exclusion region of interfering UEs under our setup is defined by the observation that the average received power from any interfering UE at y_0 needs to be lower than that received from the serving UE x_0 . Otherwise, the interfering UE will be associated to the typical BS y_0 . Formally,

$$P_i \ell_i(d_x^i) (\ell_i(r_x^i))^{-\epsilon_i} \leq P_j (\ell_j(r_0))^{1-\epsilon_j}, \forall i, j \in \{t, a\}. \quad (234)$$

7.3.2 Interference from active terrestrial users

For $j \in \{t, a\}$, the Laplace functional of the interference generated by UEs from $\tilde{\Psi}_t$ when the serving UE belongs to $\tilde{\Psi}_j$, is obtained as

$$\mathcal{L}_{I_{x_0,j}^t}(s) = \mathbb{E} \left(\exp \left(-s \sum_{x \in \tilde{\Psi}_t \setminus \{x_0 \in \tilde{\Psi}_j\}} g_x P_t \mathbf{K}^{1-\epsilon_t} (d_x^t)^{-\alpha} (r_x^t)^{\alpha \epsilon_t} \right) \right) \quad (235)$$

$$= \mathbb{E} \left(\prod_{x \in \tilde{\Psi}_t \setminus \{x_0 \in \tilde{\Psi}_j\}} \mathbb{E}_{r_x^t} \left(\frac{1}{1 + s P_t \mathbf{K}^{1-\epsilon_t} (d_x^t)^{-\alpha} (r_x^t)^{\alpha \epsilon_t}} \right) \right) \quad (236)$$

$$\stackrel{(a)}{=} \exp \left(-4\pi^2 \tilde{\lambda}_t^2 \int_0^\infty \int_0^v \frac{v w e^{-\pi \tilde{\lambda}_t w^2}}{1 + \frac{\mathbf{K}^{\epsilon_t-1} v^\alpha}{s P_t w^{\alpha \epsilon_t}}} dw dv \right), \quad (237)$$

where (a) is by averaging first over the PDF of r_x^t in Assumption 5. Next, we use the probability generating functional (PGFL) theorem where the density of the interference field is defined in Assumption 4. The integration range of $d_x = v$ starts from 0, since the closest interfering UE can be closer to y_0 than the desired UE x_0 . This is possible from (234) since, for an interferer UE from $\tilde{\Psi}_t$ with a distance to its closest BS of $r_x^t = r_0/n$ ($n > 1$), it can be closer to y_0 by r_0/n^{ϵ_t} .

7.3.3 Interference from active aerial users

The Laplace functional of the interference generated by UEs from $\tilde{\Psi}_a$ when the serving UE belongs to $\tilde{\Psi}_t$ and distant from y_0 by $r_0 = u$, is obtained as

$$\mathcal{L}_{I_{x_0,t}^a}(s) = \exp \left(-4\pi^2 \tilde{\lambda}_a^2 \int_{\varpi(u)}^\infty \int_0^v \frac{v w e^{-\pi \tilde{\lambda}_a w^2}}{1 + \frac{\mathbf{K}^{\epsilon_a-1} (v^2+h_a^2)^{\frac{\alpha}{2}}}{s P_a (w^2+h_a^2)^{\frac{\alpha \epsilon_a}{2}}}} dw dv \right), \quad (238)$$

where the starting point of the integration range with respect to $d_x = v$ is derived from (234) as

$$\varpi(u) = \begin{cases} 0 & , u < \delta \\ h_a \sqrt{\left(\frac{P_a}{P_t} \mathbf{K}^{\epsilon_t - \epsilon_a} \right)^{\frac{2}{\alpha}} \frac{u^{2(1-\epsilon_t)}}{h_a^{2(1-\epsilon_a)}} - 1} & , \text{otherwise.} \end{cases} \quad (239)$$

Similarly, the Laplace functional of the interference generated by UEs from $\tilde{\Psi}_a$ when the serving UE belongs to $\tilde{\Psi}_a$ and distant from y_0 by $r_0 = u$, is obtained as

$$\mathcal{L}_{I_{x_0,a}^a}(s) = \exp \left(-4\pi^2 \tilde{\lambda}_a^2 \int_{\pi(u)}^{\infty} \int_0^v \frac{vwe^{-\pi\tilde{\lambda}_a w^2}}{1 + \frac{K^{\epsilon_a-1}}{sP_a} \frac{(v^2+h_a^2)^{\frac{\alpha}{2}}}{(w^2+h_a^2)^{\frac{\alpha\epsilon_a}{2}}}} dw dv \right), \quad (240)$$

where $\pi(u) = h_a \sqrt{\left(\frac{u^2}{h_a^2} + 1\right)^{1-\epsilon_a} - 1}$.

7.4 Numerical Results

We consider a typical cellular network where each BS has an average of 80 smartphones and 20 quadcopter UAVs within its coverage area, i.e., $\lambda_t = 80 \lambda_b$ and $\lambda_a = 20 \lambda_b$. We have the following standard parameters: $\alpha = 4$, $f = 2.1$ GHz, $B = 5$ MHz, $\mu_t = \mu_a = 0$ dB, $P_t = 33$ dBm, $P_a = 36$ dBm, $P_{s,t} = 0.5$ Watts, and $P_{s,a} = 2.5$ Watts.

We first need to validate the expression of priority bias derived in Lemma 4. Fig. 29 illustrating the simulated and analytical expression of the aerial priority bias shows that the analytical expression in Lemma 4 is perfectly accurate.

In Fig. 30, we validate the analytical expression of the EE coverage under the mean load setup, i.e., $\mathbb{P}(\mathbf{N} = 1 + 1.28 \frac{\bar{\lambda}_t + \bar{\lambda}_a}{\lambda_b}) \simeq 1$ [403]. It has been shown that the EE coverage decays when lowering UAVs height or increasing their density by making aerial shadowing more variable, i.e., increasing σ_a . This is a similar result to [403], where shadowing is revealed to be a natural load balancing bias between tiers of BSs in the downlink. Here, it plays the role of a natural priority balancing between several classes of uplink UEs.

In Fig. 31, we illustrate the mean load terrestrial EE coverage, i.e., $\mathcal{E}_c(\mathcal{S} = \tilde{\Psi}_t)$, and the aerial priority bias \mathcal{A}_a as a function of the power control exponent $\epsilon = \epsilon_t = \epsilon_a$ and UAVs height h_a . $\mathcal{E}_c(\mathcal{S} = \tilde{\Psi}_t)$ is typically monotonically decreasing with the aerial priority bias. Reducing the latter can therefore reduce the detrimental effect of UAVs on the EE of terrestrial UEs. To achieve this, we can act not only by reducing UAVs density (as mentioned in [408]), but also by acting on other system parameters such as altitude and the power control exponent (see Fig. 29). In the general case, assuming a properly operating LTE cellular network for $\mathcal{A}_a \leq \beta < 1$, we get from (219)

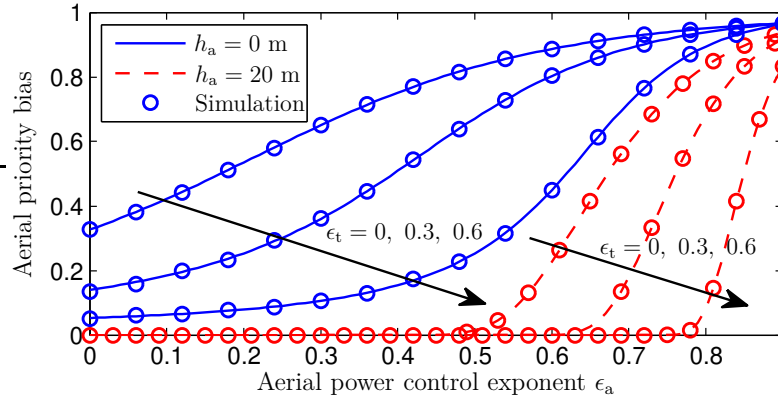


Figure 29 – Aerial priority bias as a function of terrestrial and aerial power control exponents and UAVs altitude, when $\lambda_b = 10^{-2}$, $\sigma_t = 4$ dB, and $\sigma_a = 8$ dB.

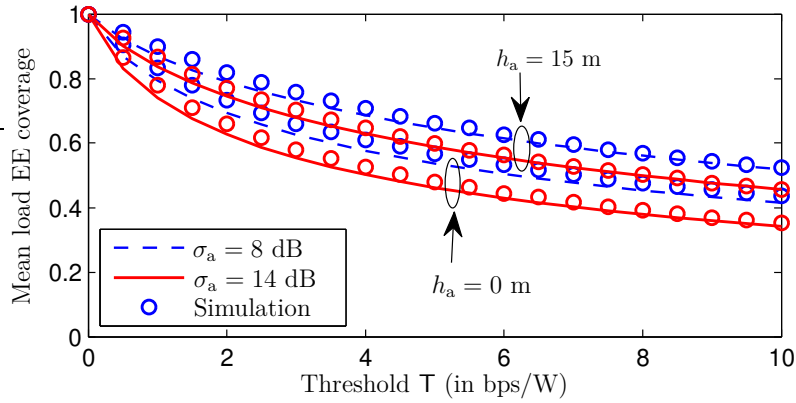


Figure 30 – Mean load approximation of the uplink EE coverage when $\lambda_b = 10^{-2}$, $\epsilon_t = \epsilon_a = 0.5$, and $\sigma_t = 0$ dB.

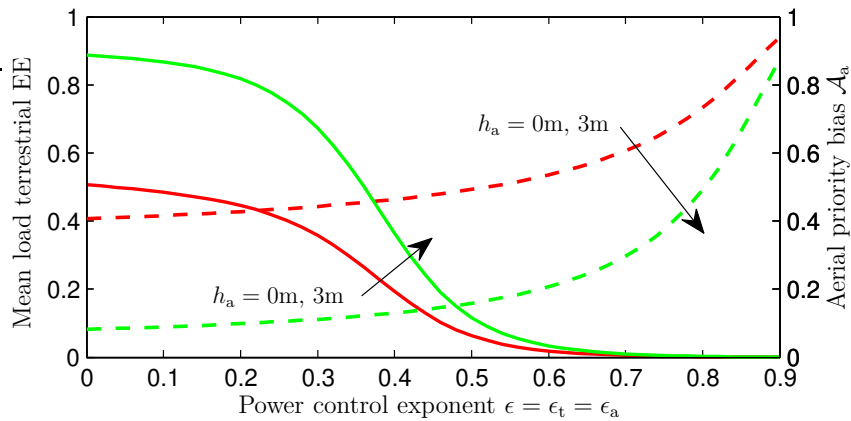


Figure 31 – Mean load approximation of the uplink terrestrial EE coverage $\mathcal{E}_c(\mathcal{S} = \tilde{\Psi}_t)$ (Solid lines) and aerial priority bias \mathcal{A}_a (Dashed lines) as a function of the power control exponent $\epsilon = \epsilon_t = \epsilon_a$ and UAVs height h_a (Arrow) when $\lambda_b = 10^{-3}$, $\sigma_t = 0$ dB, $\sigma_a = 10$ dB, and $T = 10$ bps/W.

$$\pi h_a^2 \left(\bar{\lambda}_a + \bar{\lambda}_t \left(\frac{P_t}{P_a} \right)^{\frac{2}{\alpha(1-\epsilon)}} \right) \exp \left(\pi h_a^2 \left(\bar{\lambda}_a + \bar{\lambda}_t \left(\frac{P_t}{P_a} \right)^{\frac{2}{\alpha(1-\epsilon)}} \right) \right) \geq \frac{\pi \bar{\lambda}_a h_a^2}{\beta} \exp(\pi \bar{\lambda}_a h_a^2). \quad (241)$$

Since W_0 is the inverse relation of $f(w) = we^w$, we obtain from (241) a transcendental constraint as

$$\left(\frac{P_t}{P_a} \right)^{\frac{2}{\alpha(1-\epsilon)}} \geq \frac{W_0 \left(\frac{\pi \bar{\lambda}_a h_a^2}{\beta} \exp(\pi \bar{\lambda}_a h_a^2) \right) - \pi \bar{\lambda}_a h_a^2}{\pi \bar{\lambda}_t h_a^2}. \quad (242)$$

7.5 Chapter Summary

This chapter proposed a tractable analytical framework to derive the uplink EE coverage under a setup where two classes of terrestrial and aerial UEs are considered. It has been particularly shown that increased tendency of terrestrial BSs to be connected to aerial UEs, i.e., increased aerial priority bias (not only UAVs density as reported in [408]), will have a detrimental effect on the uplink EE of ground UEs. Assuming similar power control exponents for terrestrial and aerial UEs, we have identified a compact analytical constraint for a proper operational regime of the network in terms of EE coverage.

Future generalization of this work will consider constrained transmit power at the level of each UE class, in addition to multi-tier BSs. The rationale is to investigate the impact of a decoupled uplink and downlink association scheme on EE.

RÉSUMÉ LONG EN FRANÇAIS

La géométrie stochastique (SG) est un champ de la probabilité appliquée qui vise à proposer des modèles mathématiques tractables et des méthodes statistiques appropriées pour étudier et analyser des phénomènes aléatoires sur le plan \mathbb{R}^2 ou dans des dimensions supérieures [1]. Son développement a été motivé par des applications dans divers domaines scientifiques tels que la foresterie, l'analyse d'images, la géophysique, la neurophysiologie, la cardiologie, la finance et l'économie. Dans le contexte des réseaux de communication, l'emplacement des équipements utilisateurs et des stations de base sont considérés comme des réalisations parmi un nombre énorme de possibilités, où concevoir le système pour chaque réalisation de réseau serait laborieux et exigerait beaucoup de ressources [2, 3]. Au lieu de cela, en utilisant les outils de la SG [1–8], l'emplacement des nœuds est évalué statistiquement afin de quantifier les moyennes spatiales, ce qui permet de prendre en compte toutes les réalisations possibles du réseau et de cerner généralement les dépendances fondamentales relatives à la performance du réseau (e.g., capacité/débit et fiabilité). Le travail [15] est le premier à considérer des outils de la SG pour évaluer la connectivité dans un réseau de stations représenté par un processus ponctuel de Poisson (PPP). En particulier, il a fallu attendre la fin des années 90 pour que des idées importantes de la SG trouvent leur chemin vers la modélisation et l'analyse des réseaux de communication [2, 3]. Ainsi, des outils basés sur les tessellations de Poisson-Voronoi et la triangulation de Delaunay ont été proposés pour dériver les caractéristiques géométriques des liens hiérarchiques entre les stations. Des résultats clés ont été rapportés une décennie plus tard, où la technique mathématique de base a été définie pour un réseau sans fil mono-niveau [16, 17, 56]. Ensuite, des généralisations à des modèles de SG plus avancés ont été progressivement adoptées pour des applications aux réseaux sans fil finis [59], aux réseaux multi-niveaux [18, 19], et à la liaison montante [20]. Pour plus de discussions sur ces premières extensions, veuillez consulter [21–24].

La digitalisation croissante de la société moderne fait que les réseaux de cinquième génération et au-delà (5G/B5G) sont appelés à jouer un rôle primordial dans le développement des débits de données, de l'hyper-connectivité et de la latence ultra-faible. Pour répondre à ces exigences, les futurs réseaux sans fil 5G/B5G devraient être plus hétérogènes en raison de diverses applications ciblées, en plus de l'utilisation de bandes de fréquences élevées (e.g., ondes millimétriques (mmWave) [27], communications teraHertz [28], et communications en lumière

visible (VLC) [29]) permettant la mise en place de réseaux à haut débit et à courte portée. En outre, les objets de l'environnement seront recouverts de méta-surfaces intelligentes capables de réfléchir les signaux incidents d'une manière personnalisée afin d'optimiser/recycler la propagation des signaux dans les réseaux du futur [30]. L'utilisation de systèmes aériens sans pilote (UAV) sera une technologie répandue et mature, où ils pourront être utilisés comme des stations de base volantes pour assurer la couverture terrestre dans des régions isolées, améliorer la capacité dans des zones fortement surchargées par le trafic, et même être utilisés comme UAV volants à des fins de livraison ou de supervision [31]. Il est intéressant de constater que les terminaux utilisateurs seront progressivement équipés de capacités de calcul et/ou de stockage permettant de passer du paradigme de la connectivité omniprésente à celui de l'intelligence sans fil omniprésente [32].

Ainsi, au fur et à mesure que la complexité et l'hétérogénéité des réseaux sans fil modernes augmenteront, les outils de l'intelligence artificielle et de l'apprentissage machine (ML) seront indispensables pour appréhender les aspects statiques et dynamiques de l'environnement sans fil, puis aider à prendre des décisions de contrôle optimales pour les performances du système. Dans ce contexte, la SG considérée comme un outil puissant de modélisation et d'évaluation des réseaux sans fil au cours de la dernière décennie, devrait rester un domaine de recherche effervescent dans l'avenir prévisible, pour les raisons suivantes : Premièrement, la configuration spatiale des émetteurs et des récepteurs continuera à jouer un rôle essentiel dans la prédiction des indicateurs de performance dans les réseaux sans fil 5G/B5G. Deuxièmement, une synergie entre la SG et ML peut être établie pour obtenir de meilleurs résultats en termes de précision et de flexibilité. Généralement, la SG peut être intégrée comme une classe d'hypothèses dans le processus d'apprentissage de ML pour évaluer la famille de problèmes de sélection des sous-ensembles [35,36]. Troisièmement, malgré la possibilité de construire un environnement sans fil programmable et commandé dans les réseaux 5G/B5G, grâce à l'intelligence omniprésente et à l'adoption massive de méta-surfaces, il est en fait impossible de contrôler toutes les facettes de l'environnement, par exemple le mouvement des bâtiments généré par les vents et la dilatation thermique des matériaux [37] ou le mauvais alignement des faisceaux dans les communications à haute fréquence [38]. D'où la nécessité de modéliser ces aspects non maîtrisés du réseau par des processus aléatoires, et donc le besoin omniprésent de la SG.

Dans ce travail de thèse, j'utiliserai des outils analytiques de la SG pour modéliser et analyser la liaison descendante et montante des réseaux sans fil. Les résultats obtenus dans le cadre de la présente thèse peuvent être étendus à un large éventail de configurations. Pour résumer, les contributions peuvent être présentées comme suit

-
- Chapitre 1 : Nous proposons une revue de la littérature jusqu'en 2020, sur les applications des modèles de de la SG dans la modélisation et l'analyse des communications sans fil. En particulier, nous élaborons pour la première fois une taxonomie complète de ces processus ponctuels (PPs) (voir Fig. 8). En effet, les PPs hard-core ne peuvent refléter que des structures ayant une distance de répulsion hard-core entre les points, sans pouvoir capturer des structures totalement aléatoires (PPP ou BPP) ou des maillages parfaits (perfect lattice). Les DPP qui font partie des PP soft-core peuvent capturer des structures allant du PPP à certaines structures répulsives en dessous des maillages parfaits. Toutefois, d'autres PP soft-core, tels que les maillages perturbés (perturbed lattices) et la combinaison d'un PPP et d'un maillage stationnaire, peuvent modéliser plus de structures ponctuelles allant du PPP aux maillages parfaits. Il est intéressant de noter que l'approche IDT permet de modéliser des structures ponctuelles comprises entre les deux extrêmes (entre les PPs de clustering et les maillages stationnaires). Une étude détaillée des propositions de modélisation des réseaux sans fil avec des PPs au-delà du PPP permet de constater que ces PPs sont bien plus précis que le PPP pour la modélisation des architectures sans fil émergentes. Toutefois, ils sont mathématiquement moins tractables permettant que d'approximer le comportement de l'interférence et de la performance. Par conséquent, dans certains scénarios d'analyse, il est généralement plus judicieux de privilégier la souplesse mathématique offrant des informations pratiques sur la conception du système, plutôt que d'accroître la précision de la modélisation, mais avec une perte considérable de la flexibilité mathématique. En d'autres termes, la tractabilité du PPP justifie parfois son éventuelle manque de précision. Le tableau 1 classe ces PPs selon divers degrés de tractabilité et de complexité mathématique. Une mesure importante est la capacité du PP à permettre la dérivation de la transformée de Laplace (PGFL) de l'interférence à un point arbitraire donné, ce qui permettra par la suite de dériver diverses mesures de performance comme la probabilité de couverture et le débit érgodique. Ainsi, trois classes de PPs sont identifiées : ceux qui permettent de dériver la PGFL de l'interférence, ceux qui ne permettent pas de la dériver d'où une approximation de la PGFL ou de la valeur moyenne de l'interférence est établie, et ceux dont la PGFL et la valeur moyenne de l'interférence sont inconnues.
 - Chapitre 2 : Nous examinons dans ce chapitre les nombreux choix de modélisation clés couramment utilisés dans la littérature basée sur la SG. Ainsi, nous passons en revue les préférences conceptuelles relatives i) aux éléments du réseau, par exemple le modèle de localisation (déterministe, aléatoire, stationnaire ou mobile), le type de nœud (émet-

teur, récepteur ou les deux), ii) leurs attributs, par exemple la puissance d'émission et les types d'antenne (omni, directionnelle, antennes multiples, etc), iii) les caractéristiques de l'environnement dans lequel ils opèrent, telles que les effets de propagation, et iv) les propriétés d'interaction entre les nœuds comme la stratégie d'association émetteur/récepteur, la coordination entre les nœuds du réseau et l'interaction spatiale entre eux (repulsion, attraction, ou zero interaction). Nous présentons également quelques mesures de performance fondamentales et nous exposons, de manière plus raffinée pour les non-spécialistes, les techniques d'analyse développées à ce jour dans la littérature relative à la modélisation et à l'analyse des réseaux sans fil basées sur la SG. Le tableau 3 résume les onze techniques utilisées dans la littérature pour évaluer les principales métriques de performance des réseaux sans fil sous l'abstraction PPP/BPP. Ces techniques sont classées en fonction de leur degré de précision analytique (approximation ou exacte) et de leur flexibilité mathématique. Nous avons également examiné le mapping de ces techniques avec les divers stratégies d'association émetteur/récepteur, de même qu'illustré les modèles d'évanouissement requis pour chaque technique.

- Chapitre 3: Dans ce chapitre, nous avons identifié et examiné les principaux aspects et défis relatifs à la modélisation et l'analyse des architectures RAN émergentes telles que les réseaux hétérogènes terrestres, les architectures denses (par les petites cellules, le partage des infrastructures, les relais à plusieurs hubs, et les communications D2D), réseaux non terrestres, RAN en cloud, RAN virtualisé, fog RAN. De même, nous avons investigué les caractéristiques et les défis de modélisation des technologies habilitantes pour la 5G/B5G telles que l'utilisation des bandes de fréquences élevées, la radio cognitive, les systèmes MIMO, les métasurfaces pilotées par logiciel, les communications IBFD, le schéma d'accès NOMA, et la sécurité de la couche physique, et ensuite décrire comment des travaux pertinents dans la littérature ont entrepris d'intégrer la SG dans l'évaluation de ces technologies.
- Chapitre 4: Avec la croissance rapide des applications et des appareils à forte consommation de données, le volume du trafic de données dans les années à venir devrait atteindre des niveaux beaucoup plus élevés que ceux d'aujourd'hui. Une façon de relever ce défi est de déployer des réseaux très denses (UDNs) [261]. Cependant, la densification entraînera divers zones de chevauchement de la couverture, ce qui augmente le risque d'interférence et entraîne une dégradation de la performance du réseau. Dans ce sens, les caractéristiques de l'environnement telles que le shadowing, et les paramètres RNPO (e.g., la hauteur de l'antenne [71], l'angle d'inclinaison/azimut de l'antenne [391, 393] et le biais de la puis-

sance d'émission [19]) sont fortement requis pour l'analyse des performances des UDNs puisqu'ils affectent directement la probabilité de connexions LOS et NLOS, et donc le chevauchement des cellules.

En ignorant l'effet du shadowing et de tout paramètre RNPO, le travail pionnier de [17] fournit une compréhension globale du comportement des performances des UDNs à base de la SG. Un résultat important est la propriété d'invariance du SINR, qui indique que la densité des stations de base augmente au point où le bruit devient négligeable, ensuite le SINR reste stable et indépendant de cette densité due à un équilibre entre la puissance de transmission du signal désiré et celle de l'interférence. Cependant, l'utilisation du modèle standard de perte de trajet et le fait d'ignorer les paramètres RNPO pour des scénarios de communication réalistes conduisent à des conclusions qui ne collent pas aux limites physiques [163], ce qui nécessite une révision impérative de ce modèle de perte de trajet. Ainsi, les auteurs de [162] ont établi que la propriété d'invariance du SINR n'est plus valable lorsqu'on utilise le modèle de perte de trajet à double pente. Un effet similaire est signalé dans [71] pour les stations de base avec antennes élevées, et dans [391] pour un réseau utilisant des antennes directionnelles.

La motivation derrière ce chapitre est donc de trouver une approche analytique adaptée pour étudier les performances des UDNs en incorporant des paramètres généralisés de shadowing et des paramètres RNPO dans le modèle de sélection des cellules. En se basant sur des outils de la SG, nous commençons par développer une équivalence 3D-2D où un réseau cellulaire tridimensionnel avec des paramètres de shadowing et de RNPO est statistiquement équivalent à un réseau 2D dans lequel ils ne sont pas pris en compte. Ensuite, pour des raisons de commodité mathématique, nous nous penchons sur une étude de cas basée sur un modèle de probabilité H -LOS. Ainsi, la probabilité de couverture est calculée, confirmant que notre formule est suffisamment générale pour englober plusieurs formules déjà adoptées par la communauté de recherche. Nous étudions ensuite la loi d'échelle de la densité optimale des stations de base permettant de maximiser la probabilité de couverture. Enfin, nous développons un générateur d'expressions analytiques robustes pour la probabilité de couverture dans le cadre du modèle standard de perte de trajet, ce qui généralisera la fameuse expression basée sur la fonction \mathcal{Q} dans [17].

- Chapitre 5: Les UDNs basés sur le déploiement massif de petites stations de base cellulaires sont considérés comme un outil essentiel pour améliorer la capacité des réseaux 5G/B5G [262]. L'analyse et la modélisation des UDNs nécessitent des outils mathématiques généralement puissants et des concepts nouveaux afin de saisir les paramètres

clés du système qui influent sur la fonction d'utilité intégrant la QoS des utilisateurs et l'investissement des opérateurs.

Une grande partie des études précédentes basées sur des modèles de la SG considéraient le (SINR) comme le facteur clé de la qualité d'expérience de l'utilisateur. Par conséquent, la probabilité de couverture (CCDF de SINR), est en général exprimée sous une intégrale impropre [4, 17, 18, 162], nécessitant une intégration numérique efficace et laborieuse [204], à l'exception de quelques cas particuliers où des expressions simplifiées peuvent être obtenues (e.g., l'exposant de perte de trajet égal à 4, négliger le bruit, évanouissement de Rayleigh). En outre, la quasi-totalité des études basées sur la SG dérivent le débit ergodique en intégrant la probabilité de couverture sur l'axe réel positif, ce qui aboutit à une intégrale à quatre temps [17, Appendix C], à l'exception de l'approche basée sur le lemme de Hamdi présentée dans [68], qui ne nécessite que le calcul d'une intégrale numérique à deux temps mais qui demande cependant l'utilisation de la fonction G de Meijer [68, Corollary 1].

Pour surmonter les limites susmentionnées, les auteurs de [204, 205] ont introduit une nouvelle définition de la probabilité de couverture, selon laquelle l'utilisateur typique est en couverture lorsque, i) celui-ci reçoit un signal suffisamment puissant sans que la puissance d'émission de la station de base ne soit surdimensionnée, c'est-à-dire le $\overline{\text{SNR}}$ à long terme est supérieur à un certain seuil, ii) l'utilisateur reçoit un signal de bonne qualité, c'est-à-dire que le SIR est supérieur à un seuil donné. Il est à noter que cette nouvelle définition permet de saisir davantage de paramètres au niveau du système et de générer des expressions de probabilité de couverture simplifiées, que la définition conventionnelle ne permet pas [17].

D'un autre côté, l'utilisateur dans les réseaux réalistes, peut subir des interruptions de la voix et des données en raison de la congestion lors des périodes de pointe, indépendamment de l'intensité ou de la qualité du signal reçu. La composante essentielle manquante dans la nouvelle définition de la probabilité de couverture présentée dans [204, 205], est donc une mesure de la capacité des ressources physiques et logiques sur les stations de base actives (e.g., les éléments de ressources des canaux regroupés en blocs de ressources physiques (PRB) dans la 5G New Radio (NR), ou la ressource commune des canaux de puissance comme les canaux P-CPICH dans l'UMTS).

Dans ce chapitre, nous élargissons le concept de la probabilité de couverture introduit dans [204, 205] en saisissant de façon tractable la capacité des ressources des stations de base actives. Dans ce sens, nous introduisons dans l'analyse une nouvelle mesure flexible

permettant de représenter les stations de base ayant une capacité de ressources suffisante. Ensuite, nous abordons pour la première fois l'analyse de la performance des UDNs sous ce nouveau modèle de la probabilité de couverture. Pour ce faire, nous incorporons dans l'analyse trois schémas d'ordonnancement représentatifs en termes d'équité d'accès des utilisateurs et de la complexité de mise en œuvre. Le but est de comparer leurs performances dans le cadre des UDNs. Nous considérons également la hauteur des stations de base puisque i) son effet est critique dans le contexte des UDNs [398] et ii) pour permettre d'éviter la propriété peu réaliste d'invariance du SINR [17, 162].

Il a été établi que la performance du réseau dans le cadre d'un modèle d'ordonnancement donné est exprimée en fonction de celle obtenue au moyen d'un ordonnancement non orthogonal où les utilisateurs concurrents sont desservis via le même bloc de ressources. En outre, il est révélé que l'ordonnanceur PF fournit la meilleure performance de réseau en raison du gain de diversité multi-utilisateurs, tandis que la performance sous l'ordonnanceur RR est altérée par la densité des utilisateurs et leur processus de sélection à probabilité égale. Cependant, les trois modèles d'ordonnancement sont équivalents dans le contexte des UDNs, où il est recommandé de déployer le modèle d'ordonnancement ayant la complexité de déploiement la plus réduite.

De plus, nos résultats ont montré que la hauteur des stations de base et la densité d'utilisateurs sont si préjudiciables à la probabilité de couverture et au débit moyen dans les UDNs, tandis que la capacité inhérente des ressources et la puissance d'émission ont un impact réduit au fur et à mesure que la densité des stations de base augmente, ce qui permet de mieux cerner le rôle de ces paramètres dans le cadre des UDNs.

- Chapitre 5: Un moyen efficace d'améliorer le débit de la liaison montante est le déploiement des UDNs, considérés comme la clé de la continuité de service dans les réseaux 5G/B5G [263]. De plus, le déploiement concret de nœuds dans le contexte des UDNs est opportun en raison de plusieurs facteurs socio-économiques, ce qui fait que des outils analytiques tels que la SG et la théorie des processus ponctuels sont plus efficaces pour saisir cette variabilité spatiale des nœuds [4, 24].

Le travail de [20] est le premier à considérer un modèle tractable basé sur la SG pour évaluer la probabilité de couverture de la liaison montante au niveau de la station de base typique, déployée de manière uniforme et aléatoire dans la cellule Voronoï de l'UE qui la dessert. Dans [24], le travail précédent a été légèrement étendu, où le postulat de modélisation des utilisateurs actifs en liaison montante au moyen d'un PPP ayant la même densité que le PPP des stations de base, est particulièrement validé par des

simulations. Dans [245], les auteurs ont examiné la performance de la liaison montante des réseaux cellulaires hétérogènes basés sur un contrôle de puissance fractionné avec une puissance d'émission des utilisateurs bornée. Dans [148], la puissance d'émission des utilisateurs est conçue comme une variable aléatoire mappée à la distance du lien désiré par le biais d'un contrôle de puissance d'inversion de canal tronqué. Cependant, la question de la liaison montante dans le cadre des UDNs n'a pas été explicitement abordée dans les travaux précédents, où ils ont tous considéré le modèle standard d'affaiblissement du trajet qui a démontré des tendances de performance peu réalistes dans le contexte de la liaison descendante des UDNs [162, 164]. Les auteurs de [406] ont abordé cette limitation et ont évalué la couverture de la liaison montante dans les UDNs avec des utilisateurs fixes et un modèle d'affaiblissement de trajet revisité lié à une fonction par morceaux. Cependant, il est crucial d'incorporer la mobilité des utilisateurs étant donné la taille réduite des cellules dans le contexte des UDNs.

Un examen des modèles SG tenant compte de la mobilité, indique qu'il y a particulièrement deux directions d'analyse : i) Le handoff basé sur la trajectoire dans lequel l'événement de handoff se produit tant que le récepteur franchit la bordure de la cellule de l'émetteur, et donc, le taux de handoff est dépendant à l'efficacité de quantification de la distribution statistique des frontières des cellules. Un exemple d'analyse de la liaison montante utilisant une telle méthode est présenté dans [148]. ii) Le handoff basé sur la stratégie d'association dans lequel l'événement de handoff se produit tant qu'une autre station de base vérifie le critère d'association mieux que la station de base actuelle desservant l'utilisateur [185]. Ainsi, ce chapitre est censé être le premier travail qui étend ce concept de handoff basé sur l'association à l'analyse de la liaison montante.

En général, les contributions de ce travail comportent trois volets : i) Nous étendons les modèles de [20, 24, 148, 245] en évaluant la probabilité de couverture de la liaison montante dans le cadre d'un schéma de contrôle de puissance unifié basé sur des modèles réalistes de perte de trajet et de puissance d'émission des utilisateurs limitée. ii) Inspiré du modèle de mobilité utilisé dans des simulations 3GPP [408], les utilisateurs actifs sont considérés comme effectuant intuitivement un mouvement linéaire avec une direction aléatoire afin d'améliorer leurs conditions de connectivité. Dans un tel contexte, nous dérivons le taux de handoff de la liaison montante comme une extension de l'analyse tractable de la liaison descendante dans [185]. iii) En utilisant le taux de handoff obtenu, nous évaluons également la probabilité de couverture de la liaison montante induite par ce modèle de mobilité. La validité analytique de nos résultats est ensuite validée par

des simulations où nous avons identifié quatre régimes de fonctionnement des réseaux OFDMA en liaison montante en fonction des paramètres de design du système et du modèle d'affaiblissement du trajet considéré.

En général, il a été démontré que dans le cas de réseaux suffisamment denses, l'impact du contrôle de la puissance sur la couverture de la liaison montante est limité dans le cadre du BPM, en particulier pour des niveaux de SIR faibles, où les utilisateurs plus éloignés sont plus susceptibles de brouiller le signal souhaité, indépendamment de la compensation de l'affaiblissement du trajet. Inversement, l'impact du contrôle de la puissance est significatif sous l'UPM et le DSPM en raison de la singularité à très faible distance.

— Chapitre 7:

Bien qu'ils présentent divers avantages, les drones (véhicules aériens sans pilote), en tant qu'équipement utilisateur aérien dans les réseaux de communication, peuvent néanmoins avoir un impact négatif sur les performances des équipements utilisateurs terrestres, qui se voient confier des missions plus critiques que les drones (e.g., les transactions monétaires, les prestations de santé) [410]. Le 3GPP (Third Generation Partnership Project) a inclus dans la version 15 une étude technique pour évaluer la capacité à desservir des utilisateurs aériens par le biais de déploiements LTE (Long Term Evolution) dans lesquels les antennes des stations de base (BS) ciblent les utilisateurs terrestres [408]. Les simulations montrent en particulier qu'une densité accrue des utilisateurs aériens augmentera considérablement les interférences sur la liaison montante des stations de base terrestres. Ceci est dû au fait qu'un utilisateur aérien typique connaît des conditions de propagation à visibilité directe avec une probabilité plus élevée vers davantage de cellules par rapport à un utilisateur terrestre typique. Cette augmentation des interférences sur la liaison montante nécessiterait un niveau d'utilisation des ressources plus élevé pour maintenir un niveau de débit similaire pour les utilisateurs terrestres. D'autre part, l'augmentation du niveau d'utilisation des ressources amplifie encore l'interférence sur la liaison montante du réseau, et donc dégrade davantage le débit de la liaison montante des utilisateurs aériens et terrestres.

Considérant des emplacements déterministes et un nombre fixe de stations de base terrestres, d'utilisateurs terrestres et d'utilisateurs aériens, la plupart des efforts de recherche ont généralement exploité des mesures de terrain ou des simulations [411], des analyses algorithmiques [412] et la théorie de l'optimisation [413] pour évaluer l'impact des utilisateurs aériens sur la performance des réseaux cellulaires LTE terrestres. Les précédentes

techniques sont généralement laborieuses, nécessitent des configurations personnalisées pour chaque expérience et des algorithmes complexes et puissants. Dans ce sens, il est de plus en plus nécessaire de disposer de modèles analytiques tractables. À notre connaissance, il n'existe pas de modèle analytique dans la littérature pour saisir l'impact en liaison montante des paramètres système des UAV (e.g., densité, hauteur, puissance consommée et exposant de contrôle de la puissance) sur les métriques de performance des réseaux cellulaires.

La SG et sa propre théorie des processus ponctuels est considérée comme un outil mathématique puissant pour l'analyse des réseaux sans fil au niveau système. Cependant, l'analyse de la liaison montante est très exigeante en raison du couplage des emplacements des utilisateurs actifs suite à l'utilisation d'un schéma d'accès orthogonal tel que OFDMA, et également en raison des mécanismes de contrôle de la puissance dépendant à la distance, ce qui induit une dépendance entre les emplacements des BS et ceux des utilisateurs. Plusieurs modèles clés ont été développés dans la littérature pour évaluer la performance de la liaison montante dans les réseaux cellulaires terrestres à un seul niveau [20], les réseaux sans fil à plusieurs niveaux [414], et les réseaux cellulaires denses [415]. Cependant, il reste d'importantes axes d'analyse inexplorés. Par exemple, i) considérer l'hétérogénéité au niveau des utilisateurs (terrestres et aériennes) plutôt qu'au niveau des BS (petites cellules, macrocellules). L'analyse de la liaison montante dans ce dernier cas se révèle statistiquement équivalente à celle de la configuration à un seul niveau [414, Corollaire 4]. En outre, ii) les travaux précédents ont uniquement porté sur des mesures de performance typiques telles que la probabilité de couverture et le débit, alors qu'ajuster les paramètres système pour améliorer ces métriques aurait cependant un impact négatif sur d'autres métriques aussi importantes telles que la consommation d'énergie des utilisateurs souhaitant avoir une plus grande autonomie de batterie.

Dans ce chapitre, nos contributions peuvent être résumées comme suit : i) nous considérons deux classes d'UE terrestres et aériennes avec des paramètres distinctifs en termes de shadowing, et des paramètres système. Ainsi, nous introduisons une mesure de priorité entre les niveaux d'UE, à savoir le biais de priorité de l'UE. Le but est d'évaluer le processus des utilisateurs actifs en liaison montante de chaque niveau et d'en déduire la distribution de la distance à l'UE desservant la station de base typique. ii) Déterminer le processus des utilisateurs interférents est assez difficile dans l'analyse de la liaison montante. Dans notre configuration, nous l'estimons par un processus ponctuel de Poisson (PPP) non homogène sur une région d'exclusion définie par le compromis entre les util-

isateurs interférents et la puissance moyenne reçue par l'UE desservant la station de base typique. iii) Enfin, nous dérivons la distribution de l'efficacité énergétique (EE) de la liaison montante, ce qui nous permet d'évaluer la quantité d'UE avec un bon compromis entre le débit et la consommation énergétique. Ainsi, nous illustrons l'effet préjudiciable sur l'EE de l'augmentation de la priorité de connexion aux utilisateurs aériens. Une contrainte analytique basée sur la fonction Lambert W liant les principaux paramètres système est identifiée permettant un fonctionnement approprié des réseaux cellulaires avec des utilisateurs aériens.

CONCLUSION

The insights presented in this thesis illustrate the flexibility of SG and its ability to capture the analysis of the rather unconventional scenarios; these features of SG will likely enable it to remain as an essential tool in modeling and analysis of future wireless networks.

However, after intensive use of SG in modeling and analysis of communication networks, notably during the last decade of the seminal work [17], research community begins to experience some congestion on applications of SG and some degree of duplication in the literature. This is in particular due to the following reasons: i) SG is very rich in theory but only few results are used practically in modeling and analysis of wireless networks, including Campbell's and PGFL theorems, as well as constructing properties that may preserve the Poisson law (superposition, displacement, mapping, independent thinning). ii) Given some modeling and design challenges, SG has not been sufficiently explored in the analysis of new research areas (networks with metasurfaces, molecular communication (MC), ML, FSO communications,...). iii) No bridges of interaction are created between SG and other emerging mathematical theories, which can give rise to new practical results of SG. In the following, we will outline some emerging research avenues that can revitalize the use of SG during this new decade.

7.5.1 Stochastic Geometry and Molecular Communications

One promising frontier of conventional EM communication systems is the ability to share, manipulate and control information on a very small scale in such a way to connect swarms of intelligent autonomous nano-devices, i.e., devices in a scale ranging from 1 to 100 nanometers, e.g., nano-robots, nano-processors, nano-clocks. Based on biological communication in nature where molecules are the basic carriers of information, MC is expected to be one of the next big³ ideas of communication due to its inherent biocompatibility and enhanced EE at the cost of slow propagation speed as compared to EM wave based communications [416, 417].

The vision of molecular nanonetworks is actually fraught with many challenges, among them, how information can be encoded in molecules and how such molecules are supposed to propagate from a transmitter to a receiver. Several MC propagation schemes are considered

3. As was first pointed out conceptually by the 1965 nobel laureate physicist Richard Feynman in his famous speech entitled "There's Plenty of Room at the Bottom" in Dec. 1959.

in the literature such as diffusion-based propagation, flow assisted propagation and bacteria chemotaxis. The most common approach is the free diffusion of particles where molecules can propagate from one point to another in a random Brownian motion via inherent thermal energy, which does not require any external source of energy and may induce confusion in molecules detection at the receiver, also known as inter-symbol-interference. Several ways are considered to encode information in such diffusing particles, for example encoding information according to the time of arrival of molecules at the receiver, according to molecular composition or to the variations on molecules concentration in the space.

Another major constraint in MC systems is the laborious and expensive nature of laboratory experimentation which justifies the wide use of simulation environments for MC analysis [418]. Interestingly, the authors of [419] presented a first attempt to provide some appropriate analytical tools via SG in such context of miniaturization in MC. The work proposed a mathematical framework for performance evaluation of a 3D diffusion-based large-scale MC system. The average number of sensed particles and the bit error probability at a receiver located at the origin are next characterized over many spatial realizations of a swarm of point transmitters scattered in space according to some PPP and emitting the same bit sequence (the same type of molecule) simultaneously, i.e., co-channel transmitters. Analytical evaluation of MC as a serious alternative to EM wave based systems, particularly in strong attenuation regimes of EM waves, is relatively new and several fundamental questions need actually years and years to be answered and agreed about [420]. However, many advances are expected in the near future due especially to recent development in inexpensive testbed for MC systems capable of transmitting short text messages via chemical signals [418].

7.5.2 Stochastic Geometry in the Era of Machine Learning

SG and ML have recently been considered as the most popular methods with renewed and widespread interest in the design and analysis of wireless networks [2, 17, 421, 422]. The former is actually a powerful model-driven approach aimed to enhance the tractability and accuracy of conventional probabilistic models, e.g., channel, interference, scheduling, by considering the randomness on the locations of the transmitters and the receivers, so that one can derive average performance metrics of a generative network upon several realizations of network geometry [2, 17]. The latter is however, a data-driven simulation-based approach, which by collecting sufficient amount of realistic data, i.e., *the training set*, can feed a supervised and/or unsupervised learning process deployed at the cloud components of the network, to enable the prediction of the desired result, e.g., performance metrics [421, 422].

To the best of authors knowledge, there are fundamentally two lines of thought in the literature regarding the mode of interaction that should prevail between ML and SG. The first vision is based on *an evolutionary interaction* [421, 423, 424], in which ML is conceived as a separate evolved alternative to SG enabling to overcome the shortcomings of the latter and provide more accurate representation of reality. In fact, SG model-driven approach is generally governed by a trade-off between tractability and accuracy, where tractable models are simply so superficial to reflect realistic scenarios, while accurate models are hard to derive and their resulting algorithms are too complex to implement. However, with the unprecedented availability of data, inducing the need for software-controlled and optimized operations, in addition to recent developments in smart radio environments via the use of metasurfaces [30, 298], it is almost unfeasible to develop accurate SG models that can capture such complex scenarios of analysis due to the unlimited degrees of freedom and system constraints. The second vision is based on *a collaborative interaction* [35, 36]; in which a common ground and potential cross-fertilization between SG and ML is created such that the strength of both approaches will be jointly harnessed to tackle the same issue. Typically, SG models will be integrated as a hypothesis class in the learning process of ML. One representative example is the class of problems known as *the subset selection problems*, where an optimal subset needs to be selected from a ground set. In such context, SG probabilistic models constructed by finite DPPs are used to feed ML data-driven supervised learning frameworks.

7.5.3 Stochastic Geometry as a Multi-objective Analytical Tool

From the previous discussions, it is evident that future 5G/B5G wireless networks are going to be highly heterogeneous, multi-layered, with embedded intelligence at both the core and the edge of the network, where ML is expected to play a crucial role in link and system-level decisions. In such a context, future performance metrics need to be carefully tailored to ensure the joint evaluation of throughput, latency, and reliability, which ultimately leads to the joint optimization of communication, control, localization, sensing, energy consumption, and many other parameters and resources. Interestingly, SG can be envisioned as a potential analytical candidate in this way.

For instance, Fig. 4 presents some scenarios where the SINR can be combined with useful utility functions to enable the joint analysis of communication and other related attributes, e.g., DUDA, SWIPT. Also, SG is increasingly adopted in studying the joint localization and communication of users in a given propagation environment. In particular, the authors of [425, 426] use tools from SG and its inherent PP theory to evaluate the statistics of the number of

BSs that can participate in the localization procedure of users as a function of system-level parameters and channel impairments. Typically, there is a tradeoff, known as *the hearability problem*, that needs to be considered between communication requirements that ask for a strong signal from the desired BS and a poor one from interferers, versus localization that requires a good signal from most BSs.

Furthermore, SG and its inherent random set theory are increasingly being adopted for the analysis of combined recognition, data manipulation, and movement in real-world environments. Typically, SG is used to study uncertainty in geometric objects in order to build models from IoT measurements [427, 428]. The physical environment landmarks are actually abstracted into parametric representations such as points, lines, and edges. These features are next handled as realizations of random variables modeled as a finite random set, which based on the Bayesian estimation paradigm, can allow to jointly estimate the number of objects and their states. This is relevant for example to detect and locate objects from surveillance images [427]. Besides, random set theory is gaining increased importance for providing a theoretical estimation for the famous simultaneous localization and map building (SLAM) problem that asks for the ability to place an autonomous robot at an undefined location in an undefined environment and construct a map, based only on relative ambient observations, and subsequently use this map for spatial mobility of this robot [428]. Using random finite set theory, SLAM is then presented as a Bayesian filtering problem in which the joint recursive estimation of the robot route and set-valued map are spatially distributed over time as measurements are acquired.

Future research efforts are therefore expected to identify attractive applications of SG in multi-objective optimization.

7.5.4 Grothendieck Toposes as Mathematical Bridges for Stochastic Geometry

One effective way to deal with the embarrassing trade-off between tractability and accuracy that governs SG models, is to investigate how to build more advanced and accurate SG models from tractable and easy-to-interpret models conceived by other mathematical fields. Our vision therefore is to create some abstract bridges of interaction between SG and other mathematical fields where we have reached some remarkable degree of specialization and proficiency. The rationale is to create meaningful and powerful analogies that may illuminate concepts and suggest new practical results in SG. A promising approach to meet such aims is through the concept of topos introduced by Alexandre Grothendieck during his Seminar on Algebraic Geometry in the

early sixties.

“It is the notion of topos that is this “bed” where come to be married geometry and algebra, topology and arithmetic, mathematical logic and category theory, the world of the continuous and that of discontinuous or discrete structures. It is the most vast thing I have conceived, to grasp with finesse, through the same language rich in geometric resonances, an “essence” common to situations most distant from each other, coming from one region or another of the vast universe of mathematical things.”—Alexandre Grothendieck commented in his famous text of autobiographical reflections “Récoltes et Semailles” [429].

Recently, new perspectives on the notion of topos have emerged. According to Olivia Caramello [430], Grothendieck toposes can be used as unifying spaces that can serve as bridges for transferring properties, ideas, and results between distinct mathematical theories. In our case, between SG and other mathematical fields, so that long-standing problems formulated in SG can be solved using techniques from a different field, and results in a well known area can be appropriately transferred to results in SG.

BIBLIOGRAPHY

- [1] D. Stoyan, W. Kendall, and J. Mecke, *Stochastic Geometry and Its Applications*, 2nd Edition, 2nd ed. John Wiley and Sons, 1996.
- [2] F. Baccelli, M. Klein, M. Lebourges, and S. Zuyev, "Stochastic geometry and architecture of communication networks," *J. Telecommunication Systems*, vol. 7, no. 1, pp. 209-227, Jun. 1997.
- [3] F. Baccelli and S. Zuyev, "Stochastic geometry models of mobile communication networks," *Frontiers in Queueing*, CRC Press, pp. 227-243, 1997.
- [4] F. Baccelli and B. Blaszczyzyn, *Stochastic Geometry and Wireless Networks in Foundations and Trends in Networking*, vol. 1, Now Publishers, 2009.
- [5] F. Baccelli and B. Blaszczyzyn, *Stochastic Geometry and Wireless Networks in Foundations and Trends in Networking*, vol. 2, Now Publishers, 2009.
- [6] M. Haenggi, *Stochastic Geometry for Wireless Networks*. Cambridge, U.K.: Cambridge Univ. Press, 2012.
- [7] D. J. Daley and D. Vere-Jones, *An Introduction to the Theory of Point Processes, Elementary Theory and Methods*, vol. 1, Springer-Verlag New York, 2003.
- [8] J. F. Coeurjolly, J. Møller, and R. Waagepetersen, "A tutorial on Palm distributions for spatial point processes," *Int. Stat. Review*, vol. 85(3), pp. 404-420, Dec. 2017.
- [9] R. Schneider and W. Weil, *Stochastic and integral geometry*, Probability and its Applications (New York), Springer-Verlag, Berlin, 2008.
- [10] L. A. Santaló, *Integral Geometry and Geometric Probability*. Cambridge, U.K.: Cambridge Univ. Press, 1976.
- [11] G. Matheron, *Random Sets and Integral Geometry*. New York, NY: John Wiley and Sons, 1975.
- [12] J. Grandell, "Point processes and random measures," *Advances in Applied Probability* 9, pp. 502-526, 1977.
- [13] D. Coupier, *Stochastic Geometry: Modern Research Frontiers*. Cham, Switzerland : Springer, 2019.

-
- [14] J. Illian, A. Penttinen, and H. Stoyan, *Statistical Analysis and Modelling of Spatial Point Patterns*. Statistics in Practice, Wiley-Blackwell, 2008.
- [15] E. N. Gilbert, "Random plane networks," *SIAM J.*, vol. 9, pp. 533-543, 1961.
- [16] F. Baccelli, B. Blaszczyszyn, and P. Muhlethaler, "Stochastic analysis of spatial and opportunistic aloha," *IEEE J. Sel. Areas in Commun.*, vol. 27, no. 7, pp. 1105-1119, Sep. 2009.
- [17] J. G. Andrews, F. Baccelli, and R. K. Ganti, "A tractable approach to coverage and rate in cellular networks," *IEEE Trans. Commun.*, vol. 59, no. 11, pp. 3122-3134, Nov. 2011.
- [18] H. S. Dhillon, R. K. Ganti, F. Baccelli, and J. G. Andrews, "Modeling and analysis of K-Tier downlink heterogeneous cellular networks," *IEEE J. Sel. Areas Commun.*, vol. 30, no. 3, pp. 550-560, Apr. 2012.
- [19] H.-S. Jo, Y. J. Sang, P. Xia, and J. G. Andrews, "Heterogeneous cellular networks with flexible cell association: A comprehensive downlink SINR analysis," *IEEE Trans. Wireless Commun.*, vol. 11, no. 10, pp. 3484-3495, Oct. 2012.
- [20] T. D. Novlan, H. S. Dhillon, and J. G. Andrews, "Analytical modeling of uplink cellular networks," *IEEE Trans. Wireless Commun.*, vol. 12, no. 6, pp. 2669-2679, Jun. 2013.
- [21] S. Zuyev, "Stochastic geometry and telecommunications networks," in *Stochastic Geometry: Highlights, Interactions and New Perspectives*, W. S. Kendall and I. Molchanov, Eds. Oxford University Press, 2009.
- [22] M. Haenggi, J. G. Andrews, F. Baccelli, O. Dousse, and M. Franceschetti, "Stochastic geometry and random graphs for the analysis and design of wireless networks," *IEEE J. Sel. Areas Commun.*, vol. 27, no. 7, pp. 1029-1046, Sep. 2009.
- [23] H. ElSawy, E. Hossain, and M. Haenggi, "Stochastic geometry for modeling, analysis, and design of multi-tier and cognitive cellular wireless networks: A survey," *IEEE Commun. Surveys Tuts.*, vol. 15, no. 3, pp. 996-1019, Thirdquarter 2013.
- [24] J. G. Andrews, A. K. Gupta, and H. S. Dhillon, "A primer on cellular network analysis using stochastic Geometry," arXiv preprint, Oct. 2016, [Online]. Available: <https://arxiv.org/abs/1604.03183>.
- [25] I. Chih-Lin, S. Han, Z. Xu, Q. Sun, and Z. Pan, "5G: Rethink mobile communications for 2020+," *Philosoph. Trans. Roy. Soc. A Math. Phys. Eng. Sci.*, vol. 374, no. 2062, 2016, Art. no. 20140432.

-
- [26] 6G Flagship, University of Oulu, September 2019, “Key drivers and research challenges for 6G ubiquitous wireless intelligence” [Online]. Available: <http://jultika.oulu.fi/files/isbn9789526223544.pdf>.
- [27] Z. Pi and F. Khan, “An introduction to millimeter-wave mobile broadband systems,” *IEEE Commun. Mag.*, vol. 49, no. 6, pp. 101-107, Jun. 2011.
- [28] H. Song and T. Nagatsuma, “Present and future of terahertz communications,” *IEEE Trans. Terahertz Science and Technol.*, vol. 1, no. 1, pp. 256-263, Sep. 2011.
- [29] P. H. Pathak, X. Feng, P. Hu, and P. Mohapatra, “Visible light communication, networking, and sensing: A survey, potential and challenges,” *IEEE Commun. Surveys Tuts.*, vol. 17, no. 4, pp. 2047-2077, Fourthquarter 2015.
- [30] C. Liaskos, S. Nie, A. Tsioliariidou, A. Pitsillides, S. Ioannidis, and I. Akyildiz, “A new wireless communication paradigm through software-controlled metasurfaces,” *IEEE Commun. Mag.*, vol. 56, no. 9, pp. 162-169, Sep. 2018.
- [31] M. Mozaffari, W. Saad, M. Bennis, Y. Nam, and M. Debbah, “A Tutorial on UAVs for wireless networks: Applications, challenges, and open problems,” *IEEE Commun. Surveys Tuts.*, vol. 21, no. 3, pp. 2334-2360, Thirdquarter 2019.
- [32] L. Li, G. Zhao, and R. S. Blum, “A survey of caching techniques in cellular networks: research issues and challenges in content placement and delivery strategies,” *IEEE Commun. Surveys Tuts.*, vol. 20, no. 3, pp. 1710-1732, Thirdquarter 2018.
- [33] A. K. Gupta, X. Zhang, and J. G. Andrews, “SINR and throughput scaling in ultradense urban cellular networks,” *IEEE Wireless Commun. Lett.*, vol. 4, no. 6, pp. 605-608, Dec. 2015.
- [34] A. AlAmmouri, J. G. Andrews, and F. Baccelli, “A unified asymptotic analysis of area spectral efficiency in ultradense cellular networks,” *IEEE Trans. Inf. Theory*, vol. 65, no. 2, pp. 1236-1248, Feb. 2019.
- [35] B. Blaszcyszyn and H.P. Keeler, “Determinantal thinning of point processes with network learning applications”, in *Proc. IEEE Wireless Commun. Netw. Conf. (WCNC)*, Marrakech, Morocco, Apr. 2019.
- [36] C. Saha, H. S. Dhillon, “Machine learning meets stochastic geometry: determinantal subset selection for wireless networks”, in *Proc. IEEE Glob. Commun. Conf. (GLOBECOM)*, Waikoloa, HI, Dec. 2019.
- [37] D. Kedar and S. Arnon, “Urban optical wireless communication networks: the main challenges and possible solutions,” *IEEE Commun. Mag.*, vol. 42, no. 5, pp. S2-S7, May 2004.

-
- [38] J. Wildman, P. H. J. Nardelli, M. Latva-aho, and S. Weber, "On the joint impact of beamwidth and orientation error on throughput in directional wireless Poisson networks," *IEEE Trans. Wireless Commun.*, vol. 13, no. 12, pp. 7072-7085, Dec. 2014.
- [39] J. G. Andrews, "Seven ways that HetNets are a cellular paradigm shift," *IEEE Commun. Mag.*, vol. 51, no. 3, pp. 136-144, Mar. 2013.
- [40] J. G. Andrews, R. K. Ganti, M. Haenggi, N. Jindal, and S. Weber, "A primer on spatial modeling and analysis in wireless networks," *IEEE Commun. Mag.*, vol. 48, no. 11, pp. 156-163, Nov. 2010.
- [41] D. Moltchanov, "Distance distributions in random networks," *Ad Hoc Netw.*, vol. 10, pp. 1146-1166, Aug. 2012.
- [42] M. Haenggi and R. Ganti, *Interference in Large Wireless Networks*, in Foundations and Trends in Networking, NOW Publishers, vol. 3, no. 2, pp. 127-248, 2008.
- [43] P. Cardieri, "Modeling interference in wireless ad hoc networks," *IEEE Commun. Surveys Tuts.*, vol. 12, no. 4, pp. 551-572, Fourthquarter 2010.
- [44] H. ElSawy, A. Sultan-Salem, M. Alouini, and M. Z. Win, "Modeling and analysis of cellular networks using stochastic geometry: A tutorial," *IEEE Commun. Surveys Tuts*, vol. 19, no. 1, pp. 167-203, Firstquarter 2017.
- [45] China mobile research institute, "C-RAN: the road towards green RAN", in *Proc. C-RAN Int. Workshop*, Beijing, China, Apr., 2010.
- [46] A. Checko et al., "Cloud RAN for mobile networks: A technology overview," *IEEE Commun. Surveys Tuts*, vol. 17, no. 1, pp. 405-426, Firstquarter 2015.
- [47] S. M. R. Islam, N. Avazov, O. A. Dobre, and K. Kwak, "Power-domain non-orthogonal multiple access (NOMA) in 5G Systems: potentials and challenges," *IEEE Commun. Surveys Tuts*, vol. 19, no. 2, pp. 721-742, Secondquarter 2017.
- [48] A. Sabharwal, P. Schniter, D. Guo, D. W. Bliss, S. Rangarajan, and R. Wichman, "In-band full-duplex wireless: Challenges and opportunities," *IEEE J. Sel. Areas Commun.*, vol. 32, no. 9, pp. 1637-1652, Sep. 2014.
- [49] Y. Wu, A. Khisti, C. Xiao, G. Caire, K. Wong, and X. Gao, "A survey of physical layer security techniques for 5G wireless networks and challenges ahead," *IEEE J. Sel. Areas Commun.*, vol. 36, no. 4, pp. 679-695, Apr. 2018.
- [50] B. Blaszczyzyn, "Factorial moment expansion for stochastic systems," *Stochastic Processes and their Applications*, vol. 56, no. 2, pp. 321-335, Apr. 1995.

-
- [51] B. Błaszczyszyn, M. K. Karray, and H. P. Keeler, "Using Poisson processes to model lattice cellular networks," in *Proc. IEEE INFOCOM*, pp. 773-781, Turin, Italy, Apr. 2013.
- [52] H. P. Keeler, B. Błaszczyszyn, and M. K. Karray, "SINR-based k-coverage probability in cellular networks with arbitrary shadowing," in *Proc. IEEE Int. Symp. Inf. Theory*, pp. 1167-1171, Istanbul, Turkey 2013.
- [53] I. Nakata, N. Miyoshi, "Spatial stochastic models for analysis of heterogeneous cellular networks with repulsively deployed base stations," *Perform. Eval.*, vol. 78, pp. 7-17, Aug. 2014.
- [54] P. Madhusudhanan, J. G. Restrepo, Y. Liu, and T. X. Brown, "Analysis of downlink connectivity models in a heterogeneous cellular network via stochastic geometry," *IEEE Trans. Wireless Commun.*, vol. 15, no. 6, pp. 3895-3907, Jun. 2016.
- [55] M. Haenggi, "On distances in uniformly random networks," *IEEE Trans. Inf. Theory*, vol. 51, no. 10, pp. 3584-3586, Oct. 2005.
- [56] M. Haenggi, "A geometric interpretation of fading in wireless networks: theory and applications," *IEEE Trans. Inf. Theory*, vol. 54, no. 12, pp. 5500-5510, Dec. 2008.
- [57] S. Y. Jung, H. Lee, and S. Kim, "Worst-case user analysis in Poisson Voronoi cells," *IEEE Commun. Lett.*, vol. 17, no. 8, pp. 1580-1583, Aug. 2013.
- [58] G. Nigam, P. Minero, and M. Haenggi, "Coordinated multipoint joint transmission in heterogeneous networks," *IEEE Trans. Wireless Commun.*, vol. 62, no. 11, pp. 4134-4146, Nov. 2014.
- [59] S. Srinivasa and M. Haenggi, "Distance distributions in finite uniformly random networks: theory and applications," *IEEE Trans. Veh. Technol.*, vol. 59, no. 2, pp. 940-949, Feb. 2010.
- [60] M. C. Valenti, D. Torrieri, and S. Talarico, "A direct approach to computing spatially averaged outage probability," *IEEE Commun. Lett.*, vol. 18, no. 7, pp. 1103-1106, Jul. 2014.
- [61] M. Afshang and H. S. Dhillon, "Fundamentals of modeling finite wireless networks using binomial point process," *IEEE Trans. Wireless Commun.*, vol. 16, no. 5, pp. 3355-3370, May 2017.
- [62] J. Guo, S. Durrani, and X. Zhou, "Outage probability in arbitrarily-shaped finite wireless networks," *IEEE Trans. Commun.*, vol. 62, no. 2, pp. 699-712, Feb. 2014.
- [63] D. P. Kroese and Z. I. Botev, "Spatial process generation," arXiv preprint, Aug. 2013, [Online]. Available: <https://arxiv.org/abs/1308.0399>.

-
- [64] D. B. Taylor, H. S. Dhillon, T. D. Novlan, and J. G. Andrews, "Pairwise interaction processes for modeling cellular network topology," in *Proc. IEEE Glob. Commun. Conf. (GLOBECOM)*, pp. 4524-4529, Anaheim, California, USA, Dec. 2012.
- [65] A. Guo and M. Haenggi, "Spatial stochastic models and metrics for the structure of base stations in cellular networks," *IEEE Trans. Wireless Commun.*, vol. 12, no. 11, pp. 5800-5812, Nov. 2013.
- [66] A. Baddeley and R. Turner, "Practical maximum pseudolikelihood for spatial point patterns," *Australian and New Zealand J. Stat.*, vol. 42, pp. 283-322, Sep. 2000.
- [67] M. Di Renzo, S. Wang, and X. Xi, "Inhomogeneous double thinning-modeling and analysis of cellular networks by using inhomogeneous Poisson point processes," *IEEE Trans. Wireless Commun.*, vol. 17, no. 8, pp. 5162-5182, Aug. 2018.
- [68] M. Di Renzo, A. Guidotti, and G. Corazza, "Average rate of downlink heterogeneous cellular networks over generalized fading channels: A stochastic geometry approach," *IEEE Trans. Commun.*, vol. 61, no. 7, pp. 3050-3071, Jul. 2013.
- [69] T. Bai and R. W. Heath Jr., "Coverage and rate analysis for millimeter wave cellular networks," *IEEE Trans. Wireless Commun.*, vol. 14, no. 2, pp. 1100-1114, Oct. 2014.
- [70] M. Ding, P. Wang, D. López-Pérez, G. Mao, and Z. Lin, "Performance impact of LoS and NLoS transmissions in dense cellular networks," *IEEE Trans. Wireless Commun.*, vol. 15, no. 3, pp. 2365-2380, Mar. 2016.
- [71] I. Atzeni, J. Arnau, and M. Kountouris, "Downlink cellular network analysis with LOS/NLOS propagation and elevated base stations," *IEEE Trans. Wireless Commun.*, vol. 17, no. 1, pp. 142-156, Jan. 2018.
- [72] T. Sanguanpuak, S. Guruacharya, E. Hossain, N. Rajatheva, and M. Latva-aho, "Infrastructure sharing for mobile network operators: analysis of trade-offs and market," *IEEE Trans. Mobile Comput.*, vol. 17, no. 12, pp. 2804-2817, Dec. 2018.
- [73] A. K. Gupta, J. G. Andrews, and R. W. Heath, "On the feasibility of sharing spectrum licenses in mmWave cellular systems," *IEEE Trans. Commun.*, vol. 64, no. 9, pp. 3981-3995, Sep. 2016.
- [74] A. K. Gupta, A. Alkhateeb, J. G. Andrews, and R. W. Heath, "Gains of restricted secondary licensing in millimeter wave cellular systems," *IEEE J. Sel. Areas Commun.*, vol. 34, no. 11, pp. 2935-2950, Nov. 2016.

-
- [75] J. Park, J. G. Andrews, and R. W. Heath, "Inter-operator base station coordination in spectrum-shared millimeter wave cellular networks," *IEEE Trans. Cogn. Commun. Networking*, vol. 4, no. 3, pp. 513-528, Sep. 2018.
- [76] M. Rebato, M. Mezzavilla, S. Rangan, and M. Zorzi, "Resource sharing in 5G mmWave cellular networks," in *Proc. IEEE Int. Conf. Comput. Commun. (INFOCOM Wkshps)*, pp. 271-276, San Francisco, CA, USA, Apr. 2016.
- [77] J. Kibilda, N. J. Kaminski, and L. A. DaSilva, "Radio access network and spectrum sharing in mobile networks: A stochastic geometry perspective," *IEEE Trans. Wireless Commun.*, vol. 16, no. 4, pp. 2562-2575, Apr. 2017.
- [78] R. Jurdi, A. K. Gupta, J. G. Andrews, and R. W. Heath, "Modeling infrastructure sharing in mmWave networks with shared spectrum licenses," *IEEE Trans. Cogn. Commun. and Networking*, vol. 4, no. 2, pp. 328-343, Jun. 2018.
- [79] V. V. Chetlur and H. S. Dhillon, "Coverage analysis of a vehicular network modeled as Cox process driven by Poisson line process," *IEEE Trans Wireless Commun.*, vol. 17, no. 7, pp. 4401-4416, Jul. 2018.
- [80] A. Munari, P. Mahonen, and M. Petrova, "A stochastic geometry approach to asynchronous Aloha full-duplex networks," *IEEE/ACM Trans. Netw.*, vol. 25, no. 6, pp. 3695-3708, Dec. 2017.
- [81] A. H. Sakr and E. Hossain, "Cognitive and energy harvesting-based D2D communication in cellular networks: stochastic geometry modeling and analysis," *IEEE Trans. Commun.*, vol. 63, no. 5, pp. 1867-1880, May 2015.
- [82] Q. Song, X. Lagrange, and L. Nuaymi, "Evaluation of macro diversity gain in long range ALOHA networks," *IEEE Commun. Lett.*, vol. 21, no. 11, pp. 2472-2475, Nov. 2017.
- [83] M. Di Renzo, W. Lu, and P. Guan, "The intensity matching approach: A tractable stochastic geometry approximation to system-level analysis of cellular networks," *IEEE Trans. Wireless Commun.*, vol. 15, no. 9, pp. 5963-5983, Sep. 2016.
- [84] Y. Hmamouche, M. Benjillali, and S. Saoudi, "A Stochastic geometry based approach to tractable 5G RNPO with a new H-LOS model," in *Proc. IEEE Wireless Commun. Netw. Conf. (WCNC)*, Marrakech, Morocco, Apr. 2019.
- [85] P. Madhusudhanan, J. G. Restrepo, Y. E. Liu, T. X. Brown, and K. R. Baker, "Stochastic ordering based carrier-to-interference ratio analysis for the shotgun cellular systems," *IEEE Wireless Commun. Lett.*, vol. 1, no. 6, pp. 565-568, Dec. 2012.

-
- [86] P. Madhusudhanan, J. G. Restrepo, Y. Liu, T. X. Brown, and K. R. Baker, "Downlink performance analysis for a generalized shotgun cellular system," *IEEE Trans. Wireless Commun.*, vol. 13, no. 12, pp. 6684-6696, Dec. 2014.
- [87] Y. Li, F. Baccelli, H. S. Dhillon, and J. G. Andrews, "Fitting determinantal point processes to macro base station deployments," in *Proc. IEEE Glob. Commun. Conf. (GLOBECOM)*, pp. 3641-3646, Austin, TX, USA, Dec. 2014.
- [88] R. Nasri and A. Jaziri, "Analytical tractability of hexagonal network model with random user location," *IEEE Trans. Wireless Commun.*, vol. 15, no. 5, pp. 3768-3780, May 2016.
- [89] M. Michalopoulou, J. Riihijarvi, and P. Mahonen, "Studying the relationships between spatial structures of wireless networks and population densities," in *Proc. IEEE Glob. Commun. Conf. (GLOBECOM)*, pp. 1-6, Miami, FL, USA, Dec. 2010.
- [90] H. Ghazzai, E. Yaacoub, M. Alouini, Z. Dawy, and A. Abu-Dayya, "Optimized LTE cell planning with varying spatial and temporal user densities," *IEEE Trans. Veh. Technol.*, vol. 65, no. 3, pp. 1575-1589, Mar. 2016.
- [91] A. Achtzehn, J. Riihijarvi, and P. Mahonen, "Large-scale cellular network modeling from population data: an empirical analysis," *IEEE Commun. Lett.*, vol. 20, no. 11, pp. 2292-2295, Nov. 2016.
- [92] Y. Zhou et al., "Large-scale spatial distribution identification of base stations in cellular networks," *IEEE Access*, vol. 3, pp. 2987-2999, 2015.
- [93] L. Chiaraviglio et al., "What is the best spatial distribution to model base station density? A deep dive into two european mobile networks," *IEEE Access*, vol. 4, pp. 1434-1443, 2016.
- [94] B. Matérn, "*Spatial Variation*," Lecture Notes in Statistics, vol. 36, 2nd ed. New York, NY, USA: Springer-Verlag, 1986.
- [95] M. Haenggi, "Mean Interference in hard-core wireless networks," *IEEE Commun. Lett.*, vol. 15, no. 8, pp. 792-794, Aug. 2011.
- [96] B. Cho, K. Koufos, and R. Jantti, "Bounding the mean interference in Matérn type II hard-core wireless networks," *IEEE Wireless Commun. Lett.*, vol. 2, no. 5, pp. 563-566, Oct. 2013.
- [97] A. Al-Hourani, R. J. Evans, and S. Kandeepan, "Nearest neighbor distance distribution in hard-core point processes," *IEEE Commun. Lett.*, vol. 20, no. 9, pp. 1872-1875, Sep. 2016.

-
- [98] F. Lagum, S. S. Szyszkowicz, and H. Yanikomeroglu, "CoV-based metrics for quantifying the regularity of hard-core point processes for modeling base station locations," *IEEE Wireless Commun. Lett.*, vol. 5, no. 3, pp. 276-279, Jun. 2016.
- [99] M.N.M. van Lieshout, *Markov Point Processes and their Applications*, Imperial College Press, London, 2000.
- [100] I. Flint, H.-B. Kong, N. Privault, P. Wang, and D. Niyato, "Analysis of heterogeneous wireless networks using Poisson hard-core hole process," *IEEE Trans. Wireless Commun.*, vol. 16, no. 11, pp. 7152-7167, Nov. 2017.
- [101] C. Lee and M. Haenggi, "Interference and outage in Poisson cognitive networks," *IEEE Trans. Wireless Commun.*, vol. 11, no. 4, pp. 1392-1401, Apr. 2012.
- [102] N. Deng, W. Zhou, and M. Haenggi, "Heterogeneous cellular network models with dependence," *IEEE J. Sel. Areas Commun.*, vol. 33, no. 10, pp. 2167-2181, Oct. 2015.
- [103] Z. Chen and M. Kountouris, "Decentralized opportunistic access for D2D underlaid cellular networks," *IEEE Trans. Commun.*, vol. 66, no. 10, pp. 4842-4853, Oct. 2018.
- [104] Z. Yazdanshenasan, H. S. Dhillon, M. Afshang, and P. H. J. Chong, "Poisson hole process: Theory and applications to wireless networks," *IEEE Trans. Wireless Commun.*, vol. 15, no. 11, pp. 7531-7546, Nov. 2016.
- [105] R. K. Ganti, F. Baccelli, and J. G. Andrews, "Series expansion for interference in wireless networks," *IEEE Trans. Inf. Theory*, vol. 58, no. 4, pp. 2194-2205, Apr. 2012.
- [106] Y. Li, F. Baccelli, H. S. Dhillon, and J. G. Andrews, "Statistical modeling and probabilistic analysis of cellular networks with determinantal point processes," *IEEE Trans. Commun.*, vol. 63, no. 9, pp. 3405-3422, Sep. 2015.
- [107] N. Miyoshi and T. Shirai, "A cellular network model with Ginibre configured base stations," *Research Rep. on Math. and Comp. Sciences (Tokyo Inst. of Tech.)*, Oct. 2012.
- [108] I. Nakata and N. Miyoshi, "Spatial stochastic models for analysis of heterogeneous cellular networks with repulsively deployed base stations," *Tokyo Institute of Technology Preprint*, Oct. 2013.
- [109] N. Deng, W. Zhou, and M. Haenggi, "The Ginibre point process as a model for wireless networks with repulsion," *IEEE Trans. Wireless Commun.*, vol. 14, no. 1, pp. 107-121, Jan. 2015.
- [110] Han-Bae Kong, Ping Wang, Dusit Niyato, Yu Cheng, "Physical layer security in wireless networks with Ginibre point processes," *IEEE Trans. Wireless Commun.*, vol. 17, no. 8, pp. 5132-5147, May 2018.

-
- [111] F. Lavancier, J. Møller, and E. Rubak, "Statistical aspects of determinantal point processes," arXiv preprint, Jun. 2014, [Online]. Available: <https://arxiv.org/abs/1205.4818>.
- [112] S. A. Banani, A. W. Eckford, and R. S. Adve, "The penalty for random deployment in hexagonal lattice networks with perturbed interferers," in *Proc. IEEE Globecom Workshops*, pp. 1272-1277, Austin, TX, USA, Dec. 2014.
- [113] S. A. Banani, R. S. Adve, and A. W. Eckford, "A perturbed hexagonal lattice to model basestation locations in real-world cellular networks," in *Proc. IEEE Globecom Workshops*, pp. 1-6, San Diego, CA, USA, Dec. 2015.
- [114] F. Lagum, S. S. Szyszkowicz, and H. Yanikomeroglu, "Quantifying the regularity of perturbed triangular lattices using CoV-Based metrics for modeling the locations of base stations in HetNets," in *Proc. IEEE 84th Veh. Technol. Conf. (VTC-Fall)*, pp. 1-5, Montreal, QC, Canada, 2016.
- [115] Q.-N. Le-The, T. Beitelmal, F. Lagum, S. S. Szyszkowicz, H. Yanikomeroglu, "Cell switch-off algorithms for spatially irregular base station deployments," *IEEE Wireless Commun. Lett.*, vol. 6, no. 3, pp. 354-357, Apr. 2017.
- [116] F. Lagum, Q.-N. Le-The, T. Beitelmal, S. S. Szyszkowicz, H. Yanikomeroglu, "Cell switch-off for networks deployed with variable spatial regularity," *IEEE Wireless Commun. Lett.*, vol. 6, no. 2, pp. 234-237, Feb. 2017.
- [117] M. Mirahsan, R. Schoenen and H. Yanikomeroglu, "HetHetNets: heterogeneous traffic distribution in heterogeneous wireless cellular networks," *IEEE J. Sel. Areas Commun.*, vol. 33, no. 10, pp. 2252-2265, Oct. 2015.
- [118] M. Tanemura, "Statistical distributions of poisson Voronoi cells in two and three dimensions," *Forma*, vol. 18, no. 4, pp. 221-247, Nov. 2003.
- [119] C. Choi, J. O. Woo, and J. G. Andrews, "An analytical framework for modeling a spatially repulsive cellular network," *IEEE Trans. on Commun.*, vol. 66, no. 2, pp. 862-874, Feb. 2018.
- [120] R. K. Ganti and M. Haenggi, "Interference and outage in clustered wireless AdHoc networks," *IEEE Trans. Inf. Theory*, vol. 55, no. 9, pp. 4067-4086, Sep. 2009.
- [121] Y. J. Chun, M. O. Hasna, and A. Ghayeb, "Modeling heterogeneous cellular networks interference using Poisson cluster processes," *IEEE J. Sel. Areas Commun.*, vol. 33, no. 10, pp. 2182-2195, Oct. 2015.

-
- [122] C. Saha, M. Afshang, and H. S. Dhillon, "Enriched K-tier HetNet model to enable the analysis of user-centric small cell deployments," *IEEE Trans. Wireless Commun.*, vol. 16, no. 3, pp. 1593-1608, Mar. 2017.
- [123] C. Saha, M. Afshang, and H. S. Dhillon, "3GPP-inspired HetNet model using Poisson cluster process: sum-product functionals and downlink coverage," *IEEE Trans. Commun.*, vol. 66, no. 5, pp. 2219-2234, May 2018.
- [124] P. D. Mankar, G. Das, and S. S. Pathak, "Modeling and coverage analysis of BS-centric clustered users in a random wireless network," *IEEE Wireless Commun. Lett.*, vol. 5, no. 2, pp. 208-211, Apr. 2016.
- [125] M. Afshang and H. S. Dhillon, "Poisson cluster process based analysis of HetNets with correlated user and base station locations," *IEEE Trans. Wireless Commun.*, vol. 17, no. 4, pp. 2417-2431, Apr. 2018.
- [126] R. Li, Z. Zhao, Y. Zhong, C. Qi, and H. Zhang, "The stochastic geometry analyses of cellular networks with α -stable self-similarity," *IEEE Trans. Commun.*, vol. 67, no. 3, pp. 2487-2503, Mar. 2019.
- [127] Y. Zhou, R. Li, Z. Zhao, X. Zhou, and H. Zhang, "On the α -stable distribution of base stations in cellular networks," *IEEE Commun. Lett.*, vol. 19, no. 10, pp. 1750-1753, Oct. 2015.
- [128] J. Møller, "Shot noise Cox processes," *Adv. Appl. Probab.*, vol. 35, no. 3, pp. 4-26, Sep. 2003.
- [129] C. Choi and F. Baccelli, "Poisson Cox point processes for vehicular networks," *IEEE Trans. Veh. Technol.*, vol. 67, no. 10, pp. 10160-10165, Oct. 2018.
- [130] C. Choi and F. Baccelli, "An analytical framework for coverage in cellular networks leveraging vehicles," *IEEE Trans. Commun.*, vol. 66, no. 10, pp. 4950-4964, Oct. 2018.
- [131] Z. Wang, R. Schoenen, H. Yanikomeroglu, and M. St-Hilaire, "The impact of user spatial heterogeneity in heterogeneous cellular networks," in *Proc. IEEE Globecom Workshops (GC Wkshps)*, pp. 1278-1283, Austin, TX, USA, Dec. 2014.
- [132] J. Kibiłda, B. Galkin, and L. A. DaSilva, "Modelling multi-operator base station deployment patterns in cellular networks," *IEEE Trans. Mobile Comput.*, vol. 15, no. 12, pp. 3087-3099, Dec. 2016.
- [133] Q. Cui, N. Wang, and M. Haenggi, "Vehicle distributions in large and small cities: spatial models and applications," *IEEE Trans. Veh. Technol.*, vol. 67, no. 11, pp. 10176-10189, Nov. 2018.

-
- [134] A. Guo, Y. Zhong, W. Zhang, and M. Haenggi, "The Gauss-Poisson process for wireless networks and the benefits of cooperation," *IEEE Trans. Commun.*, vol. 64, no. 5, pp. 1916-1929, May 2016.
- [135] N. Deng and M. Haenggi, "The benefits of hybrid caching in Gauss-Poisson D2D networks," *IEEE J. Sel. Areas Commun.*, vol. 36, no. 6, pp. 1217-1230, Jun. 2018.
- [136] H. S. Dhillon, R. K. Ganti, and J. G. Andrews, "Modeling non-uniform UE distributions in downlink cellular networks," *IEEE Wireless Commun. Lett.*, vol. 2, no. 3, pp. 339-342, Jun. 2013.
- [137] H. S. Dhillon, R. K. Ganti, and J. G. Andrews, "Load-aware modeling and analysis of heterogeneous cellular networks," *IEEE Trans. Wireless Commun.*, vol. 12, no. 4, pp. 1666-1677, Apr. 2013.
- [138] S. Lee and K. Huang, "Coverage and economy of cellular networks with many base stations," *IEEE Commun. Lett.*, vol. 16, no. 7, pp. 1038-1040, Jul. 2012.
- [139] M. Haenggi, "The mean interference-to-signal ratio and its key role in cellular and amorphous networks," *IEEE Wireless Commun. Lett.*, pp. 597-600, Dec. 2014.
- [140] A. Guo and M. Haenggi, "Asymptotic deployment gain: A simple approach to characterize the SINR distribution in general cellular networks," *IEEE Trans. Commun.*, vol. 63, pp. 962-976, Mar. 2015.
- [141] R. K. Ganti and M. Haenggi, "Asymptotics and approximation of the SIR distribution in general cellular networks," *IEEE Trans. Wireless Commun.*, vol. 15, no. 3, pp. 2130-2143, Mar. 2016.
- [142] B. Błaszczyszyn and D. Yogeshwaran, "Directionally convex ordering of random measures, shot-noise fields and some applications to wireless networks," *Adv. Appl. Prob.*, vol. 41, pp. 623-646, Jun. 2009.
- [143] J. Lee and C. Tepedelenlioglu, "Stochastic ordering of interference in large-scale wireless networks," *IEEE Trans. Signal Process.*, vol. 62, no. 3, pp. 729-740, Feb., 2014.
- [144] M. Van Lieshout and A. Baddeley, "A nonparametric measure of spatial interaction in point patterns," *Statistica Neerlandica*, vol. 50, pp. 344-361, 1996.
- [145] C. Chen, R. C. Elliott, W. A. Krzymień, and J. Melzer, "Modeling of cellular networks using stationary and nonstationary point processes," *IEEE Access*, vol. 6, pp. 47144-47162, 2018.

-
- [146] A. Okabe, B. Boots, K. Sugihara, and S. N. Chiu, *Spatial Tessellations: Concepts and Applications of Voronoi Diagrams*, 2nd Ed..Chichester, West Sussex, England: John Wiley & Sons, 1999.
- [147] S. Krishnan and H. S. Dhillon, "Spatio-temporal interference correlation and joint coverage in cellular networks," *IEEE Trans. Wireless Commun.*, vol. 16, no. 9, pp. 5659-5672, Sep. 2017.
- [148] H. ElSawy and E. Hossain, "On stochastic geometry modeling of cellular uplink transmission with truncated channel inversion power control," *IEEE Trans. Wireless Commun.*, vol. 13, no. 8, pp. 4454-4469, Aug. 2014.
- [149] P. Herath, C. Tellambura, and W. A. Krzymien, "Stochastic geometry modeling of cellular uplink power control under composite Rayleigh-Lognormal fading," in *Proc. IEEE 82nd Veh. Technol. Conf. (VTC2015-Fall)*, pp. 1-5, Boston, MA, 2015.
- [150] S. Singh, X. Zhang, and J. G. Andrews, "Joint rate and SINR coverage analysis for decoupled uplink-downlink biased cell associations in HetNets," *IEEE Trans. Wireless Commun.*, vol. 14, no. 10, pp. 5360-5373, Oct. 2015.
- [151] L. Zhang, W. Nie, G. Feng, F. Zheng, and S. Qin, "Uplink performance improvement by decoupling uplink/downlink access in HetNets," *IEEE Trans. Veh. Technol.*, vol. 66, no. 8, pp. 6862-6876, Aug. 2017.
- [152] F. Boccardi et al., "Why to decouple the uplink and downlink in cellular networks and how to do it," *IEEE Commun. Mag.*, vol. 54, no. 3, pp. 110-117, Mar. 2016.
- [153] M. Haenggi, "User point processes in cellular networks," *IEEE Wireless Commun. Lett.*, vol. 6, no. 2, pp. 258-261, Apr. 2017.
- [154] M. Afshang, H. S. Dhillon, and P. H. Joo Chong, "Modeling and performance analysis of clustered device-to-device networks," *IEEE Trans. Wireless Commun.*, vol. 15, no. 7, pp. 4957-4972, Jul. 2016.
- [155] M. Afshang, H. S. Dhillon, and P. H. J. Chong, "Fundamentals of cluster-centric content placement in cache-enabled device-to-device networks," *IEEE Trans. Commun.*, vol. 64, no. 6, pp. 2511-2526, Jun. 2016.
- [156] W. Yi, Y. Liu, and A. Nallanathan, "Modeling and analysis of D2D millimeter-wave networks with Poisson cluster processes," *IEEE Trans. Commun.*, vol. 65, no. 12, pp. 5574-5588, Dec. 2017.

-
- [157] X. Lin, J. G. Andrews, and A. Ghosh, "Spectrum sharing for device-to-device communication in cellular networks," *IEEE Trans. Wireless Commun.*, vol. 13, no. 12, pp. 6727-6740, Dec. 2014.
- [158] S. Singh, M. N. Kulkarni, A. Ghosh, and J. G. Andrews, "Tractable model for rate in self-backhauled millimeter wave cellular networks," *IEEE J. Sel. Areas Commun.*, vol. 33, no. 10, pp. 2196-2211, Oct. 2015.
- [159] M. Di Renzo, "Stochastic geometry modeling and analysis of multi-tier millimeter wave cellular networks," *IEEE Trans. Wireless Commun.*, vol. 14, no. 9, pp. 5038-5057, Sep. 2015.
- [160] T. Bai, R. Vaze, and R. W. Heath, "Analysis of blockage effects on urban cellular networks," *IEEE Trans. Wireless Commun.*, vol. 13, no. 9, pp. 5070-5083, Sep. 2014.
- [161] H. Inaltekin, M. Chiang, H. V. Poor, and S. B. Wicker, "On unbounded path-loss models: effects of singularity on wireless network performance," *IEEE J. Sel. Areas Commun.*, vol. 27, no. 7, pp. 1078-1092, Sep. 2009.
- [162] X. Zhang and J. G. Andrews, "Downlink cellular network analysis with multi-slope path loss models," *IEEE Trans. Commun.*, vol. 63, no. 5, pp. 1881-1894, May 2015.
- [163] J. G. Andrews, X. Zhang, G. D. Durgin, and A. K. Gupta, "Are we approaching the fundamental limits of wireless network densification?," *IEEE Commun. Mag.*, vol. 54, no. 10, pp. 184-190, Oct. 2016.
- [164] J. Liu, M. Sheng, L. Liu, and J. Li, "Effect of densification on cellular network performance with bounded pathloss model," *IEEE Commun. Lett.*, vol. 21, no. 2, pp. 346-349, Feb. 2017.
- [165] A. AlAmmouri, J. G. Andrews, and F. Baccelli, "SINR and throughput of dense cellular networks with stretched exponential path loss," *IEEE Trans. on Wireless Commun.*, vol. 17, no. 2, pp. 1147-1160, Feb. 2018.
- [166] J. G. Andrews, T. Bai, M. N. Kulkarni, A. Alkhateeb, A. K. Gupta, and R. W. Heath, "Modeling and analyzing millimeter wave cellular systems," *IEEE Trans. Commun.*, vol. 65, no. 1, pp. 403-430, Jan. 2017.
- [167] A. Al-Hourani, S. Kandeepan, and A. Jamalipour, "Modeling air-to-ground path loss for low altitude platforms in urban environments," in *Proc. IEEE Glob. Commun. Conf. (GLOBECOM)*, pp. 2898-2904, Austin, TX, USA, Dec. 2014.
- [168] A. Al-Hourani, S. Kandeepan, and S. Lardner, "Optimal LAP altitude for maximum coverage," *IEEE Wireless Commun. Lett.*, vol. 3, no. 6, pp. 569-572, Dec. 2014.

-
- [169] A. A. Khuwaja, Y. Chen, N. Zhao, M. Alouini, and P. Dobbins, "A survey of channel modeling for UAV communications," *IEEE Commun. Surveys Tuts*, vol. 20, no. 4, pp. 2804-2821, Fourthquarter 2018.
- [170] J. Liu, M. Sheng, L. Liu, and J. Li, "Performance of small cell networks under multislope bounded pathloss model: from sparse to ultradense deployment," *IEEE Trans. Veh. Technol.*, vol. 67, no. 11, pp. 11022-11034, Nov. 2018.
- [171] C. Galiotto, N. K. Pratas, N. Marchetti, and L. Doyle, "A stochastic geometry framework for LOS/NLOS propagation in dense small cell networks," in *Proc. IEEE Int. Conf. Commun. (ICC)*, pp. 2851-2856, London, UK, 2015.
- [172] M. Ding, and D. López-Pérez, "Performance impact of base station antenna heights in dense cellular networks," *IEEE Trans. Wireless Commun.*, vol. 16, no. 12, pp. 8147-8161, Dec. 2017.
- [173] Z. Zhang and R. Qingyang Hu, "Dense cellular network analysis with LoS/NLoS propagation and bounded path loss model," *IEEE Commun. Lett.*, vol. 22, no. 11, pp. 2386-2389, Nov. 2018.
- [174] Q. Ye, B. Rong, Y. Chen, M. Al-Shalash, C. Caramanis, and J. G. Andrews, "User association for load balancing in heterogeneous cellular networks," *IEEE Trans. Wireless Commun.*, vol. 12, no. 6, pp. 2706-2716, Jun. 2013.
- [175] S. Singh, H. S. Dhillon, and J. G. Andrews, "Offloading in heterogeneous networks: modeling, analysis, and design insights," *IEEE Trans. Wireless Commun.*, vol. 12, no. 5, pp. 2484-2497, May 2013.
- [176] S. Singh and J. G. Andrews, "Joint resource partitioning and offloading in heterogeneous cellular networks," *IEEE Trans. Wireless Commun.*, vol. 13, no. 2, pp. 888-901, Feb. 2014.
- [177] A. H. Sakr and E. Hossain, "On user association in multi-tier full-duplex cellular networks," *IEEE Trans. Commun.*, vol. 65, no. 9, pp. 4080-4095, Sep. 2017.
- [178] I. Rhee, M. Shin, S. Hong, K. Lee, S. J. Kim, and S. Chong, "On the Levy-walk nature of human mobility," *IEEE/ACM Trans. on Netw.*, vol. 19, no. 3, pp. 630-643, Jun. 2011.
- [179] J. B. T. Camp and V. Davies, "A survey of mobility models for adhoc network research," *Wireless Commun. Mobile Comput. Special Issue on Mobile Ad Hoc Netw.: Research, Trends and Applications*, vol. 2, no. 5, pp. 483-502, 2002.
- [180] X. Lin, R. K. Ganti, P. J. Fleming, and J. G. Andrews, "Towards understanding the fundamentals of mobility in cellular networks," *IEEE Trans. Wireless Commun.*, vol. 12, no. 4, pp. 1686-1698, Apr. 2013.

-
- [181] W. Bao and B. Liang, "Stochastic geometric analysis of user mobility in heterogeneous wireless networks," *IEEE J. Sel. Areas Commun.*, vol. 33, no. 10, pp. 2212-2225, Oct. 2015.
- [182] X. Xu, Z. Sun, X. Dai, T. Svensson, and X. Tao, "Modeling and analyzing the cross-tier handover in heterogeneous networks," *IEEE Trans. Wireless Commun.*, vol. 16, no. 12, pp. 7859-7869, Dec. 2017
- [183] X. Ge, J. Ye, Y. Yang, and Q. Li, "User mobility evaluation for 5G small cell networks based on individual mobility model," *IEEE J. Sel. Areas Commun.*, vol. 34, no. 3, pp. 528-541, Mar. 2016.
- [184] R. Arshad, H. ElSawy, S. Sorour, T. Y. Al-Naffouri, and M. Alouini, "Velocity-aware handover management in two-tier cellular networks," *IEEE Trans. Wireless Commun.*, vol. 16, no. 3, pp. 1851-1867, Mar. 2017.
- [185] S. Sadr and R. S. Adve, "Handoff rate and coverage analysis in multi-tier heterogeneous networks," *IEEE Trans. Wireless Commun.*, vol. 14, no. 5, pp. 2626-2638, May 2015.
- [186] S. Hsueh and K. Liu, "An equivalent analysis for handoff probability in heterogeneous cellular networks," *IEEE Commun. Lett.*, vol. 21, no. 6, pp. 1405-1408, Jun. 2017.
- [187] H. Tabassum, M. Salehi and E. Hossain, "Fundamentals of Mobility-Aware Performance Characterization of Cellular Networks: A Tutorial," *IEEE Commun. Surveys Tuts*, vol. 21, no. 3, pp. 2288-2308, Thirdquarter 2019.
- [188] C. E. Shannon, "Two-way communication channels," in *Proc. 4th Berkeley Symp. Math. Statist. And Prob.*, vol. 1, pp. 611-644, 1961.
- [189] Y. Zhong, T. Q. S. Quek, and X. Ge, "Heterogeneous cellular networks with spatio-temporal traffic: delay analysis and scheduling," *IEEE J. Sel. Areas Commun.*, vol. 35, no. 6, pp. 1373-1386, Jun 2017.
- [190] M. Salehi, A. Mohammadi, and M. Haenggi, "Analysis of D2D underlaid cellular networks: SIR Meta distribution and mean local delay," *IEEE Trans. Commun.*, vol. 65, pp. 2904-2916, Jul. 2017.
- [191] Y. Zhong, M. Haenggi, F. Zheng, W. Zhang, T. Q. S. Quek, and W. Nie, "Toward a tractable delay analysis in ultra-dense networks," *IEEE Commun. Mag.*, vol. 55, no. 12, pp. 103-109, Dec. 2017.
- [192] D. C. Chen, T. Q. S. Quek, and M. Kountouris, "Backhauling in heterogeneous cellular networks: modeling and tradeoffs," *IEEE Trans. Wireless Commun.*, vol. 14, no. 6, pp. 3194-3206, Jun. 2015.

-
- [193] M. A. Abd-Elmagid, N. Pappas, and H. S. Dhillon, "On the role of age of information in the internet of things," *IEEE Commun. Mag.*, vol. 57, no. 12, pp. 72-77, Dec. 2019.
- [194] Y. Hu, Y. Zhong, and W. Zhang, "Age of information in Poisson networks," in *Proc. 10th Int. Conf. Wireless Commun. Signal Process. (WCSP)*, Oct. 2018, pp. 1-6.
- [195] M. Emara, H. Elsaywy, and G. Bauch, "A spatiotemporal model for peak AoI in uplink IoT networks: time versus event-triggered traffic," *IEEE Internet Things J.*, vol. 7, no. 8, pp. 6762-6777, Aug. 2020.
- [196] H. H. Yang, A. Arafa, T. Q. Quek, and V. Poor, "Optimizing information freshness in wireless networks: A stochastic geometry approach," *IEEE Trans. Mobile Comput.*, to appear.
- [197] P. Chang and G. Miao, "Energy and spectral efficiency of cellular networks with discontinuous transmission," *IEEE Trans. Commun.*, vol. 16, no. 5, pp. 2991-3002, May 2017.
- [198] M. Haenggi, "The Meta distribution of the SIR in Poisson bipolar and cellular networks," *IEEE Trans. Wireless Commun.*, vol. 15, no. 4, pp. 2577-2589, Apr. 2016.
- [199] H. Ji, S. Park, J. Yeo, Y. Kim, J. Lee, and B. Shim, "Ultra-reliable and low-latency communications in 5G downlink: physical layer aspects," *IEEE Wireless Commun.*, vol. 25, no. 3, pp. 124-130, Jun. 2018.
- [200] I. Ramezanipour, P. Nouri, H. Alves, P. H. J. Nardelli, R. D. Souza, and A. Pouttu, "Finite blocklength communications in smart grids for dynamic spectrum access and locally licensed scenarios," *IEEE Sensors J.*, vol. 18, no. 13, pp. 5610-5621, Jul. 2018.
- [201] Y. Polyanskiy, H. V. Poor, and S. Verdú, "Channel coding rate in the finite blocklength regime," *IEEE Trans. Inf. Theory*, vol. 56, no. 5, pp. 2307-2359, May 2010.
- [202] M. Alouini and A. J. Goldsmith, "Area spectral efficiency of cellular mobile radio systems," *IEEE Trans. Veh. Technol.*, vol. 48, no. 4, pp. 1047-1066, Jul. 1999.
- [203] C. Li, J. Zhang, J. G. Andrews, and K. B. Letaief, "Success probability and area Spectral efficiency in multiuser MIMO hetNets," *IEEE Trans. on Commun.*, vol. 64, no. 4, pp. 1544-1556, Apr. 2016.
- [204] M. Di Renzo, A. Zappone, T. T. Lam, and M. Debbah, "System-level modeling and optimization of the energy efficiency in cellular networks – A stochastic geometry framework," *IEEE Trans. Wireless Commun.*, vol. 17, no. 4, pp. 2539-2556, Apr. 2018.
- [205] M. Di Renzo, T. T. Lam, A. Zappone, and M. Debbah, "A tractable closed-form expression of the coverage probability in Poisson cellular networks," *IEEE Wireless Commun. Lett.*, vol. 8, no. 1, pp. 249-252, Feb. 2019.

-
- [206] W. Lu, M. Di Renzo, and T. Q. Duong, "On Stochastic Geometry Analysis and Optimization of Wireless-Powered Cellular Networks," in *Proc. IEEE Glob. Commun. Conf. (GLOBECOM)*, pp. 1-7, San Diego, CA, Dec. 2015.
- [207] S. Guruacharya, H. Tabassum, and E. Hossain, "Integral approximations for coverage probability," *IEEE Wireless Commun. Lett.*, vol. 5, no. 1, pp. 24-27, Feb. 2016.
- [208] Y. Hmamouche, M. Benjillali, and S. Saoudi, "Stochastic analysis of UDNs with resource capacity and user scheduling," in *Proc. IEEE Wireless Commun. and Netw. Conf. (WCNC)*, Marrakech, Morocco, Apr. 2019.
- [209] S. Guruacharya and E. Hossain, "Approximation of Meta distribution and its moments for Poisson cellular networks," *IEEE Wireless Commun. Lett.*, vol. 7, no. 6, pp. 1074-1077, Dec. 2018.
- [210] M. Haenggi, "Efficient calculation of Meta distributions and the performance of user percentiles," *IEEE Wireless Commun. Lett.*, vol. 7, no. 6, pp. 982-985, Dec. 2018.
- [211] S. S. Kalamkar and M. Haenggi, "Simple approximations of the SIR meta distribution in general cellular networks," *IEEE Trans. Commun.*, vol. 67, no. 6, pp. 4393-4406, Jun. 2019.
- [212] M. Salehi, A. Mohammadi, and M. Haenggi, "Analysis of D2D underlaid cellular networks: SIR Meta distribution and mean local delay," *IEEE Trans. Commun.*, vol. 65, pp. 2904-2916, Jul. 2017.
- [213] N. Deng and M. Haenggi, "A fine-grained analysis of millimeter-wave device-to-device networks," *IEEE Trans. Commun.*, vol. 65, no. 11, pp. 4940-4954, Nov. 2017.
- [214] Q. Cui, X. Yu, Y. Wang, and M. Haenggi, "The SIR Meta distribution in Poisson cellular networks with base station cooperation," *IEEE Trans. Commun.*, vol. 66, pp. 1234-1249, Mar. 2018.
- [215] Y. Wang, M. Haenggi, and Z. Tan, "The Meta distribution of the SIR for cellular networks with power control," *IEEE Trans. Commun.*, vol. 66, no. 4, pp. 1745-1757, Apr. 2018.
- [216] Q. Cui, X. Yu, Y. Wang, and M. Haenggi, "The SIR Meta distribution in Poisson cellular networks with base station cooperation," *IEEE Trans. Commun.*, vol. 66, no. 3, pp. 1234-1249, Mar. 2018.
- [217] J. Tang, G. Chen, and J. P. Coon, "Meta distribution of the secrecy rate in the presence of randomly located eavesdroppers," *IEEE Wireless Commun. Lett.*, vol. 7, no. 4, pp. 630-633, Aug. 2018.

-
- [218] N. Deng and M. Haenggi, "The Energy and rate Meta distributions in wirelessly powered D2D networks," *IEEE J. Sel. Areas Commun.*, vol. 37, no. 2, pp. 269-282, Feb. 2019.
- [219] K. S. Ali, H. El Sawy, and M. Alouini, "Meta distribution of downlink non-orthogonal multiple access (NOMA) in Poisson networks," *IEEE Wireless Commun. Lett.*, vol. 8, no. 2, pp. 572-575, Apr. 2019.
- [220] V. V. Chetlur and H. S. Dhillon, "Downlink coverage analysis for a finite 3-D wireless network of unmanned aerial vehicles," *IEEE Trans. Commun.*, vol. 65, no. 10, pp. 4543-4558, Oct. 2017.
- [221] X. Wang, H. Zhang, Y. Tian, and V. C. M. Leung, "Modeling and analysis of aerial base station-assisted cellular networks in finite areas under LoS and NLoS propagation," *IEEE Trans. Wireless Commun.*, vol. 17, no. 10, pp. 6985-7000, Oct. 2018.
- [222] Z. Khalid and S. Durrani, "Distance distributions in regular polygons," *IEEE Trans. Veh. Technol.*, vol. 62, no. 5, pp. 2363-2368, Jun. 2013.
- [223] C. Tepedelenlioglu, A. Abdi, and G. B. Giannakis, "The Ricean K factor: estimation and performance analysis," *IEEE Trans. Wireless Commun.*, vol. 2, no. 4, pp. 799-810, Jul. 2003.
- [224] O. Georgiou, "Polarized rician fading models for performance analysis in cellular networks," *IEEE Commun. Lett.*, vol. 20, no. 6, pp. 1255-1258, Jun. 2016.
- [225] A. M. Hunter, J. G. Andrews, and S. Weber, "Transmission capacity of ad hoc networks with spatial diversity," *IEEE Trans. Wireless Commun.*, vol. 7, no. 12, pp. 5058-5071, Dec. 2008.
- [226] A. K. Gupta, H. S. Dhillon, S. Vishwanath, and J. G. Andrews, "Downlink multi-antenna heterogeneous cellular network with load balancing," *IEEE Trans. Commun.*, vol. 62, no. 11, pp. 4052-4067, Nov. 2014.
- [227] M. Bacha, Y. Wu, and B. Clerckx, "Downlink and uplink decoupling in two-tier heterogeneous networks with multi-antenna base stations," *IEEE Trans. Wireless Commun.*, vol. 16, no. 5, pp. 2760-2775, May 2017.
- [228] R. Tanbourgi, H. S. Dhillon, and F. K. Jondral, "Analysis of joint transmit–receive diversity in downlink MIMO heterogeneous cellular networks," *IEEE Trans. Wireless Commun.*, vol. 14, no. 12, pp. 6695-6709, Dec. 2015.
- [229] W. P. Johnson, "The curious history of Faa di Bruno's formula," *Amer. Math. Monthly*, vol. 109, no. 3, pp. 217-234, Mar. 2002.

-
- [230] C. Li, J. Zhang, and K. B. Letaief, "Throughput and energy efficiency analysis of small cell networks with multi-antenna base stations," *IEEE Trans. Wireless Commun.*, vol. 13, no. 5, pp. 2505-2517, May 2014.
- [231] S. Mukherjee, "Downlink SINR distribution in a heterogeneous cellular wireless network with max-SINR connectivity," in *Proc. 49th Annual Allerton Conf. Commun., Control, and Comput. (Allerton)*, pp. 1649-1656, Monticello, IL, USA, 2011.
- [232] S. Mukherjee, "Distribution of downlink SINR in heterogeneous cellular networks," *IEEE J. Sel. Areas Commun.*, vol. 30, no. 3, pp. 575-585, Apr. 2012.
- [233] B. Błaszczyszyn and H. P. Keeler, "Studying the SINR process of the typical user in Poisson networks using its factorial moment measures," *IEEE Trans. Inf. Theory*, vol. 61, no. 12, pp. 6774-6794, Dec. 2015.
- [234] J. Gil-Pelaez, "Note on the inversion theorem," *Biometrika*, vol. 38, no. 3/4, pp. 481-482, Dec. 1951.
- [235] M. Di Renzo and P. Guan, "Stochastic geometry modeling of coverage and rate of cellular networks using the Gil-Pelaez inversion theorem," *IEEE Commun. Lett.*, vol. 18, no. 9, pp. 1575-1578, Sep. 2014.
- [236] Y. Kim, T. Lee, and D. I. Kim, "Joint information and power transfer in SWIPT-enabled CRFID networks," *IEEE Wireless Commun. Lett.*, vol. 7, no. 2, pp. 186-189, Apr. 2018.
- [237] M. G. Khoshkholgh and V. C. M. Leung, "Coverage analysis of Max-SIR cell association in HetNets under Nakagami fading," *IEEE Trans. Veh. Technol.*, vol. 67, no. 3, pp. 2420-2438, Mar. 2018.
- [238] B. Yang, M. Ding, G. Mao, and X. Ge, "Performance analysis of dense small cell networks with generalized fading," in *Proc. IEEE Int. Conf. Commun. (ICC)*, pp. 1-7, Paris, France, 2017.
- [239] M. Win, P. Pinto, and L. Shepp, "A mathematical theory of network interference and its applications," *Proc. IEEE*, vol. 97, no. 2, pp. 205-230, Feb. 2009.
- [240] R. W. Heath, M. Kountouris, and T. Bai, "Modeling heterogeneous network interference using Poisson point processes," *IEEE Trans. Sig. Process.*, vol. 61, no. 16, pp. 4114-4126, Aug. 2013.
- [241] K. Hamdi, "A useful lemma for capacity analysis of fading interference channels," *IEEE Trans. Commun.*, vol. 58, no. 2, pp. 411-416, Feb. 2010.

-
- [242] H. Tabassum, F. Yilmaz, Z. Dawy, and M. Alouini, "A framework for uplink intercell interference modeling with channel-based scheduling," *IEEE Trans. Wireless Commun.*, vol. 12, no. 1, pp. 206-217, Jan. 2013.
- [243] M. Kamel, W. Hamouda, and A. Youssef, "Performance analysis of multiple association in ultra-dense networks," *IEEE trans. Commun.*, vol. 65, no. 9, pp. 3818-3831, Sep. 2017.
- [244] H. ElSawy and E. Hossain, "On stochastic geometry modeling of cellular uplink transmission with truncated channel inversion power control," *IEEE Trans. Wireless Commun.*, vol. 13, no. 8, pp. 4454-4469, Aug. 2014.
- [245] M. Di Renzo and P. Guan, "Stochastic geometry modeling and system-level analysis of uplink heterogeneous cellular networks with multi-antenna base stations," *IEEE Trans. Commun.*, vol. 64, no. 6, pp. 2453-2476, Jun. 2016.
- [246] H. Tabassum, E. Hossain, and J. Hossain, "Modeling and analysis of uplink non-orthogonal multiple access in large-scale cellular networks using Poisson cluster processes," *IEEE Trans. Commun.*, vol. 65, no. 8, pp. 3555-3570, Aug. 2017.
- [247] M. Ding, D. López-Pérez, G. Mao, and Z. Lin, "Performance impact of idle mode capability on dense small cell networks," *IEEE Trans. Veh. Technol.*, vol. 66, no. 11, pp. 10446-10460, Nov. 2017.
- [248] I. Bor-Yaliniz and H. Yanikomeroglu, "The new frontier in RAN heterogeneity: Multi-tier drone-cells," *IEEE Commun. Mag.*, vol. 54, no. 11, pp. 48-55, Nov. 2016.
- [249] S. Sekander, H. Tabassum, and E. Hossain, "Multi-tier drone architecture for 5G/B5G cellular networks: challenges, trends, and prospects," *IEEE Commun. Mag.*, vol. 56, no. 3, pp. 96-103, Mar. 2018.
- [250] Y. Zeng, R. Zhang, and T. J. Lim, "Throughput maximization for UAV-enabled mobile relaying systems," *IEEE Trans. Commun.*, vol. 64, no. 12, pp. 4983-4996, Dec. 2016.
- [251] Q. Wu, Y. Zeng, and R. Zhang, "Joint trajectory and communication design for multi-UAV enabled wireless networks," *IEEE Trans. Wireless Commun.*, vol. 17, no. 3, pp. 2109-2121, Mar. 2018.
- [252] H. El Hammouti, M. Benjillali, B. Shihada, and M.-S. Alouini, "A distributed mechanism for joint 3D placement and user association in UAV-assisted networks," in *Proc. IEEE Wireless Commun. Netw. Conf. (WCNC'19)*, Marrakech, Morocco, Apr. 2019.
- [253] M. Mozaffari, W. Saad, M. Bennis, and M. Debbah, "Wireless communication using unmanned aerial vehicles (UAVs): optimal transport theory for hover time optimization," *IEEE Trans. Wireless Commun.*, vol. 16, no. 12, pp. 8052-8066, Dec. 2017.

-
- [254] E. Kalantari, H. Yanikomeroglu, and A. Yongacoglu, "On the number and 3D placement of drone base stations in wireless cellular networks," in *Proc. IEEE VTC-Fall*, Montreal, Canada, 2016.
- [255] M. Mozaffari, W. Saad, M. Bennis, and M. Debbah, "Unmanned aerial vehicle with underlaid device-to-device communications: performance and tradeoffs," *IEEE Trans. Wireless Commun.*, vol. 15, no. 6, pp. 3949-3963, Jun. 2016.
- [256] E. Turgut and M. C. Gursoy, "Downlink analysis in unmanned aerial vehicle (UAV) assisted cellular networks with clustered users," *IEEE Access*, vol. 6, pp. 36313-36324, 2018.
- [257] A. M. Hayajneh, S. A. R. Zaidi, D. C. McLernon, M. Di Renzo, and M. Ghogho, "Performance analysis of UAV enabled disaster recovery networks: A stochastic geometric framework based on cluster processes," *IEEE Access*, vol. 6, pp. 26215-26230, 2018.
- [258] X. Zhou, J. Guo, S. Durrani, and H. Yanikomeroglu, "Uplink coverage performance of an underlay drone cell for temporary events," in *Proc. IEEE Int. Conf. Commun. Workshops (ICC Workshops)*, pp. 1-6, Kansas City, MO, USA 2018.
- [259] B. Galkin, J. Kibilda, and L. A. DaSilva, "Backhaul for low-altitude UAVs in urban environments," in *Proc. IEEE Int. Conf. Commun. (ICC)*, pp. 1-6, Kansas City, MO, USA 2018.
- [260] T. Hou, Y. Liu, Z. Song, X. Sun, and Y. Chen, "Multiple antenna aided NOMA in UAV networks: A stochastic geometry approach," *IEEE Trans. Commun.*, vol. 67, no. 2, pp. 1031-1044, Feb. 2019.
- [261] N. Bhushan et al., "Network densification: the dominant theme for wireless evolution into 5G," *IEEE Commun. Mag.*, vol. 52, no. 2, pp. 82-89, Feb. 2014.
- [262] D. López-Pérez, M. Ding, H. Claussen, and A. H. Jafari, "Towards 1 Gbps/UE in cellular systems: understanding ultra-dense small cell deployments," *IEEE Commun. Surveys Tuts.*, vol. 17, no. 4, pp. 2078-2101, Fourthquarter 2015.
- [263] M. Kamel, W. Hamouda, and A. Youssef, "Ultra-dense networks: A survey," *IEEE Commun. Surveys Tuts.*, vol. 18, no. 4, pp. 2522-2545, Fourthquarter 2016.
- [264] D. Lopez-Perez, I. Guvenc, G. de la Roche, M. Kountouris, T. Q. S. Quek, and J. Zhang, "Enhanced intercell interference coordination challenges in heterogeneous networks," *IEEE Wireless Commun.*, vol. 18, no. 3, pp. 22-30, Jun. 2011.
- [265] I. Hwang, B. Song, and S. S. Soliman, "A holistic view on hyper-dense heterogeneous and small cell networks," *IEEE Commun. Mag.*, vol. 51, no. 6, pp. 20-27, Jun. 2013.

-
- [266] E. Bastug, M. Bennis, M. Kountouris, and M. Debbah, "Cache-enabled small cell networks: Modeling and tradeoffs," *EURASIP J. Wireless Commun. Netw.*, vol. 2015, no. 1, p. 41, Feb. 2015.
- [267] J. G. Andrews, H. Claussen, M. Dohler, S. Rangan, and M. C. Reed, "Femtocells: past, present, and future," *IEEE J. Sel. Areas Commun.*, vol. 30, no. 3, pp. 497-508, Apr. 2012.
- [268] T. Frisanco, P. Tafertshofer, P. Lurin, and R. Ang, "Infrastructure sharing and shared operations for mobile network operators: From a deployment and operations view," in *Proc. IEEE Int. Conf. Commun. (ICC)*, pp. 2193-2200, Beijing, China, 2008.
- [269] A. Khan, W. Kellerer, K. Kozu, and M. Yabusaki, "Network sharing in the next mobile network: TCO reduction, management flexibility, and operational independence," *IEEE Commun. Mag.*, vol. 49, no. 10, pp. 134-142, Oct. 2011.
- [270] F. Boccardi et al., "Spectrum pooling in MmWave networks: opportunities, challenges, and enablers," *IEEE Commun. Mag.*, vol. 54, no. 11, pp. 33-39, Nov. 2016.
- [271] A. A. M. Saleh, A. J. Rustako, and R. S. Roman, "Distributed antennas for indoor radio communications," *IEEE Trans. Commun.*, vol. 35, pp. 1245-1251, Dec. 1987.
- [272] J. Zhang and J. G. Andrews, "Distributed antenna systems with randomness," *IEEE Trans. Wireless Commun.*, vol. 7, no. 9, pp. 3636-3646, Sep. 2008.
- [273] Y. Lin and W. Yu, "Downlink spectral efficiency of distributed antenna systems under a stochastic model," *IEEE Trans. on Wireless Commun.*, vol. 13, no. 12, pp. 6891-6902, Dec. 2014.
- [274] M. Cheng and J. Wang, "Downlink transmission capacity analysis for virtual cell based distributed antenna systems," in *Proc. IEEE Int. Conf. Commun. (ICC)*, pp. 1-6, France, Paris, 2017.
- [275] M. Di Renzo and P. Guan, "A mathematical framework to the computation of the error probability of downlink MIMO cellular networks by using stochastic geometry," *IEEE Trans. Commun.*, vol. 62, no. 8, pp. 2860-2879, Aug. 2014.
- [276] V. Chandrasekhar, M. Kountouris, and J. G. Andrews, "Coverage in multi-antenna two-tier networks," *IEEE Trans. Wireless Commun.*, vol. 8, no. 10, pp. 5314-5327, Oct. 2009.
- [277] H. S. Dhillon, M. Kountouris, and J. G. Andrews, "Downlink MIMO hetNets: modeling, ordering results and performance analysis," *IEEE Trans. Wireless Commun.*, vol. 12, no. 10, pp. 5208-5222, Oct. 2013.

-
- [278] T. Bai and R. W. Heath, "Analyzing uplink SINR and rate in massive MIMO systems using stochastic geometry," *IEEE Trans. on Commun.*, vol. 64, no. 11, pp. 4592-4606, Nov. 2016.
- [279] G. Hattab and D. Cabric, "Joint resource allocation and user association in multi-antenna heterogeneous networks," in *Proc. IEEE Glob. Commun. Conf. (GLOBECOM)*, pp. 1-7, Washington, DC, USA, Dec. 2016.
- [280] A. Adhikary, H. S. Dhillon, and G. Caire, "Massive-MIMO meets hetnet: interference coordination through spatial blanking," *IEEE J. Sel. Areas Commun.*, vol. 33, no. 6, pp. 1171-1186, Jun. 2015.
- [281] A. Shojaeifard, K. Wong, M. Di Renzo, G. Zheng, K. A. Hamdi, and J. Tang, "Massive MIMO-enabled full-duplex cellular networks," *IEEE Trans. Commun.*, vol. 65, no. 11, pp. 4734-4750, Nov. 2017.
- [282] Z. Ding, R. Schober, and H. V. Poor, "A general MIMO framework for NOMA downlink and uplink transmission based on signal alignment," *IEEE Trans. Wireless Commun.*, vol. 15, no. 6, pp. 4438-4454, Jun. 2016.
- [283] M. N. Kulkarni, A. Ghosh, and J. G. Andrews, "A comparison of MIMO techniques in downlink millimeter wave cellular networks with hybrid beamforming," *IEEE Trans. Commun.*, vol. 64, no. 5, pp. 1952-1967, May 2016.
- [284] X. Lin, R. W. Heath, and J. G. Andrews, "The interplay between massive MIMO and underlaid D2D networking," *IEEE Trans. Wireless Commun.*, vol. 14, no. 6, pp. 3337-3351, Jun. 2015.
- [285] A. Lo and I. Niemegeers, "Multi-hop relay architectures for 3GPP LTE-advanced," in *Proc. IEEE 9th Int. Conf. Commun. (ICC)*, pp. 123-127, 2009, Kuala Lumpur, Malaysia.
- [286] G. Liu, F. R. Yu, H. Ji, V. C. M. Leung, and X. Li, "In-band full-duplex relaying: A survey, research issues and challenges," *IEEE Commun. Surveys Tuts*, vol. 17, no. 2, pp. 500-524, Secondquarter 2015.
- [287] J. He et al., "A Tutorial on lossy forwarding cooperative relaying," *IEEE Commun. Surveys Tuts*, vol. 21, no. 1, pp. 66-87, Firstquarter 2019.
- [288] N. Nomikos et al., "A survey on buffer-aided relay selection," *IEEE Commun. Surveys Tuts*, vol. 18, no. 2, pp. 1073-1097, Secondquarter 2016.
- [289] R. K. Ganti and M. Haenggi, "Spatial analysis of opportunistic downlink relaying in a two-hop cellular system," *IEEE Trans. Commun.*, vol. 60, no. 5, pp. 1443-1450, May 2012.

-
- [290] I. Krikidis, "Simultaneous information and energy transfer in large-scale networks with/without relaying," *IEEE Trans. Commun.*, vol. 62, no. 3, pp. 900-912, Mar. 2014.
- [291] Z. Ding, I. Krikidis, B. Sharif, and H. V. Poor, "Wireless information and power transfer in cooperative networks with spatially random relays," *IEEE Trans. on Wireless Commun.*, vol. 13, no. 8, pp. 4440-4453, Aug. 2014.
- [292] J. Wen, M. Sheng, X. Wang, J. Li, and H. Sun, "On the capacity of downlink multi-hop heterogeneous cellular networks," *IEEE Trans. Wireless Commun.*, vol. 13, no. 8, pp. 4092-4103, Aug. 2014.
- [293] W. Lu and M. Di Renzo, "Stochastic geometry modeling and system-level analysis & optimization of relay-aided downlink cellular networks," *IEEE Trans. Commun.*, vol. 63, no. 11, pp. 4063-4085, Nov. 2015.
- [294] K. Ntontin, M. Di Renzo, and C. Verikoukis, "On the feasibility of full-duplex relaying in multiple-antenna cellular networks," *IEEE Trans. Commun.*, vol. 65, no. 5, pp. 2234-2249, May 2017.
- [295] E. Basar, M. Di Renzo, J. De Rosny, M. Debbah, M. Alouini, and R. Zhang, "Wireless Communications Through Reconfigurable Intelligent Surfaces," *IEEE Access*, vol. 7, pp. 116753-116773, 2019.
- [296] M. Di Renzo et al., "Smart radio environments empowered by reconfigurable AI metasurfaces: an idea whose time has come," *EURASIP J. Wireless Commun. Netw.*, vol. 129, no. 1, pp. 1-20, May 2019.
- [297] S. Han and K. G. Shin, "Enhancing wireless performance using reflectors," in *Proc. IEEE Conf. on Comput. Commun. (INFOCOM)*, pp. 1-9, Atlanta, GA, USA 2017.
- [298] M. Di Renzo and J. Song, "Reflection probability in wireless networks with metasurface-coated environmental objects: an approach based on random spatial processes," *EURASIP J. Wireless Commun. Netw.*, Vol. 99, pp. 1-15, Apr. 2019.
- [299] A. Asadi, Q. Wang, and V. Mancuso, "A survey on device-to-device communication in cellular networks," *IEEE Commun. Surveys Tuts.*, vol. 16, no. 4, pp. 1801-1819, Fourthquarter 2014.
- [300] F. Jameel, Z. Hamid, F. Jabeen, S. Zeadally, and M. A. Javed, "A survey of device-to-device communications: research issues and challenges," *IEEE Commun. Surveys Tuts.*, vol. 20, no. 3, pp. 2133-2168, Thirdquarter 2018.

-
- [301] X. Lin, J. G. Andrews, and A. Ghosh, "Spectrum sharing for device-to-device communication in cellular networks," *IEEE Trans. Wireless Commun.*, vol. 13, no. 12, pp. 6727-6740, Dec. 2014.
- [302] F. Wu, H. Zhang, B. Di, J. Wu and L. Song, "Device-to-device communications underlaying cellular networks: To use unlicensed spectrum or not?," *IEEE Trans. Commun.*, vol. 67, no. 9, pp. 6598-6611, Sept. 2019.
- [303] M. Peng, Y. Li, T. Q. S. Quek, and C. Wang, "Device-to-device underlaid cellular networks under Rician fading channels," *IEEE Trans. Wireless Commun.*, vol. 13, no. 8, pp. 4247-4259, Aug. 2014.
- [304] S. Andreev, O. Galinina, A. Pyattaev, K. Johnsson, and Y. Koucheryavy, "Analyzing assisted offloading of cellular user sessions onto D2D links in unlicensed bands," *IEEE J. Sel. Areas Commun.*, vol. 33, no. 1, pp. 67-80, Jan. 2015.
- [305] H. ElSawy, E. Hossain, and M. Alouini, "Analytical modeling of mode selection and power control for underlay D2D communication in cellular networks," *IEEE Trans. Commun.*, vol. 62, no. 11, pp. 4147-4161, Nov. 2014.
- [306] H. V. Vu, N. H. Tran, and T. Le-Ngoc, "Full-duplex device-to-device cellular networks: power control and performance analysis," *IEEE Trans. Veh. Technol.*, vol. 68, no. 4, pp. 3952-3966, Apr. 2019.
- [307] V. Suryaprakash, P. Rost, and G. Fettweis, "Are heterogeneous cloud-based radio access networks cost effective?," *IEEE J. Sel. Areas Commun.*, vol. 33, no. 10, pp. 2239-2251, Oct. 2015.
- [308] F. A. Khan, H. He, J. Xue, and T. Ratnarajah, "Performance analysis of cloud radio access networks with distributed multiple antenna remote radio heads," *IEEE Trans. Sig. Process.*, vol. 63, no. 18, pp. 4784-4799, Sep. 2015.
- [309] H. He, J. Xue, T. Ratnarajah, F. A. Khan, and C. B. Papadias, "Modeling and analysis of cloud radio access networks using Matérn hard-core point processes," *IEEE Trans. Wireless Commun.*, vol. 15, no. 6, pp. 4074-4087, Jun. 2016.
- [310] S. T. Veetil, K. Kuchi, and R. K. Ganti, "Coverage analysis of cloud radio networks with finite clustering," *IEEE Trans. Wireless Commun.*, vol. 16, no. 1, pp. 594-606, Jan. 2017.
- [311] J. Liu, M. Sheng, T. Q. S. Quek, and J. Li, "D2D enhanced co-ordinated multipoint in cloud radio access networks," *IEEE Trans. Wireless Commun.*, vol. 15, no. 6, pp. 4248-4262, Jun. 2016.

-
- [312] M. Mohammadi, H. A. Suraweera, and C. Tellambura, "Uplink/downlink rate analysis and impact of power allocation for full-duplex cloud-RANs," *IEEE Trans. Wireless Commun.*, vol. 17, no. 9, pp. 5774-5788, Sep. 2018.
- [313] X. Gu, X. Ji, Z. Ding, W. Wu, and M. Peng, "Outage probability analysis of non-orthogonal multiple access in cloud radio access networks," *IEEE Commun. Lett.*, vol. 22, no. 1, pp. 149-152, Jan. 2018.
- [314] M. Y. Arslan, K. Sundaresan, and S. Rangarajan, "Software-defined networking in cellular radio access networks: Potential and challenges," *IEEE Commun. Mag.*, vol. 53, no. 1, pp. 150-156, Jan. 2015.
- [315] H. Ishii, Y. Kishiyama, and H. Takahashi, "A novel architecture for LTE-B: C-plane/U-plane split and phantom cell concept," in *Proc. IEEE Globecom Workshops*, pp. 624-630, Anaheim, CA, USA, Dec. 2012.
- [316] A. Zakrzewska, D. López-Pérez, S. Kucera, and H. Claussen, "Dual connectivity in LTE HetNets with split control- and user-plane," in *Proc. IEEE Globecom Workshops (GC Wkshps)*, pp. 391-396, Atlanta, GA, USA, Dec. 2013.
- [317] O. Semiari, W. Saad, M. Bennis, and M. Debbah, "Integrated millimeter wave and sub-6 GHz wireless networks: A roadmap for joint mobile broadband and ultra-reliable low-latency communications," *IEEE Wireless Commun.*, vol. 26, no. 2, pp. 109-115, Apr. 2019.
- [318] M. Peng, Y. Li, J. Jiang, J. Li, and C. Wang, "Heterogeneous cloud radio access networks: a new perspective for enhancing spectral and energy efficiencies," *IEEE Wireless Commun.*, vol. 21, no. 6, pp. 126-135, Dec. 2014.
- [319] S. Mukherjee and H. Ishii, "Energy efficiency in the phantom cell enhanced local area architecture," in *Proc. IEEE Wireless Commun. Netw. Conf. (WCNC)*, pp. 1267-1272, Shanghai, China, 2013.
- [320] T. Han et al., "Small cell offloading through cooperative communication in software-defined heterogeneous networks," *IEEE Sensors J.*, vol. 16, no. 20, pp. 7381-7392, Oct. 2016.
- [321] H. Ibrahim, H. ElSawy, U. T. Nguyen, and M. Alouini, "Mobility-aware modeling and analysis of dense cellular networks with C-plane/U-plane split architecture," *IEEE Trans. Commun.*, vol. 64, no. 11, pp. 4879-4894, Nov. 2016.

-
- [322] B. Yang, X. Yang, X. Ge, and Q. Li, "Coverage and handover analysis of ultra-dense millimeter-wave networks with control and user plane separation architecture," *IEEE Access*, vol. 6, pp. 54739-54750, 2018.
- [323] R. Arshad, L. Lampe, H. ElSawy, and M. J. Hossain, "Integrating UAVs into existing wireless networks: A stochastic geometry approach," in *Proc. IEEE Globecom Workshops (GC Wkshps)*, pp. 1-6, Abu Dhabi, UAE, Dec. 2018.
- [324] Y. Mao, C. You, J. Zhang, K. Huang, and K. B. Letaief, "A survey on mobile edge computing: The communication perspective," *IEEE Commun. Surveys Tuts.*, vol. 19, no. 4, pp. 2322-2358, Fourthquarter 2017.
- [325] H. Kong, I. Flint, P. Wang, D. Niyato, and N. Privault, "Fog radio access networks: Ginibre point process modeling and analysis," *IEEE Trans. on Wireless Commun.*, vol. 17, no. 8, pp. 5564-5580, Aug. 2018.
- [326] D. Malak, M. Al-Shalash, and J. G. Andrews, "Spatially correlated content caching for device-to-device communications," *IEEE Trans. Wireless Commun.*, vol. 17, no. 1, pp. 56-70, Jan. 2018.
- [327] B. Blaszczyszyn and A. Giovanidis, "Optimal geographic caching in cellular networks," in *Proc. IEEE Int. Conf. Commun. (ICC)*, pp. 3358-3363, London, UK, 2015.
- [328] J. Wen, K. Huang, S. Yang, and V. O. K. Li, "Cache-enabled heterogeneous cellular networks: optimal tier-level content placement," *IEEE Trans. Wireless Commun.*, vol. 16, no. 9, pp. 5939-5952, Sep. 2017.
- [329] C. Yang, Y. Yao, Z. Chen, and B. Xia, "Analysis on cache-enabled wireless heterogeneous networks," *IEEE Trans. Wireless Commun.*, vol. 15, no. 1, pp. 131-145, Jan. 2016.
- [330] Y. Cui, Y. Wu, and D. Jiang, "Analysis and optimization of caching and multicasting in large-scale cache-enabled information-centric networks," *IEEE Glob. Commun. Conf. (GLOBECOM)*, pp. 1-7, San Diego, CA, USA, Dec. 2015.
- [331] Z. Zhao, M. Peng, Z. Ding, W. Wang, and H. V. Poor, "Cluster content caching: an energy-efficient approach to improve quality of service in cloud radio access networks," *IEEE J. Sel. Areas Commun.*, vol. 34, no. 5, pp. 1207-1221, May 2016.
- [332] M. R. Akdeniz et al., "Millimeter wave channel modeling and cellular capacity evaluation," *IEEE J. Sel. Areas Commun.*, vol. 32, no. 6, pp. 1164-1179, Jun. 2014.
- [333] J. Park, S. Kim, and J. Zander, "Tractable resource management with uplink decoupled millimeter-wave overlay in ultra-dense cellular networks," *IEEE Trans. Wireless Commun.*, vol. 15, no. 6, pp. 4362-4379, Jun. 2016.

-
- [334] H. Elshaer, M. N. Kulkarni, F. Boccardi, J. G. Andrews, and M. Dohler, "Downlink and uplink cell association with traditional macrocells and millimeter wave small cells," *IEEE Trans. Wireless Commun.*, vol. 15, no. 9, pp. 6244-6258, Sep. 2016.
- [335] G. Zhang, T. Q. S. Quek, M. Kountouris, A. Huang, and H. Shan, "Fundamentals of heterogeneous backhaul design-analysis and optimization," *IEEE Trans. Commun.*, vol. 64, no. 2, pp. 876-889, Feb. 2016.
- [336] M. N. Kulkarni, A. Ghosh, and J. G. Andrews, "A comparison of MIMO techniques in downlink millimeter wave cellular networks with hybrid beamforming," *IEEE Trans. Commun.*, vol. 64, no. 5, pp. 1952-1967, May 2016.
- [337] J. M. Jornet and I. F. Akyildiz, "Channel modeling and capacity analysis for electromagnetic wireless nanonetworks in the terahertz band," *IEEE Trans. Wireless Commun.*, vol. 10, no. 10, pp. 3211-3221, Oct. 2011.
- [338] V. Petrov, M. Komarov, D. Moltchanov, J. M. Jornet, and Y. Koucheryavy, "Interference and SINR in millimeter wave and terahertz communication systems with blocking and directional antennas," *IEEE Trans. Wireless Commun.*, vol. 16, no. 3, pp. 1791-1808, Mar. 2017.
- [339] J. Kokkonen, J. Lehtomäki, and M. Juntti, "Stochastic geometry analysis for mean interference power and outage probability in THz networks," *IEEE Trans. Wireless Commun.*, vol. 16, no. 5, pp. 3017-3028, May 2017.
- [340] K. Ntontin and C. Verikoukis, "Toward the performance enhancement of microwave cellular networks through THz links," *IEEE Trans. Veh. Technol.*, vol. 66, no. 7, pp. 5635-5646, Jul. 2017.
- [341] C. Chen, D. A. Basnayaka, and H. Haas, "Downlink performance of optical attocell networks," *J. Lightwave Technol.*, vol. 34, no. 1, pp. 137-156, Jan. 2016.
- [342] L. Yin and H. Haas, "Coverage analysis of multiuser visible light communication networks," *IEEE Trans. Wireless Commun.*, vol. 17, no. 3, pp. 1630-1643, Mar. 2018.
- [343] H. Tabassum and E. Hossain, "Coverage and rate analysis for co-existing RF/VLC downlink cellular networks," *IEEE Trans. Wireless Commun.*, vol. 17, no. 4, pp. 2588-2601, Apr. 2018.
- [344] J. Kong, M. Ismail, E. Serpedin, and K. A. Qaraqe, "Energy efficient optimization of base station intensities for hybrid RF/VLC networks," *IEEE Trans. Wireless Commun.*, vol. 18, no. 8, pp. 4171-4183, Aug. 2019.

-
- [345] G. Pan, J. Ye, and Z. Ding, "Secure hybrid VLC-RF systems with light energy harvesting," *IEEE Trans. Commun.*, vol. 65, no. 10, pp. 4348-4359, Oct. 2017.
- [346] L. Yin and H. Haas, "Physical-layer security in multiuser visible light communication networks," *IEEE J. Sel. Areas Commun.*, vol. 36, no. 1, pp. 162-174, Jan. 2018.
- [347] S. Cho, G. Chen, and J. P. Coon, "Securing visible light communication systems by beamforming in the presence of randomly distributed eavesdroppers," *IEEE Trans. on Wireless Commun.*, vol. 17, no. 5, pp. 2918-2931, May 2018.
- [348] M. A. Khalighi and M. Uysal, "Survey on free space optical communication: A communication theory perspective," *IEEE Commun. Surveys Tuts.*, vol. 16, no. 4, pp. 2231-2258, Fourthquarter 2014.
- [349] M. Lahmeri, M. A. Kishk, and M. Alouini, "Stochastic Geometry-based analysis of Airborne Base Stations with Laser-powered UAVs," *IEEE Commun. Lett.*, to appear.
- [350] F. Nadeem, V. Kvicera, M. S. Awan, E. Leitgeb, S. S. Muhammad, and G. Kandung, "Weather effects on hybrid FSO/RF communication link," *IEEE J. Sel. Areas Commun.*, vol. 27, no. 9, pp. 1687-1697, Dec. 2009.
- [351] A. Vavoulas, H. G. Sandalidis, and D. Varoutas, "Weather effects on FSO network connectivity," *IEEE/OSA J. of Optical Commun. and Netw.*, vol. 4, no. 10, pp. 734-740, Oct. 2012.
- [352] N. Letzepis and A. Guillen i Fabregas, "Outage probability of the free-space optical channel with doubly stochastic scintillation," *IEEE Trans. Commun.*, vol. 57, no. 10, pp. 2899-2902, Oct. 2009.
- [353] V. G. Sidorovich, "Solar background effects in wireless optical communications," in *Proc. of SPIE, Optical Wireless Commun.*, vol. 4873, pp. 133-142, 2002.
- [354] S. Haykin, "Cognitive radio: brain-empowered wireless communications," *IEEE J. Sel. Areas Commun.*, vol. 23, no. 2, pp. 201-220, Feb. 2005.
- [355] U. Tefek and T. J. Lim, "Interference management through exclusion zones in two-tier cognitive networks," *IEEE Trans. Wireless Commun.*, vol. 15, no. 3, pp. 2292-2302, Mar. 2016.
- [356] X. Song, C. Yin, D. Liu, and R. Zhang, "Spatial throughput characterization in cognitive radio networks with threshold-based opportunistic spectrum access," *IEEE J. Sel. Areas Commun.*, vol. 32, no. 11, pp. 2190-2204, Nov. 2014.

-
- [357] J. Bang, J. Lee, S. Kim, and D. Hong, "An efficient relay selection strategy for random cognitive relay networks," *IEEE Trans. Wireless Commun.*, vol. 14, no. 3, pp. 1555-1566, Mar. 2015.
- [358] S. Cheng, W. C. Ao, F. Tseng, and K. Chen, "Design and analysis of downlink spectrum sharing in two-tier cognitive femto networks," *IEEE Trans. Veh. Technol.*, vol. 61, no. 5, pp. 2194-2207, Jun. 2012.
- [359] Y. Saito, Y. Kishiyama, A. Benjebbour, T. Nakamura, A. Li, and K. Higuchi, "Non-orthogonal multiple access (NOMA) for cellular future radio access," in *Proc. IEEE 77th Veh. Technol. Conf. (VTC Spring)*, pp. 1-5, Dresden, Germany, 2013.
- [360] H. Tabassum, E. Hossain, and J. Hossain, "Modeling and analysis of uplink non-orthogonal multiple access in large-scale cellular networks using poisson cluster processes," *IEEE Trans. Commun.*, vol. 65, no. 8, pp. 3555-3570, Aug. 2017.
- [361] Y. Liu, Z. Qin, M. ElKashlan, Y. Gao, and A. Nallanathan, "Non-orthogonal multiple access in massive MIMO aided heterogeneous networks," in *Proc. IEEE Glob. Commun. Conf. (GLOBECOM)*, pp. 1-6, Washington, DC, USA, Dec. 2016.
- [362] Z. Zhang, H. Sun, and R. Q. Hu, "Downlink and uplink non-orthogonal multiple access in a dense wireless network," *IEEE J. Sel. Areas Commun.*, vol. 35, no. 12, pp. 2771-2784, Dec. 2017.
- [363] F. J. Martin-Vega, Y. Liu, G. Gomez, M. C. Aguayo-Torres, and M. ElKashlan, "Modeling and analysis of NOMA enabled CRAN with cluster point process," in *Proc. Glob. Commun. Conf. (GLOBECOM)*, pp. 1-6, Singapore, Dec. 2017.
- [364] X. Gu, X. Ji, Z. Ding, W. Wu, and M. Peng, "Outage probability analysis of non-orthogonal multiple access in cloud radio access networks," *IEEE Commun. Lett.*, vol. 22, no. 1, pp. 149-152, Jan. 2018.
- [365] C. Liu and D. Liang, "Heterogeneous networks with power-domain NOMA: coverage, throughput, and power allocation analysis," *IEEE Trans. Wireless Commun.*, vol. 17, no. 5, pp. 3524-3539, May 2018.
- [366] Z. Zhang, Z. Ma, M. Xiao, X. Lei, Z. Ding, and P. Fan, "Fundamental tradeoffs of non-orthogonal multicast, multicast, and unicast in ultra-dense networks," *IEEE Trans. Commun.*, vol. 66, no. 8, pp. 3555-3570, Aug. 2018.
- [367] T. Hou, Y. Liu, Z. Song, X. Sun, and Y. Chen, "Multiple antenna aided NOMA in UAV networks: A stochastic geometry approach," *IEEE Trans. Commun.*, vol. 67, no. 2, pp. 1031-1044, Feb. 2019.

-
- [368] P. Swami, V. Bhatia, S. Vuppala, and T. Ratnarajah, "On user offloading in NOMA-hetnet using repulsive point process," *IEEE Systems J.*, vol. 13, no. 2, pp. 1409-1420, Jun. 2019.
- [369] K. Ali, H. Elsayy, and M. Alouini, "Meta distribution of downlink non-orthogonal multiple access (NOMA) in Poisson networks," *IEEE Wireless Communications Letters*, vol. 8, no. 2, pp. 572-575, Apr. 2019.
- [370] K. Ali, H. Elsayy, and M. Alouini, "Meta distribution of downlink non-orthogonal multiple access (NOMA) in Poisson networks," *IEEE Wireless Commun. Lett.*, vol. 8, no. 2, pp. 572-575, Apr. 2019.
- [371] M. Salehi, H. Tabassum, and E. Hossain, "Meta distribution of SIR in large-scale uplink and downlink NOMA networks," *IEEE Trans. on Commun.*, vol. 67, no. 4, pp. 3009-3025, Apr. 2019.
- [372] J. Lee and T. Q. S. Quek, "Hybrid full-/half-duplex system analysis in heterogeneous wireless networks," *IEEE Trans. Wireless Commun.*, vol. 14, no. 5, pp. 2883-2895, May 2015.
- [373] Z. Tong and M. Haenggi, "Throughput analysis for full-duplex wireless networks with imperfect self-interference cancellation," *IEEE Trans. Commun.*, vol. 63, no. 11, pp. 4490-4500, Nov. 2015.
- [374] H. Tabassum, A. H. Sakr, and E. Hossain, "Analysis of massive MIMO-enabled downlink wireless backhauling for full-duplex small cells," *IEEE Trans. Commun.*, vol. 64, no. 6, pp. 2354-2369, Jun. 2016.
- [375] K. Ntontin, M. Di Renzo, and C. Verikoukis, "On the feasibility of full-duplex relaying in multiple-antenna cellular networks," *IEEE Trans. Commun.*, vol. 65, no. 5, pp. 2234-2249, May 2017.
- [376] A. H. Sakr and E. Hossain, "On user association in multi-tier full-duplex cellular networks," *IEEE Trans. Commun.*, vol. 65, no. 9, pp. 4080-4095, Sep. 2017.
- [377] A. Shojaeifard, K. Wong, M. Di Renzo, G. Zheng, K. A. Hamdi, and J. Tang, "Massive MIMO-enabled full-duplex cellular networks," *IEEE Trans. on Commun.*, vol. 65, no. 11, pp. 4734-4750, Nov. 2017.
- [378] A. Sharma, R. K. Ganti, and J. K. Milleth, "Joint backhaul-access analysis of full duplex self-backhauling heterogeneous networks," *IEEE Trans. Wireless Commun.*, vol. 16, no. 3, pp. 1727-1740, Mar. 2017.

-
- [379] I. Atzeni and M. Kountouris, "Full-duplex MIMO small-cell networks with interference cancellation," *IEEE Trans. Wireless Commun.*, vol. 16, no. 12, pp. 8362-8376, Dec. 2017.
- [380] X. Zhou, R. K. Ganti, J. G. Andrews, and A. Hjørungnes, "On the throughput cost of physical layer security in decentralized wireless networks," *IEEE Trans. Wireless Commun.*, vol. 10, no. 8, pp. 2764-2775, Aug. 2011.
- [381] H. Wang, X. Zhou, and M. C. Reed, "Physical layer security in cellular networks: A stochastic geometry approach," *IEEE Trans. Wireless Commun.*, vol. 12, no. 6, pp. 2776-2787, Jun. 2013.
- [382] H. Wu, X. Tao, N. Li, and J. Xu, "Secrecy outage probability in multi-RAT heterogeneous networks," *IEEE Commun. Lett.*, vol. 20, no. 1, pp. 53-56, Jan. 2016.
- [383] H. Wang, T. Zheng, J. Yuan, D. Towsley, and M. H. Lee, "Physical layer security in heterogeneous cellular networks," *IEEE Trans. on Commun.*, vol. 64, no. 3, pp. 1204-1219, Mar. 2016.
- [384] Y. Liu, Z. Qin, M. ElKashlan, Y. Gao, and L. Hanzo, "Enhancing the physical layer security of non-orthogonal multiple access in large-scale networks," *IEEE Trans. Wireless Commun.*, vol. 16, no. 3, pp. 1656-1672, Mar. 2017.
- [385] W. Wang, K. C. Teh, and K. H. Li, "Artificial noise aided physical layer security in multi-antenna small-cell networks," *IEEE Trans. Inf. Forensics and Security*, vol. 12, no. 6, pp. 1470-1482, Jun. 2017.
- [386] C. Ma, J. Liu, X. Tian, H. Yu, Y. Cui, and X. Wang, "Interference exploitation in D2D-enabled cellular networks: A secrecy perspective," *IEEE Trans. Commun.*, vol. 63, no. 1, pp. 229-242, Jan. 2015.
- [387] S. Vuppala, S. Biswas, and T. Ratnarajah, "An analysis on secure communication in millimeter/micro-wave hybrid networks," *IEEE Trans. Commun.*, vol. 64, no. 8, pp. 3507-3519, Aug. 2016.
- [388] H. Wang, C. Wang, T. Zheng, and T. Q. S. Quek, "Impact of artificial noise on cellular networks: A stochastic geometry approach," *IEEE Trans. Wireless Commun.*, vol. 15, no. 11, pp. 7390-7404, Nov. 2016.
- [389] W. Tang, S. Feng, Y. Ding, and Y. Liu, "Physical layer security in heterogeneous networks With jammer selection and full-duplex users," *IEEE Trans. Wireless Commun.*, vol. 16, no. 12, pp. 7982-7995, Dec. 2017.

-
- [390] H. Kong, P. Wang, D. Niyato, and Y. Cheng, "Physical layer security in wireless networks with Ginibre point processes," *IEEE Trans. Wireless Commun.*, vol. 17, no. 8, pp. 5132-5147, Aug. 2018.
- [391] A. Merwaday, R. Vannithamby, M. M. Rashid, Y. Zhang, C. Chen, and X. Wu, "On the performance of directional communications in ultra-dense networks," in *Proc. IEEE Int. Conf. Commun. Workshops (ICC)*, Paris, France, 2017, pp. 522-527.
- [392] R. Hernandez-Aquino, S. A. R. Zaidi, D. McLernon, M. Ghogho, and A. Imran, "Tilt angle optimization in two-tier cellular networks – A stochastic geometry approach," *IEEE Trans. Commun.*, vol. 63, no. 12, pp. 5162-5177, Dec. 2015.
- [393] B. Blaszczyszyn, and M. K. Karray, "Spatial distribution of the SINR in Poisson cellular networks with sector antennas," *IEEE Trans. Wireless Commun.*, vol. 15, no. 1, pp. 581-593, Jan. 2016.
- [394] B. Blaszczyszyn, and H. P. Keeler, "Equivalence and comparison of heterogeneous cellular networks," in *Proc. IEEE 24th Annu. Symp. Pers. Indoor Mobile Radio Commun. Workshops (PIMRC)*, London, U.K., 2013, pp. 153-157.
- [395] S. Sun, T. A. Thomas, T. S. Rappaport, H. Nguyen, I. Z. Kovacs, and I. Rodriguez, "Path loss, shadow fading, and line-of-sight probability models for 5G urban macro-cellular scenarios," in *Proc. IEEE Glob. Conf. Workshops (GLOBECOM)*, San Diego, CA, USA, 2015, pp. 1-7.
- [396] A. P. Prundnikov, Y. A. Brychkov, and O. I. Marichev, *Integrals and Series, Vol. 3: More Special Functions*, Philadelphia, USA: Gordon and Breach Science Publishers, 1990.
- [397] I. S. Gradshteyn, I. M. Ryzhik, *Table of Integrals, Series, and Products*, 7th ed. Academic Press, Elsevier Inc, 2007.
- [398] M. Ding and D. Lopez Perez, "Please Lower Small Cell Antenna Heights in 5G," 2016 IEEE Global Communications Conference (GLOBECOM), Washington, DC, 2016, pp. 1-6.
- [399] S. M. Yu and S.-L. Kim, "Downlink capacity and base station density in cellular networks", *IEEE Workshop on Spatial Stochastic Models for Wireless Networks*, pp. 1-7, May 2013.
- [400] M. Ding, D. Lopez Perez, A. H. Jafari, G. Mao and Z. Lin, "Ultra-Dense Networks: A New Look at the Proportional Fair Scheduler," *GLOBECOM 2017 - 2017 IEEE Global Communications Conference*, Singapore, pp. 1-7, Dec. 2017.
- [401] S. G. Foss, S. A. Zuyev, "On a Voronoi Aggregative Process Related to a Bivariate Poisson Process," *Adv. Appl. Probab.*, vol. 28, no. 4, 965-981, 1996.

-
- [402] P. Calka, "Precise formulae for the distributions of the principal geometric characteristics of the typical cells of a two-dimensional Poisson voronoi tessellation and a Poisson line process", *Adv. Appl. Prob.*, vol. 35, pp. 551-562, Sep. 2003.
- [403] H. S. Dhillon and J. G. Andrews, "Downlink Rate Distribution in Heterogeneous Cellular Networks under Generalized Cell Selection," in *IEEE Wireless Communications Letters*, vol. 3, no. 1, pp. 42-45, Feb. 2014.
- [404] M. Ding, D. L. Perez, G. Mao, and Z. Lin, "Study on the idle mode capability with los and nlos transmissions," in *2016 IEEE Global Communications Conference (GLOBECOM)*, pp. 1–6, Dec. 2016.
- [405] *Ericsson Mobility Report on the Pulse of the Networked Society*, Nov. 2016, Stockholm, Sweden. [Online]. Available: <https://www.ericsson.com/assets/local/mobility-report/documents/2016/ericsson-mobility-report-november-2016.pdf>
- [406] T. Ding, M. Ding, G. Mao, Z. Lin, D. López-Pérez, and A. Y. Zomaya, "Uplink performance analysis of dense cellular networks with LoS and NLoS transmissions," *IEEE Trans. Wireless Commun.*, vol. 16, no. 4, pp. 2601-2613, Apr. 2017.
- [407] R. Arshad, H. Elsayy, S. Sorour, M. Alouini, and T. Y. Al-Naffouri, "Mobility-aware user association in uplink cellular networks," *IEEE Commun. Lett.*, vol. 21, no. 11, pp. 2452-2455, Nov. 2017.
- [408] 3GPP, "Enhanced LTE support for aerial vehicles," 3rd Generation Partnership Project (3GPP), Tech. Rep. 36.777, 01 2018, version 1.1.0.
- [409] Y. Sun, R. P. Jover, and X. Wang, "Uplink interference mitigation for OFDMA femtocell networks," *IEEE Trans. Wireless Commun.*, vol. 11, no. 2, pp. 614-625, Feb. 2012.
- [410] B. Van Der Bergh, A. Chiumento, and S. Pollin, "LTE in the sky: trading off propagation benefits with interference costs for aerial nodes," *IEEE Commun. Mag.*, vol. 54, no. 5, pp. 44-50, May 2016.
- [411] R. Amorim et al., "Measured uplink interference caused by aerial vehicles in LTE cellular networks," *IEEE Wireless Commun. Lett.*, vol. 7, no. 6, pp. 958-961, Dec. 2018.
- [412] W. Mei, Q. Wu and R. Zhang, "Cellular-connected UAV: uplink association, power control and interference coordination," *IEEE Trans. Wireless Commun.*, vol. 18, no. 11, pp. 5380-5393, Nov. 2019.

-
- [413] L. Liu, S. Zhang and R. Zhang, "Multi-beam UAV communication in cellular uplink: cooperative interference cancellation and sum-rate maximization," *IEEE Trans. Wireless Commun.*, vol. 18, no. 10, pp. 4679-4691, Oct. 2019.
- [414] S. Singh, X. Zhang and J. G. Andrews, "Uplink rate distribution in heterogeneous cellular networks with power control and load balancing," in *Proc. IEEE Int. Conf. Commun. (ICC) Workshops*, pp. 1275-1280, London, UK, 2015.
- [415] T. Ding, M. Ding, G. Mao, Z. Lin, D. López-Pérez and A. Y. Zomaya, "Uplink performance analysis of dense cellular networks With LoS and NLoS transmissions," *IEEE Trans. Wireless Commun.*, vol. 16, no. 4, pp. 2601-2613, Apr. 2017.
- [416] N. Rikhtegar and M. Keshtgary, "A brief survey on molecular and electromagnetic communications in nano-networks," *Int. J. Comput. Appl.*, vol. 79, pp. 16-28, Oct. 2013.
- [417] N. Farsad, H. B. Yilmaz, A. Eckford, C. Chae, and W. Guo, "A comprehensive survey of recent advancements in molecular communication," *IEEE Commun. Surveys Tuts*, vol. 18, no. 3, pp. 1887-1919, Thirdquarter 2016.
- [418] N. Farsad, W. Guo, and A. W. Eckford, "Tabletop molecular communication: Text messages through chemical signals," *PLoS One*, vol. 8, Dec. 2013.
- [419] Y. Deng, A. Noel, W. Guo, A. Nallanathan, and M. ElKashlan, "Analyzing large-scale multiuser molecular communication via 3-D stochastic geometry," *IEEE Trans. Molecular, Biological and Multi-Scale Commun.*, vol. 3, no. 2, pp. 118-133, Jun. 2017.
- [420] W. Guo, C. Mias, N. Farsad, and J. Wu, "Molecular versus electromagnetic wave propagation loss in macro-scale environments," *IEEE Trans. Molecular, Biological and Multi-Scale Commun.*, vol. 1, no. 1, pp. 18-25, Mar. 2015.
- [421] O. Simeone, "A very brief introduction to machine learning with applications to communication systems," *IEEE Trans. on Cogn. Commun. Netw.*, vol. 4, no. 4, pp. 648-664, Dec. 2018.
- [422] Y. Sun, M. Peng, Y. Zhou, Y. Huang, and S. Mao, "Application of machine learning in wireless networks: key techniques and open issues," *IEEE Commun. Surveys Tuts*, to appear.
- [423] H. E. Hammouti, M. Ghogho, and S. A. Raza Zaidi, "A machine learning approach to predicting coverage in random wireless networks," in *Proc. IEEE Globecom Workshops (GC Wkshps)*, pp. 1-6, Abu Dhabi, UAE, Dec. 2018.

-
- [424] A. Zappone, M. Di Renzo, M. Debbah, "Wireless networks design in the era of deep learning: model-based, AI-based, or both?," *IEEE Trans. Commun.*, vol. 67, no. 10, pp. 7331-7376, Oct. 2019.
- [425] J. Schloemann, H. S. Dhillon, and R. M. Buehrer, "Toward a tractable analysis of localization fundamentals in cellular networks," *IEEE Trans. Wireless Commun.*, vol. 15, no. 3, pp. 1768-1782, Mar. 2016.
- [426] C. E. O'Lone, H. S. Dhillon, and R. M. Buehrer, "A statistical characterization of localization performance in wireless networks," *IEEE Trans. Wireless Commun.*, vol. 17, no. 9, pp. 5841-5856, Sept. 2018.
- [427] B. Vo, B. Vo, N. Pham, and D. Suter, "Joint detection and estimation of multiple objects from image observations," *IEEE Trans Signal Process.*, vol. 58, no. 10, pp. 5129-5141, Oct. 2010.
- [428] J. Mullane, B. Vo, M. D. Adams, and B. Vo, "A random-finite-set approach to bayesian SLAM," *IEEE Trans. Robot.*, vol. 27, no. 2, pp. 268-282, Apr. 2011.
- [429] A. Grothendieck, "*Récoltes et Semailles*". [Online]. Available: https://www.quarante-deux.org/archives/klein/prefaces/Romans_1965-1969/Recoltes_et_semailles.pdf.
- [430] O. Caramello, "The unification of mathematics via topos theory," arXiv preprint, Jun. 2010, [Online]. Available: <https://arxiv.org/abs/1006.3930>.

Titre : Applications de la Géométrie Stochastique pour l'Analyse et la Modélisation des Réseaux sans Fil

Mot clés : Réseaux de 5ème génération (5G) et au-delà (B5G), rapport signal sur interférence plus bruit, géométrie stochastique

Résumé : Les réseaux sans fil de la cinquième génération (5G) et au-delà (B5G), devraient être très hétérogènes, multicouches, et dotés d'une intelligence intégrée à la fois au cœur et à la périphérie du réseau. Dans un tel contexte, l'évaluation des performances au niveau du système revêtira une importance cruciale pour formuler des enseignements judicieux sur les compromis qui régissent un tel système complexe et ainsi prévenir le besoin de simulations logicielles coûteuses et fastidieuses. Au cours de la dernière décennie, la géométrie stochastique est considérée comme un puissant outil d'analyse permettant d'évaluer les performances des réseaux sans fil au niveau du système et de cerner leur tendance à l'hétérogénéité. Cette thèse examine les nouveaux modèles et techniques de la géométrie stochastique développés au cours de la précédente décennie en matière de modélisation et d'analyse des réseaux sans fil du futur. Les discussions sont suffisamment affinées

pour être accessibles aux lecteurs peu spécialisés et faire en sorte que les lecteurs débutants, intermédiaires ou avancés puissent se familiariser rapidement avec ce domaine de recherche. Ensuite, nous nous appuyons sur la géométrie stochastique pour examiner plusieurs aspects des réseaux sans fil 5G et B5G, afin d'illustrer sa flexibilité mathématique et sa capacité à saisir l'analyse de scénarii peu conventionnels. Nous discutons également de nouvelles perspectives qui apporteront un nouveau souffle à l'utilisation de la géométrie stochastique au cours de cette décennie cruciale. En bref, les discussions furent étendues à des thématiques plus larges telles que les communications optiques en espace libre (FSO), les communications en lumière visible, les systèmes de drones, l'architecture d'accès radio en brouillard (F-RAN), l'intelligence artificielle et l'apprentissage machine, ainsi que les communications moléculaires.

Title: Applications of Stochastic Geometry in the Modeling and Analysis of Wireless Networks

Keywords: Fifth-generation (5G) and beyond fifth-generation (B5G) networks, signal-to-interference-and-noise-ratio, stochastic geometry

Abstract: Next generation wireless networks, i.e., fifth generation (5G) and beyond (B5G), are expected to be highly heterogeneous, multi-layered, with embedded intelligence at both the core and edge of the network. In such a context, system-level performance evaluation will be very important to formulate relevant insights into tradeoffs that govern such a complex system and then prevent the need for onerous and time-consuming computer simulations. Over the past decade, stochastic geometry has emerged as a powerful analytical tool to evaluate system-level performance of wireless networks and capture their tendency towards heterogeneity. This dissertation reviews first novel stochastic geometry models and techniques developed during the last decade in modeling and analysis of modern wireless networks. The discussions are refined

enough to be accessible for non-specialist readers and help new, intermediate, or advanced readers familiarize quickly with this field of research. Next, we leverage stochastic geometry frameworks to investigate several aspects of 5G and B5G wireless networks and then illustrate its mathematical flexibility and ability to capture the analysis of the rather unconventional scenarios. Also, new perspectives that will breathe new life into the use of stochastic geometry during this crucial decade are discussed. In a nutshell, extensive discussions were held on broader topics such as free space (FSO) optical communications, visible light communications, unmanned aerial vehicle systems, fog radio access architecture (F-RAN), artificial intelligence and machine learning, and molecular communications.